

NATURAL CIRCULATION STUDIES ON LEAD BISMUTH EUTECTIC COOLANT

By

ANANTA BORGOHAIN

ENGG01201004012

Bhabha Atomic Research Centre, Mumbai

A thesis submitted to the

*Board of Studies in Engineering Sciences
In partial fulfillment of requirements for the Degree of*

DOCTOR OF PHILOSOPHY

of

HOMI BHABHA NATIONAL INSTITUTE



August, 2017

HOMI BHABHA NATIONAL INSTITUTE

Recommendations of Viva Voce Board

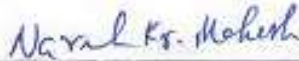
As members of the Vice Voce Board, we certify that we have read the dissertation prepared by Ananta Borgohain, enrollment number ENGG01201004012 titled "Natural Circulation Studies on Lead Bismuth Eutectic Coolant" and recommend that it may be accepted as fulfilling the dissertation requirement for the degree of Doctor of Philosophy.

Dr. P. K. Vijayan
Chairman



Date 20/6/18

Dr. N. K. Maheshwari
Guide/Convener



Date 20/6/18

Dr. A. K. Nayak
Member



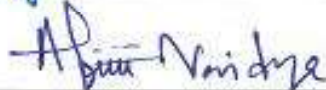
Date 20/6/18

Prof. Atul Sharma
Member



Date 20/6/18

Dr. A.M. Vaidya
Member



Date 20/6/18

Prof. Ashwin W. Patwardhan
Examiner

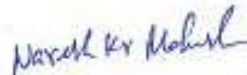


Date 20/06/2018

Final approval and acceptance of this dissertation is contingent upon the candidate's submission of the final copies of the dissertation of HBNI.

I hereby certify that I have read this dissertation prepared under my direction and recommend that it may be accepted as fulfilling the dissertation requirements.

Guide:



Date 20/6/2018 Place Mumbai

STATEMENT BY AUTHOR

This dissertation has been submitted in partial fulfilment of requirements for an advanced degree at Homi Bhabha National Institute (HBNI) and is deposited in the library to be made available to borrowers under rules of the HBNI. Brief quotations from this dissertation are allowable without special permission, provided that accurate acknowledgement of source is made. Requests for permission for extended quotation from or reproduction of this manuscript in whole or in part may be granted by the Competent Authority of HBNI when in his or her judgment the proposed use of the material is in the interests of scholarship. In all other instances, however, permission must be obtained from the author.



Ananta Borgohain

DECLARATION

I, hereby declare that the investigation presented in the thesis has been carried out by me. The work is original and has not been submitted earlier as a whole or in part for a degree/diploma at this or any other Institution / University.

A handwritten signature in blue ink, appearing to read 'Ananta Borgohain', with a stylized flourish at the end.

Ananta Borgohain

DEDICATIONS

I dedicate this thesis to my parents and my beloved family.

ACKNOWLEDGEMENTS

I would like to express my sincere gratitude to my guide Dr. N. K. Maheshwari for the guidance and encouragement to work to the best of my abilities. His knowledge, insightfulness and consistent care for the best output have been great assets without which research would not have been possible. I would like to thank my co-guide Dr. P. K. Vijayan for the constant encouragement helps in experimental and theoretical work. I am indebted to the chairman and other members of doctoral committee for their valuable comments and suggestions during the review presentations, oral, general comprehensive examinations and pre-synopsis viva-voce. My sincere thanks to Shri S. S. Jana, Shri. A. K. Shrivastava, Shri. B. Jaiswal and Shri. B. M. Lingade for their support and encouragement during this research work. I would like to express my sincere thanks to all the colleagues of RED workshop, Electrical group and Instrumentation Group for their invaluable supports. I also thank to our Operation staff of RED, who have helped to operate the loops round the clock with utmost care and generated the invaluable data required for the present work. I would like to thank Dr. R Tewari, MSD, BARC and his colleague for developing the KTL loop material. It is special thanks to the colleagues of NFC, Hyderabad for developing the KTL loop and for giving invaluable experience on Nb-alloy loop fabrication.

I am highly grateful to Prof. A. W. Patwardhan, (ICT, Mumbai) and Dr. Nathalie Marie, (CEA, France) for their invaluable comments during review of this thesis. I thank to all those who have also contributed towards this work whose names are inadvertently missed out here.



Ananta Borgohain

List of Publications arising from the thesis

Journal

1. “Natural Circulation Studies in a Lead Bismuth Eutectic Loop”, A. Borgohain, B. K. Jaiswal, N. K. Maheshwari, P. K. Vijayan, D. Saha and R. K. Sinha, *J. Progress in Nucl. Energy* 2011, vol 53, p 308-319.
2. “Natural circulation studies in a LBE loop for a wide range of temperature", A. Borgohain, A.K. Srivastava, S.S. Jana, N.K. Maheshwari, R.D. Kulkarni, P.K. Vijayan, R. Tewari, A. Maruthi Ram, S.K. Jha; *Nuclear Engineering and Design*, 2016, Volt. 300, p 358–375.
3. “Experimental and CFD Study on Natural circulation Phenomenon in Lead Bismuth Eutectic Loop”, P. Naphade, A. Borgohain, R. Thundil Karuppa Raj, N.K. Maheshwari, *J. Procedia Engineering*, 2013, vol. 64, p 936-945.
4. “Natural Circulation Experiments in a Non-uniform Diameter Lead Bismuth loop and validation of LeBENC code”, A. Borgohain, N. K. Maheshwari and P. K. Vijayan, , *J. Progress in Nucl. Energy*, 2016, vol 91, p 68-82.’

International Conference

1. “CFD Analysis on Heat Transfer in Low Prandtl Number Fluid Flows”, A. Borgohain, B. K. Jaiswal, N. K. Maheshwari, P. K. Vijayan, D. Saha and R. K. Sinha, 2011, 14th International Topical Meeting on Nuclear Reactor Thermal hydraulics, NURETH-14, September 25-30, 2011, Toronto, Ontario, Canada.

2. “Natural circulation studies in lead bismuth eutectic loops”, A. Borgohain, A. K. Srivastava, S. S. Jana, N. K. Maheshwari and P. K. Vijayan, 2015, , International Thorium Energy Conference, ThEC-15, October 12-15, 2015, BARC, Mumbai, India.

National Conference

1. “CFD Analysis of Heat Transfer in a Vertical Annular Gas Gap”, A. Borgohain, N.K. Maheshwari and P. K. Vijayan, 2011, 4th National Conference on Nuclear Reactor Technology (NRT-4), Mar 04-06, 2011, BARC, Mumbai, India.

Contents

SYNOPSIS	viii
LIST OF FIGURES	xi
LIST OF TABLES	xvii
NOMENCLATURE	xviii
ABBREVIATIONS	xxi
CHAPTER 1 INTRODUCTION	1
1.1 Natural Circulation	3
1.2 Natural Circulation in Liquid Metal	5
1.3 Motivation and Problem Statement	5
1.4 Objectives of This Work	7
1.4.1 Investigation of steady state and transient behaviour natural circulation of LBE in the operating range of CHTR	7
1.4.2 Development of computer code for thermal hydraulic analysis LBE and its validation.	7
1.4.3 Parametric influence on the LBE natural circulation.	8
1.5 Organisation of the Thesis	8
1.6 Closure.	11
CHAPTER 2 LITERATURE REVIEW	12
2.1 Liquid Metals as Coolant	12
2.2 Liquid Metal Cooled Reactors	15
2.3 Natural Circulation	17
2.4 Liquid Metal Loops for Natural Circulation Studies	20
2.5 Theoretical Studies in Liquid Metal Loops.	22
2.6 Literature Review Carried out for Construction of the Lead Bismuth Facilities	26
2.6.1 Attributes of Lead Bismuth Eutectic (LBE)	27

2.6.1.1 Thermo-physical properties of LBE	27
2.6.1.2 Liquid metal experimental loops	30
2.6.1.3 LBE corrosion and suitable material of construction	40
2.6.1.4 Dissolved oxygen measurement	44
2.6.1.5 Safety aspects of molten lead alloy	45
2.7 Liquid Metals Thermal Hydraulics and Factors Affecting the Natural Circulation.	46
2.8 Summary of Findings from the literature Survey.	48
CHAPTER 3 DEVELOPMENT OF LIQUID METAL LOOP (LML) AND EXPERIMENTAL STUDIES	50
3.1 Introduction.	50
3.2 Design of the Loop.	51
3.3 Description of the Lead-Bismuth Loop.	52
3.3.1 Heating system.	53
3.3.2 Heat exchanger.	55
3.3.3 Instrumentation.	56
3.3.4 Oxygen measurement and Control.	60
3.4 Safety design aspects of the loop	65
3.5 Characterisation of the Loop.	67
3.5.1 Heat exchanger performance analysis.	67
3.5.2 Heat loss in the loop	71
3.5.3 Experimental test matrix in the loop.	73
3.6 . Operation of the Loop	73
3.7. Results and Discussions.	76
3.7.1 Steady state analysis.	76
3.7.2 Transient studies.	81
3.7.2.1 Start-up operation.	81
3.7.2.2 Loss of heat sink.	85
3.7.2.3 Step change in heater power	87

3.7.2.4 Effect of coolant flow in heat exchanger.	90
3.8 Summary of Major Findings	91
CHAPTER 4 DEVELOPMENT OF KILO TEMPERATURE LOOP AND EXPERIMENTAL STUDIES.	93
4.1 Introduction	93
4.2 Developmental Work for High Temperature Loop.	93
4.3 Design of the Loop with Nb-alloy	94
4.4 Description of Kilo Temperature Loop (KTL)	98
4.5 Enclosure for Inert Gas and Oxygen Scavenging System	103
4.6 Loop Operating Procedure	107
4.7. Results and Discussions	108
4.7.1 Steady state experiments.	108
4.7.2 Comparison of steady state natural circulation flow equations with experimental data	111
4.7.3 Transient studies	113
4.7.3.1 Start-up operation	113
4.7.3.2 Loss of heat source	115
4.7.3.3 Step change of heater power	117
4.8 Summary of Major Findings/achievements	119
CHAPTER 5 EVALUATION OF LBE HEAT TRANSFER COEFFICIENT AT DIFFERENT FLOW REGIMES	121
5.1 Introduction	121
5.2 Different Flow Regimes in Natural Circulation	123
5.2.1 Free convection	123
5.2.2 Mixed convection	124
5.2.3 Heat transfer in forced laminar flow	125
5.2.4 Forced convection turbulent flow	126
5.3 CFD Application for Liquid Metal Heat Transfer.	
5.3.1 Turbulent Prandtl number	127

5.3.2 Turbulence models and mesh distribution	129
5.3.3 Evaluation of Nusselt number from PHOENICS results	131
5.3.4 Thermo-physical properties of lead bismuth eutectic	131
5.3.5 Heat transfer in developing flow.	131
5.4 Heat Transfer Formulations in Different Parts of the Loops	132
5.4.1 Heater section	132
5.4.2 Piping	132
5.4.3 Heat exchanger.	133
5.5 Results and Discussions	133
5.5.1 Free convection	135
5.5.2 Mixed convection	137
5.5.3 Forced convection	139
5.5.4 Heat transfer analysis at higher Reynolds number	139
5.5.4.1 Effect of mesh size	141
5.5.4.2 Turbulent Prandtl number effect	143
5.5.4.3 Effect of turbulence models	145
5.5.4.4 Developing length	147
5.6 Summary of Major Findings.	147
CHAPTER 6 DEVELOPMENT OF COMPUTER CODE LeBENC	149
6.1 Introduction	149
6.2. Numerical Code, LeBENC	149
6.2.1 Mathematical formulation of LeBENC code for LML	150
6.2.1.1 Momentum equation for fluid	150
6.2.1.2 Energy equation for fluid	151
6.2.1.3 Conduction equation for the wall	151
6.2.2 Discretization of the governing equations	151
6.2.2.1 Discretization of momentum equation	151
6.2.2.2 Discretization of energy equation	152

6.2.2.3 Discretization of conduction equation for the wall	153
6.2.3 Solution procedure adopted in the code	155
6.2.4 Discretisation of LML	156
6.2.5 Constitutive equations	157
6.3 Formulation of LeBENC Code for KTL.	159
6.3.1 Mathematical formulation of LeBENC code for KTL.	159
6.3.1.1 Momentum equation for fluid	160
6.3.1.2 Energy equation for fluid	161
6.3.1.3 Conduction equation for the wall	161
6.3.2 Modelling of heat exchanger	162
6.3.2.1 Nodal discretisation and coupling of the primary and secondary side parameters	163
6.3.2.2 Finding inlet temperature of argon gas in the secondary side of the heat exchanger of KTL	164
6.3.3 Discretization of the governing equations and the loop	166
6.4 Validation of LeBENC Code with LML	167
6.4.1 Steady state analysis	167
6.4.2 Transient analysis	168
6.4.2.1 Start up experiment	168
6.4.2.2 Loss of heat sink	169
6.4.2.3 Effect of the step change in power	173
6.4.2.4 Effect of the change in the secondary coolant flow rate	174
6.5 Validation of LeBENC Code with KTL Experimental Data	174
6.5.1 Steady state analysis	174
6.5.2 Transient studies	178
6.5.2.1 Start-up simulation test	178
6.5.2.2 Loss of heat source	179
6.5.2.3 Step change of heater power	179
6.6 Summary of Major Findings	181

CHAPTER 7 EFFECT OF VARIOUS PARAMETERS ON LBE NATURAL CIRCULATION.....	183
7.1 Introduction	183
7.2 Different Parameters Which may Affect Natural Circulation of LBE	183
7.3 Results of the Parametric Analysis and Discussion	185
7.3.1 Effect of thermal conduction of LBE.	185
7.3.1.1 Axial temperature variation	186
7.3.1.2 Effect on natural circulation flow rate	188
7.3.1.3 Effect of radial conduction of LBE on natural convection	189
7.3.2 Effect of surface roughness of the piping	190
7.3.3 Effect of heat transfer coefficients	191
7.3.4 Effect of heat loss in piping	195
7.4 Summary of Major Findings.	197
CHAPTER 8 SUMMARY AND SCOPE FOR FUTURE WORK.....	199
8.1 Introduction	199
8.2 Experimental Work on Natural Circulation of LBE in two Loops, LML and KTL	199
8.3 Development of Computer Code LeBENC and its Validation.. . .	201
8.4 Studies on the Effect of Different Parameters on LBE Natural Circulation.....	201
8.5 Suggestions for Future Work	202
8.5.1 Experimental studies	202
8.5.2 Computational studies	202
8.5.3 Stability analysis	203
Appendix 4.1 Calculation of wall thickness of KTL components	204
Appendix 4.2 Heat transfer analysis of the enclosure of KTL	206
Appendix 4.3 Oxidation of the Niobium at high temperature	213
Appendix 4.4 Calculation of non-dimensionlised numbers of different liquid metal loops	217

Appendix 4.5 Error Analysis	227
Appendix 6.1 Effect of acceleration pressure drop in the secondary side of KTL..	232
REFERENCEES	237

SYNOPSIS

The design of the Compact High Temperature Reactor (CHTR) is in progress in BARC. CHTR is a 100 kW_{th} power, ²³³U-Thorium fuelled, Lead Bismuth Eutectic (LBE) cooled and beryllium oxide moderated reactor. The reactor is being designed to operate with natural circulation cooling and at about 1000 °C, to facilitate demonstration of technologies for high temperature process heat applications such as hydrogen production by thermo-chemical processes. The high boiling point (1670 °C) of LBE ensures that the reactor can be operated at high temperatures at near atmospheric pressure without the risk of coolant boiling, which improves the thermal efficiency. It also improves the plant safety by reducing the risk of leakage at high temperatures as pressurization is not required.

In natural circulation, the driving force is the buoyancy head developed due to the heating in the core and cooling in the primary heat exchanger. The flow of the coolant depends on the relative vertical positions of the core and the heat exchanger. Moreover the geometry of the primary heat transport system plays an important role on the coolant flow rate. In CHTR the range of modified Grashof number, Gr_m, which is a measure of buoyancy force in natural convection, is in the range of 10¹¹ to 10¹³. Extensive literature survey was carried out on the liquid metal experimental studies, but no literature on the natural circulation studies in the operating range of CHTR could be found. So specific experiments are required to study the behaviour of the coolant in a particular reactor design. The theoretical modelling is also required to simulate natural circulation of LBE for entire temperature range of CHTR including all the factors which may affect the natural circulation of LBE at high temperature.

To conduct natural circulation experiments two liquid metal loops have been made. One of the loop is named Liquid Metal Loop and the other is Kilo Temperature Loop (KTL). The experiments in the loop covers a wide temperature range i.e. (200-780 °C) and the entire Gr_m range of CHTR design. The LML was designed on the basis of the knowledge gained from literature review. To simulate the CHTR conditions, hydraulic diameter of the single fuel tube is simulated in the heater section. The maximum power of the heater section of the loop is equivalent to full power the single fuel tube full power. The vertical distance between the cooler and heater centreline is maintained to simulate the buoyancy head of the reactor. The LBE inventory of the loop is same as that in CHTR. Accurate measurement of the dissolved oxygen concentration in liquid LBE was a critical issue for the active chemistry control in the system. An oxygen sensor was developed to measure dissolved oxygen level in LBE and used in the loop. A number of steady state and transient natural circulation experiments are carried out for different power levels with air and water as the secondary fluids. The results are compared with natural circulation correlations available in literature.

To conduct experiment beyond 500 °C, KTL was constructed from high temperature material which is compatible with molten LBE. The in-house developed niobium alloy (Nb-1 % Zr-0.1C) was used as the construction material. All the components of the loop are Electron Beam (EB) welded. The loop was kept in an inert gas enclosure to avoid oxidation of Nb alloy at higher temperature. The loop was operated up to 1100 °C and natural circulation studies were carried out. Natural circulation data of LBE could be generated in the temperature range of (bulk coolant temperature) 200-780 °C.

Transient studies were carried out to simulate some postulated accident scenarios in the reactor. The main objective was to observe the LBE coolant behaviour during various transient conditions. The transient experimental studies include start-up of the loop from zero power conditions, heater trip and step power change. For heat transfer simulation, as the heat

transfer correlations are different from the water based coolants, literature survey was carried out and found that there are several correlations for liquid metal heat transfer. The help of CFD is taken for verification of the heat transfer correlations for forced flow and mixed convection flow for LBE application.

A computer code named LeBENC (Lead Bismuth Eutectic Natural Circulation) was developed to study steady state and stability (transient) behaviour of natural circulation rectangular loops for various orientations of heated section and heat exchanger. The code has the capability to handle, (a) non-uniform diameter loops, (b) different working fluid in primary and secondary side of the loop, (c) trace heating and surface heat loss from the walls to ambient and (d) axial conduction through liquid metal and the pipe wall. The details of the mathematical formulation of the code are described in the thesis. The code was used to analyse the experimental studies of both KTL and LML. Both steady state and transient natural circulation analyses were carried out using the code. It was found that the maximum difference in experimental data and code prediction is $\pm 20\%$ in all the predictions. The code was used to study the effect of various parameters like axial thermal conduction, heat loss through the piping, heat transfer coefficients, etc. The effect of variation heat transfer coefficient on the transient cases was found to be negligible. The heat loss in the piping has considerably reduced the loop temperatures during both steady state as well as transient natural circulations cases. However the natural circulation flow rate has not been affected by the heat loss. The effect of axial conduction was also found to be negligible on the flow rate. But the some effect is found on the axial temperature profile especially at the inlet of the heater. The effect of the surface roughness on the natural circulation was found to be negligible.

LIST OF FIGURES

Fig 1.1	Schematic of CHTR	2
Fig 2.1	Flow sheet of PFBR [6]	15
Fig 2.2	Schematic of natural circulation flow path in SSTAR [7]	16
Fig 2.3(a)	Variation of density of lead bismuth eutectic with temperature	28
Fig 2.3(b)	Variation of thermal conductivity of lead bismuth eutectic with temperature	28
Fig 2.3(c)	Variation of specific heat of lead bismuth eutectic with temperature	29
Fig 2.3(d)	Variation of dynamic viscosity of lead bismuth eutectic with temperature	29
Fig 2.3(e)	Variation of volumetric thermal expansion coefficient of lead bismuth eutectic with temperature	30
Fig 2.4	Corrosion/oxidation of stainless in lead at 550°C [106]	41
Fig. 3.1(a)	Isometric view of Liquid Metal Loop.	52
Fig. 3.1(b)	Photo of a part of Liquid Metal Loop.	52
Fig.3.2	View of the main heater of the Loop.	55
Fig. 3.3	Schematic of the heat exchanger of the Loop.	55
Fig. 3.4	Flow sheet of Liquid Metal Loop.	57
Fig 3.5	Instrumentation panel of LML.	58
Fig 3.6	Mimic for monitoring and control of LML.	58
Fig 3.7	Schematic of the discrete type level sensor used in LML.	59
Fig 3.8 (a)	Schematic of continuous level measurement sensor based on gas bubbling	59
Fig 3.8 (b)	Response of the continuous level sensor during loop filling	60
Fig. 3.9	Working principle of YSZ Oxygen sensor.	61
Fig 3.10	Variation of EMF in the oxygen sensor with temperature at different dissolved O ₂ concentration (% wt) in LBE.	62
Fig. 3.11	Schematic and view of the oxygen sensor used in LML	64

Fig. 3.12	Variation of EMF in a oxygen sensor with time.	64
Fig. 3.13 (a)	View of the Argon gas scrubber of LML	65
Fig. 3.13 (b)	P&I diagram of the Argon gas scrubber of LML	66
Fig 3.14	Schematic of the ventilation system with enclosure of LML.	67
Fig 3.15	Test results of the heat exchanger in high temperature water loop before installing in the LML.	69
Fig 3.16	Radial dimensions considered [Eq (3.9) and Eq (3.10)] across the walls of the heat exchanger	70
Fig 3.17	Variation of ΔT_{in} and overall Heat transfer Coefficient in the heat exchanger of the loop.	71
Fig 3.18	Heat removed by the heat exchanger and heat loss in the loop piping in LML.	72
Fig 3.19	Calculated mass flow rate during steady state natural circulation at different power levels.	77
Fig 3.20	Comparison of steady state correlation [Eq. (3.9)] with experimental data. ...	78
Fig 3.21(a)	Steady state temperature distribution along the length of the loop at main heater power= 2400W with air as the secondary side coolant.	78
Fig 3.21(b)	Steady state temperature distribution along the length of the Loop at Main Heater Power= 2400W with water as the secondary side coolant.	79
Fig 3.22 (a)	Steady state axial temperature distribution of the loop at 900 W power.	79
Fig 3.22 (b)	Steady state axial temperature distribution of the loop at 4200 W power.	80
Fig 3.23(a)	Temperature variation at outlets of heater and heat exchanger during start-up of the loop from near stagnation condition with Power 1200 W.	82
Fig. 3.23 (b)	Temperature difference across the heater section and heat exchanger during start-up of the loop from stagnation condition Power 1200 W.	82
Fig 3.24 (a)	Temperature variation at outlets of heater and heat exchanger during start-up of the loop from stagnation condition at power 2400 W	83
Fig 3.24 (b)	Temperature difference across the heater section and heat exchanger during start-up of the loop from near stagnation condition at Power 2400 W.	84
Fig 3.25 (a)	Temperature variation at outlets of heater and heat exchanger during start-up of the loop from stagnation condition at 3000 W power.	85
Fig 3.25 (b)	Temperature difference across the heater section and heat exchanger during start-up of the loop from stagnation condition at 3000 W power.	86

Fig 3.26 (a)	Variation of inlet and outlet temperature of heated section during the simulation of loss of heat sink with initial steady state power 2400W.	87
Fig. 3.26 (b)	Variation of inlet and outlet temperature of heat exchanger during the simulation of loss of heat sink with initial steady state power 2400W.	88
Fig. 3.27 (a)	Variation of the difference of LBE inlet and outlet temperature of heated section and heat exchanger, during the simulation of loss of heat sink with initial steady state power 1200 W.	88
Fig. 3.27 (b)	Variation of the difference of LBE inlet and outlet temperature of heated section and heat exchanger, during the simulation of loss of heat sink with initial steady state power 2400 W.	89
Fig. 3.28	Variation of temperature difference in LML during step change in power 2100 W-1200 W-2100 W.	89
Fig 3.29	Temperature variation in the loop when secondary air flow was decreased from 320LPM to 100LPM with 2280W loop power.	90
Fig 4.1	Isometric view of the KTL made jointly with NFC, Hyderabad.	95
Fig 4.2	Schematic of the support of KTL.	96
Fig 4.3	KTL components and loop assembly fabricated in NFC, Hyderabad.	97
Fig 4.4	Joint between Nb alloy part and SS part of the loop.	99
Fig. 4.5	Schematic of heat exchanger of the loop.	100
Fig 4.6	P&I diagram of KTL.	102
Fig 4.7	Solid model of the enclosure of KTL (top finned plate is not shown for clarity).	104
Fig 4.8	KTL facility with the enclosure.	105
Fig 4.9	Flow sheet of oxygen scavenging system the KTL enclosure.	106
Fig 4.10 (a)	Temperature rise across heated section during steady state natural circulation at different power levels.	109
Fig 4.10 (b)	Mass flow rate of LBE during steady state natural circulation at different power levels.	109
Fig. 4.11	Fluid and wall temperature distribution in the axial direction of the loop at 360W power.	110
Fig 4.12	Comparison of Steady state natural circulation correlations with experimental data for flow range of $100 < Re < 10^5$	113

Fig 4.13 (a)	Start up experimental results at 800 W and with loop avg temperature 350 °C	114
Fig 4.13 (b)	Start up experimental results at 800 W and with loop avg temperature 475 °C.	115
Fig 4.14 (a)	Temperature variation in the loop during heater trip experiments at power 200 W.	116
Fig 4.14 (b)	Temperature variation in the loop during heater trip experiments at power 700 W.	116
Fig. 4.15	Variation of loop temperature during step change in power 440-300-200-0 W.	117
Fig. 4.16	Variation of temperatures during different power levels in the loop.	118
Fig. 4.17	Variation of loop temperature during step change in power from 1100 W to 1200 W.	118
Fig 5.1	Regimes of free, mixed and forced convection flow through vertical tubes [117].	122
Fig 5.2	Influence of buoyancy on heat transfer to sodium [120].	125
Fig. 5.3	2D axi-symmetry section of a tube with mesh distribution.	134
Fig 5.4	Prediction of CFD results for free convection heat transfer and comparison with correlations developed for vertical heated surfaces.	136
Fig 5.5	The prediction of free convection heat transfer and comparison with the data for mixed convection (Jackson et al., 1994) [120].	136
Fig 5.6	Variation of Nusselt number with Reynolds number for the range, $50 < Re < 4000$	138
Fig 5.7	CFD results of the buoyancy aided mixed convection with LBE.	138
Fig 5.8	CFD results of LBE heat transfer in vertical tube for flow range $4000 < Re < 38500$ and comparison with various correlations.	140
Fig 5.9	Comparison of liquid metal heat transfer correlations with experimental results.	141
Fig. 5.10	Variation of fully developed Nusselt Number with y_1^+ with k- ϵ turbulence model.	142
Fig. 5.11	Variation of turbulent Prandtl Number with Peclet Number for liquid metal.	143
Fig. 5.12	Comparison of CFD prediction using standard k- ϵ model for different Pr_t with empirical correlation for Nusselt number.	144
Fig. 5.13	Comparison of CFD prediction using different turbulence models with empirical correlations for Nusselt number.	146
Fig. 5.14	Variation of local Nusselt number along the axial distance.	146
Fig. 6.1	Discretisation of the loop geometry for analysis using LeBENC code	156
Fig 6.2	Schematic of the heat exchanger and nodal discretization for LeBENC code.	163

Fig. 6.3	Discretisation of the KTL main loop geometry for analysis using LeBENC code	165
Fig 6.4	Steady state natural circulation prediction by LeBENC code and comparison with experimental data of LML.	167
Fig. 6.5 (a)	Steady state temperature distribution along the length of the loop at main heater power= 2400 W with air as the secondary side fluid.	168
Fig. 6.5 (b)	Steady state temperature distribution along the length of the loop at main heater power= 2400 W with water as the secondary side fluid.	170
Fig 6.6 (a)	Steady state axial temperature distribution in LML at 900 W power.	170
Fig 6.6 (b)	Steady state axial temperature distribution in LML at 4500 W power.	171
Fig. 6.7	Simulation of start-up experiment in LML at Power 1200 W.	171
Fig 6.8	Simulation of start-up experiment in LML at 2400 W power.	172
Fig. 6.9	Comparison of the LeBENC prediction with the experimental data of the variation of temperature difference across the heat exchanger during the simulation of Loss of Heat Sink with initial steady state Power 1200 W.	172
Fig. 6.10	Comparison of the LeBENC prediction with the experimental data of the variation of temperature difference across the heater section and the Heat Exchanger during the step change in power experiment.	173
Fig 6.11	Variation in temperature differences across the heater section and the heat exchanger of LML with step change in secondary air flow 200-320-200LPM with 1500 W.	175
Fig 6.12 (a)	Temperature rise across heated section during steady state natural circulation results at different power levels	175
Fig 6.12 (b)	Calculated steady state natural circulation LBE mass flow rate in LML at different power levels	176
Fig. 6.13	Variation of main heater section inlet temperature of LBE at different steady state power levels.	177
Fig. 6.14	Fluid and wall temperature distribution in the axial direction of the loop at 360 W power.	177
Fig. 6.15 (a)	Temperature variation during start-up experiment of the loop from zero power condition to 360 W power level.	178
Fig. 6.15 (b)	Temperature variation during start-up experiment of the loop from zero power condition to 700 W power level.	179
Fig 6.16	Temperature variation in the loop during loss of heat sink with initial power 1000 W.	180
Fig. 6.17	Variation of loop temperature during step change in power from 720 W to 480 W in step of 40 W.	180

Fig. 6.18	Variation of loop temperature during step change in power from 1100 W to 1200 W.	181
Fig 7.1	Prediction of axial temperature distribution of LBE at different power levels.	186
Fig 7.2	Prediction of axial temperature distribution of water and LBE at 50 W power level.	187
Fig 7.3	Prediction of variation of temperature in KTL with different thermal conductivities of the working fluid at 700 W loop power.	188
Fig 7.4	Buoyancy head developed at different thermal conductivities of LBE with heat loss in the piping.	190
Fig 7.5	LeBENC predictions on the effect of pipe surface roughness on the natural circulation of LBE during start-up experiment at 700 W power.	191
Fig 7.6	Effect of LBE heat transfer coefficients on the temperature variation with time during start up experiments at 700 W power in KTL.	193
Fig 7.7	Effect of LBE heat transfer coefficients on the temperature difference between average wall and fluid temperatures in the heater sectin of KTL.	194
Fig. 7.8	Start-up at 900 W power and comparison with LeBENC data considering different boundary conditions at the secondary side.	194
Fig 7.9	Variation of temperature difference across the heater section during start up experiment simulation at 900 W in LML with different heat loss conditions in the piping.	196
Fig 7.10	Prediction of buoyancy head developed in the LML at 900 W power at various conditions of heat loss in the piping.	196
Fig 7.11	Prediction of LBE mass flow rate in the LML at 900 W power at various conditions of heat loss in the piping.	197

LIST OF TABLES

Table 1.1	Major design and operating characteristics of CHTR.	4
Table 2.1	Thermo physical properties of different liquid metal coolants.	13
Table 2.2	Liquid metal coolants its use and its merits and demerits.	14
Table 2.3	Working range (in terms of Gr_m) and maximum operating temperature of CHTR and different liquid metal loops available from literature.	23
Table 2.4	Summary theoretical codes used for liquid metal systems.	24
Table 2.5	Liquid metal loops operating up to 550 °C.	32
Table 2.6	Summary of the experimental loops operated at and above 550 °C.	37
Table 2.7	Maximum allowable concentration of lead in air and blood.	46
Table 3.1	Comparative design parameters of CHTR and Liquid Metal Loop (LML).	51
Table 3.2	Design parameters of LML.	54
Table 3.3	Postulated events and measures for safety.	68
Table 3.4	Natural circulation test matrix of the Liquid Metal Loop.	73
Table 4.1	Design parameters of KTL.	98
Table 4.2	The values of coefficients of Eq (4.1) recommended by different authors.	112
Table 5.1	Correlations available for free convection heat transfer for low Prandtl number fluids in vertical plate.	124
Table 5.2	Literature review of heat transfer correlations in liquid metal flow in pipe with uniform wall heat flux.	126
Table 5.3	Parameters for the LBE heat transfer analysis.	134
Table 5.4	Heat Transfer correlations used for fully developed flow.	148
Table 6.1	Values of the coefficients in Eq. (6.10) and Eq. (6.14).	154
Table 6.2	Loop parameters used in the code (Fig 6.1).	157
Table 6.3	Correlations for pressure loss coefficients used in the LeBENC analysis.	158

NOMENCLATURE

A	Area (m ²)	k	Local loss coefficient
B _o	Liquid Metal Buoyancy parameter,	l	Length (m)
$\left[\frac{Gr^*}{\left\{ Re^{1.825} \left(5 + 0.025 Pe^{0.8} \right)^2 \right\}} \right]$		N	Node
a _{pb}	activity of lead (dimensionless)	N _G	Geometrical parameter (dimensionless)
C _o	Oxygen concentration (%wt)	Nu	Nusselt Number (h _{in} d _{in} /K)
C _p	specific heat (J/kg-K)	Nu'	Nusselt number based on the annular spacing, Eq. (6.24),(dimensionless)
Co	Courant number (dimensionless)	P	Pressure (N/m ²)
D	diameter (m)	Pe	Peclet Number
d _h	hydraulic diameter (m)	Pr _t	turbulent Prandtl number, $\left(\frac{\epsilon_M}{\epsilon_H} \right)$
E	Emf (V)	q	Heat flux rate (W/m ²)
F	Faraday constant, (C/mol)	Q	Heat transfer rate (W)
ΔF	Free Energy of formation, (J/K-mol)	r	radius, m
f	Friction factor (dimensionless)	r ₁	radius of the annular gas gap, m
F _o	Fourier number (dimensionless)	R _{gap}	gap resistance (mK/W)
Gr _m	Modified Grashof number $= \frac{D_r^3 \rho_o^2 \beta g Q_h \Delta Z_c}{A_r \mu^3 C_p}$	R	Gas constant (J/K-mol)
Gr*	Grashof number in vertical plate, $\left(= \frac{g \beta q x^4}{K \nu^2} \right) \text{ for tube } x=D.$	Ra	Rayleigh number
g	Acceleration due to gravity (m/s ²)	Re _o	Reynolds number corresponding to the departure from Hagen-Poiseuille law for pressure drop coefficient
H	loop height (m)	Re ₁	Reynolds number indication the flow regime change from laminar to transition.
h	Heat transfer coefficient (W/m ² -K)	Re ₂	Reynolds number indication the flow regime change from transition to turbulent.

K	Thermal conductivity (W/mK)		
t	Time (seconds)	ζ	Perimeter (m)
T	Temperature (°C)	ρ	Density (kg/m ³)
T _o	Reference temperature (°C)	Fe ₃ O ₄	Iron Oxide
u	velocity (m/s)	ρ_o	Density at reference temperature
u ⁺	dimensionless velocity (u/u _τ)		(kg/m ³)
v	Velocity (m/sec)	Δ	roughness (m)
w	thickness (m)	$\overline{\Delta} = \frac{\Delta}{D_h}$, dimensionless
W	Mass flow rate (kg/sec)	ε_H	eddy diffusivity of heat transfer (m ² /s),
x	Length wise distance (m)	ε_M	eddy diffusivity of momentum transfer
y	Radial distance from the wall, m/s.		(m ² /s),
y ⁺	dimensionless distance to wall	μ	dynamic viscosity, Ns/m ²
$y^+ = \frac{y}{v} \frac{u}{\left(\frac{\tau_s}{\rho}\right)^{1/2}}$		ν	kinematic viscosity, m ² /s
y ⁺¹	dimensionless distance to wall at the first mesh	τ_s	shear stress, (N/m ²)
Z	height (m)	ν_t	turbulent kinematic viscosity (m ² /s)
Z _c	Central Height (m)	σ	stress
U	overall heat transfer coefficient (W/m ² -K)	Subscript	
Δp	pressure drop (N/m ²)	1	first loop
Δx	length difference (m)	2	second loop
Greek		Ar	argon
α	Thermal diffusivity in liquid, (m ² /s)	atm	atmosphere
β	Thermal expansion coefficient, K ⁻¹	a	ambient
		acc	acceleration
		Bi ₂ O ₃	Bismuth Oxide
		eff	effective

encl	enclosure	Superscript	
f	Fluid	n	n-th time step
h	Heater		
hx	heat exchanger		
i	i-th node, section		
in	Inside		
LBE	Lead bismuth Eutectic		
ln	Logarithmic mean		
m	mean		
max.	Maximum		
min.	Minimum		
O ₂	Oxygen		
o	Outside		
PbO	Lead Oxide		
r	reference		
s	secondary side		
t	total		
c	coolant		
ss	steady state		
w	wall		

ABBREVIATIONS

ADS	Acceleration Driven System
ALEX	Argonne Liquid metal EXperiment (ALEX)
ALLF	Argonne Lead Loop Facility
ANL	Argonne National Laboratory
ASME	American Society for Mechanical Engineers
ATHENA	Advanced Thermal Energy Network Analysis
BARC	Bhabha Atomic Research Centre
CEA	Commisionarate Energie Atomique
CFD	Computational Fluid Dynamics
CHTR	Compact High Temperature Reactor
CHEOPE	CHEmistry and OPERations
CV	Control Valve
CIAE	China Institute of Atomic Energy
CIEMAT	Centro de Investigaciones Energéticas Medioambientales y Tecnológicas
CIRCE	CIRColazione Eutettico
COLONRI	COnvection LOop NRI
CORRIDA	CORROsion In Dynamic lead Alloys
CRIEPI	Central Research Institute of Electric Power Industry
DACS	Data Acquisition and Control System
DELTA	Development of Lead-alloy Technology and Applications
DEMO	DEMOstration
DYNAM	DYNAMic

EB	Electron Beam
EM	Electro Magnetic
EMF	Electro Motive Force
ENEA	Italian National Agency for New Technologies, Energy and Sustainable Economic Development
FBR	Fast Breeder Reactor
FBTR	Fast Breeder Test Reactor
FDS	Fusion Design Study
FZK	Forschungszentrum Küste
GIF	Generation IV International Forum
HELIOS	Heavy Eutectic Liquid Metal Loop for Integral test of Operability and Safety of PEACER Proliferation-resistant, Environment-friendly, Accident-tolerant, Continual and Economical Reactor
HTL	High Temperature Loop
HTR	High Temperature Reactor
HHHC	Horizontal Heater Horizontal Cooler
HHVC	Horizontal Heater Vertical Cooler
HTGR	High Temperature Gas cooled Reactor
HTR	High Temperature Reactor
ICE	Integral Circulation Experiments
IGCAR	Indira Gandhi Centre for Atomic Research
INL	Idaho National laboratory
IPPE	Institute of Physics and Power Engineering
IR	Infra Red
ITER	International Thermonuclear Experimental Reactor

JAERI	Japan Atomic Energy Research Institute
IAEA	Japan Atomic Energy Agency
JLBL	JAERI lead-bismuth loop for material corrosion
JNC	Japan Nuclear Cycle Development Institute (JNC)
KPAL	KAERI Pb-Alloy Loop
KTL	Kilo Temperature Loop
LANL	Los Alamos National Laboratory
LBE	Lead Bismuth Eutectic
LeBENC	Lead Bismuth Eutectic Natural Circulation Code
LECOR	LeadCORrosion
LFR	Lead-cooled Fast Reactor
LIFUS	Lithium for fusion
LIMITS	Liquid metal integrated test system
LiSoR	Liquid metal–solid metal reaction
LML	Liquid Metal Loop
LMFBR	Liquid Metal Fast Breeder Reactor
LPM	Litre Per Minute
MaPle	Magnetohydrodynamic PbLi Experiment
MDSNP	Modified Dynamic Simulator for Nuclear Power Plants
MESLOOP	Mitsui Engineering & Ship-building Co. Ltd Loop
MHD	Magneto Hydro Dynamics
NACIE	Natural Circulation Experiment
NASA	National Aeronautics Space Agency
NCL	Natural Circulation Loop
NEA	Nuclear Energy Agency

NFC	Nuclear Fuel Complex
NRV	Non Return Valve
OECD	Organisation for Economic Co-operation and Development
OEC-PNC	O-arai Engineering Center - Power Reactor and Nuclear Fuel Development Corporation
ORNL	Oak Ridge National Laboratory
OSHA	Occupational Safety and Health Administration
PEACER	Proliferation resistant Environment-friendly Accident-tolerant Continuable-energy Economical Reactor
PEL	Permissible Exposure Limit
PFBR	Prototype Fast Breeder Reactor
PHT	Primary Heat Transport
PLANDTL	Plant Dynamics Test Loop
PLC	Programmable Logic Controller
PRV	Pressure Regulating Valve
RELAP	Reactor Excursion and Leak Analysis Program
RIT	Royal Institute of Technology
SADHANA	Safety grade Decay Heat removal in Sodium
SAS	Safety Analysis code System
SBO	Station Black Out
SEM	Scanning Electron Microscopy
SFR	Sodium-cooled Fast Reactor
SGDHR	Safety Grade Decay Heat Removal
SNAP	Systems Nuclear Auxiliary Power
SS	Stainless Steel

SSTAR	Small, Sealed, Transportable, Autonomous Reactor
STAR-LM	Secure, Transportable, Autonomous Reactor-Liquid Metal variant
STELLA	Standard Technology Loop for Lead Alloy
TALL	Thermal-hydraulic ADS Lead-bismuth Loop
THEADES	Thermal-hydraulics and ADS Design
THESYS	Technology for Heavy Liquid Metals Systems
TIT	Tokyo Institute of Technology
TRISO	TRistructural ISOtropic
TZM	Titanium-Zirconium-Molybdenum alloy
UCLA	University of California at Los Angeles
UNIST	Ulsan National Institute of Science and Technology
UTK	University of Tennessee, Knoxville
UWISC	University of Wisconsin–Madison
VHHC	Vertical Heater Horizontal Cooler
VHVC	Vertical Heater Vertical Cooler
WHO	World Health Organisation
YSZ	Yttria Stabilised Zirconia

Chapter 1

INTRODUCTION

Renewed interest in nuclear reactor power plants in the wake of the concern for sustainable energy development and climate change, has led to the development of numerous designs and innovative concepts for nuclear reactors with a view to increase their economic competitiveness and to enhance safety. The main emphasis is to simplify the design of power plants by incorporating several passive features. New high temperature power plants are attractive for hydrogen generation and as a power pack for remote areas, where the current ability to generate electric power depends on costly shipments of fossil fuels. There are many evolving designs of nuclear reactors with different coolants other than water. Reactor designs based on heavy liquid metal as coolant have been envisaged by various countries as the source of high temperature heat for applications such as hydrogen production by thermochemical processes. Heavy liquid metal systems are excellent spallation targets for Accelerator Driven Systems (ADS). Liquid metal especially lead-lithium is also considered for the blanket in the International Thermonuclear Experimental Reactor (ITER). Natural circulation of liquid metal coolant is being considered as the normal core cooling mode in some advanced reactor designs including the Lead cooled Fast Reactors (LFR) being developed by some member countries of Generation IV International Forum, (GIF Annual Report, 2014) [1].

The design of the Compact High Temperature Reactor (CHTR) is in progress in BARC (Dulera and Sinha, 2006) [2]. CHTR is a ^{233}U -Thorium fuelled, Lead Bismuth Eutectic (LBE) cooled and beryllium oxide moderated reactor. This reactor is being developed to generate about 100 kW_{th} power, with refuelling interval of 15 years and several

advanced passive safety features to enable its operation as compact power pack in remote areas not connected to the electrical grid. The reactor is being designed to operate at about 1000°C , to demonstrate the technologies for high temperature reactor and the process heat applications such as hydrogen production by thermo-chemical processes.

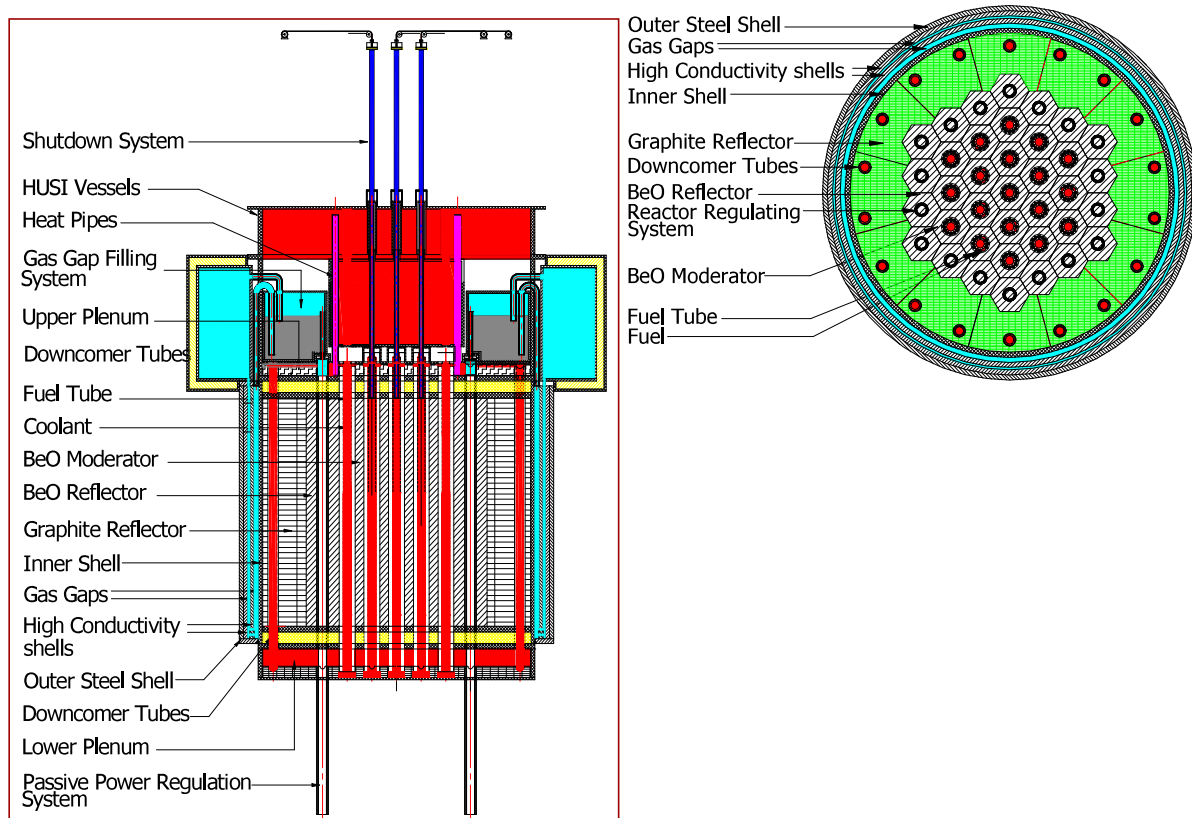


Fig 1.1 Schematic of CHTR

Fig. 1.1 shows the schematic of the reactor. The cross-sectional view of the reactor core is also shown. The reactor core consists of nineteen prismatic beryllium oxide (BeO) moderator blocks. These 19 blocks contain centrally located graphite fuel tubes. Each fuel tube has 12 equi-spaced longitudinal bores made in its wall, in which fuel compacts are inserted. The fuel tube also serves as coolant channel. The fuel is based on TRISO coated particle fuel. Eighteen blocks of beryllium oxide reflector surround the moderator blocks. Graphite reflector blocks surround these beryllium oxide reflector blocks. The fuel,

moderator and reflector blocks are contained in a reactor shell made of high temperature and liquid metal corrosion resistant material. Top plenum and bottom plenum are provided for primary coolant inlet and outlet of the core respectively. These plenums have flow guiding blocks, having passages for coolant flow. The reactor shell is surrounded by two gas gaps that act as insulators during normal reactor operation and reduce heat loss in the radial direction. There is an outer steel shell, surrounded by a large heat sink. This outer shell has fins to improve heat dissipation. During accidental conditions if the temperature of the core increases, the gaps will be filled with molten metal and the core heat is transferred to the heat sink by various modes of heat transfer. Table 1.1 gives the major parameter of the reactor.

The high boiling point (1670 °C) of LBE ensures that the coolant can be operated at high temperatures at atmospheric pressure without the risk of coolant boiling, which improves the thermal efficiency. It also improves the plant safety by reducing the risk of leakage at high temperatures as pressurization is not required. Also, LBE does not react readily with air or water and thus, an intermediate coolant is not essential in the reactor. The various desirable properties as a coolant make LBE the most suitable choice for CHTR. In order to design the reactor, it is necessary to study the thermal hydraulic behaviour of liquid LBE under various operating and accidental conditions.

1.1 NATURAL CIRCULATION

The natural circulation is an important safety phenomenon in nuclear reactor. During failure of pump or Station Black Out (SBO), the reactor core decay heat is removed through natural circulation of primary coolant. Some of the advanced reactors are designed for natural circulation even during normal operating conditions.

Table1.1: Major design and operating characteristics of CHTR

Attributes	Design Parameters
Reactor Power	100kW(th)
Core configuration	Vertical, prismatic block type
Fuel	$^{233}\text{UC}_2 + \text{ThC}_2$ based TRISO coated fuel particles shaped into fuel compacts with graphite matrix
Moderator	BeO
Reflector	BeO and Graphite
Coolant	Molten Pb-Bi eutectic alloy
Mode of core heat removal	Natural circulation
Coolant flow rate	6.7kg/sec
Coolant inlet/outlet temperature	900°C/ 1000°C
Primary coolant circuit height	1.4 m
Core dia/height	1.27m/1.0m

These reactors do not have any primary circulation pump, thereby eliminating the cost of the pump and its maintenance and associated events like pump failure. Natural circulation in a system depends on many parameters like, the system geometry, characteristics of heat addition and removal rate from the system, thermo-physical properties of the coolant and the system conditions like pressure and temperature. Another important parameter for natural circulation is the pressure drop. Since the driving head for this type of system is much less than the forced circulation system, the pressure drop in the system is to be accurately

calculated during the natural circulation. This pressure drop includes mainly frictional drop and local pressure drop due to flow area and direction change.

1.2 NATURAL CIRCULATION IN LIQUID METAL

As mentioned above, natural circulation depends on the thermo-physical properties of the liquid. For example liquid metal has higher thermal conductivity than water or air, which makes the heat transfer phenomena different from the common fluid. This may further affect the natural circulation behaviour of the liquid especially during transient conditions. The heat transfer coefficient and thermal conductivity of the liquid metal coolant affect the behaviour of the natural circulation. The studies on natural circulation of liquid metals are important for the design of liquid metal cooled reactors.. Except few conceptual designs, so far the liquid metal reactor systems with natural circulation cooling were not considered. So the experimental studies on liquid metal are also very few and not sufficient to understand the natural circulation behaviour of the coolant especially at high temperature and low flow rate.

1.3 MOTIVATION AND PROBLEM STATEMENT

The design of the CHTR needs detailed knowledge of the behaviour of the LBE as coolant during normal operation as well as accidental scenarios. Effective cooling of the reactor core by natural circulation of the coolant at all scenarios is important requirement for the reactor design. The sudden temperature rise of the coolant in any part of the reactor primary system may cause thermal stresses in the refractory material components of the core. The reactor is to be started from low temperature (200 °C) and slowly the temperature is to be raised in steps by nuclear heating to the operating temperature (1000 °C). So, natural circulation behaviour of the coolant is required to be understood for entire temperature range, before the design of the reactor. Establishing a full scale experimental facility to study the

thermal hydraulic behaviour at operating conditions of the reactor is difficult and an expensive option. Theoretical analysis on the behaviour of the reactor, by well validated computer code, is the effective solution. But validation of the code with the experimental data is important before using them.

In natural circulation the driving force is the buoyancy head developed due to the density difference caused by heating in the core and cooling in the primary heat exchanger. The flow of the coolant depends on the relative vertical positions of the core and the heat exchanger. Moreover, the geometry of the primary heat transport system plays an important role on the coolant flow rate. Grashof number is an important parameter to characterise a natural circulation system. In CHTR the range of modified Grashof number, Gr_m (as defined by Vijayan, 2002 [3]), which is a measure of buoyancy force in natural convection, is in the range of 10^{11} to 10^{13} . The inventory of the coolant in the PHT circuit plays a great role on the natural circulation especially during transient conditions. So specific experiments are required to study the behaviour of the coolant in a particular reactor design.

There were several liquid metal experimental facilities made during last sixty years. Detailed literature review was required to evaluate the experimental studies carried out so far. Accordingly, a detailed literature survey was carried out for different liquid metal coolant experimental studies. It was found that though there were many experimental facilities with operating temperature ranging from 200 to 1450 °C, a very few facilities were made for natural circulation studies. Moreover there was no facility which studies natural circulation in the operating range of CHTR. In fact, no facility was found where natural circulation studies were carried out beyond 550°C. So there was a need to generate the experimental data in the flow and temperature range of CHTR. Moreover without a computer code to handle liquid metal natural circulation, it is not possible to design reactor systems. A code is to be developed to simulate various aspects of liquid metal systems, like heat loss through the

pipings, axial conduction of the fluid, temperature dependent thermo physical properties of different high temperature fluids etc. In addition to make it generic, it should also be capable of simulating non-uniform diameter loops and different type of heat sources as well as sink with different orientations. The code has to be extensively validated with experimental data.

1.4 OBJECTIVES OF THIS WORK

1.4.1 Investigation of Steady State and Transient Behaviour of Natural Circulation of LBE in the Operating Range of CHTR

As discussed above, the experimental data for the operating range of CHTR was not available. Experimental facilities are essential for the natural circulation studies for CHTR. Since the technologies for molten lead bismuth eutectic are not available readily, those are to be developed for successful operation of the loops. Natural circulation data were to be generated for Gr_m range from 10^{11} to 10^{13} and the temperature range from 200 to 1000°C.

1.4.2. Development of Computer Code for LBE Natural Circulation Studies and its Validation.

A computer code was to be developed for theoretical studies on natural circulation of LBE in closed loops. The code can handle various aspects related to high temperature natural circulation LBE loop, like (a) non-uniform diameter loops, (b) different working fluid in primary and secondary side of the loop, (c) trace heating and surface heat loss from the walls to ambient and (d) axial conduction through liquid metal and the pipe wall. (e) various orientations of heated section and heat exchanger, etc. The code was required to be validated with both steady state and transient natural circulation experimental results from the LBE loops.

1.4.3 Parametric Influence on the LBE Natural Circulation

The various parameters like heat loss in the piping, thermo physical properties of the fluid, heat transfer coefficients, etc. may affect natural circulation of LBE in the CHTR operating range. Hence, it was essential to study the parametric effects on both steady state and transient natural circulations, using the computer code.

1.5 ORGANISATION OF THE THESIS

Chapter 2 presents a comprehensive literature review of the experimental studies using liquid metal test facilities. The objectives of each of the facility, materials of constructions, operating range, etc., are summarised. In the review 39 liquid metal loops were found which were operating up to 550°C and 21 loops were found to be operating beyond 550°C. The facilities, where natural circulation of liquid metal was studied, are briefed separately. The computer codes which are being used for liquid metal related studies are also reviewed and briefed in this chapter. The thermal hydraulics in liquid metals especially heat transfer studies are reviewed. The different parameters that may affect the natural circulation in liquid metal natural circulation at high temperatures are discussed in light of the work carried out by other researchers.

Chapter 3 gives the details of the Liquid Metal Loop (LML), its fabrication, installation, commissioning and experiments performed. The instrumentation developed and the experiences gained during the operation were briefed. A number of steady state and transient natural circulation experiments were carried out for different power levels with air and water as the secondary fluids. The steady state experiments were carried out for the power range from 900 W to 5000 W. In transient studies different postulated events were simulated in the loop and the results obtained are discussed in detail.

Chapter 4 describes the details of the Kilo Temperature Loop which was designed to operate at 1000 °C. After the literature survey it was found that Nb and Mo based refractory alloys can be used as the loop material for high temperature experiments. The in-house development of the loop is described in detail. As the Nb-alloy picks up the oxygen present in the ambient air at higher temperature and gets oxidized quickly, the main Nb-alloy loop was kept in an inert gas enclosure equipped with an oxygen scavenging system. The design and development of the inert gas circulation system was described in the chapter. The loop was operated up to 1100 °C and natural circulation studies were carried out. Natural circulation data of LBE could be generated in the temperature range of (bulk coolant temperature) 200-780 °C and power level range 200 W to 1200 W. The natural circulation correlations available in literature are compared with experimental results of the various liquid metal loops including experimental data obtained from LML and KTL.

Chapter 5 gives details of the evaluation of the heat transfer coefficients for liquid LBE during different operating conditions. During experiments when the flow rate of LBE varies with time, different modes of convective heat transfer were envisaged during the experiments, especially in the heater section. When the loop was started with stagnant LBE in the loop, the LBE in the heater section will experience free convection near the heater surface. The free convection will initiate the LBE flow in the loop slowly. As the bulk flow of LBE in the loop starts, free convection will change to mixed convection in the heater section. When the bulk flow through the heater slowly dominates over the local free convection in the heater section the flow become forced convection type and may become turbulent if the flow rate is high. The heat transfer coefficient will also vary with the flow rate. The correlations for LBE heat transfer coefficients in free convection and mixed convection flow regimes were evaluated with the help of CFD analysis. For forced convection turbulent regime the existing correlations were assessed by comparing with

experimental results available in literature and also from CFD analysis. From the analysis, the heat transfer correlations for different flow range were defined so that those can be used for the theoretical calculations on natural circulation flow rate.

Chapter 6 describes the development of a computer code LeBENC (Lead Bismuth Eutectic Natural Circulation) and its validation. LeBENC is an one dimensional finite difference code, developed to study the steady state and transient behaviour of liquid metal natural circulation in closed loop. The 1-D momentum and energy equations were solved in the code. In the formulation of the governing equations for the fluid, incompressible flow was considered and Boussinesq approximation was assumed to be valid. The fluid axial conduction was considered in the energy equation as it might play an important role in LBE loop. To account for the thermal conduction and energy stored in the pipe wall, separate conduction equation was solved in the code. The results obtained from the theoretical analysis have been compared with the steady state and transient experimental results of LML and KTL.

Chapter 7 describes the parametric studies of various factors like axial conduction, heat loss through piping, surface roughness on the natural circulation of LBE. After the validation of the LeBENC code, it was used to study the natural circulation by changing the parameters like thermal conductivity of the fluid, surface roughness factor and heat loss to the ambient from the piping. The results obtained are discussed in detail.

Chapter 8 presents the summary of the work both experimental and theoretical studies. The important findings from the work are prescribed. The future work needed in this topic was also discussed.

1.6 CLOSURE

In this chapter the brief description of the Compact High Temperature Reactor (CHTR), a LBE natural circulation cooled reactor being designed in BARC, is given. Motivation of the present work was to study natural circulation at the operating range of CHTR. The problem involves both experimental and theoretical work related to LBE natural circulation in the operating range of CHTR. Two experimental loops, Liquid Metal Loop (LML) which operates with maximum temperature 500°C and Kilo Temperature Loop (KTL) with maximum working temperature 1100°C were made for natural circulation studies with LBE at specified operating ranges. Natural circulation experimental data for LBE were generated for temperature range 200-780 °C for the first time. As there was no in house computer code available to study the natural circulation behaviour of LBE, a code was proposed to be developed and validated for theoretical analysis. This code was then used to study the effect of various factors affecting the natural circulation of LBE at high temperature.

Chapter 2

LITERATURE REVIEW

The experimental studies on liquid metal requires specific knowledge, because of its high melting point and other thermo-physical properties, which are different from conventional fluids like air and water. There are limited knowledge on liquid metal thermal hydraulics especially on lead-bismuth eutectic. So extensive literature survey is required before starting the work on liquid metal thermal hydraulics.

In the literature survey, different liquid metals which are being used as the nuclear reactor coolants were reviewed. Different kinds of reactor were also reviewed which are cooled by liquid metals. Since liquid metal systems are different from water based nuclear reactor systems, extensive review was essential before handling liquid metal and designing the systems. The different aspects of the Lead Bismuth Eutectic (LBE) alloy were reviewed in detail. After that the different liquid metal experimental facilities were reviewed on their objectives, operating conditions and the main design features. The experimental facilities where the natural circulation studies had been carried out were studied in more detail. The theoretical codes available for liquid metal thermal hydraulics were also reviewed. The different factors which are to be considered for theoretical analysis on liquid metal natural circulation range were studied. The following sections give the details of the literature review.

2.1 LIQUID METAL AS COOLANT

The use of liquid metal as nuclear reactor coolant has originated from the inception of the nuclear reactor systems. Clamentine was the first reactor to be operated in 1943 using

mercury as the coolant [4]. The various liquid metals considered for reactor coolant are briefed in Table 2.1. It could be seen that the boiling point of LBE is much more than the operating temperature of CHTR. Hence unlike water cooled reactors, CHTR can be operated at atmospheric pressure even at high temperature ($\sim 1000^\circ\text{C}$). The high thermal conductivity ensures excellent heat transfer even at low flow rate. The specific heat of LBE is 25 times less than water; however, ρC_p is only 4 times less than the water.

Table 2.1 Thermo physical properties of different liquid metal coolants

Coolant	T_m/T_{bp} at 1 atm. (K)	ρ (kg/m^3)	μ Pa-s/m (10^{-4})	K W/mK	C_p J/kgK	B (K^{-1}) (10^{-4})	Prandtl number	Cost (Rs/kg)
Water (at 333K)	273/373	983.0	4.66	0.65	4185.0	2.14	3.00	-
Lead Bismuth*	396.5/1943	10169.5	14.51	13.37	146.0	1.30	0.0158	1500
Lead*	600.5/2022	10531.0	20.95	16.21	147.6	1.13	0.0191	200
Sodium*	370.72/1156	849.5	2.64	71.10	1280.0	2.77	0.0048	1400
Pb-Li*	508/1983	9272.6	13.82	15.60	201.38	1.81	0.0178	220
Li*	452/1590	493.3	3.63	51.19	4249.1	0.944	0.0301	700
Mercury (at 523K)	234.2/629.7	13028.0	10.00	13.05	136.0	1.79	0.0104	150
NaK*	262/1058	1129.18	2.26	26.00	395.49	2.82	0.0034	15000

*Properties at 700K

The Prandtl number of all the liquid metals is much lower than water. This implies that the thermal conduction has major contribution in heat transfer in liquid metal compared to that of water. Various merits and demerits of liquid metals used as the nuclear coolants are also listed in Table 2.2.

Table 2.2 Liquid metal coolants its use and its merits and demerits

Sl No	Liquid metal Coolants	Use in reactors	Advantages	Disadvantages
1	Mercury	Clamentine	<ul style="list-style-type: none"> Low melting point Good thermal properties 	<ul style="list-style-type: none"> low boiling point High toxicity High neutron absorption cross section
2	Lithium	Space reactors	<ul style="list-style-type: none"> Lowest density liquid metal, Highest specific heat, High vapour pressure 	<ul style="list-style-type: none"> high melting point, high corrosion activity, Reactive with air and water
3	Sodium	Fast Breeder Reactors	<ul style="list-style-type: none"> Good thermo-physical properties. Good neutronic properties, Less corrosive to structural metals. 	<ul style="list-style-type: none"> High Chemical activity with air and water Radioactivity due to Na-24 and N-22,
4	Nak	Space reactors	<ul style="list-style-type: none"> Very low melting point (-12.3°C), 	<ul style="list-style-type: none"> High vapour pressure of the eutectic mixture More reactive to air and water.
5	Lead	BREST reactor	<ul style="list-style-type: none"> Excellent neutronic properties, Good shielding against gamma rays Inert to air and water 	<ul style="list-style-type: none"> Requires higher pumping power. Corrosive to nickel based high temperature alloys.
6	Lead Bismuth Eutectic (Pb-45.5%-Bi 55.5%)	SVBR, alpha class Submarines reactor	<ul style="list-style-type: none"> Lower melting points Excellent neutronic properties, Inert to air and water 	<ul style="list-style-type: none"> Highly corrosive nature of bismuth limits structural metal at high temperature. Po-210 and its activity is most troublesome.
7	Lead Lithium (Pb-83%, Li-17%)	Fusion reactors for cooling and tritium breeding	Excellent choice in Fusion reactor application because it is the good source of tritium as well as good cooling media.	<ul style="list-style-type: none"> Lithium is highly corrosive. The tritium management is critical

2.2 LIQUID METAL COOLED REACTORS

Liquid metal cooled reactors are under development for last sixty years. As per IAEA Tecdoc-1531 (2006) [5] the fast reactors are divided into three categories, 1) Experimental Fast reactors, 2) Demonstration or Prototype Fast Reactors, 4) Commercial Size Reactors. The review of the liquid metal fast reactors was carried out from the inception to the present day design. The concepts of future reactors were also reviewed. Here two designs of liquid metal cooled reactor are briefed.

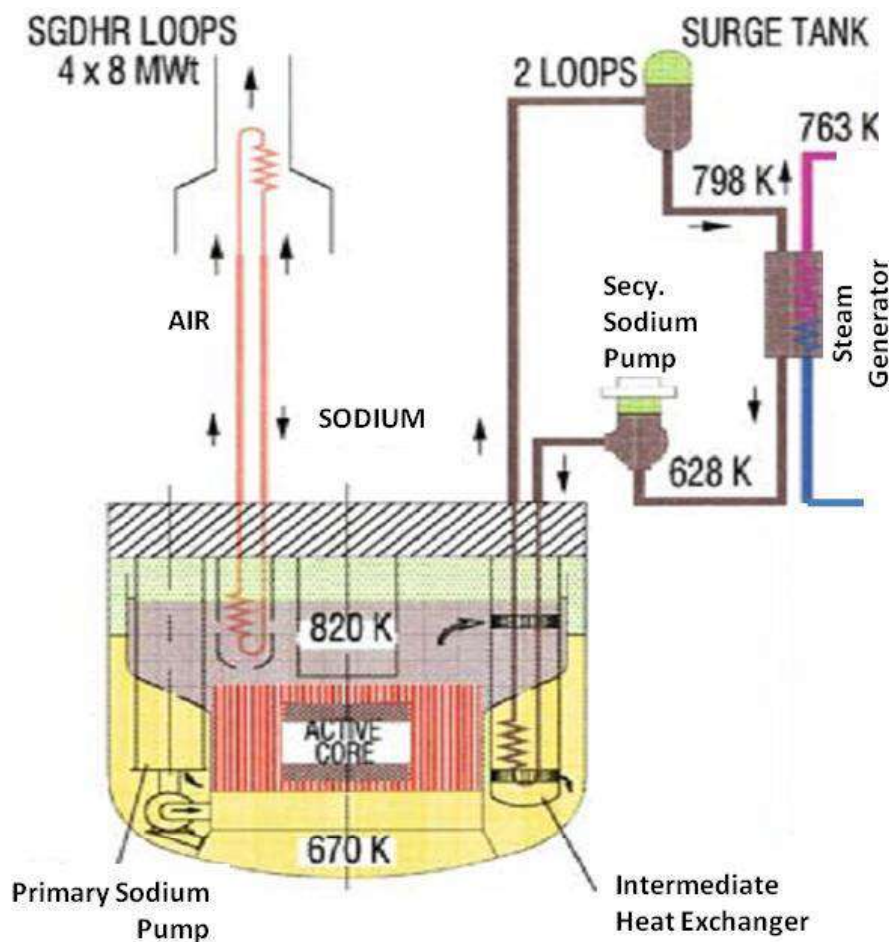


Fig 2.1 Flow sheet of PFBR [6]

Figure 2.1 shows a flow sheet of Prototype Fast Breeder Reactor (PFBR) being built in India. The reactor is a pool type and sodium is used as the coolant in the primary and

secondary circuit. The primary heat exchangers and primary sodium pumps are submerged in the sodium pool. During normal operation the core heat is removed by the forced flow of the sodium coolant. In order to improve safety, a Safety Grade Decay Heat Removal System (SGDHR) is incorporated to remove the decay heat to atmosphere passively by natural circulation of sodium. Another reactor design, Small Secure Transportable Autonomous Reactor (SSTAR) reactor is shown in Fig 2.2, which is a molten lead natural circulation cooled reactor. The secondary system is supercritical CO₂ cycle and the intermediate heat exchanger is directly submerged in the molten lead. This type of natural circulation cooled system offers simple design of the reactor with high thermal efficiency.

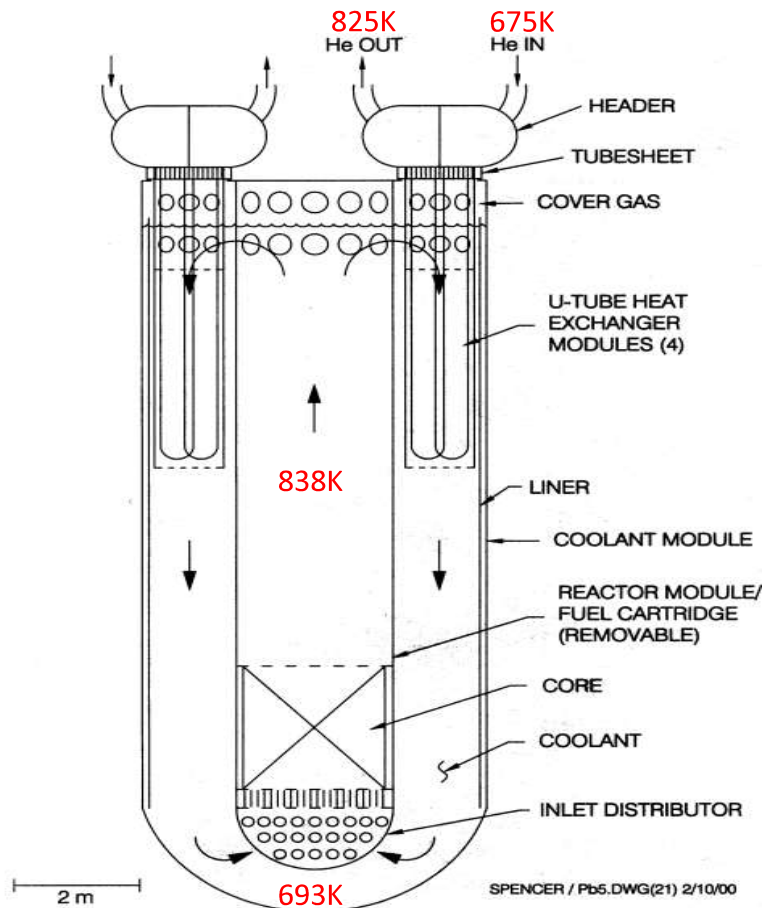


Fig 2.2 Schematic of natural circulation flow path in SSTAR [7]

A total of 40 more designs have been reviewed, which are already operated or under advanced design stage. It was found that most of the reactors are Na cooled and reactors with

wide range of power were made and maximum operating temperature was limited to 550°C. The new concepts of liquid metal reactor systems were also reviewed and it was found that most of the design was lead/lead bismuth alloy cooled. Total 21 concept designs were found and the maximum operating temperature of the reactor was below 600°C, except CHTR. The primary geometry is mainly pool type configuration which may give the advantages like large thermal inertia and lower possibility of leakage. Three concepts were found, which are designed for natural circulation cooling during normal operating conditions. Most of the other designs depend on the natural circulation of the coolant for passive decay heat removal during any accidental conditions. So the natural circulation has become important for both normal operating conditions and accidental conditions.

2.3 NATURAL CIRCULATION

There are number of application of natural circulation in engineering. The application includes, nuclear reactor core cooling, transformer cooling, solar water heaters, gas turbine blade cooling, geothermal power extraction, computer cooling, etc. One of the applications of the natural circulation, for different type of fluids, is corrosion studies in low velocity flow. The literature review is limited on the single phase liquid metal natural circulation considering the present work. There are number of studies on single phase water natural circulation. The general reviews on single-phase NCLs can be found in Zvirin (1981) [8], Mertol and Greif (1985) [9], Greif (1988) [10] and Vijayan (2001) [11]. The basic requirement of understanding steady state and stability behaviour of natural circulation is the availability of generalised dimensionless groups which are not loop specific. These dimensionless groups facilitate the comparison of the behaviour of different loops and extend the data from experimental loops to the prototype. Considerable work have been carried out on this by Welander (1967) [12], Creveling et al. (1975) [13], Chen (1983) [14], Bau and

Torrance (1981) [15], Huang and Zelaya (1988) [16], Vijayan et al. (1992) [17]. This study was extended for non-uniform diameter loops by Vijayan (2002) [3]. For steady state natural circulation, he showed that the flow in single phase uniform or non-uniform diameter natural circulation loops can be expressed as,

$$\text{Re}_{ss} = c \left(\frac{Gr_m}{N_G} \right)^p \quad (2.1)$$

$$\text{Where, } \text{Re}_{ss} = \frac{D_r W_{ss}}{A_r \mu}, \quad D_r = \frac{1}{L_t} \sum_{i=1}^N D_i L_i, \quad A_r = \frac{1}{L_t} \sum_{i=1}^N A_i L_i, \quad L_t = \sum_{i=1}^N L_i, \quad Gr_m = \frac{D_r^3 \rho_o^2 \beta g Q_h \Delta Z_c}{A_r \mu^3 C_p}$$

Equation (2.1) defines the steady state flow rate in a closed loop with defined geometry and heater power. Gr_m is the modified Grashof number and is a measure of natural circulation driving force.

N_G is a geometric parameter of the loop and defined as,

$$N_G = \frac{L_t}{D_r} \sum_{i=1}^N \left(\frac{\bar{L}_{eff}}{\bar{D}^{1+b} \bar{A}^{2-b}} \right)_i \quad (2.2)$$

$$\text{Where, } (\bar{L}_{eff})_i = \frac{(L_{eff})_i}{L_t}, \quad (L_{eff})_i = L_{ei} + L_i, \quad k_i = \frac{f_i L_{ei}}{D_r}, \quad \bar{A}_i = \frac{A_i}{A_r}, \quad \bar{D}_i = \frac{D_i}{D_r}, \quad \bar{L}_i = \frac{L_i}{H},$$

$$c = \left(\frac{2}{a} \right)^{1/(3-b)} \quad \text{and} \quad p = 1/(3-b)$$

For laminar flow, $a=64$ and $b=1$. For turbulent flow, $a=0.316$ and $b=0.25$, if Blassius friction factor correlation is used. L_{ei} is the equivalent length to absorb the local loss coefficient k_i . The coefficients of the Eq (2.1), i.e. ‘c’ and ‘p’ were modified by different authors based on

their experimental and theoretical analysis. The studies by Pilkhwal et al. (2007) [18], Swapnalee et al. (2011) [19], Kumar et al. (2011) [20] are few of the examples of this type of work.

Stability analysis is one of the most important part of the transient studies in a natural circulation loop. Zivirin (1981) [8] pointed out that there are three type of instabilities associated with natural circulation loops, (a) stability of the rest state, which may occur due to heating in the horizontal leg in stagnation conditions, local boiling in the loop or very low temperature difference across the heater section. (b) Metastable equilibrium with multiple steady states, which was seen especially in loops with parallel vertical channels ([21], [22] [17]). (c) Small-amplitude oscillations that grow and may lead to flow reversals, which was first shown analytically by Welander (1967) [12] and experimentally observed by many researchers ([13], [23], [24], [25]). It was observed that the instabilities may occur in any of the orientation, Horizontal Heater Horizontal Cooler (HHHC), Horizontal Heater Vertical Cooler (HHVC), Vertical Heater Horizontal Cooler (VHHHC) and Vertical Heater Vertical Cooler (VHVC). The HHHC position was found to be most unstable but instability were also found in the other orientations [25]. The best way to represent the conditions or parameters which affect the instability was the generation of stability map. It clearly defines the stable conditions for a particular system where the stable natural circulation exists.

Proper scaling philosophy was required to design experimental facility where the natural circulation behaviour of the medium was to be simulated as in the prototype. Vijayan and Austregesilo (1994) [26] used the power-to-volume scaling laws for the design of a scaled test facility simulating the primary heat transport system of nuclear power plants, which results in loops of the same elevation with reduced diameters. They checked adequacy of the scaling laws for simulating single phase natural circulation by testing in three rectangular loops, each having same elevation but different diameters. The experiments

showed that the power-to-volume scaling principle adequately describe the steady state behaviour. But the transient and the stability behaviours were found to be significantly affected by the loop diameter and modified Stanton number. So the stability map generated in the scaled experimental facility may not be applicable to nuclear power plant.

2.4 LIQUID METAL LOOPS FOR NATURAL CIRCULATION STUDIES

There is lot of interest in natural circulation flow of LBE in various nuclear reactor systems but very few experimental studies have been carried out so far. Takahashi et al. (2005a) [27] have carried out experimental studies in LBE-water two-phase loop. Single phase natural circulation studies were carried out before LBE-water two phase boiling experiments [28] . The loop consists of a heater section where an immersion heater with four rod bundle was used. Single phase LBE experiment was carried out up to 304°C with maximum power of 7.7kW. The LBE flow rate was found to be increasing with increase in power. The LBE flow rate was found to be steady when the power was constant.

Another experimental study was carried out by Ma et al. (2007) [29] in TALL facility with forced flow and natural circulation of LBE for ADS systems. The studies carried out in the natural circulation experiments are, (a) start-up of natural circulation at different operating conditions, (b) stability of natural circulation (c) effect of influencing parameters: loop power, secondary side flow and flow resistance; (d) the capability of natural circulation. In the start-up experiments it was found that the flow rate picks up quickly from stagnant condition but takes considerable time to stabilise at certain power. The natural circulation flow was found to be stable and the direction was forward when the loop was started from the stagnant condition. To observe the stability of the natural circulation, the flow of LBE was reversed with the help of an EM pump. When the pump was stopped and the natural circulation flow was continued, it was found that the flow remained in reversed direction.

Coccoluto et al. (2011) [30] carried out experimental studies in a LBE loop, NACIE (Natural Circulation Experiment) to characterize the natural and gas enhanced circulation flow regimes and to qualify components for heavy liquid metal applications. The study was carried out in support of the Integral Circulation Experiments (ICE) in CIRCE facility. The fuel rod cluster simulators were tested at different power to see the performance of the fuel simulators during natural circulation. Both high heat flux bundle and low heat flux bundle were tested. Recently natural and mixed convection studies were carried out in the loop with a wire spaced 19 rod fuel simulator rod bundle in the range of sub channel Reynolds number 1000 to 10,000 [31]. The local Nusselt numbers in the sub channels were calculated and compared with the experimental results. Cho et al. (2011) [32] carried out benchmarking exercise on thermal hydraulics of LBE in HELIOS (Heavy Eutectic Liquid Metal Loop for Integral test of Operability and Safety of PEACER). PEACER (Proliferation resistant Environment-friendly Accident-tolerant Continuable-energy Economical Reactor) is a LBE cooled transmutation reactor being developed in the Republic of Korea.

Agostini et al. (2002) [33] carried out natural circulation experimental studies in CHEOPE-III loop with LBE as coolant. The decrease in flow in the loop after a pump shutdown and reaching steady state condition of natural circulation with a heater power was one of the main studies in the loop. Kang et al. (2013) [34] carried out steady state natural circulation experiments in a loop with molten gallium. Steady state natural circulation tests were carried out for different power of the loop. Padmakumar et al. (2013) [35] studied the natural circulation in a sodium loop SADHANA, to assess the passive decay heat removal capability of the Safety Grade Decay Heat Removal (SGDHR) System. The loop was a natural circulation system which removes heat from a constant temperature sodium pool and rejects to atmosphere through an air heat exchanger. The experiments in SADHANA proved

that the performance of SGDHR of the reactor was sufficient to remove the decay heat after shut down.

The details of each of the liquid metal loops discussed above were studied and the values of Gr_m and Re_{ss} as defined in Eq (2.1) were found for different power levels. Table 2.3 shows the operating parameters of the liquid metal loops along with the calculated parameters of the CHTR. It can be seen that except gallium loop the range of Gr_m is higher than that of the CHTR.

Limited steady state natural circulation experimental data of the Gallium loop is available which is not sufficient for the design study of CHTR. The operating temperature of the loops was also much lower than the CHTR. There was no steady state and transient natural circulation experimental data of LBE , which can be used for the thermal hydraulic design of the CHTR. Experimental data were to be generated for LBE natural circulation at the operating range of CHTR. For that, experimental facilities were to be made.

2.5 THEORETICAL STUDIES IN LIQUID METAL LOOPS

In the studies of natural circulation of LBE in TALL loop [36], the experiments were simulated using TRAC/AAA and RELAP5 codes and the numerical results were compared the experimental results. The results of the steady state and transient simulation analysis were in good conformity with the experimental results. Wu and Sienichi (2003) [37] carried out 1D linear stability analysis for a uniform diameter rectangular natural circulation LBE loop, Argonne Lead Loop Facility (ALLF). The Nyquist criterion and a root search method were employed to find the linear stability boundary of both forward and backward circulations. Lumped minor loss coefficient was used for the uniform diameter loop. It was found that single phase LBE could be unstable in a high Reynolds number region. Any increase in loop

friction makes the forward circulation more stable, but the backward flow unstable with same heating/cooling conditions.

Table 2.3 Operating conditions of CHTR and different liquid metal loops reported in literature.

Reactor/ Facility	Modified Grashof number, Gr_m	Max. $T_{Coolant}$ ($^{\circ}C$)	Coolant	Re_{ss}	Uniform/Non-uniform diameter
CHTR [2]	10^{12} - 10^{13}	1000	LBE	1000-2300	Non-uniform
SADHANA [35]	10^{16} - 10^{17}	550	Sodium	>10000	Non-uniform
LBE loop [28]	10^{13} - 5×10^{13}	450	LBE	2000-4000	Non-uniform
TALL [29]	7×10^{13} - 5×10^{14}	475	LBE	4000-10000	Non-uniform
NACIE [30]	1.3×10^{15} - 2×10^{15}	450	LBE	>10000	Non-uniform
Gallium [34]	5.0×10^{11} - 1.0×10^{12}	350	Gallium	2500-4000	Uniform

The pre-test analysis was carried out on the NACIE loop [38] using RELAP 5 and coupled analysis using FLUENT-RELAP 5 code. The analysis gave a good insight of the heat transfer in the heater bundle of the loop during natural circulation of LBE. The results of the coupled analysis results were found to be in good agreement at low flow rate. Agostini et al. (2002) [33] carried out pre-test and post-test analysis of the CHEOPE-III loop. The pre-test analysis helped to make the operating procedure of the loop. The post-test analysis was carried out to assess the capability of the RELAP 5/Mod3.2 code to simulate the steady state and transient experiments in the LBE loop. Kang et al. (2013) [34] carried out CFD analysis to simulate steady state natural circulation experiments in a loop with molten gallium. The loop was modelled as a rectangular in shape with uniform diameter and the steady state flow rate and temperature distribution in the loop were predicted at different power levels. The

results were compared with the experimental results. Though the heat loss through the piping was ~12%, its effect on the natural circulation flow rate was not studied.

Sabharwall et al. (2012) [39] studied the effect of axial conduction on natural circulation in liquid metal systems and found that for Reynolds number beyond 3.0×10^3 , the effect of axial conduction was negligible. This was derived from the fact that for Peclet number < 1 only the axial conduction has effect on the axial temperature distribution. It was commented that the effect of axial conduction might have influence on the stability in some set of loop geometries, especially preventing flow reversal during unstable behaviour of the loop. A literature survey was carried out for use of different codes for liquid metal system analysis. Table 2.4 gives the summary of the review.

Table 2.4 Summary of computer codes used for liquid metal systems

Sl No	Code	Country/Institute	Features	Example of use in Liquid metal systems	References of the users
1	TRACE	USA/NRC	System code for reactor safety analysis	Natural circulation in LBE loops	Batra, 2013) [40], Shao (2011) [41] and Ma et al., (2006) [36]
2	CATHARE	France/CEA	System code for reactor thermal hydraulics	Sodium reactor System thermal hydraulics	Tenchine et al. (2013) [42]
3	CFX	USA/ANSYS	General purpose CFD code	SFR design and analysis, 3D CFD analysis of various liquid metal loops.	Velushamy et al. (2013) [43], Naphade et al. (2013) [44], Tarantino et al., (2008) [45] and Cho et al.(2011) [32].
4	FLUENT	USA/ANSYS			
5	PHOENICS	UK/CHAM			
6	TRIO-U	France/CEA	CFD code for nuclear thermal hydraulics	SFR design and analysis	Tenchine et al. (2012) [46] and Vasile (2012) [47]
7	MASKA-LM	Russia/IPPE	2-D code for lead cooled reactor thermal hydraulics and	System analysis of BREST type of reactor	Kumayev et al.(2005) [48]

			mass transport analysis		
8	SAS-4A	USA/ANL	Detail thermal hydraulic code for reactor analysis	Accelerator driven system dynamics	Cheng et al. (2004) [49]
9	ATHENA	USA/INL	System code for reactor safety analysis	Pool type LBE cooled reactor design analysis	Davis (2003) [50]
10	DEMO	USA/Westing-house Ltd	Thermal hydraulics of pool type Fast reactor	LMFBR reactor thermal hydraulics	Albright and Bari (1978), [51]
11	NATDEM O	USA/ANL	Code for thermal hydraulic system dynamics of Fast reactor systems	Transient thermal hydraulic analysis of LMFBR	Mohr and Feldman (1981) [52]
12	DYNAM	India/IGCAR	Code for thermal hydraulics of fast reactor core	System dynamics studies of FBTR core.	Vaidyanathan et al. (2010), [53]
13	MELANI	USA/-	Thermal hydraulics of molten metal in reactor pool.	Decay heat removal by natural circulation in the reactor pool.	Durham (1976), [54]
14	MDSNP	USA/California Univ.	Thermal hydraulics of molten metal in reactor pool.	Decay heat removal by natural circulation in the reactor pool.	Hung and Dhir, (1990), [55]
15	SIMMER	Japan/JNC, Germany/FZK, France/CEA	2D thermal hydraulics code for reactor safety analysis.	Fast severe reactor accident analysis.	Yamano et al. (2009), [56]
16	THYC-2D	India/IGCAR	2D thermal hydraulic code for liquid metal thermal hydraulics.	Natural convection in an enclosure of PFBR	Rajakumar et al. (1987), [57]
17	THYC-3D	India/IGCAR	3D thermal hydraulic code for liquid metal thermal hydraulics.	Flow analysis in sodium pool and piping of FBR	Kumar (1990), [58]

Thus, it is seen from Table 2.4 that system codes like TRACE and CATHARE were used for the natural circulation analysis. These codes can handle non uniform diameter loops also. The codes are still being validated with experimental results.

Analytical methods were also used to study natural circulation in LBE loops. But these were limited to the uniform diameter loops. The minor loss coefficients in different parts of the loop were lumped into one. This formulation limits the study of the local phenomena like temperature variation in the joint of two pipes with different diameters. The application of CFD codes is still limited to the simulation of steady state natural circulation in LBE. The transient analysis of LBE loop using CFD code was not found. System level codes are essential and more convenient for the theoretical analysis of natural circulation in a loop. But since there was no system code available for LBE application with the author, a code was to be developed which will include all aspects of LBE natural circulation at high temperature.

2.6 LITERATURE REVIEW CARRIED OUT FOR CONSTRUCTION OF THE LEAD BISMUTH FACILITIES

Due to the lack of previous knowledge and experience on lead bismuth systems, an extensive literature survey was to be carried out before making a LBE loop. Accordingly the literature review was done which encompass the following,

1. Lead bismuth eutectic material, its properties and handling issues,
2. Experimental facilities of liquid metals to review its instrumentation, different essential components and its design, material of constructions, etc.
3. Thermal hydraulic parameters affecting the natural circulation of LBE at high temperature and the formulations of each one.

The following sections give the details of the review,

2.6.1 Attributes of Lead Bismuth Eutectic (LBE)

As discussed above LBE is one of the potential high temperature coolants and it has been successfully used in nuclear submarine reactors in Russia. There are recent interests in the studies of heavy liquid metal for innovative reactor design. However the experience base with lead alloy reactor is less robust than sodium cooled system. In India, there was no LBE experimental facilities built for thermal hydraulic studies, so literature review were carried out for the required fields of LBE to make experimental facilities and the findings are briefed below,

2.6.1.1 Thermo physical properties of LBE

As shown in Table 2.1 the density of LBE is high and similar to lead coolant. The lower specific heat of the coolant makes it cool quickly in the pipe line. So care has to be taken to reduce heat loss in the piping. The viscosity is similar to water and it is a Newtonian fluid. The isothermal pressure drop correlations developed for water is applicable to LBE also [59]. Figure 2.3 (a) to Figure 2.3 (d) show the variation of different properties of LBE with temperature. The temperature variable correlations for the data are plotted up to 1300 K.

It can be seen that there are considerable variation of properties of LBE in the temperature range of 500 to 1250 K. The thermal conductivity increases by 100% and the viscosity decreases by 62.5%. The study on the effect of these variations on natural circulation is important for high temperature reactor design. The volumetric thermal expansion coefficient has been calculated and plotted. Figure 2.3 (e) shows the variation and it can be seen that the thermal expansion coefficient increases with temperature.

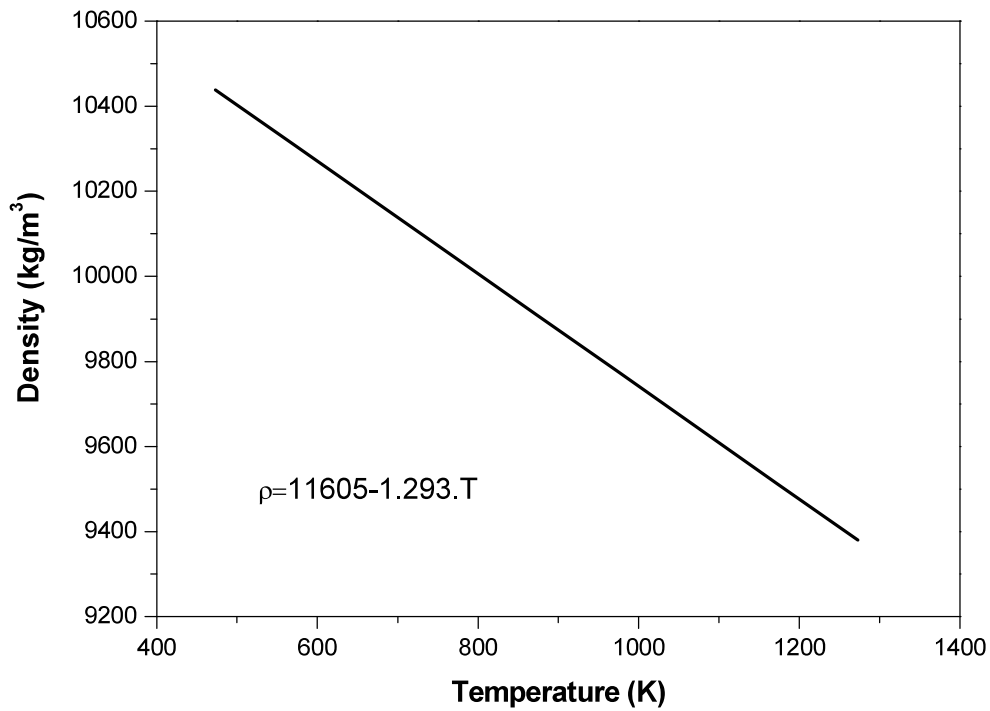


Fig 2.3 (a) Variation of density of lead bismuth eutectic with temperature

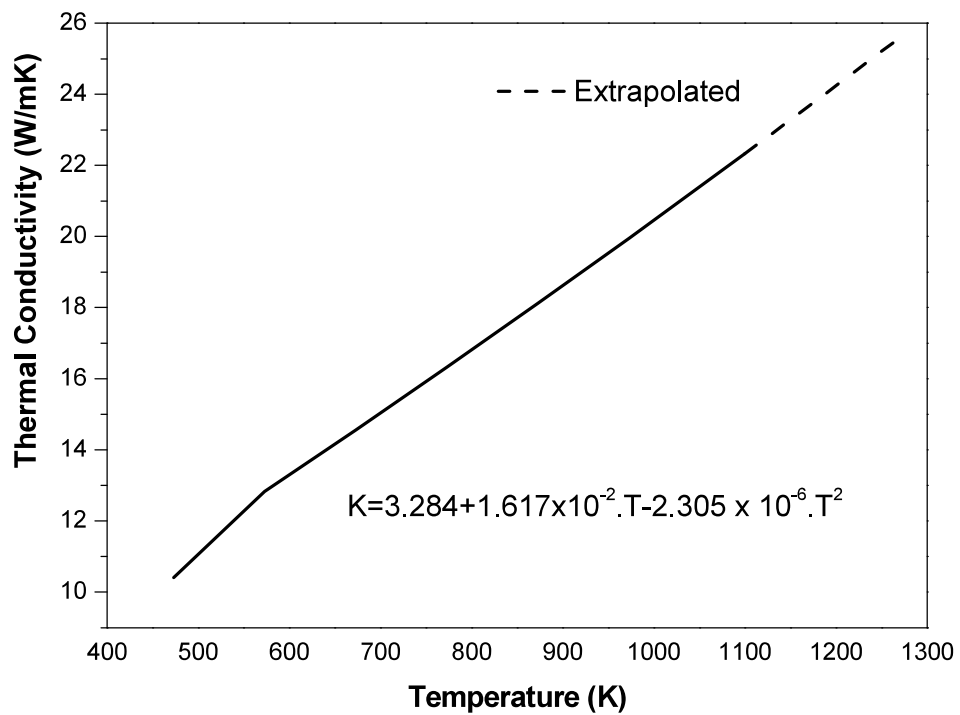


Fig 2.3 (b) Variation of thermal conductivity of lead bismuth eutectic with temperature

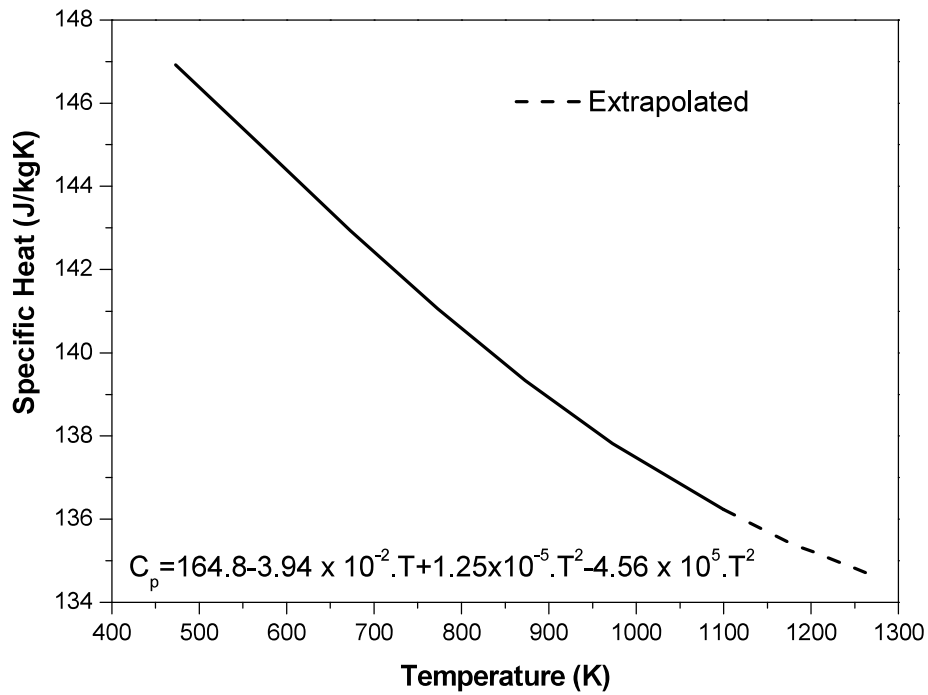


Fig 2.3 (c) Variation of specific heat of lead bismuth eutectic with temperature

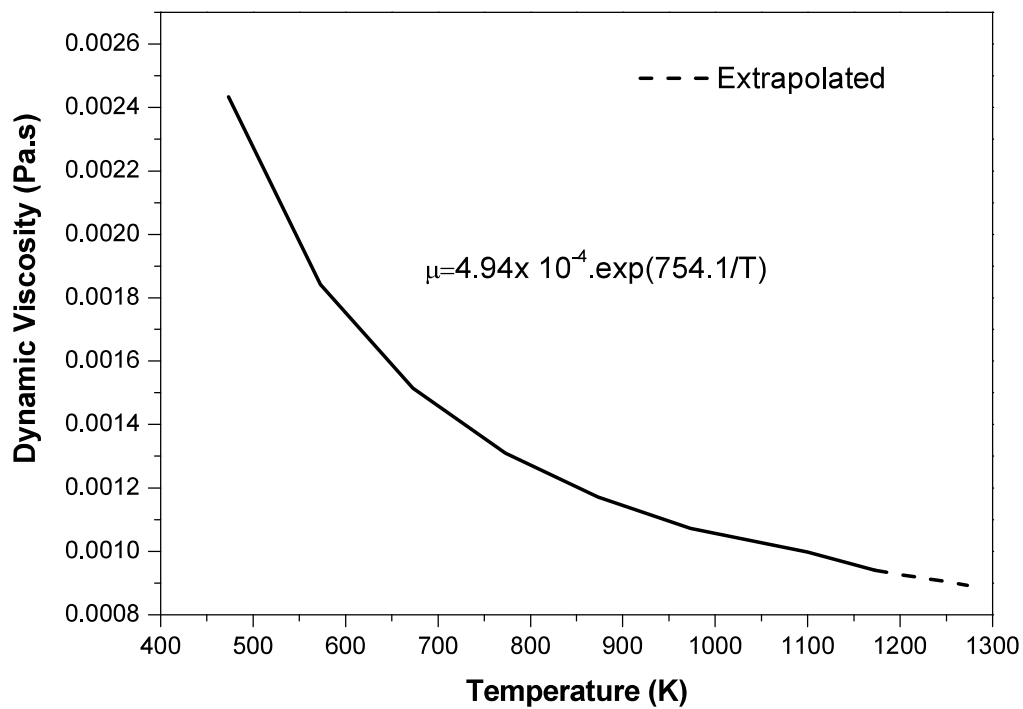


Fig 2.3 (d) Variation of dynamic viscosity of lead bismuth eutectic with temperature

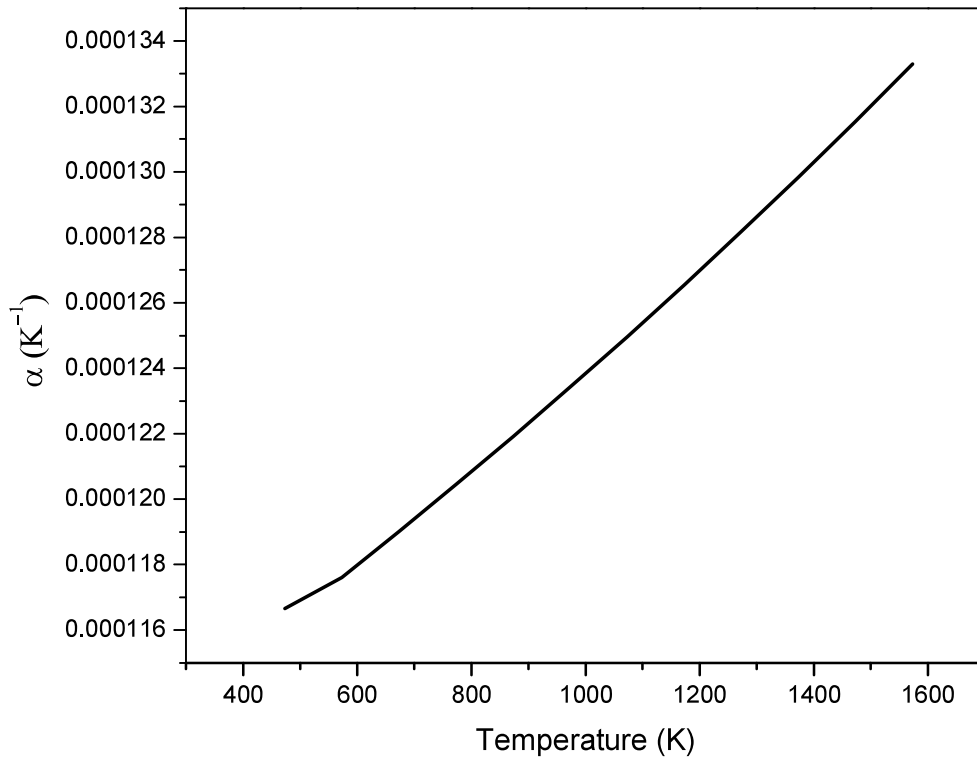


Fig 2.3 (e) Variation of volumetric thermal expansion coefficient of lead bismuth eutectic with temperature

2.6.1.2 Liquid metal experimental loops

A literature survey is carried out for experimental loops using liquid metal as working fluid. Table 2.5 gives the list of the loops with maximum operating temperature up to 550 °C. Few loops were found where natural circulation studies were carried out, which will be briefed below. Most of the loops were found to be used for material compatibility and coolant chemistry control related studies under forced flow. The loops used for these studies are, STELLA [60], LECOR [61], DELTA [62], JLBL-1 [63], MESLOOP2001 [64], CORRIDA [65], LISOR [66], CorrWett, CIRCO [67], LINCE [68], KPAL-1 [69], Natural convection quartz harp loop [70], LBE corrosion test loop [71], DRAGON-1 [72], KYLIN-I & KYLIN-II [73] and LIFUS-3 [74]. Few loops were found where material compatibility studies were carried out under natural circulation also. The loops were DRAGON-I [72], KYLIN-I [73], KYLIN-II [73] and the thermal convection loop reported by Pawel et al. (2014) [75]. The

experimental studies on forced flow heat transfer in heater rod bundles were carried out in several loops like THESYS [76], TALL [36] and HELIOS [32]. The two phase flow studies were also carried out in some loops as reported by Loewen and Tokuhiko (2003) [77] and Abdulla et al. (2001) [78]. The facilities like THEADES [79], CHEOPE [67] and JLBL-3 [63] were used for thermal hydraulic design and testing of ADS components. MHD effect on thermal hydraulics is important in fusion reactor technology development. Facilities like MaPLE [80], MHD loop reported by Uda et al. (2001) [81], LIMITS [82] were made to study the effect of MHD on heat transfer and flow pattern in liquid metals. There were large facilities like CIRCE [83] and ATENA [84], where full scale components and system level studies of ADS were carried out. The loops were used for instrument development especially for flow measurement. The loops JLBL-2 [63] and JLBL-4 [85] were extensively used for advanced flow measurement technique development.

Literature survey was also carried out for experimental loops operating above 550°C. Table 2.6 briefs some of the loops reported in literature. It can be seen from the table that most of the high temperature corrosion loops were natural circulation based. COLONRI-I [86], COLONRI-II [87], DRAGON-II [72], Sodium loops in CIAE, China [88], thermal convection loops reported by Scheuermann (1974) [89], Devan et al.(1966) [90], Bryhan and Chan (1993) [91], Rowkamp (2013) [92] and Harrison (1970) [93] have studied the different high temperature material compatibility in liquid metals. Forced flow high temperature corrosion loops were few as compared to the loops reported in Table 2.6. The loops reported by Hvasta et al.(2010) [94], Devan et al.(1966) [90], Harrison (1970) [91] were used for material compatibility studies in forced flow of liquid metals. Loops simulating integrated power conversion system were found which were mainly developed for design validation of space nuclear power systems. SNAP-8 simulation facility [95], the T-111 loop reported by Harrison (1970) [93] were two such facilities given in Table-2.5. For sodium cooled fast

reactors high temperature loops were made to study special issues at high temperature like thermal fatigue of structural material [84] and sodium two phase thermal hydraulics ([96], and [97]). High temperature liquid metal loops were made to test components like EM pump [98] and dissimilar material joints [99], etc.

From the literature survey as discussed above it was found that though many liquid metal natural circulation loops were made but most of them were for mainly corrosion related studies. Extensive natural circulation studies were carried out in very few loops. It was seen that all the natural circulation experimental studies carried out so far, are in the temperature range of 250-550°C only. The studies above 550°C could not be found in literature except the work reported by Haga (1983) [96] where two phase sodium coolant natural circulation studies were carried out. There was no LBE loop except the present loop KTL, which has operated up to 1100°C. The following sections describe the important aspects of liquid metal experimental set ups gained from literature review.

Table 2.5 Liquid metal loops operating up to 550 °C

Sl No	References	Name of the facility/ Institute/ country	T _{Max.} (°C)	Flow rate (LPM)/ Nature of flow	Inven- tory (L)	Coolant	Remarks
1.	Knebel and Goschel (2003) [76]	THESYS /FZK/ Denmark	550	58, FC	100	LBE	Heat transfer studies in rod bundle and single heater rod were carried out for CFD code validation.
2.	LBE Handbook (2007) [67]	CHEOPE I/ ENEA/Italy	550	FC	900	LBE	Component level thermal hydraulic studies of ADS and pumping system development and testing were carried out.
3.	Beauchamp et al. (2010) [60]	STELLA /CEA/ France	550	16.7, FC	32	LBE	Apart from LBE chemistry control, purification filter

							development and testing and characterisation of different impurities were carried out.
4.	Mikinori et al.(2003) [64]	MESLOOP2001/MES/Japan	550	15, FC	-	LBE	Corrosion of steels and coolant chemistry control were studied.
5.	Carsten et al.(2011) [65]	CORRIDA/FZK/Denmark	550	2-4m/s, FC	-	LBE	The loop was devoted for corrosion experiment with varying oxygen by gas/liquid transfer. The longest sample was tested for 20000 hrs.
6.	Hosemann (2008) [62]	DELTA /LANL/USA	550	2-5 m/s, FC	200	LBE	Corrosion tests for different metal including ODS steels were carried out in high flow rate of LBE.
7.	Kikuhchi (2009) [63]	JLBL-3/JAERI/Japan		500, FC	450	LBE	Heat transfer characteristics around beam window and testing of mechanical pump.
8.	LBE handbook (2007) [67]	CIRCO/CIEMAT/Spain	550	NC	1	LBE	Long term corrosion was studied.
9.	Agostini et al. (2002) [33]	CHEOPE- III/ENEA/France	550	67, FC/NC	30	LBE	Natural circulation studies and material compatibility under forced flow were carried out.
10.	Cho et al. (2006) [69]	KPAL-1/KAERI/Korea	550	60, FC	30	LBE	Long term corrosion experiments for cladding and structural materials were carried out.
11.	Abraham et al. (2000) [70]	Natural convection quartz harp/ANL/USA	550	0.01 m/s FC		LBE	Quartz was used as the structural material for the loop different steel samples were tested for corrosion in LBE.
12.	Takahashi (2002) [71]	LBE corrosion test loop/	550	6, FC	22	LBE	Corrosion studies on different steels were

		TIT/Japan					carried out. The role of Si on the formation of stable oxide inner layer was found to be effective.
13.	Ma(2005) [36]	TALL/RIT/Sweden	550	40, FC	-	LBE	Thermal hydraulic studies with fuel rod bundle were carried out.
14.	Abdulla et al. (2001) [78]	Wisconsin Tantalus/UW/USA	550	230, FC	-	LBE	Studies on molten LBE and water interaction and related heat transfer was carried out.
15.	Wu et al. (2014) [73]	KYLIN-II	550	FC/NC		LBE	Test run of the loop was completed.
16.	Uda et al. (2001) [81]	MHD loop/Osaka Univ/Japan	550	13, FC	230	Li	MHD effect on Heat transfer in lithium flowing in annular channel was studied.
17.	NEA report (2011) [84]	ATENA/JAE A/Japan	550	31500, FC	10^3	Na	The complex of loops has been made to simulate the heat removal system of JSFR with installed heat load of 60 MW.
18.	Pawel et al. (2014) [75]	Thermal convection loop, ORNL/USA	550	0.14, NC	-	PbLi	Made of Kanthal APM alloy, designed for 800 °C. Corrosion studies were carried out up to 550 °C.
19.	Coccoluto et al. (2011) [30]	NACIE/ENEA / ITALY	550	40, NC	100	LBE	Thermal hydraulic studies were carried out to find pressure drop in fuel rod bundles.
20.	Wu et al. (2014) [73]	KYLIN-I/FDS/China	500	NC	2	LBE	Corrosion studies on SS316 and clam steel was carried out.
21.	Padmakumar et al. (2013) [35]	SADHANA/IGCAR/India	500	110, NC	3500	Na	Natural circulation experiments have been carried out to validate the capability of SGDHR system to remove the decay heat

							from the fast breeder reactor core after its shutdown.
22.	Toshinobu and Hiroyuki (2014) [85]	JLBL-4		40, FC	-	LBE	Development of advanced flow measurement techniques like, use of UVP.
23.	Kikuhchi (2009) [63]	JLBL-2/JAERI/Japan	500	50, FC	-	LBE	It was a tube-in-tube type compact flow set up where target flow was simulated and testing of Ultrasonic Doppler method and EM flow meter were carried out.
24.	Fazio et al. (2003) [61]	LECOR/ENEA/ITALY	500	75, FC	600	LBE	Corrosion and mechanical stress test studies of steels and refractory metals like W and Mo.
25.	Borghaine et al. (2011) [100]	LML/BARC/INDIA	500	1, NC	50	LBE	Natural circulation was carried out at different operating conditions.
26.	Cinotti (2012) [68]	LINCE/CIEMAT/Spain	500	40, FC	170	LBE	Corrosion studies were carried out for steel. Weight loss of steel samples was observed after 5000 hrs and at 450°C.
27.	Wu et al. (2012) [72]	DRAGON-I/FDS/China	480	0.08m/s, NC	1	PbLi	Experience gained on Pb-Li and corrosion studies on SS316 and Chinese martensitic steel samples were done.
28.	Takahashi (2005a) [27]	LBE test loop/TIT/Japan	460	36, FC	-	LBE	Natural circulation studies on of single phase LBE and two phases LBE-steam were carried out.
29.	Bandini et al. (2015) [83]	CIRCE/ENEA/Italy	450	900, FC	9000	LBE	Integral thermal hydraulic experiments on ADS were done. Natural circulations in

							pool type geometry including thermal stratification were studied.
30.	Schulenberg et al. (2005) [79]	THEADES/FZK/Denmark	450	1670, FC	4000	LBE	The loop with 4 MW capacity was used for testing full scale component testing of ADS.
31.	Kikuhchi (2009) [63]	JLBL-1/JAERI/Japan	450	18, FC	-	LBE	The loop was used for erosion-corrosion experiment.
32.	Kang et al. (2013) [34]	-/UNIST/Korea	450	13, NC	-	Ga	Natural circulation experiment was carried out in a rectangular loop.
33.	Tanaka (2004) [82]	LIMITS/Sandia NL/USA	425	FC	-	Li	The loop was well equipped to study the free surface of lithium which was required for flow studies on the surface under MHD.
34.	Cho et al. (2011) [32]	HELIOS/SNU/Korea	400	2m/s, FC	1800	LBE	Benchmark exercise has been carried out for isothermal pressure drop in the loop.
35.	Kirchner et al. (2003) [66]	LISOR/PSI/Switzerland	350	1 m/s, FC	18	LBE	T91 steel embrittlement was found to be more under irradiation. Coated T91 shows good resistance.
36.	LBE Handbook (2007) [67]	CorrWett/PSI/Switzerland	350	0.8 m/s, FC	-	LBE	Corrosion studies were carried out on coated samples in LBE and found that TiN coating gives the best result.
37.	Smolentsev et al. (2013) [70]	MaPle/UCLA/USA	350	50, FC	20	PbLi	The MHD pressure drop reduction and the compatibility of different coated samples were studied.
38.	Technical Report (2009) [74]	LIFUS-3/ENEA/Italy	350	30, FC	46	Li	Material corrosion and erosion studies in lithium were carried

							out. Experience on lithium purification and handling were gained.
39.	Loewen and Tokuhiro (2003) [77]	Pb-Bi TH/ CREIPI/Japan	300	100, FC	-	LBE	The heat transfer and LBE-gas two phase flow characteristics were studied.

Table 2.6: Summary of the experimental loops operated at and above 550°C

Sl. No	References	Name of the facility/ Institute/Country	T _{Max.} (°C)	Flow rate (LPM)/ Nature of flow	Inven-tory (L)	Coolant	Remarks
1	Devan et al.(1966) [90]	ORNL/ USA	1400	FC/ NC	-	Li, K	Made of Nb-1% Zr alloy, Material compatibility studies were carried out.
2	Scheuermann (1974) [89]	Thermal convection loop /NASA/ USA	1370	NC	-	Li	The loop was made of Tantalum alloy T-111. Corrosion studies were carried out to find the materials suitable for lithium cooled space systems.
3	Harrison (1970) [93]	T-111 corrosion test loop /GE/USA	1235	3.28, K-0.56 FC	-	Li and K	The material compatibility and Rankine cycle performance was studied for SP-100 space nuclear reactor. Primary loop has Li and Secondary loop has 2 phase Potassium.
4	Annual report (2010) [98]	STL-300 /Univ. Latvia/ Latvia	1200	FC	-	Li	The loop was made of Nb-alloy and used for testing of high temperature EM pumps.
5	Borgohain	KTL /BARC/	1100	0.75,	32	LBE	Natural

	et al. (2016) [101]	India		NC			circulation experiments were carried out for temperature range 200-1100 °C.
6	Harrison (1970) [93]	Thermal convection loop /GE/USA	1040	FC	3.5	Li	The loop was made of T-111 alloy and used for corrosion related studies.
7	Gnadt et al. (1979) [97]	THORS /ORNL/ USA	1010	FC	-	Na	The 2.0 MW capacity heater bundle was made from Hastelloy-X. The bundle thermal hydraulics were carried out for both single phase and 2 phase of sodium.
8	Noborio et al. (2011) [99]	Kyoto Univ/ Japan	926	3, FC	-	PbLi	The high temperature section was made of SiC _f /SiC. The heat transfer between PbLi loop and high pressure helium loop was studied.
9	Haga (1983) [96]	SIENA/ OEC-PNC/Japan	887	0.29 m/s, NC	-	Na	The different regimes of flow boiling and dry out conditions were studied to evaluate the capability of cooling of the core by two phase natural circulation during reactor shutdown.
10	Cathcart and Manly (1956) [102]	Thermal convection loop/ ORNL/USA	800	0.6, NC	-	Pb	The quartz loop was used to test the compatibility of 24 different metal/alloys in molten lead.

11	Bryhan and Chan (1993) [91]	Thermal convection loop /NASA/ USA	732	NC	1	Li	Made of Nb alloy. Corrosion attack by molten lithium weldments in presence of contaminates like oxygen and nitrogen were studied.
12	Valerino et al.(1968) [95]	Snap-8 simulation facility/ NASA/USA	704	NaK 280 Hg 5.0, FC	-	NaK, Hg	The performance of the nuclear reactor with non nuclear heating was carried out to evaluate the energy conversion system consisting of coupled NaK-Hg loops.
13	Gabriele et al.(2014) [86]	COLONRI II/ REZ/CZ	700	1-2 cm/s, NC	-	Pb	Loop was made from SS321. Different coated samples were tested up to 600 °C in flowing lead.
14	Wu et al. (2012) [72]	DRAGON-II /FDS/China	700	NC	10	PbLi	Made of high temperature alloy. Corrosion studies on TBM alloy and coatings were carried out.
15	Xu Mi (2007) [88]	Several loops /CIAE/ China	700	12 m/s, FC/ NC	60	Na	Large number of sodium loops has been operated in CIAE since 1968.
16	ANL Website [103]	ALEX /ANL/ USA	700	FC/NC	-	NaK, Na, Li	This was a facility has the provision for various experiments with different coolants.
17	OECD/NE A report (2011) [84]	TTS /JAEA/ Japan	650	400, FC	75000	Na	Mixing of high temperature and low temperature sodium to simulate high temperature fluctuation for

							thermal fatigue behavior of the structural material of different components were studied.
18	Rowkamp (2013) [92]	UTK/ USA	650	2.4 NC	-	NaK	A compact loop was designed to fit in a glove box and the flow measurement by thermal spike was tested.
19	OECD/NEA report (2011) [84]	PLANDTL /JAEA/ Japan	625	1200, FC	1000	Na	The coupled thermal hydraulic studies were carried out with max heat flux 2 MW/m ² in the fuel simulator.
20	Hvasta et al. (2010) [94]	Univ of Wisconsin/US A	600	100, FC	30	Na	High temperature high flow system for testing materials for fusion and fast reactor.
21	Gabriele and Kosek (2013) [86]	COLONRI I /REZ/CZ	600	1-2 cm/s, NC	-	LBE	Effect of different element content in steel on corrosion rate in LBE with different oxygen concentration was studied.

FC: Forced Circulation, NC: Natural Circulation

2.6.1.3 LBE corrosion and material of construction

Structural materials exposed to liquid metals can undergo corrosion by: (1) direct dissolution of the structural material in the liquid metal by a surface reaction involving atoms from the solid and the liquid metals or impurities present in the liquid metal, and (2) by intergranular attack. In the dissolution process or leaching, one component of the alloy was

preferentially dissolved, as in the case of nickel that is leached from stainless steels by lead and lead bismuth eutectic [104]. Intergranular attack occurs because the atoms at the grain boundary have a higher potential energy than the atoms inside the grains. If the concentration of higher solubility elements increases in the grain boundaries, the dissolution rate may increase due to the preferential dissolution of these elements [105]. Oxygen concentration in liquid lead alloys is a key parameter for the corrosion of structural materials. Figure 2.4 shows the effect of oxygen concentration on corrosion resistance for stainless steels. There is a minimum in material loss associated with the formation of a protective oxide film.

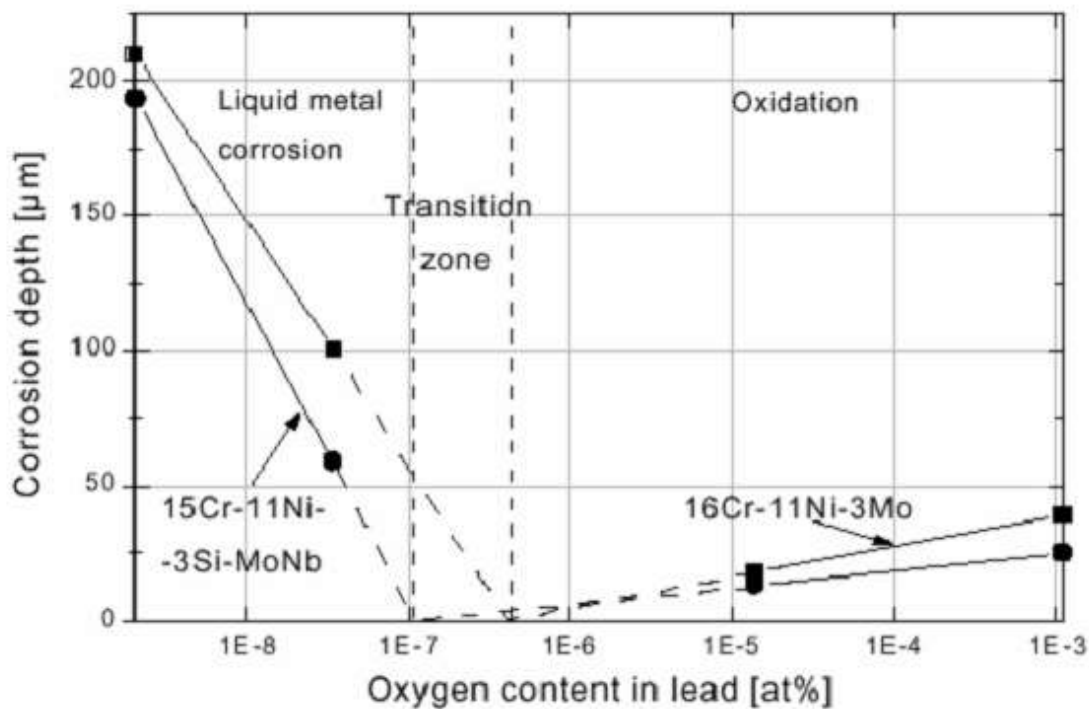


Fig 2.4 Corrosion/oxidation of stainless in lead at 550°C [106]

With appropriate control of the oxygen concentration in the liquid metal, the formation of oxide films on the surface of the structural materials occurs, limiting further dissolution. For Fe containing alloys, such as structural steels, the minimum oxygen concentration is defined by the magnetite (Fe_3O_4) decomposition potential, considering this

oxide the less stable of the ones that can be formed on structural steels. The maximum value is fixed by the precipitation of lead oxide. It was found that the dissolved oxygen level was to be maintained between 10^{-5} to 10^{-7} wt.% for operating range of LBE from 300 to 500 °C.

Data on the influence of other elements on the corrosion resistance of structural steels in liquid lead alloys have been provided by Gorynin, et al. (1998) [107] and Gorynin (1999) [106]. The effect of other alloying elements such as Cr, Ti, Nb, Si and Al on low alloy steels corrosion in flowing lead-bismuth at 600°C was studied by the same authors. A significant decrease of the dissolution was observed for concentrations of Si and Al around 2% whereas for the rest of the elements, concentrations higher than 3% seem to be needed to obtain similar effects. In general, in reducing environments, in which the formation of protective oxide layers was not possible, steels with lower chromium concentration show lower dissolution rate. Austenitic steels suffer accelerated attack in lead and lead-bismuth due to the high nickel solubility. Yachmeniov et al. (1998) [108] has recommended limiting temperatures for the application of non-protected stainless steels to around 450°C for ferritic-martensitic steels and 400°C for austenitic steels.

Corrosion tests of a wide variety of materials under wide ranging conditions have been carried out in both stagnant and flowing LBE/Pb [67]. It was concluded that for tests conducted both in stagnant and in dynamic (flowing) LBE/Pb within the oxygen control band, most Fe-Cr and Fe-Cr-Ni steels form oxides that are protective below 550°C, specially for an oxygen concentration above 10^{-6} wt.% for short- to medium-term applications. Austenitic steels show thinner oxide layers. For oxygen concentrations lower than 10^{-6} wt.%, dissolution takes place in most of the steels, especially austenitic steels, due to the high solubility of nickel in LBE/Pb. For tests temperatures higher than 550°C, the layer of oxides is not stable and the protection usually fails due to dissolution for long time.

Therefore, structural parts exposed to high thermal loads like cladding tubes, which could reach temperatures above 550°C, need additional protection measures. In LBE handbook (2007) [67] the activities on the corrosion control at elevated temperature were reviewed and the following materials and modifications were being proposed,

- (i) Steel was appropriately alloyed with Al especially on the surface to form stable oxide layers and Si in the bulk volume to increase the corrosion resistance. This method needs improvement for perfection especially on the uniformity of the Alumina layer on components.
- (ii) The coatings help to form protective oxide layers in LBE containing very low oxygen concentration. The coating has not been successful as it has a rough surface because of the relatively large spray droplets, contains pores and also the adhesion on the bulk material was not perfect [109]. The coating with the refractory metals on steel were found to be satisfactory for the material, but the coating technology is not yet ready for industrial level use [67].
- (iii) Use of inhibitors like Zr dissolved in LBE that cause formation of protective layer on the structural material which reduces corrosion to great extent [110] but proper mixing procedures to assure a homogenous distribution of the inhibitor within the LBE as well as maintaining its amount at a constant level during the whole loop operation are crucial here [67].
- (iv) The use of high temperature refractory alloys was found to be the only option for very high temperature application in LBE [111]. The Ta and W cannot be

considered in reactor design because of its high neutron absorption cross-section. Mo can be considered if suitable joining techniques could be developed. Nb alloy is suitable for LBE application but the oxidation of the material at high temperature in air is to be prevented. The corrosion resistance for ceramic based materials like SiC, Ti_3SiC_2 , SiC-SiC composites were also studied in LBE. The experiments which were carried out in static LBE up to 700°C reveals that SiC and Ti_3SiC_2 are compatible with LBE. LBE penetrates into SiC-SiC composites due to its porous nature and forms cracks.

From the review it was found that for experiments up to 500°C , a few options of stainless steels, as construction materials for LBE application were available. However beyond this temperature and up to 1000°C , refractory alloys of Nb or Mo are the only choice for structural material in molten lead alloys. But to use them as the structural material for high temperature application the oxidation by air has to be prevented either by protective coating or providing inert gas environment to the material.

2.6.1.4 Dissolved oxygen measurement

As discussed above dissolved oxygen control in LBE is essential for coolant chemistry control. This required accurate online measurement of oxygen in LBE at high temperature. The sensors based on solid electrolyte electrochemical cell proved efficient for measuring the dissolved oxygen of the lead alloys systems, despite a number of limitations, which are quite typical of this kind of measurement. However, it was not commercially available, so that for a day-to-day use on experimental facilities, the sensors were to be developed with sound theoretical background. The most widely used oxygen sensor for measuring dissolved oxygen in lead alloy is Ytria Stabilized Zirconia (YSZ) based

concentration cells. The potential difference (EMF) developed between the electrodes of the cell depends on the partial pressures of the molecular oxygen (O_2). The control of oxygen is done by several ways. The most common technique is injection of $Ar+H_2$ if the oxygen is to be reduced or injection of $Ar+O_2$ if oxygen is to be increased. The other method which is more robust is use of PbO pellet balls to release or consume dissolved oxygen as per requirement from the LBE system. The release rate of oxygen from the oxide balls depend on the temperature and flow rate of LBE through it ([112], [67]). So a suitable design of the system is possible so that confinement of the LBE system is maintained and complex gas circulation system can be avoided. However extensive development is required before using this technique for oxygen control.

2.6.1.5 Safety aspects of molten lead alloy

Lead is a cumulative toxicant that affects multiple body systems and is distributed to the brain, liver, kidney and bones [113]. Human exposure is usually assessed through the measurement of lead in blood. Exposure to lead through inhalation or ingestion can cause serious health effects in a variety of body systems. Such health effects may arise from acute (short-term) or chronic (long-term) exposures. A short-term, high-dose lead exposure can cause kidney, nerve, and brain damage that may lead to seizures, coma, and death within a matter of days. As per WHO's report there is no known level of lead exposure that is considered safe. Table 2.7 gives the maximum allowable limit of the lead in air and human blood. In practice, if we use the lead and LBE vapour pressures from the literature ([114], [115]), the 50-100 g/m^3 PEL corresponds to 530-550°C for LBE. However it is to be noted that if the working area is under ventilation the lead concentration will be lower at these temperature.

Table 2.7 Maximum allowable concentration of lead in air and blood

Medium	Maximum Permissible Concentration	References
Air	50-100 g/m ³	(WHO, 1989) [113]
Blood	70 μ g/decileter	OSHA standards

The detailed guidelines for safe operation of lead alloy systems are given in the LBE handbook (2007) [67]. The general operation steps include setting up apparatus, preparation, melting, filling, insertion, sealing, heating, gas injection, cooling, opening, extraction, cleaning, freezing, transferring, draining, circulating, etc. As per the handbook the danger posed by lead to human health and environment is very real and serious, and should not be overlooked in the research and development of lead-alloy coolant technology. However if rules and regulations are properly observed and safe work practices and controls are employed and effectively utilised, lead hazards are manageable.

2.7 LIQUID METAL THERMAL HYDRAULICS AND FACTORS AFFECTING NATURAL CIRCULATION

The theoretical modelling of natural circulation in a loop consists solving the coupled governing equations of mass, momentum and energy equations. The continuity equation in a closed loop is not required to be solved, because the mass flow rate at any section is equal at particular time, due to LBE being an incompressible fluid. The axial conduction of LBE can be part of the energy equation as shown by Vijayan (2002) [3]. The wall conduction equation was also to be solved as heat is transferred to and from the LBE at different locations in the loop. Moreover the thermal inertia of structural material of the wall plays an important part in natural circulation especially during transient conditions [116].

The heat transfer coefficient is important parameter in the natural circulation formulation [11]. The correlations for the heat transfer coefficient were to be properly selected for different flow regimes of LBE. When the loop was started from stagnant conditions at certain heater power, the flow of the LBE in the loop, especially in the heater section undergoes different flow regimes such as, free convection, mixed convection, forced laminar flow and forced turbulent flow. The different flow regimes were given by Metais and Eckert (1964) [117] is shown in a single graph. The graph is discussed in more detail in chapter 5. For free convection the heat transfer coefficient for liquid metal was given by Sherrif and Devis (1978) [118]. There were some studies on heat transfer in mixed convection done by different researchers, ([119], [120], [121]). Jackson et al. (1994) [120] studied the mixed convection heat transfer in vertical tube for sodium extensively. It was found that the mixed convection heat transfer was different from the normal fluid like water. In the studies the radial velocity profiles were found to be similar to other fluids, however the temperature distribution was very different. For LBE, no such studies were found in literature. For forced convection laminar flow regime, the Nusselt number correlations for common fluids were found to be applicable for LBE also [67]. The literature review on the heat transfer in forced convection turbulent flow of LBE, revealed that there are number of correlations available. The best suitable correlations for the present work were to be evaluated from these.

LBE natural circulation at high temperature may be affected by different parameters. Since LBE has high thermal conductivity the axial conduction effect may be prominent especially at low flow conditions. Several authors have studied the effect of axial conduction on liquid metal flow. Ambrosini et al. (2001) [122] and Misale et al. (2000) [116] studied the effect of this on natural circulation in single phase water loop. Girgin and Turker (2011) [123] studied the effect of axial conduction on fluid temperature in a circular tube for wide

range of Prandtl number. Sabharwall et al. (2012) [39] carried out analytical studies in a uniform diameter LBE loop for high Reynolds number. But there were no extensive studies for natural circulation with low flow rate of LBE in closed loops. Heat loss in the piping is undesirable but not totally avoidable. The effect of this on natural circulation was not studied so far. At high temperatures the heat loss in the piping is considerable and its effect on the natural circulation is important to study. Another parameter is the surface roughness. Since LBE is corrosive at high temperature, it may make the surface rough by corrosion. This may eventually increase the frictional pressure drop in the loop. This study is not found in literature so far.

2.8 SUMMARY OF FINDINGS FROM THE LITERATURE SURVEY

Following are major finding from the literature survey,

1. Various liquid metals were used in nuclear reactors. Sodium is the most widely used for fast reactor, due to its good thermo-physical and neutronic properties. Recently interest in LBE has increased due to its low melting point compared to lead and inertness to air and water.
2. It was seen that the studies on natural circulation in liquid metal have been increased only recently. This may be due to design of the passive decay heat removal systems in advanced reactor designs and the development of natural circulation liquid metal cooled reactor systems.
3. The literature survey shows that most of the natural circulation loops were made for material corrosion studies. There were few loops which were made for mainly natural

circulation experimental studies. But there were no loops where natural circulation studies were carried out in the operating range of CHTR.

4. As a structural material for LBE systems there are few options of stainless steel up to 550 °C along with the use of dissolved oxygen control mechanism. The different operational aspects of LBE were also reviewed. It was found that monitoring and control of dissolved oxygen in LBE monitoring were essential for operation of LBE loops. For temperature range more than 550 °C, very few structural materials are available and in the temperature range of 700-1000 °C, only Mo and Nb based alloys were found to be suitable for LBE application.
5. Limited studies were carried out on the effect of various parameters of LBE on the natural circulation of LBE. The effect of different of factors like thermal conduction of LBE, heat loss in the piping, heat transfer coefficient, etc. are not studied so far.
6. There are various computer codes developed for the thermal hydraulic studies related to liquid metal cooled reactor systems. System codes are still being validated with experimental results. The analytical methods are limited to simple geometries like uniform diameter loops for natural circulation in LBE. The applications of CFD codes are also still limited to the simulation of steady state natural circulation in LBE. So an in-house system code is required to be developed which will include all aspects of LBE natural circulation at high temperature so that extensive parametric studies can be carried out.

Chapter 3

DEVELOPMENT OF LIQUID METAL LOOP (LML) AND EXPERIMENTAL STUDIES

3.1 INTRODUCTION

It was found from literature review that there was no natural circulation data available for the operating range of CHTR. So, experimental study in high temperature loop was planned to generate the data for the CHTR natural circulation. Since there was no previous knowledge and experience in design and operation of LBE facility, an extensive literature survey was carried out to make a loop which can be operated up to ~ 1000 °C. Initially a loop to operate at such a high temperature could not be made mainly due to the unavailability of structural material to withstand such a high temperature in LBE medium. So a loop was designed with structural material SS316, which can operate up to 500 °C with the dissolved oxygen control in LBE within certain range. Since this kind of study with LBE was done for the first time in India, the design and development of the facility was carried out entirely based on the literature review. The loop mainly consists of a heated section, air heat exchanger, valves, various tanks and argon gas control system. All the components and piping are made of SS316. The instrumentation like oxygen sensor and level sensor were also developed for high temperature LBE application. The auxiliary systems of the loop like ventilation system water and scrubber were also designed for safe operation of the loop. This chapter includes the design, development of liquid metal loop, its commissioning and natural circulation experiments at various operating conditions. The details of the loop and the experimental studies carried out with loop power levels varying from 900 W to 5000 W are described in this chapter. The analysis and results of the performance of the heat exchanger with air and

water as the secondary coolants are also discussed. Transient studies simulating various events like heat sink loss, start up from stagnant condition and step power change as well as secondary side flow change are also discussed.

3.2 DESIGN OF THE LOOP

To simulate the thermal hydraulics of a prototype, the experimental facility was to be scaled properly. Nayak et al. (1998) [124] describes about the power to volume approach for scaling of the natural circulation experimental facilities. The loop was designed to maintain the scaling of important parameters of CHTR in LML. Table 3.1 gives the values of the parameters which could be maintained for LML.

Table 3.1 Comparative design parameters of CHTR and Liquid Metal Loop (LML)

Sr. No	Parameters	CHTR	LML	Ratio (CHTR :LML)
1	Normal Power per fuel tube, W	5263	5263	1
2	Volume of LBE/ fuel tube, m ³	0.01834	0.01667	~1
3	Vertical height between the centres of the heater and heat exchanger, m	0.475	0.475	1
4	Fuel tube hydraulic diameter, m	0.035	0.038	~1
5	Gr_m/N_G , as given in Eq (2.1), at normal operating conditions	$\sim 10^7$ - 10^8	$\sim 10^7$ - 10^8	1
6	Re_{ss}	0-2000	800-2000	1
7	Mass flux, (kg/m ²	310	220	1.71
8	Heat flux, (in heat exchanger) kW/m ²	60.63	41.65	1.45

Immersion heaters were used to simulate the heat generation in the fuel with maximum power 6000 W. The heater power can be varied from 0 to 6000 W to study the natural circulation at different powers.

3.3 DESCRIPTION OF THE LEAD-BISMUTH LOOP

The LBE loop mainly consists of a heated section, air heat exchanger, valves, various tanks and piping system (Fig. 3.1a). All the components and piping were made of SS316. Figure 3.1 (b) shows a view of the loop. High temperature graphoil filled metallic gaskets were used in the loop. The gaskets were tested at high temperature in LBE before using it in the loop..

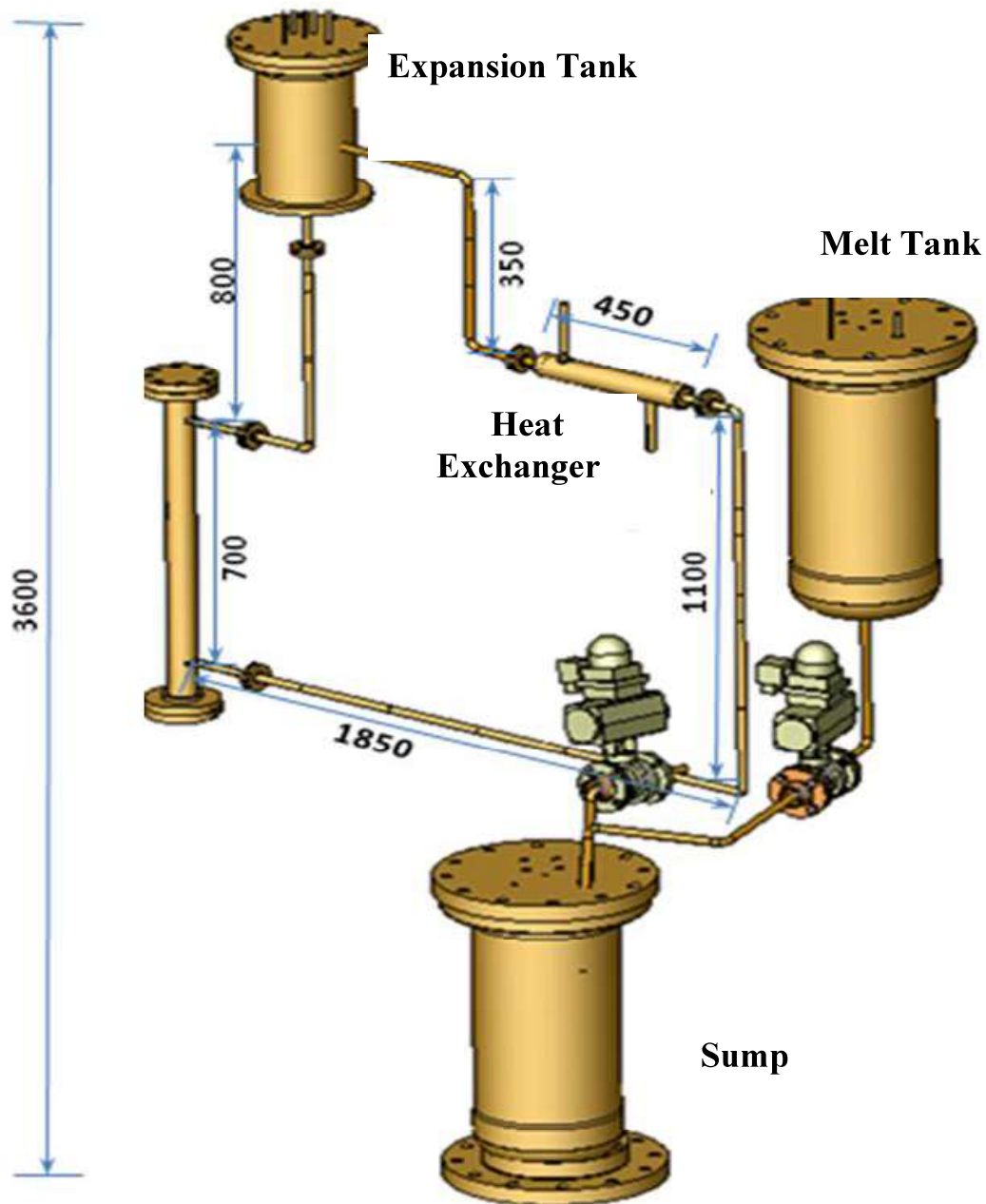


Fig. 3.1(a). Isometric view of Liquid Metal Loop

Adequate instrumentation and control system were designed and used in the loop for smooth and safe operation of the loop Table 3.2 gives detailed specifications of the loop. The different components of the loop are discussed in the following sections.

3.3.1 Heating System

There were three types of heaters used, in the loop. Band heaters were used to melt the LBE in the melt/sump tank and other vessels. Immersion heaters were provided inside heated section. Surface heaters were be used to maintain the piping temperature above the melting point of LBE during the starting of the loop.



Fig. 3.1(b) Photo of a part of Liquid Metal Loop

The surface heaters were installed in segments and covers entire length of the piping. Thick ceramic wool insulation was provided to reduce heat loss to the atmosphere. In the main heater section, the heat generated by the immersion heater was transferred to the liquid metal as sensible heat. It mainly consists of ‘U’ shaped mineral insulated heater elements mounted on a SS flange. The heating filament was made of Kanthal and the sheath material was SS316. A. C. power supply was used for resistance heating. Figure 3.2 shows the view of the heater section.

Table 3.2. Design parameters of LML

Sl. No.	Parameters	Values
1.	Fluid used	Lead Bismuth Eutectic
2.	Fluid circulation mode	Natural circulation
3.	Line size	15 mmNB(1/2”) Sch 80
4.	Centreline elevation difference between heat exchanger and heated section	475 mm
5.	Total circulation length	5500 mm
6.	Loop material	SS 316L
7.	Design pressure of the loop	5 kgf/cm ²
8.	LBE inventory	500 kg
9.	Maximum main heater power	6.0 kW
10.	Design temperature	550 °C
11.	LBE mass flow rate	0.09 to 0.15 kg/s

3.3.2 Heat Exchanger

The heat exchanger was specially designed tube-in-tube type (Fig 3.3). The liquid metal flows in the central pipe and cooling air/water flows in the outer annular jacket. A radial air gap thickness of 1 mm, was provided between the central pipe and water jacket.

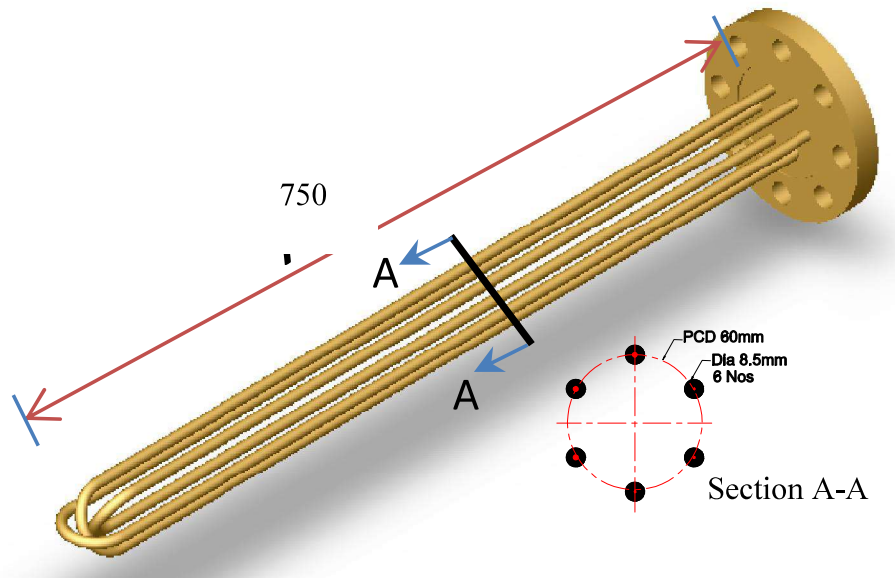


Fig.3.2. View of the main heater of the Loop

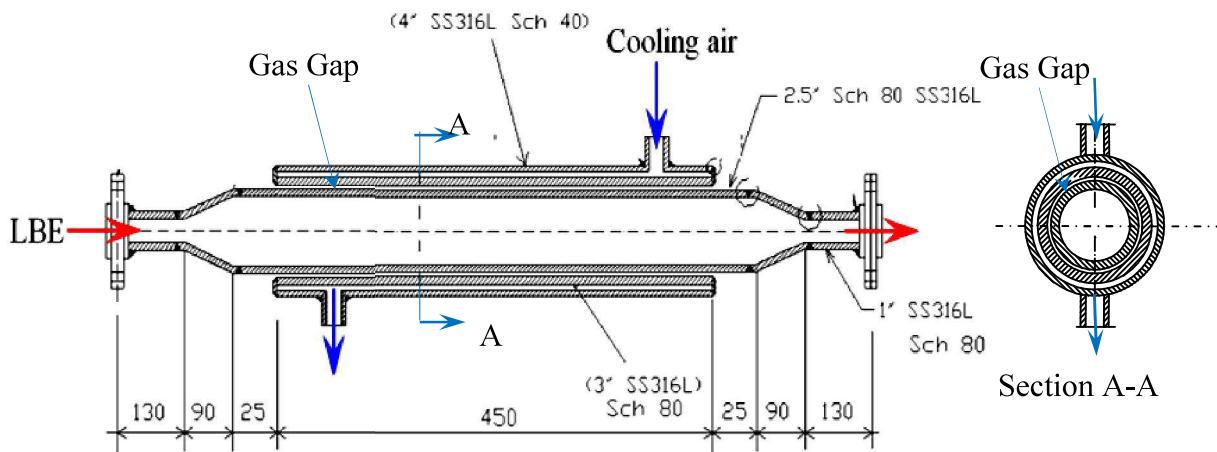


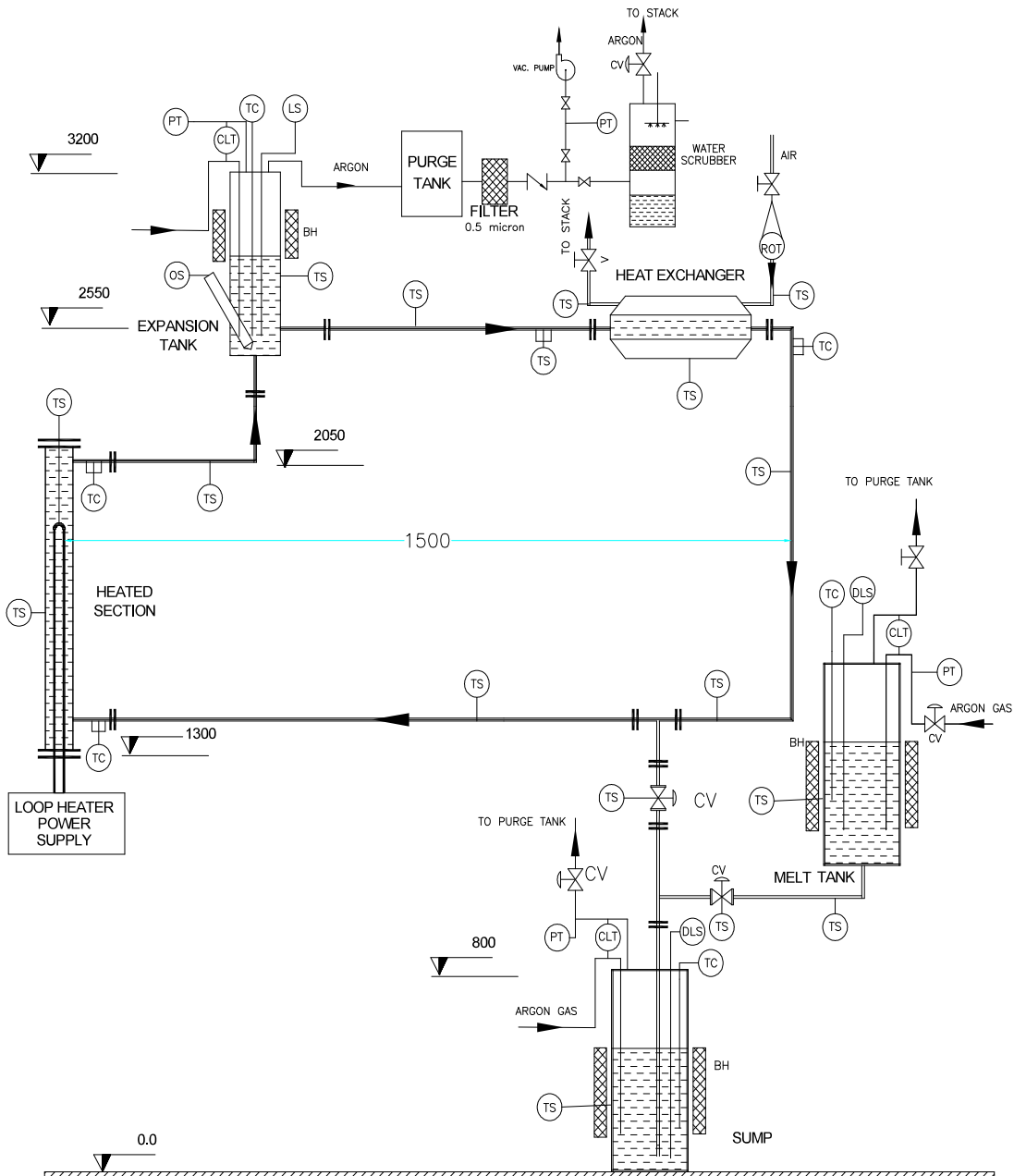
Fig. 3.3 Schematic of the heat exchanger of the Loop

The gap prevents the direct contact of cooling water with the high temperature tube surface and this prevents solidification of LBE due to overcooling. The heat exchanger was tested and the gas gap resistance was estimated in a High Temperature water Loop (HTL).

3.3.3 Instrumentation

The instrumentation and control of the LBE loop was realized by means of a Programmable Logic Controller (PLC) based Data Acquisition and Control System (DACS). Monitoring of various parameters like pressure, temperature, levels in different components of the loop, valve positions etc. was done through DACS. All operational and safety conditions were built into the program. Levels in the tanks, temperatures in the loop, dissolved oxygen in LBE, cover gas pressure; flow and other parameters were measured. Figure 3.4 shows the flow diagram of the loop with cover gas system. High Temperature pneumatically operated Control Valves (CV) and Pressure Regulating Valves (PRV) were used for the control and operation of the loop.

Figure 3.5 shows a view of the cover gas distribution panel of LML. Pressure relief valves were used to relieve argon gas in case of high system pressure. All the valves were made of SS316L and were PLC controlled. The instrumentation and control systems were designed in such a way that the loop can be operated remotely as far as possible. Pressure transmitters which can work at high temperature were used to measure the fluid pressure and gas pressure in the main loop. Fifty six ungrounded K-type, SS (Stainless Steel) sheathed thermocouples were installed in the loop. Most of the thermocouples were installed on the surface and some were inserted into the piping and vessels through special fittings. Figure 3.6 shows the mimic in the computer located at the control room for monitoring and control of the loop. Since the LBE level measurement was very important requirement of the loop, two types of level sensors were used; discrete type and continuous type. The discrete type was based on electrical conduction principle, where the electrical circuit was closed when liquid LBE surface touches a metallic rod hanging from the top flange of expansion tank. Figure 3.7 shows the schematic of the working principle of the discrete type level sensor.



BH: Band Heater

OS: Oxygen Sensor

CLT: Continuous Level Transducer

PT: Pressure Transducer

CV: Control Valve

TC: Temperature sensor in coolant

DLS: Discrete Level Switch

TS: Temperature sensor on the piping surface

Fig. 3.4 Flow sheet of Liquid Metal Loop

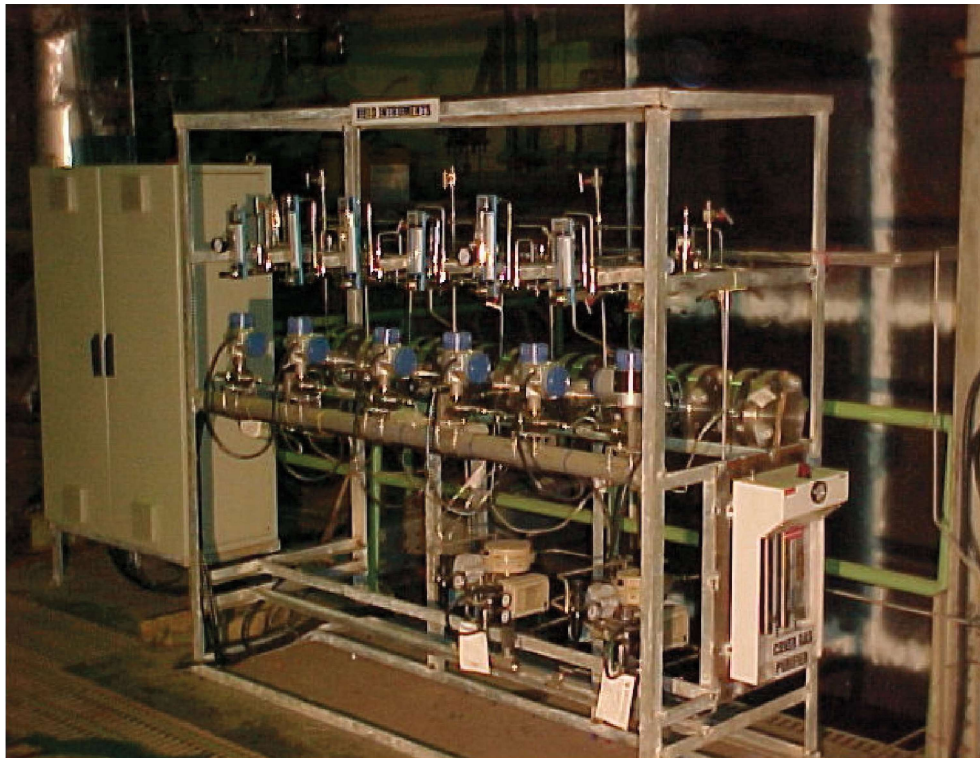


Fig 3.5 Instrumentation panel of LML

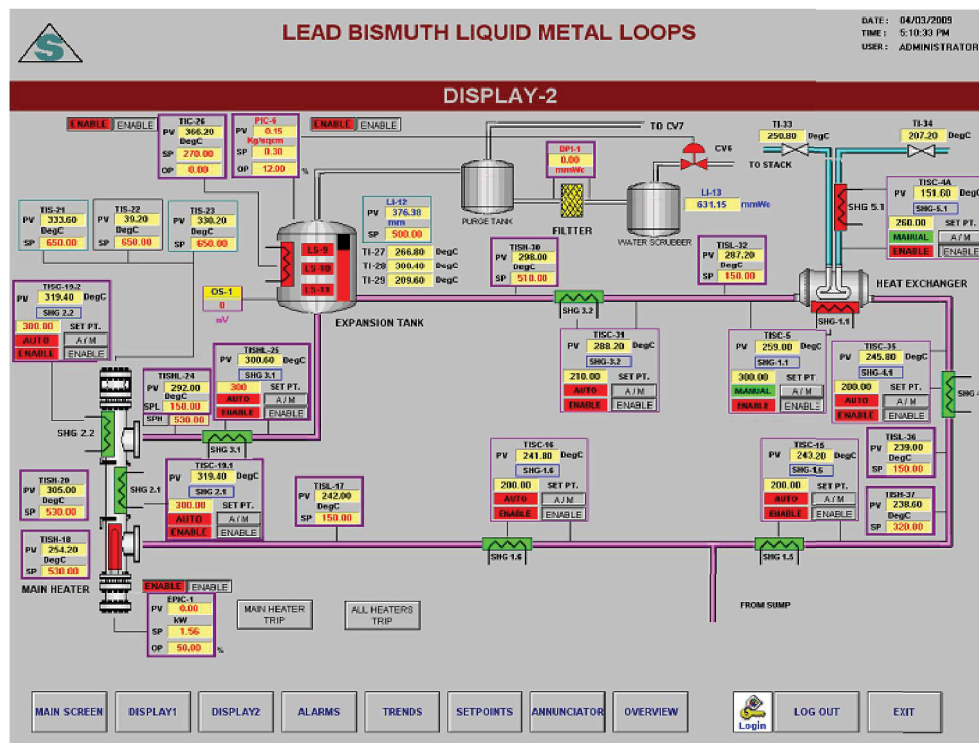


Fig 3.6 Mimic for monitoring and control of LML

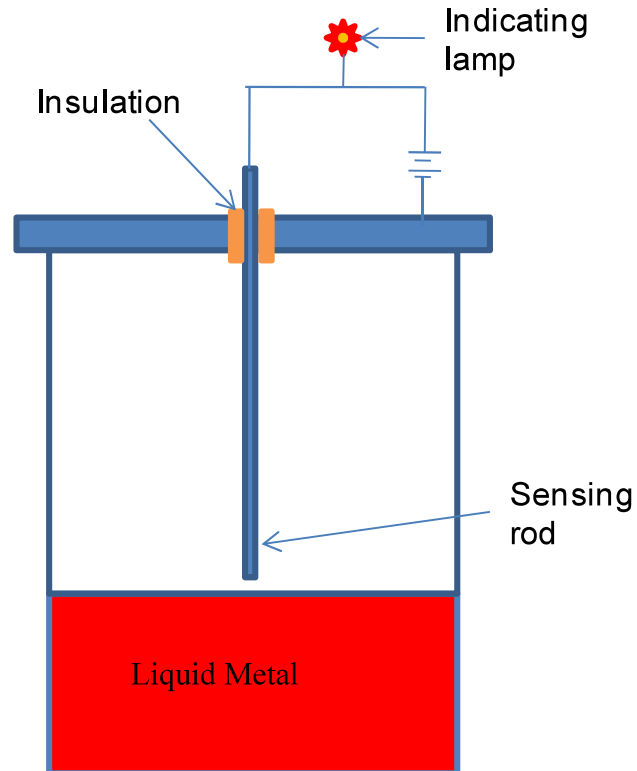


Fig 3.7 Schematic of the discrete type level sensor used in LML

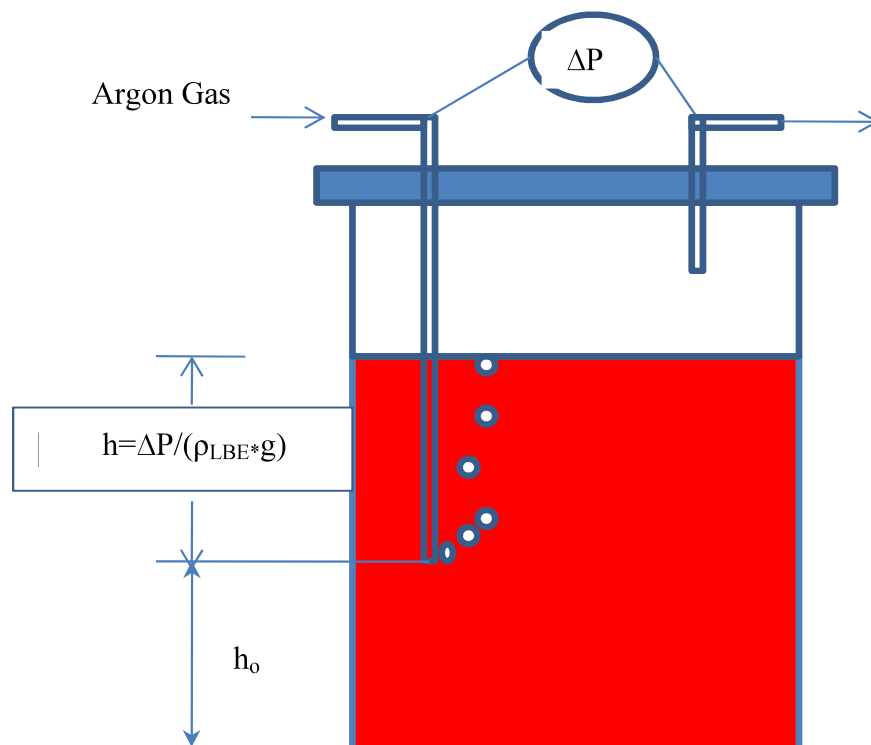


Fig 3.8 (a) Schematic of continuous level measurement sensor based on gas bubbling

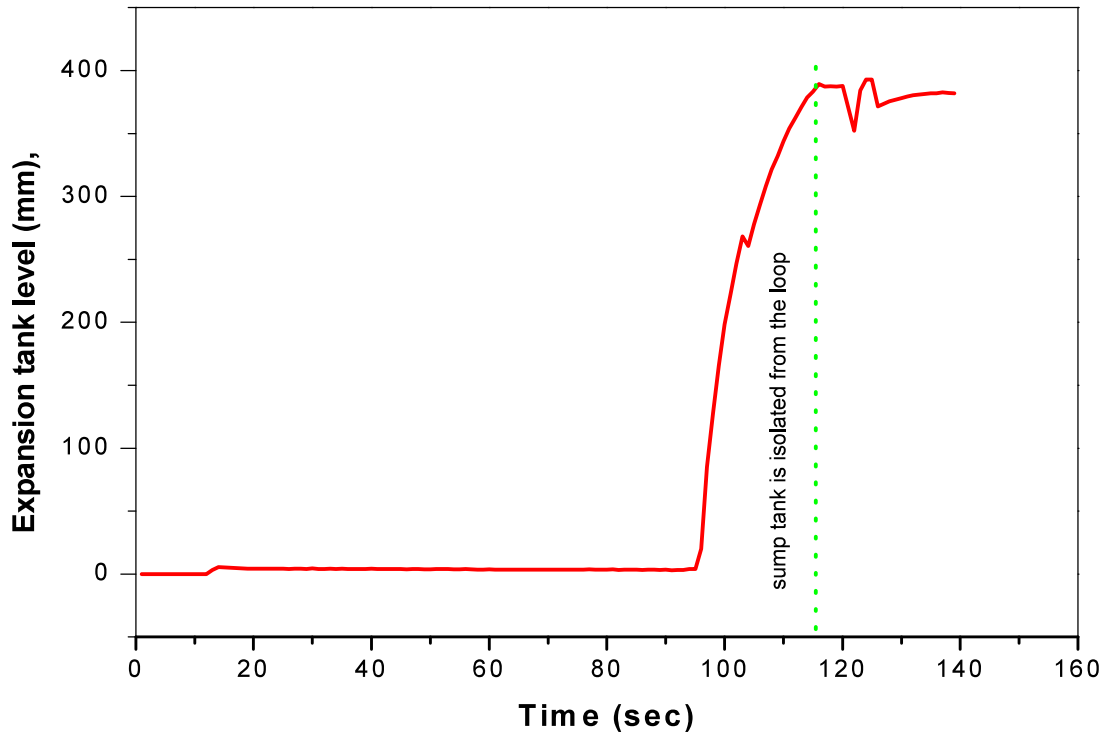


Fig 3.8 (b) Response of the continuous level sensor during loop filling

The continuous type was based on gas bubbling technique. In this type of sensor, the argon gas is bubbled at the LBE tank in a controlled rate. If the differential pressure required to maintain minimum argon gas flow, is measured the hydrostatic height can be obtained as shown in Fig 3.8 (a). The sensor is calibrated with the discrete type sensor before using in the loop. Figure 3.8 (b) shows the response of the continuous level sensor used in LML.

3.3.4 Oxygen Measurement and Control

Accurate measurement of the dissolved oxygen concentration in liquid LBE was a critical issue for the active chemistry control in the system. Oxygen enters the loop mainly during start-up operations and also due to incidental contamination. If the dissolved oxygen level reaches above a certain value, it leads to the formation of oxides in the liquid metal, resulting in plugging and degradation of heat transfer. On the other hand, if the oxygen level

falls below a certain value, the protective oxide layer on the structural material dissolves, leading to corrosion. Hence, the oxygen level must be constantly monitored and kept within a certain range. In a typical operating temperature range of 350°C to 550°C, the upper limit of oxygen concentration in LBE is 5.5×10^{-5} wt%, and the minimum oxygen concentration is 1.0×10^{-8} wt% [125]. The lower limit of the dissolved oxygen in LBE was defined as the concentration of oxygen required to form Fe_3O_4 protective oxide layer and the upper limit as the saturation level of oxygen at a particular temperature, beyond which the formation of PbO starts. The limits were obtained from the following two reactions taking place in LBE,



In terms of free energy of formation of Fe_3O_4 and PbO , using Henry's law, the limits of partial pressure of oxygen can be expressed, by following equation [126],

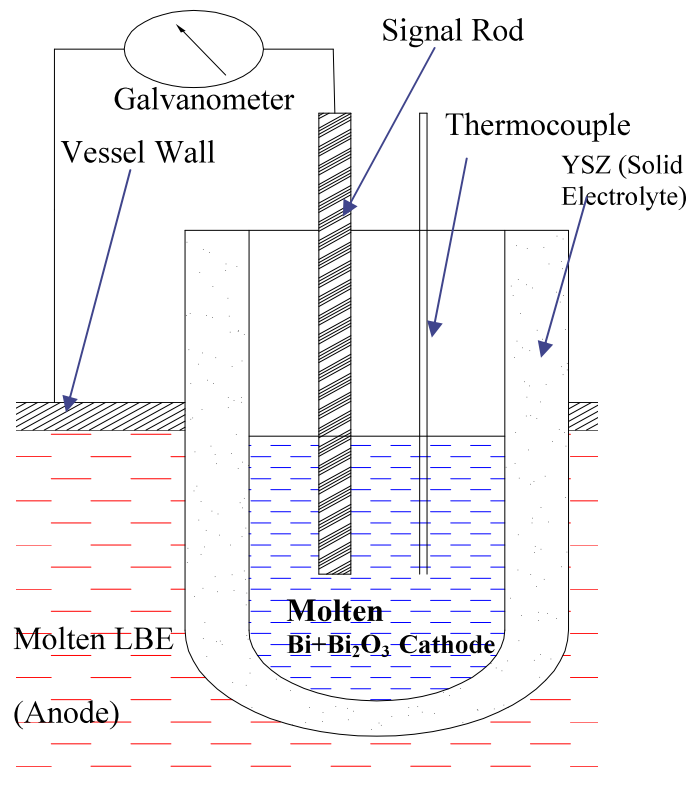


Fig. 3.9 Working principle of an YSZ oxygen sensor

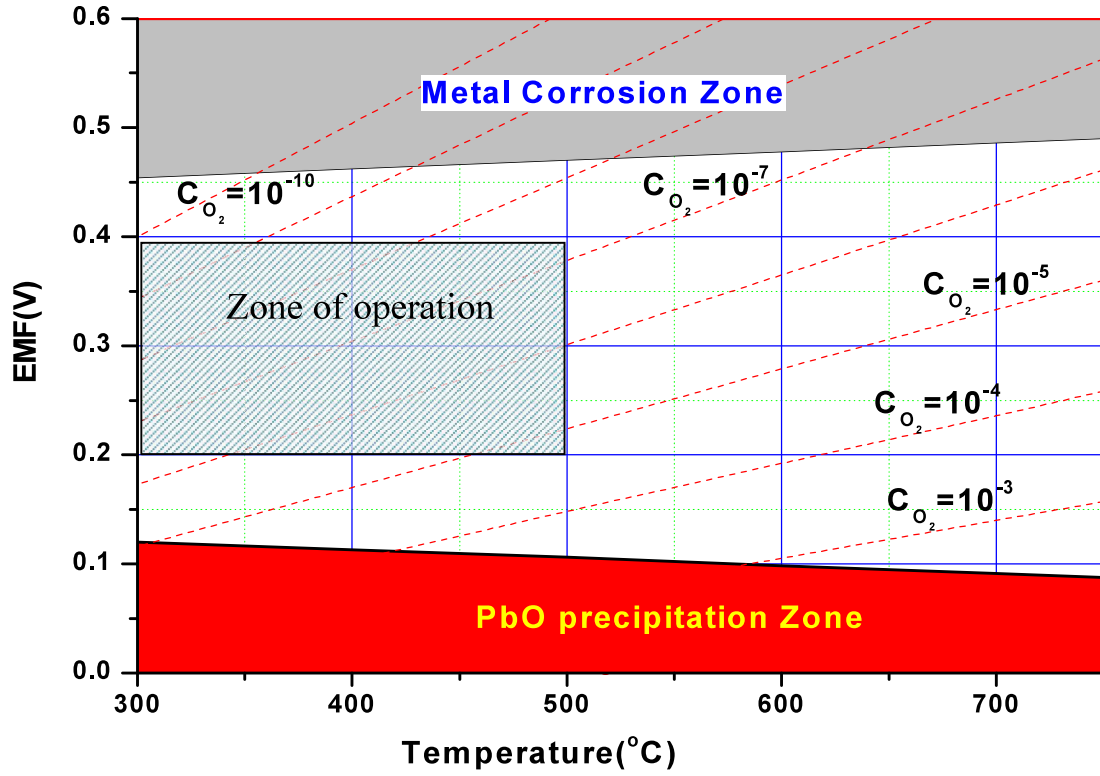


Fig 3.10 Variation of EMF in the oxygen sensor with temperature for different dissolved O₂ concentrations (%wt) in LBE.

$$\frac{1}{2} \Delta F_{Fe_3O_4} < RT \ln P_{O_2} < 2\Delta F_{PbO} - 2RT \ln a_{Pb} \quad (3.3)$$

Figure 3.9 shows a schematic of an oxygen sensor consisting of a one-end closed Yttria Stabilised Zirconia (YSZ) tube as solid electrolyte with molten Bi+Bi₂O₃ mixture as reference electrode. The molten lead alloy in which the tube was immersed serves as the other electrode. The potential difference developed across the electrodes due to the difference in oxygen concentration, can be calculated from Nernst Equation as [125],

$$\begin{aligned} E &= \frac{RT}{4F} \ln \frac{P'_{O_2}}{P_{O_2}} \\ &= \frac{1}{2} F \left(\frac{1}{3} \Delta F_{Bi_2O_3} - \Delta F_{PbO} - RT \ln a_{PbO} + RT \ln a_{Pb} \right) \end{aligned} \quad (3.4)$$

The unit of T in above equation is in K. P'_{O_2} and P_{O_2} are the partial pressures of the dissolved oxygen in reference electrode and liquid metal respectively. Using Eq (3.3), Eq (3.4) and

referring Oxide Handbook [127] for ΔF 's, the limits of the sensor voltage can be expressed as,

$$E_{\max} = 8.123 \times 10^{-5} T + 0.4304 \quad (3.5)$$

$$E_{\min} = -7.264 \times 10^{-5} T + 0.142 \quad (3.6)$$

The unit of T in Eq (3.5) and (3.6) is degree Celsius. Figure 3.10 shows the predicted variation of emf generated in the oxygen sensor as a function of different temperature for different oxygen concentration (% wt) in LBE. From the figure, it can be seen that if the EMF value of the sensor goes below 0.1 Volts then PbO oxide layer formation starts. If EMF goes above 0.45 Volts the protective oxide layer on the metal surface becomes unstable which may lead to corrosion. For normal operation range (i.e. 300 to 500 °C) the concentration of oxygen, 10^{-7} to 10^{-5} % wt is assumed as 'safe zone of operation'. In terms of EMF, it is 0.2 V to 0.4 V which is safe for the above mentioned temperature range. An oxygen sensor was developed to measure dissolved oxygen level in LBE. The oxygen sensor consists of a one-end closed YSZ tube. The tube was partially filled with laboratory grade Bi+Bi₂O₃ mixture, which was the reference electrode of the sensor. A Molybdenum rod (signal rod, for electrical connection between molten reference electrode and vessel wall) and a SS sheathed thermocouple (for temperature measurement) were immersed in the mixture. The tube was sealed with a Teflon[®] cap and high temperature silicon sealant. The detailed construction and testing of the sensor can be found in Borgohain et al., 2008 [128]. Figure 3.11 shows schematic and photo of the oxygen sensor used in the loop. Fig 3.12 shows the variation of EMF of the sensor for some period during operation of the loop. The sensor is installed in the expansion tank with specially made leak tight fittings. When the Ar+H₂ gas bubbling is started in the expansion tank, the hydrogen gas combines with oxygen and forms moisture. The moisture goes away with the purge gas.

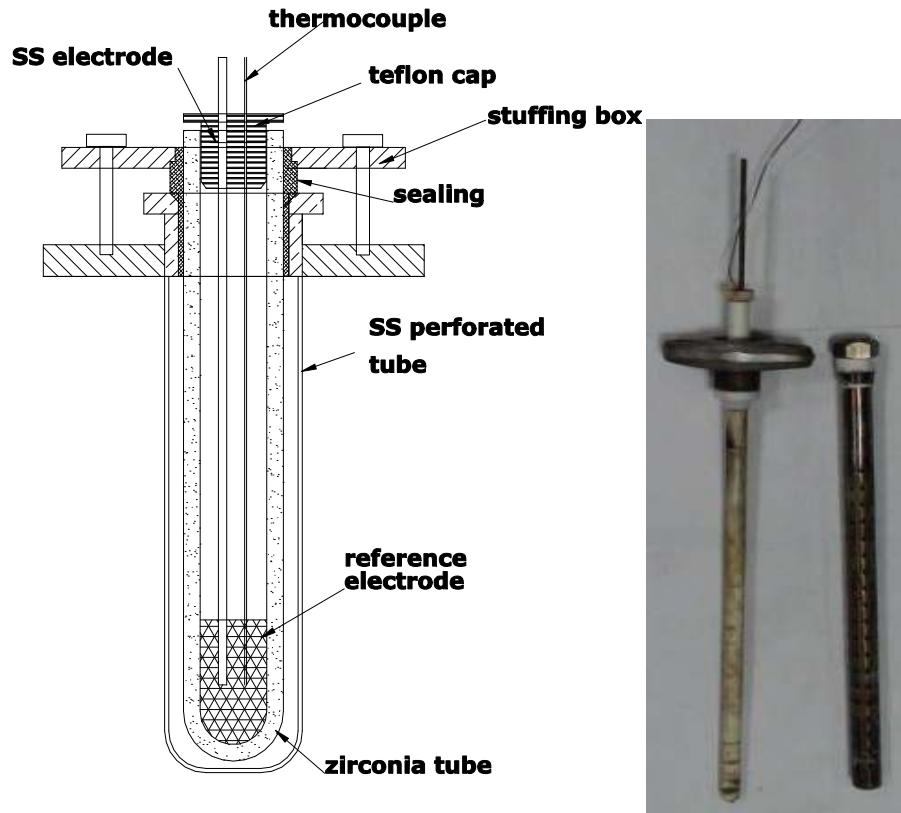


Fig. 3.11 Schematic and view of the oxygen sensor used in LML

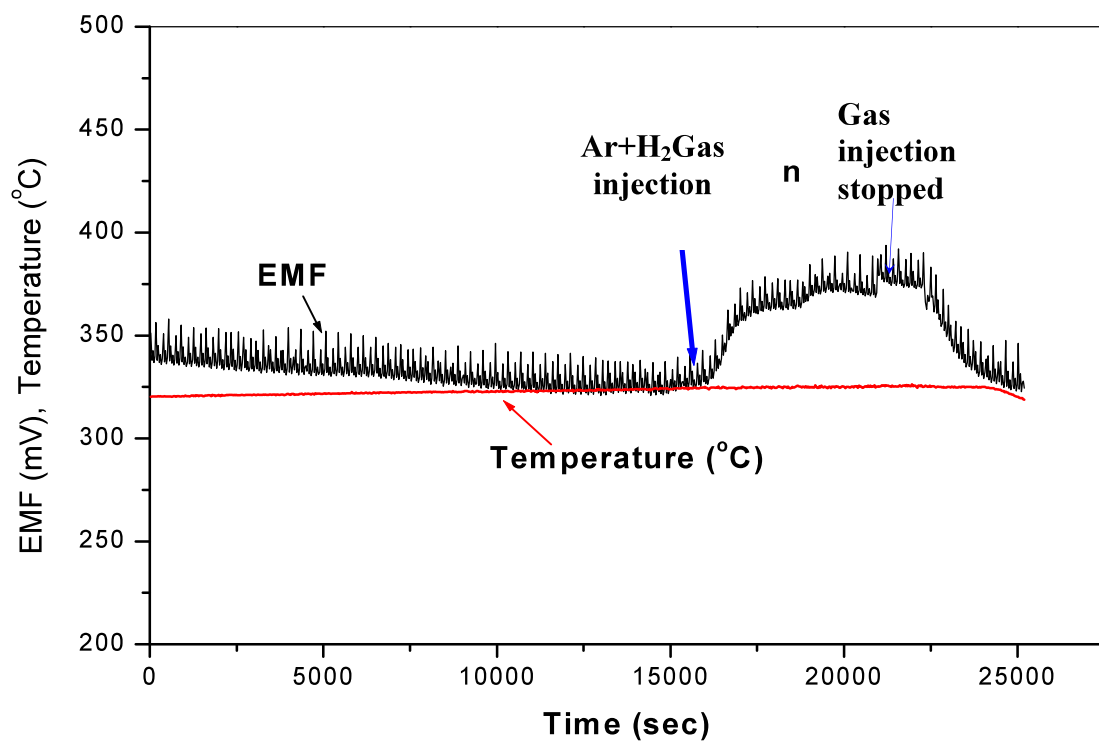


Fig. 3.12 Variation of temperature and EMF with time

The partial pressure of the dissolved oxygen decreases with decreasing concentration of oxygen in LBE. As per Eq (3.4), the EMF generated in the oxygen sensor is inversely proportional to the partial pressure of oxygen in LBE. So the EMF started increasing, as shown in Fig 3.12. When the Ar+H₂ gas bubbling is stopped the EMF reduces as the oxygen level in the LBE in the tank rises again by mixing with LBE of the loop.

3.4 SAFETY DESIGN ASPECTS OF THE LOOP

For safe operation of the loop, all possible events, during operation of the loop were to be envisaged and design of the loop should take care of these so that loop can be operated safely. Table 3.3 highlights the events of the loop that can occur during the operation and the design features of the loop to mitigate those..

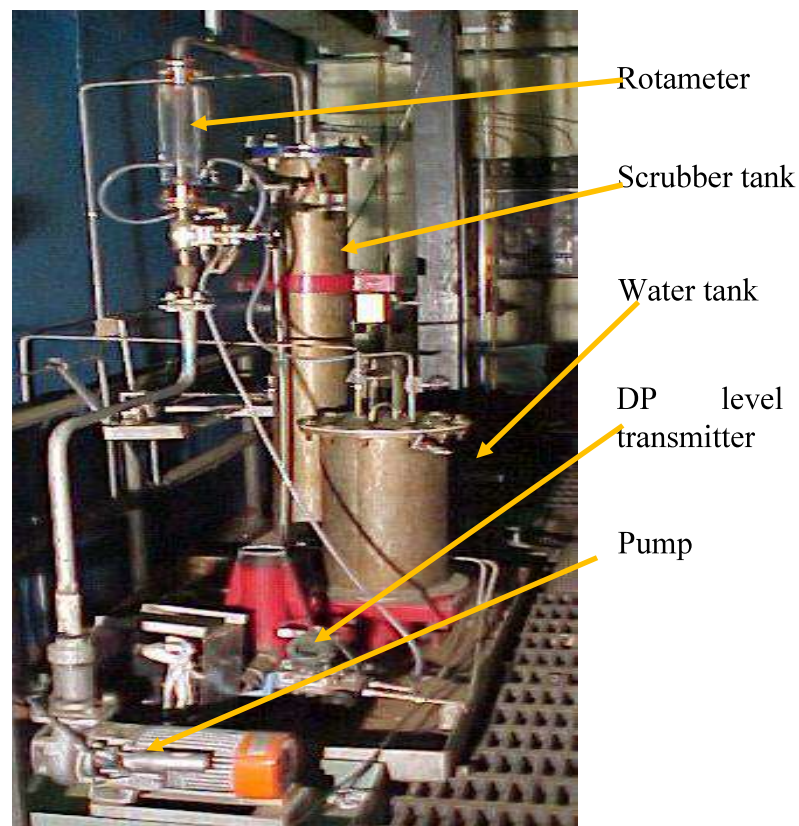


Fig 3.13 (a) View of the Argon gas scrubber of LML

For personnel safety also a ventilation system has been made to prevent any spread of lead fume or dust during any accidents. It was calculated that the equilibrium concentration of LBE vapour at 500⁰ C was 42.0x10⁻⁶ mg/litre [67], considering that the air in the operational area was stagnant i.e. it was not ventilated. This level is below the permissible limit (50-100 x 10⁻⁶ mg/Lit). However, the prevention of carrying fine LBE dust with the argon cover gas was ensured by providing high efficiency mechanical filter and scrubber at the exhaust of argon gas of the loop. The process flow sheet of scrubber system is shown in Fig 3.4. Fig 3.13 (a) shows the view of the system.

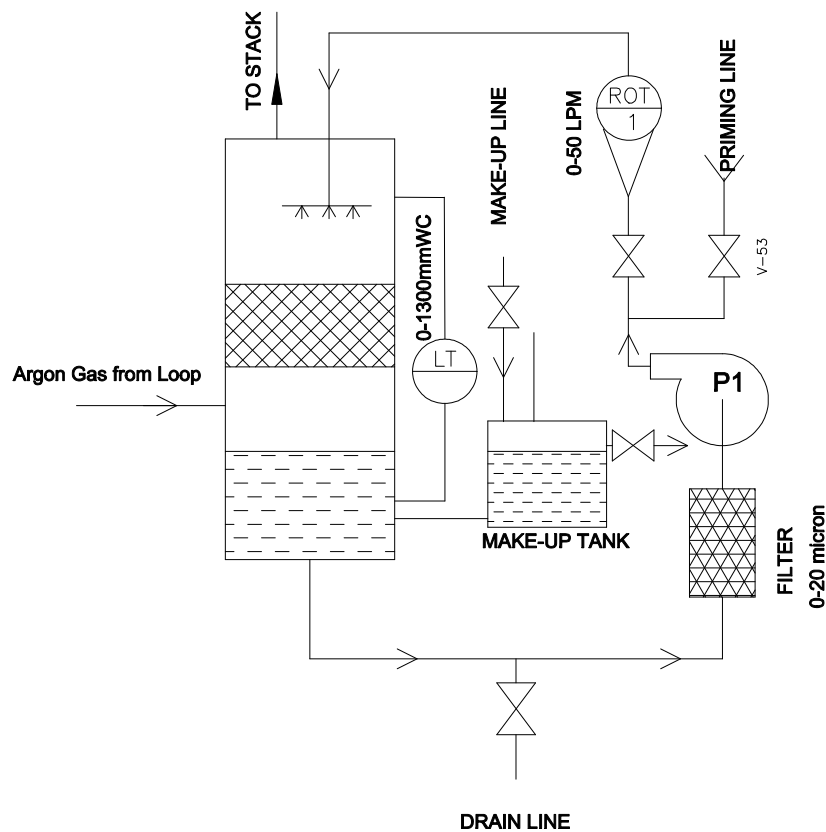


Fig 3.13 (b) P&I diagram of the Argon gas scrubber of LML

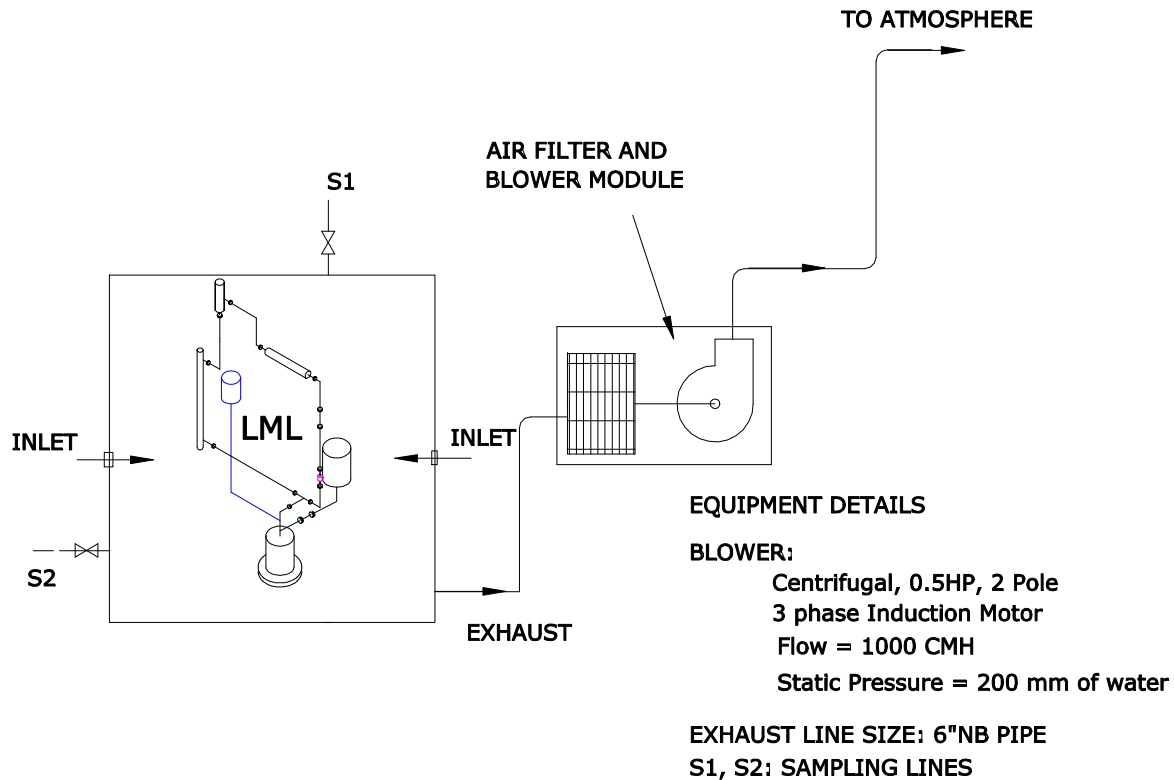


Fig 3.14 Schematic of the ventilation system with enclosure of LML

The P&I diagram of the set up is shown in Fig 3.13 (b). The whole loop was kept inside an enclosure. The enclosure was welded at the bottom with a MS plate on which the loop was installed. The pressure inside the enclosure was kept slightly negative with the help of blower and ventilation system. The air from the enclosure was passed through double-stage filtration system where the air was filtered to remove fumes and lead dust particles and the clean air was discharged to atmosphere. Figure 3.14 shows the schematic of the ventilation system of the loop.

3.5 CHARACTERISATION OF THE LOOP

3.5.1 Heat Exchanger Performance Analysis

The heat exchanger is a tube-in-tube type with an annular air gap between the primary and the secondary sides. The schematic of the heat exchanger is already shown in Fig 3.3. Air

is used as the secondary fluid for low power studies in the loop and water is used for higher power studies.

Table 3.3 Postulated events and measures for safety

SI No	Events	Action
1	Failure of power and air compressor to operate the pneumatic valves	In the event of Power failure, the heater will be tripped; subsequently valves were operated by opening the pneumatic bypass supply valve, to dump the molten LBE in the sump tank.
2	Temperature of the LBE at the outlet of heated section goes beyond normal operating temperature due to abnormal heater operation or failure of cooling water supply in the heat exchanger.	High temperature trip will be generated in the PLC, the heaters will be tripped, valves will be opened and LBE will be dumped in the sump tank.
3	Heater failure in the loop	When temperature at any location of the loop drops below 150°C, all the heaters will be tripped automatically and all the LBE will be dumped from the main loop.
4	Pressure rise in the sump tank.	The control valve for the argon gas supply will be closed. Relief valve was provided at the Argon exhaust line.
5	Decrease in pressure in the expansion tank	The Non Return Valve (NRV) was provided between the purge tank and scrubber to prevent the air ingress from the water scrubber. The control valve at the Argon exhaust line will be closed.
6	Overflow of LBE from expansion tank	A purge tank was provided in the exhaust line to collect LBE, which will avoid outflow of LBE from the loop.
7	Leakage of LBE from the loop	If there is any leakage in the loop, the level of LBE in the expansion tank will decrease. The decrease in level will prompt trip of the heaters in the loop and consequently the isolation valve will open to dump the LBE in the sump. Any spillage of the LBE will be accumulated in solid form on the tray provided at the bottom of the loop.

To find the air gap resistance, the heat exchanger was tested in a separate water loop, High Temperature and high pressure water Loop (HTL) which has maximum operating temperature and pressure of 270 °C and 70.0 bar. The secondary side of the heat exchanger is cooled by service water. Figure 3.15 shows the results of the tests. Since the radial gap is very small (~1mm), the gap resistance is modelled as the contact resistance for this heat exchanger. It can be seen that with contact resistance of $1.2 \times 10^{-3} \text{ m}^2 \text{ }^\circ\text{C/W}$, the prediction of the overall heat transfer coefficient matches well. So for the calculation of the overall heat transfer coefficient of the heat exchanger, the contact gap resistance is taken as $1.2 \times 10^{-3} \text{ m}^2 \text{ }^\circ\text{C/W}$. This contact resistance has been used for estimating the secondary side heat transfer coefficient of the heat exchanger when it is installed in the lead bismuth loop, which is required for the theoretical analysis.

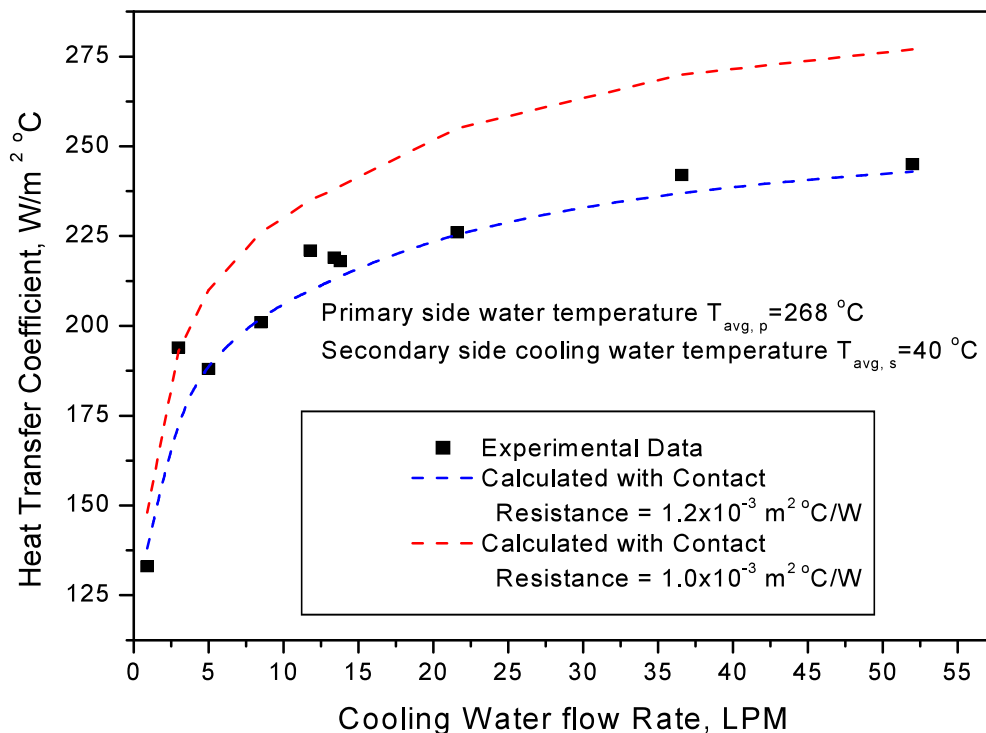


Fig 3.15 Test results of the heat exchanger in high temperature water Loop before installing in the LML.

After the test in HTL, the heat exchanger is installed in the lead bismuth loop. In the natural circulation experiments with LBE the overall heat transfer of the heat exchanger is found as,

$$U_o = \frac{Q_s}{A_o \Delta T_{ln}} \quad (3.7)$$

ΔT_{ln} can be found from the experimental data and Q_s is calculated as follows,

$$Q_s = W_s C_{ps} (T_{s,out} - T_{s,in}) \quad (3.8)$$

Considering the radial dimensions across the wall, as shown in Fig 3.16, the overall heat transfer coefficient in the heat exchanger is also given as,

$$\frac{1}{U_o} = \frac{r_o}{h_{in} r_{in}} + \frac{r_o \ln\left(\frac{r_o}{r_{in}}\right)}{k_{eff}} + \frac{1}{h_s} \quad (3.9)$$

The effective thermal conductivity, k_{eff} , across the wall thickness in the heat exchanger includes three parameters, the inside wall resistance, the gap resistance and the inner wall resistance of the water jacket. The value of k_{eff} is found as,

$$\frac{\ln\left(\frac{r_o}{r_{in}}\right)}{k_{eff}} = \frac{\ln\left(\frac{r_1}{r_{in}}\right)}{k_{in,w}} + \frac{R_{gap}}{r_1} + \frac{\ln\left(\frac{r_o}{r_1}\right)}{k_{o,w}} \quad (3.10)$$

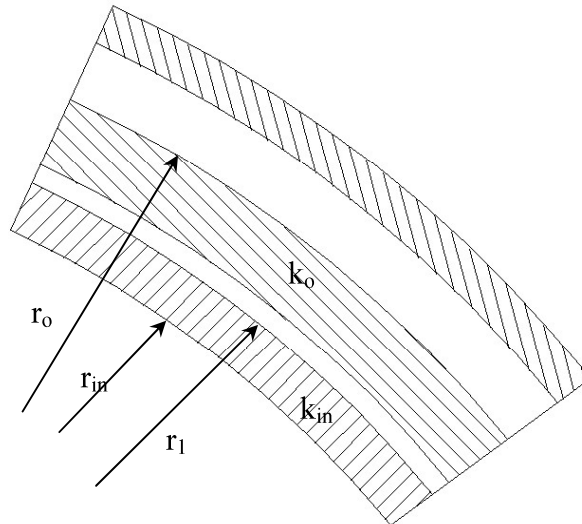


Fig 3.16 Radial dimensions considered [Eq (3.9) and Eq (3.10)] across the walls of the heat exchanger

After calculating U_o from Eq (3.7), h_{in} for LBE was calculated from the correlation given by Holman (1964) [129], k_{eff} from Eq (3.9) and h_s can be calculated from Eq (3.10). The value of h_s is required for theoretical simulation of natural circulation in the loop as discussed in chapter 6. The overall heat transfer coefficient U_o and ΔT_{in} of the heat exchanger are calculated for steady state natural circulation with different power levels and shown in Fig 3.17. In general it is seen that with air cooling in the secondary side, U_o is found to be lower than the cases with water cooling.

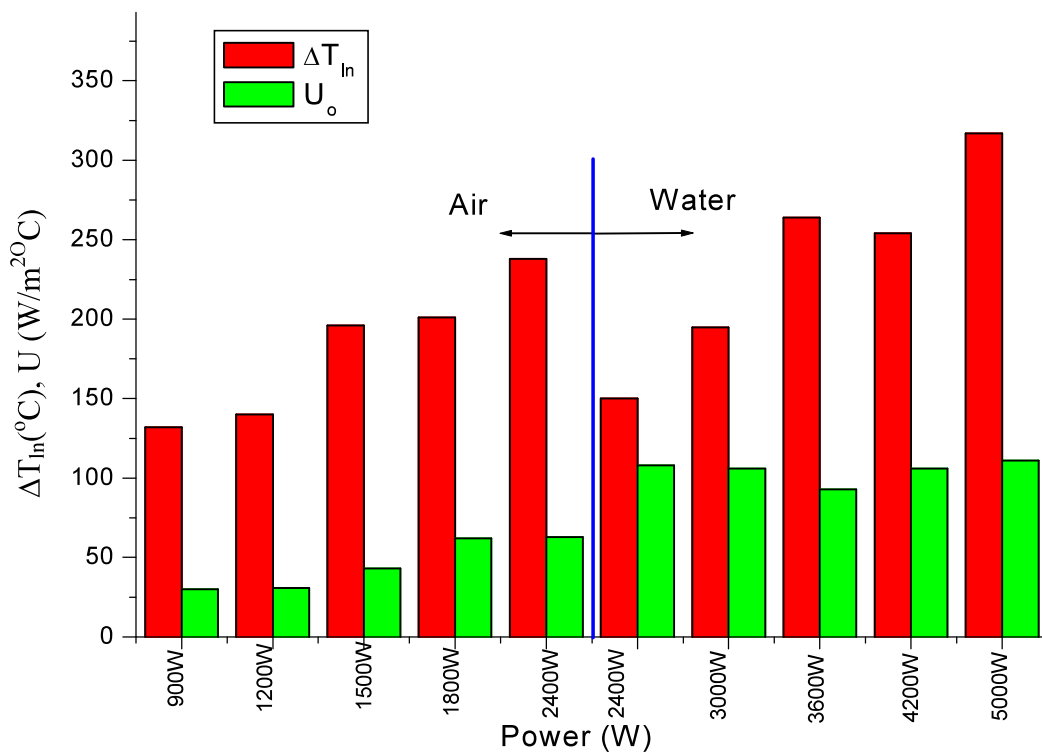


Fig 3.17 Variation of ΔT_{in} and overall heat transfer coefficient in the heat exchanger of the loop.

3.5.2 Heat Loss in the Loop

In ideal situation the heat should be removed only in the heat exchanger of the loop. But at high temperature the heat loss through the insulation could not be avoided in spite of providing sufficient insulation. The heat removed by the heat exchanger and heat loss in the piping is shown in Fig 3.18. The secondary side flow was kept in such a way that the heat

exchanger can remove maximum possible heat from the LBE. At the same time the temperature at the heat exchanger outlet was monitored so that the LBE does not solidify in the heat exchanger due to over cooling. Up to 2400 W, air has been used as the working fluid in the secondary side. Above this power the heat loss in the piping increases as the effectiveness of the heat exchanger does not increase with power. So, heat exchanger was cooled by water when the main heater power was more than 2400 W. The water was preheated before entering the heat exchanger for power from 2400 W to 3600 W to avoid solidification in the primary side. At higher power the heating was not required. It can be seen that the heat loss through the piping was much low in spite of the high power levels in the loop. This was due to the increase in effectiveness of the heat exchanger with water cooling in the secondary side.

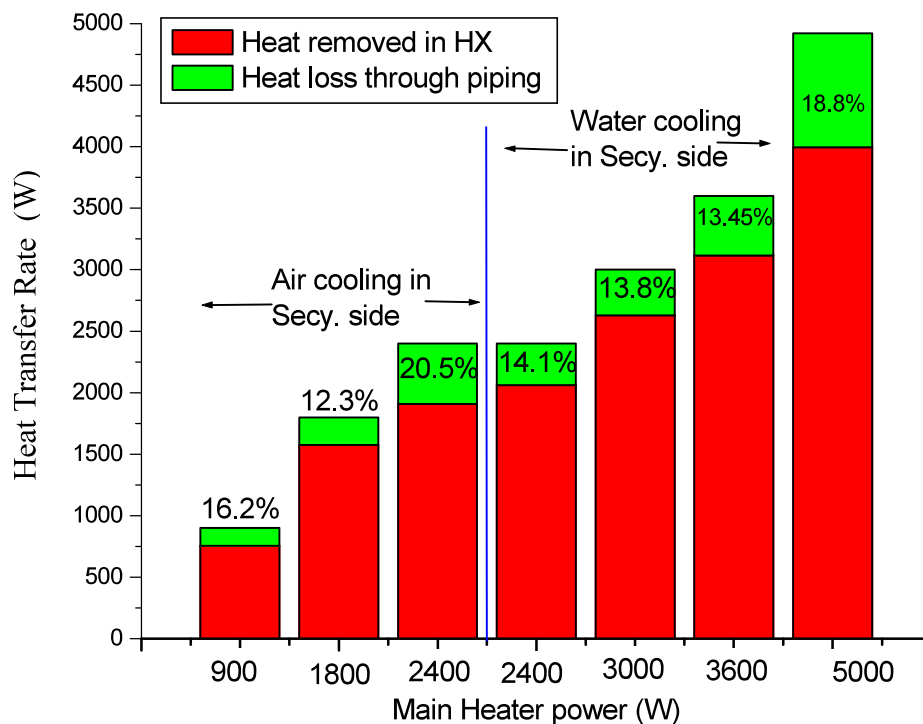


Fig 3.18. Heat removed by the heat exchanger and heat loss in the loop piping in LML.

3.5.3 Experimental Test Matrix in the Loop

A number of steady state and transient natural circulation experiments were carried out for different power levels with air and water as the secondary fluids. The experimental test matrix is shown in Table 3.4. The results of the experiments were discussed in the next section.

Table 3.4 Natural circulation test matrix of the Liquid Metal Loop

SI No	Experiments	Power	Secondary side fluid	Avg. loop temperature
1.0	Steady state:			
1.1		900 W to 2400 W	Air	250 to 350 °C
1.2		2400W to 5000W	Water	350 to 500 °C
2.0	Transient			
2.1	Start up experiment	At 1200W, 1500W, 1800W, 2400W and 3000W	Air	250 to 375 °C
2.1.1		For 3000W power, water was used as the secy fluid	water	350 °C
2.2	Heat sink loss	At heater power 2400W	Air	400 °C
2.3	Step change in heater power			
2.3.1	Step power up	1500-1800-1500W	Air	320 °C
2.3.2	Step power down	2100-1200-1800W	Air	275 °C
2.4	Secondary side coolant flow effect			
2.4.1	Step rise of coolant flow rate	200-320-200 LPM at 1500 W	Air	280 °C
2.4.2	Step down of coolant flow rate	320-100-320 LPM at 2280 W	Air	350 °C

3.6. Operation of the Loop

Following steps are followed during operation of the loop

1. Before operation of the loop, the leak test of the whole loop was done by pressurising the loop with air up to the operating pressure ($\sim 2.0 \text{ kg/cm}^2$). The pressure drop of the pressurised loop was monitored for 30 minutes. If the drop in pressure is less than 20% of the initial value the loop is considered to be sufficiently leak proof.

After the leak test the loop was evacuated to take out air from the loop, with the help of vacuum pump, up to 0.25 bar-abs. Then refilled with argon gas and pressurised to 0.5kg/cm². The loop was again evacuated to 0.25 bar-abs.

2. This cycle was then repeated for 4 times. After that the loop is filled with argon and 0.2 bar pressure is maintained in the loop.
3. Solid ingots of the LBE of required quantity was filled in the melt tank and melted by raising melt tank temperature to 200°C. The solid oxide layer from the LBE free surface was removed mechanically. Personal safety was maintained by following safety guide lines provided by LBE Handbook (2007) [67]. The melt tank was then closed and Ar+H₂ gas was bubbled to remove the dissolved oxygen gas from LBE.
4. The whole loop was then heated with trace heater and maintained at 300°C for 8 hours. This long heating time ensures maintaining the whole loop temperature well above the melting point of LBE. After that the valve between the melt tank and the sump was opened to drain the LBE from the melt tank to the sump.
5. The LBE coolant in the sump tank was then pressurized by argon gas system. Due to pressurization molten LBE flows into the loop and subsequently fills up the loop. After filling the loop up to a required level in the expansion tank, the loop was isolated from the sump tank by a valve.

6. The main loop power is increased and the cooling air flow in the secondary side of the heat exchanger is started. Natural circulation of LBE takes place in the loop due to heating of the LBE in the heated section and cooling in the heat exchanger.
7. Adequate care has been taken to prevent contact of air with the molten LBE to avoid formation of insoluble metal oxide which may block the piping of the loop. The oxygen level in LBE was monitored and if the level of O₂ goes above the prescribed limit Ar+H₂ gas mixture is directly purged in LBE at the expansion tank.
8. Experimental studies at different temperatures and power were carried out by controlling the main heater power and the secondary flow rate in the heat exchanger. The loop temperature was maintained between 200 to 500 °C during the experiments. If the temperature of the loop goes beyond this range all the LBE will be dumped after opening the isolation valve and the heaters will be tripped automatically.
9. After the experiments or in case of any anomaly in the loop, it was shut down. To shut down the power of the main heater and the secondary side coolant flow was reduced to zero. Then the valve between the main loop and the sump was opened. Care was taken that the argon pressure in the expansion tank was maintained at least 1.2 bar-absolute, so that air ingress during the dumping of LBE is avoided.
10. After dumping if the loop is to be shut down for a long time, all heaters were switched off and natural cooling of LBE was allowed. Positive argon gas pressure is maintained in the loop till the LBE is solidified and loop temperature comes down below 100 °C.

3.7. Results and Discussions

3.7.1 Steady State Analysis

In the steady state natural circulation experiments, the loop was allowed to reach steady state conditions at different heater powers. The mass flow rate in the loop was estimated from the heater power and the temperature difference between the inlet and outlet of the heated section. For heater power 900 W to 5000 W the flow was found to be varying from 0.095 kg/s to 0.135 kg/s. Figure 3.19 shows the variation of calculated mass flow rate with heater power. It can be seen that as the loop power increases mass flow rate also increases. The steady state natural circulation results are also given in tabular form in Appendix 4.4. For steady state natural circulation, Vijayan (2002) [3] showed that the flow in single phase uniform or non-uniform diameter natural circulation loops can be expressed as,

$$\text{Re}_{ss} = c \left(\frac{Gr_m}{N_G} \right)^r \quad (3.11)$$

Where, constant ‘ c ’ and ‘ r ’ depends upon the nature of flow (i.e., laminar or turbulent). Parameter N_G depends on geometry of the loop and the details of Eq (3.11) is given in Chapter 2. Re_{ss} and Gr_m are based on the reference diameter.

Figure 3.20 shows the comparison of the correlation with the experimental data for the present loop. At low flow the correlation under predicts by 17% maximum, whereas at higher flow it over predicts the experimental results by 13%. The comparison with other correlations available in literature is discussed in Chapter 4. The temperature distributions over the whole length of the loop at 2400 W power are shown in Fig 3.21 (a) and Fig. 3.21 (b). Figure 3.21 (a) shows temperature distribution with air as the secondary side fluid. The increase in air temperature in the secondary side of the heat exchanger was much higher compared to the drop in LBE temperature in primary side due to lower heat capacity of air. The minimum temperature of the loop was around 300 °C. Figure 3.21 (b) shows the axial

variation of temperature with water cooling in the secondary side. The axial variations in temperature in the heat exchanger were approximately same in the both sides. With the water cooling, the minimum temperature of the loop was found to be 235 °C. Hence it is evident that as a coolant, water is better than air in this case.

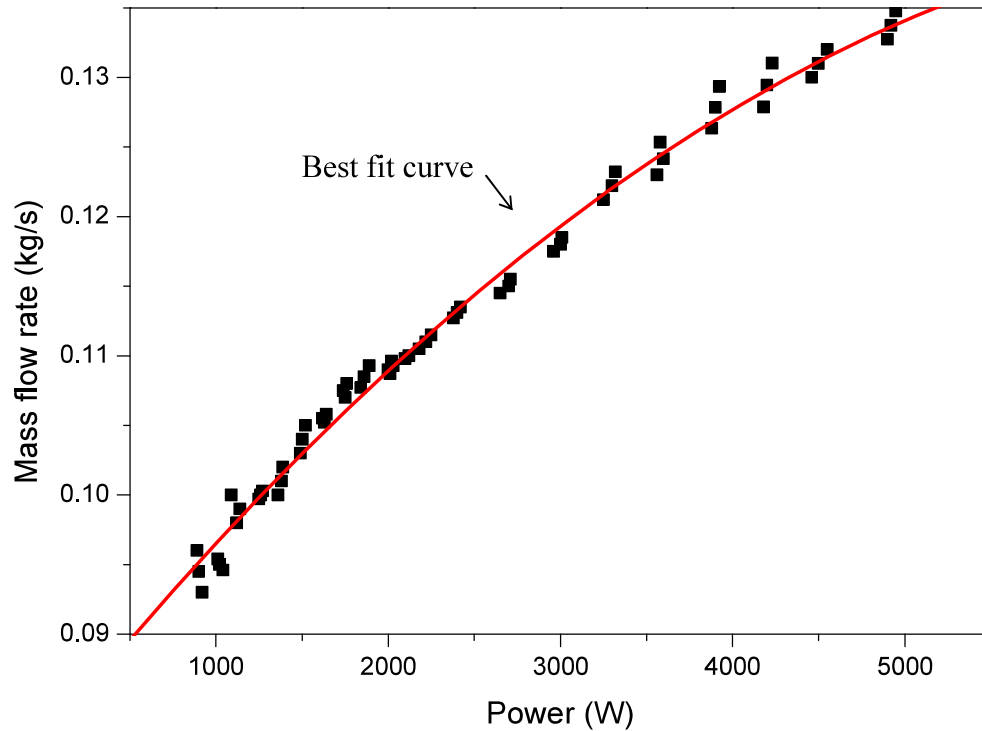


Fig. 3.19 Calculated mass flow rate during steady state natural circulation at different power levels

But water was to be at higher pressure so that it remains in single phase even at temperature above the melting point of LBE. In both the figures steady rise in temperature could be seen in the heated section of the loop. In the piping there was small temperature drop due to heat loss through the insulation. The temperature drop in the expansion tank was found to be more than other parts of the piping because of the heat loss from vessel wall, flanges, gas purging lines, oxygen sensor fittings, etc.

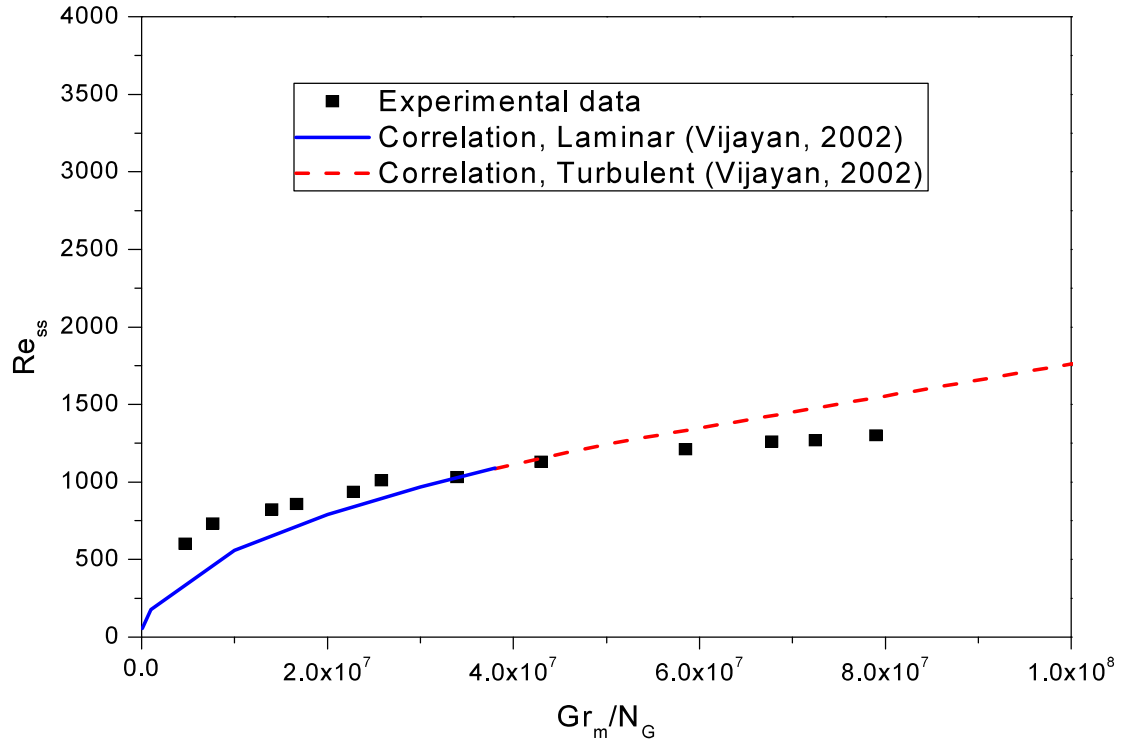


Fig. 3.20 Comparison of steady state correlation [Eq. (3.9)] with experimental data.

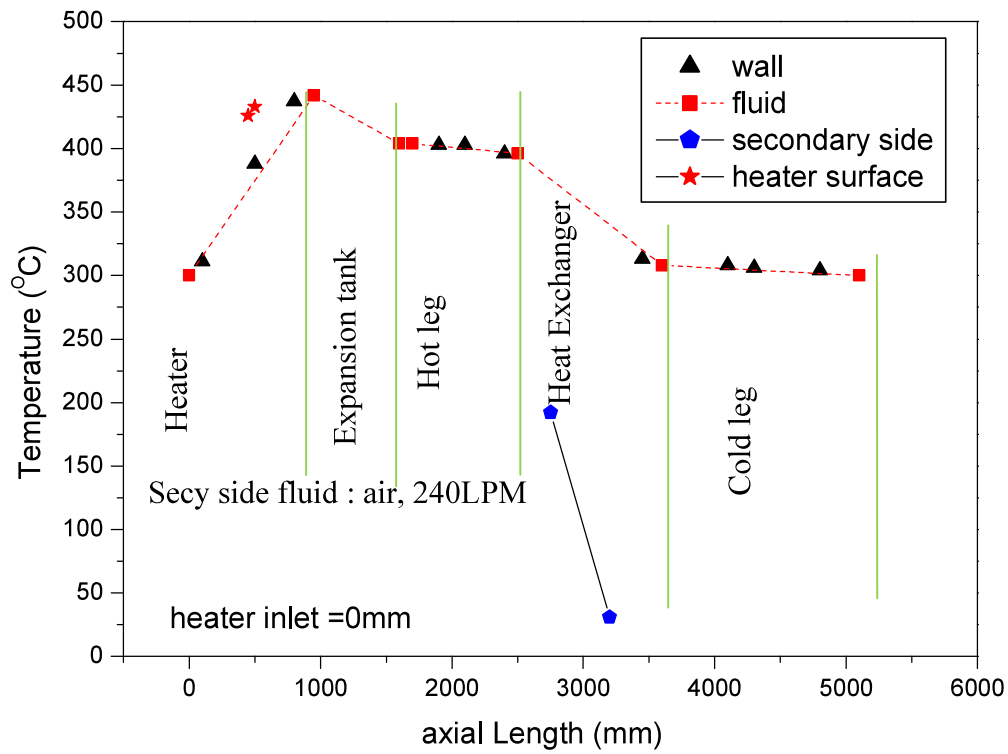


Fig. 3.21(a) Steady state temperature distribution along the length of the loop at main heater power= 2400 W with air as the secondary side coolant.

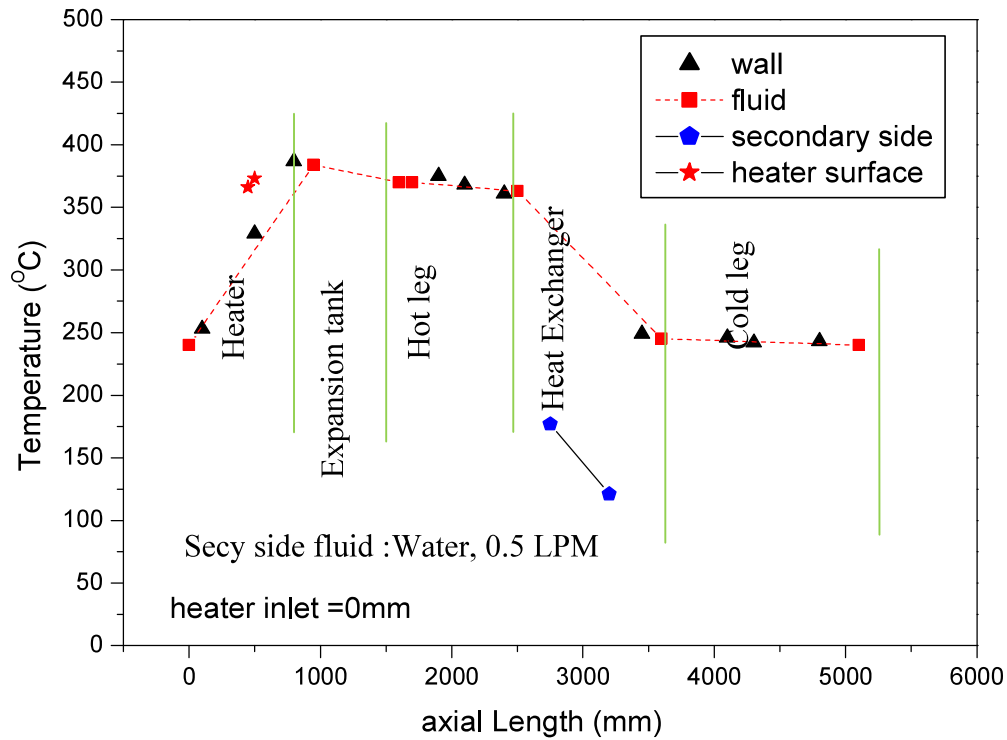


Fig. 3.21(b) Steady state temperature distribution along the length of the loop at main heater power= 2400 W with water as the secondary side coolant

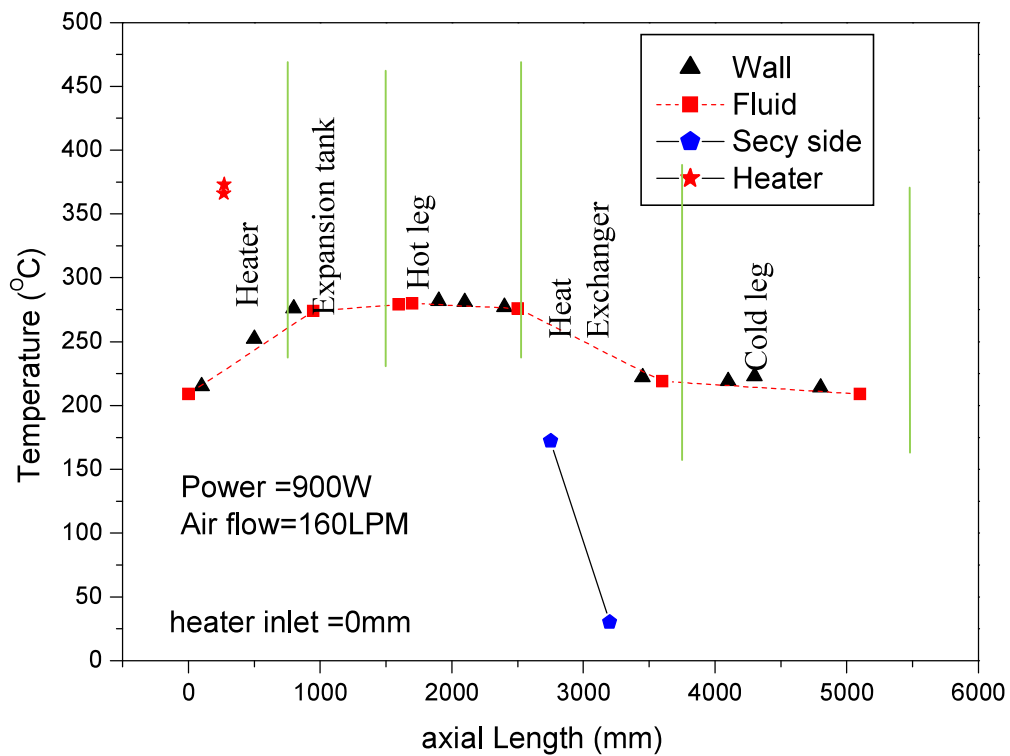


Fig 3.22(a) Steady state axial temperature distribution of the loop at 900 W power

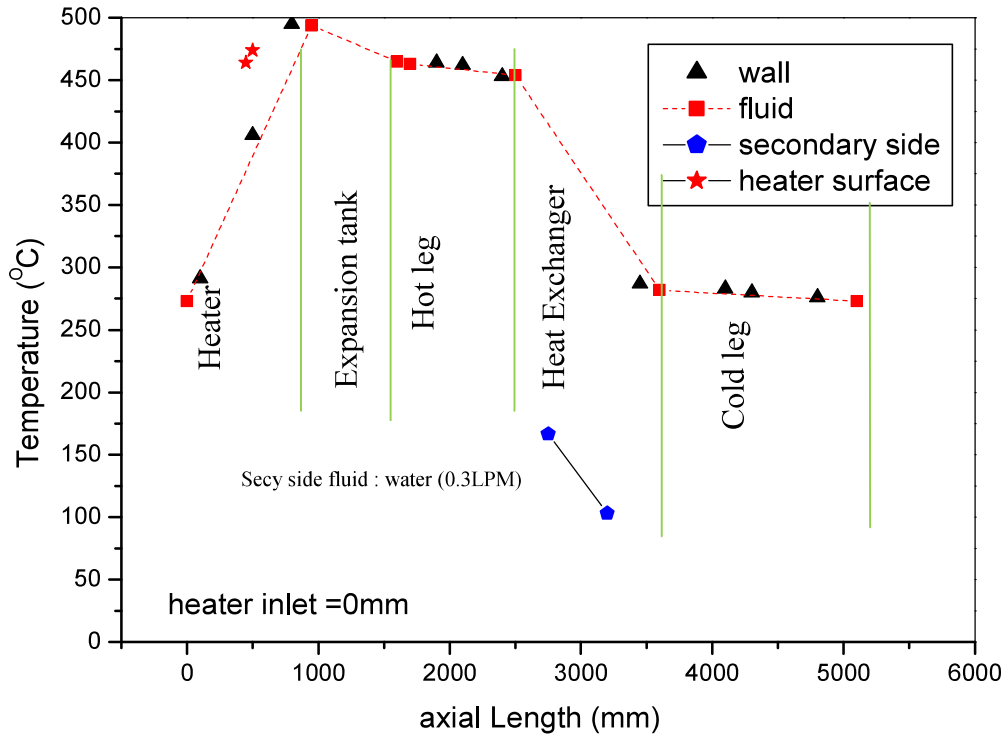


Fig 3.22(b) Steady state axial temperature distribution of the loop at 4200 W power

Figure 3.22 (a) shows the axial temperature distribution in the loop at 900 W power with air cooling in the secondary side of the heat exchanger. The temperature difference between inlet and outlet of the heater was found to be 67 °C. Figure 3.22 (b) shows the axial temperature distribution for power of 4200 W with water cooling. The temperature difference between the heater section inlet and outlet in this case was found to be 220 °C. Hence in case of natural circulation, the higher temperature gradient in the loop at high power was observed which was needed to generate higher buoyancy driving force so that it can overcome the hydraulic resistance offered by LBE at higher flow rate. The heater surface temperatures which were given by two thermocouples located at around 2/3rd of the axial length of the heater from inlet were also shown in Figures 3.21 and 3.22.

3.7.2 Transient Studies

Transient studies were carried out to simulate some postulated accident scenario in the reactor. The main objective was to observe the LBE behaviour during various transient conditions. The transient experimental studies include start-up of the loop from near stagnant conditions, loss of heat sink and step power change.

3.7.2.1 Start-up operation

Start-up operation from near zero flow condition for various power levels was carried out. Here, the start up at main heater power levels of 1200 W, 2400 W and 3000 W have been discussed. Initially, the steady state of natural circulation of LBE was achieved by maintaining same operating conditions for long time. Then the main heater was put off and secondary side air flow in the heat exchanger was stopped. The cold leg temperature slowly increased to the hot leg temperature by starting the trace heaters in the cold leg. In this way, near no flow condition was achieved by reducing the LBE temperature differences across the heated section and heat exchanger near to zero. After achieving near zero flow condition, all the trace heaters were put off and main heater was put on. The secondary side air flow in the heat exchanger was started. The temperature variation in the heated section outlet and heat exchanger outlet was observed till steady state condition was achieved. Figure 3.23 (a) shows the temperature variation at the outlets of the heated section heat exchanger for 1200 W power. Here the driving force of the LBE circulation was the buoyancy force developed due to temperature difference created between hot leg and cold leg in the loop. At initial stage the LBE starts to flow from stagnant condition. Due to initial low flow, temperature at the heated section outlet rises. As the flow approaches steady state the temperature reduces and stabilises. The peak temperature achieved during this start up experiment was 318 °C which was 10.0 % higher than the steady state temperature (~290 °C).

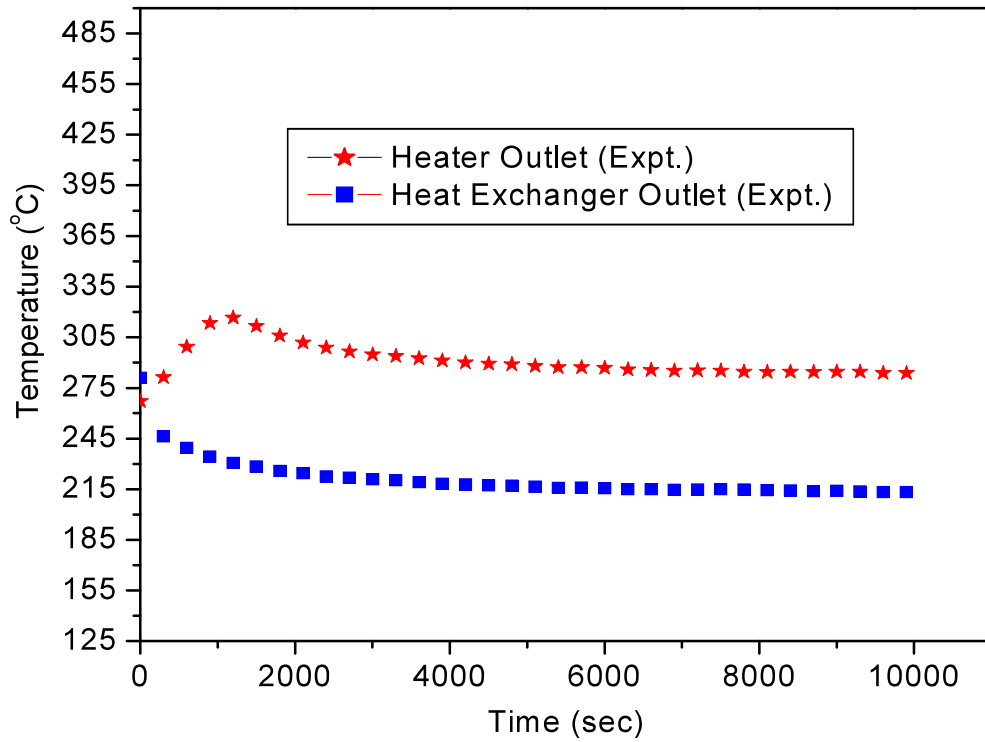


Fig. 3.23 (a) Temperature variation at outlets of heater and heat exchanger during start-up of the loop from near stagnation condition with Power 1200 W.

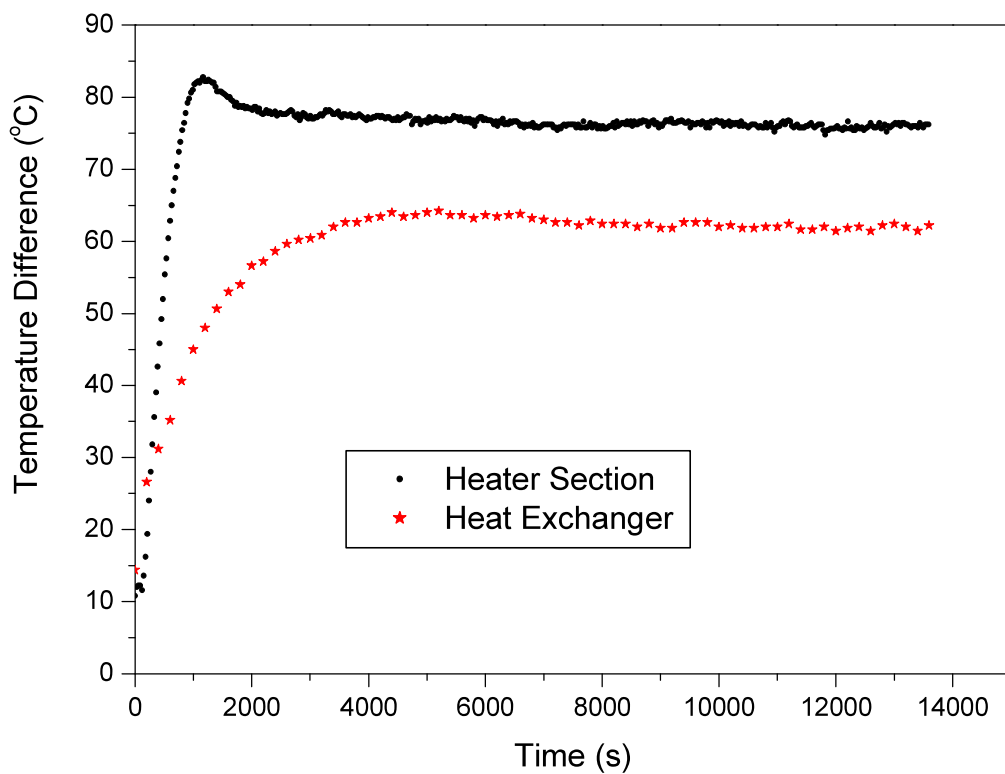


Fig. 3.23 (b). Temperature difference across the heater section and heat exchanger during start-up of the loop from stagnation condition at Power 1200 W.

It can be seen from Fig 3.23(a) that the heat exchanger outlet temperature decreases rapidly and stabilises after some time. Due to initial low flow of LBE, the heat exchanger cools down the LBE drastically. But as the flow increases, further fall in the temperature reduces. It can be further seen that the temperature stabilises smoothly after sometime. Figure 3.23 (b) shows the temperature difference across the heater section and heat exchanger for 1200 W power experiment. It could be seen that the steady state temperature difference is reached across the heater section more quickly than that of the heat exchanger section. Figure 3.24 (a) shows results for 2400 W power level.

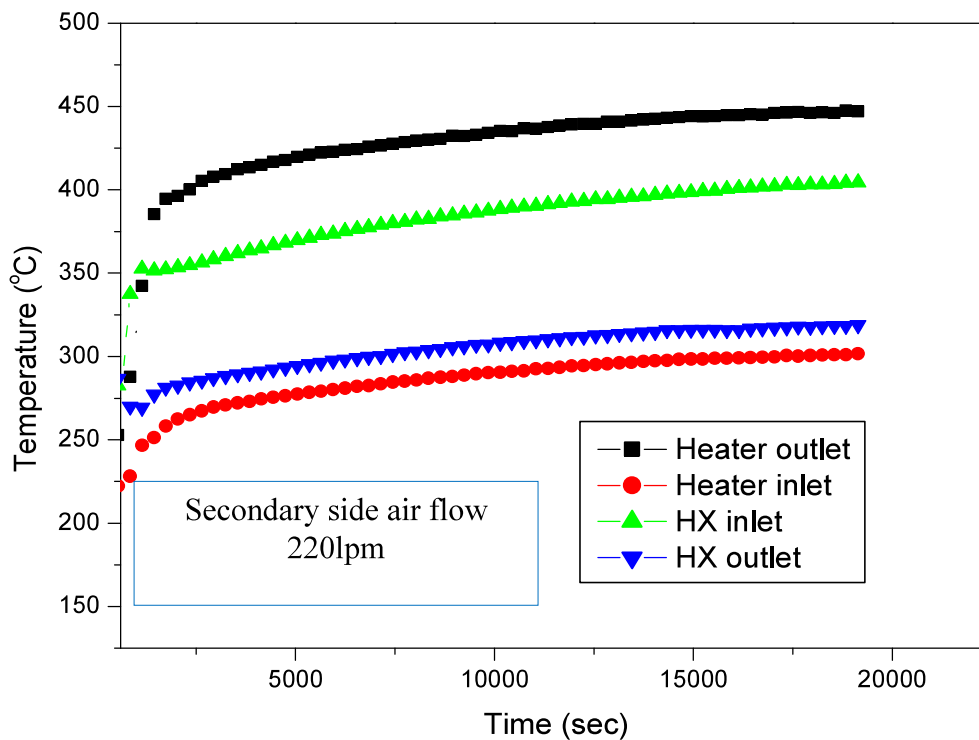


Fig. 3.24 (a) Temperature variation at outlets of heater and heat exchanger during start-up of the loop from stagnation condition at power 2400 W.

Here the initial LBE temperature in the heat exchanger was lower than the steady state temperature. From Fig 3.24 (b) it can be seen that the temperature difference in the heat exchanger reaches steady state more quickly than the 1200 W power experiment. So the initial temperature value, especially in the heat exchanger is important for the time required

to reach steady state during start up experiment. Figure 3.25 (a) shows the temperature variation in the loop for 3000 W power with 0.3 lpm cooling water flow rate in the secondary side. The heat exchanger outlet temperature drops drastically during initial moment due to low flow rate of LBE in the primary side and high heat removal rate in by water flowing in the secondary side. After 35000 s, oscillation in the heat exchanger outlet temperature was observed, which was due to the local boiling of the cooling water in the secondary side. The water flow was increased marginally after 52000 s in the secondary side which caused the disappearance of oscillation, but increase in water flow rate caused decrease in temperature of the LBE.

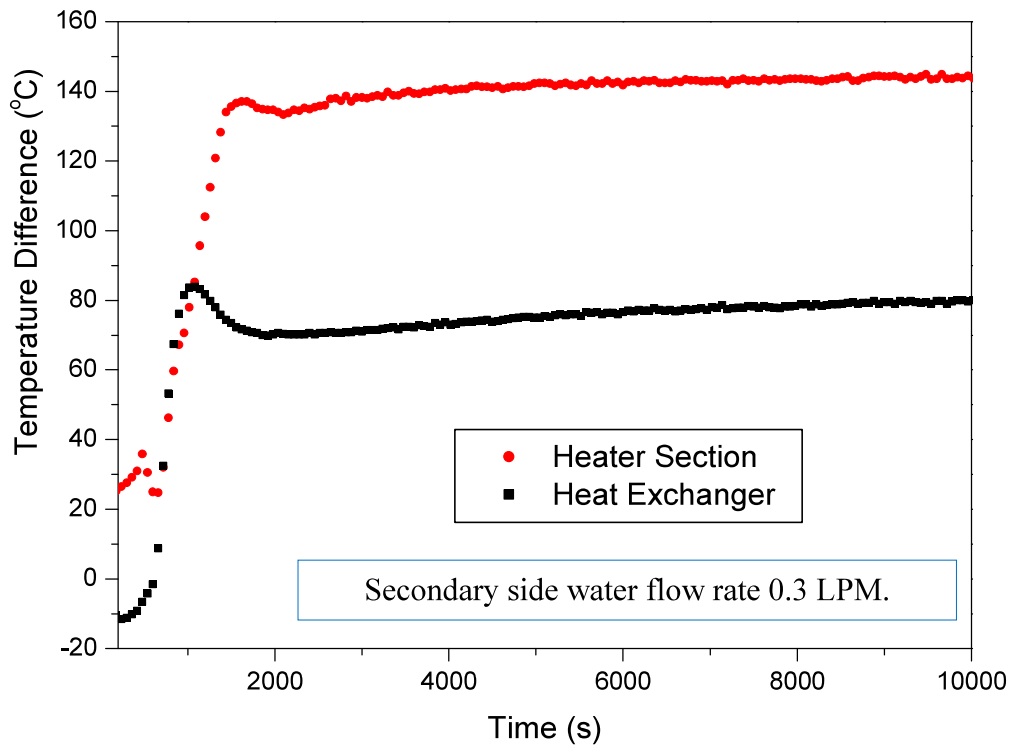


Fig. 3.24 (b) Temperature difference across the heater section and heat exchanger during start-up of the loop from near stagnation condition at Power 2400 W.

Fig 3.25 (b) shows that the steady state temperature difference in the heater section is reached more quickly than the previous two cases. This is due to high heat removal rate of water during the experiment. In the heat exchanger the steady state temperature difference is

achieved more slowly than that of the heater section. The initial decrease in LBE temperature in the heat exchanger caused the delay in achieving the steady state.

As shown in Fig 3.24 (b), it was found that the time to start the natural circulation in the loop were 240 s for power 3000 W. The time required to start natural circulation for power 1200 W and 2400 W were found to be 600 s and 400 s, respectively. So it can be inferred that higher the power, lesser was the time required to start natural circulation. More discussions on the start-up of natural circulation and its theoretical validation are done in chapter 6.

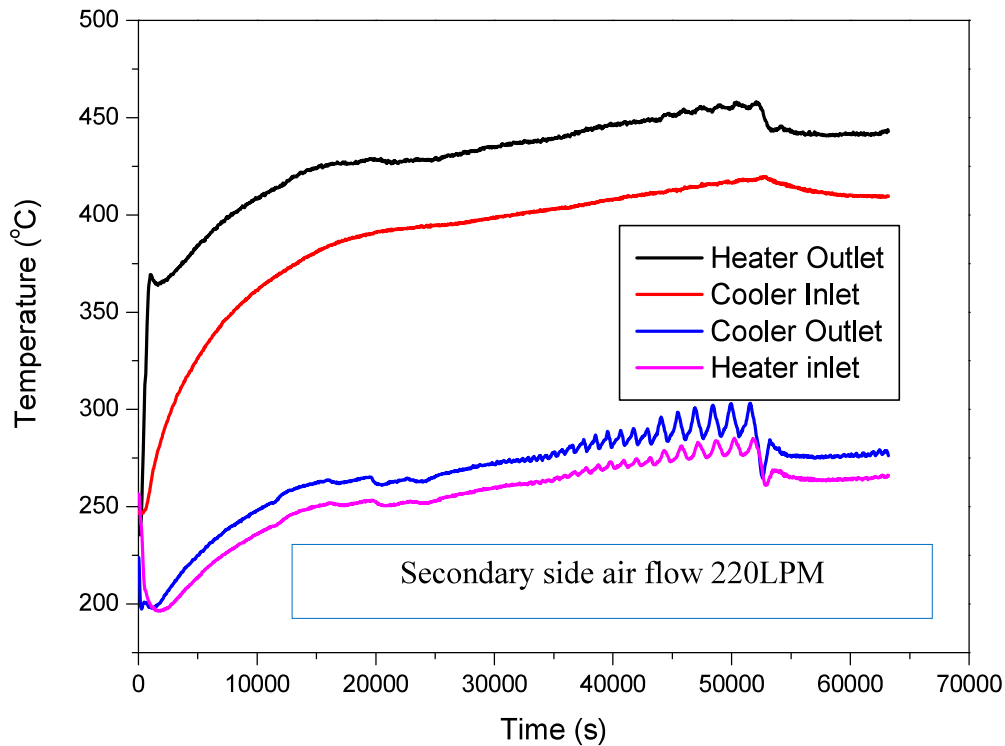


Fig 3.25 (a) Temperature variation at outlets of heater and heat exchanger during start-up of the Loop from near stagnation condition at 3000 W power.

3.7.2.2 Loss of heat sink

The loss of heat sink was considered in the safety analysis of the reactors and good prediction was necessary to ensure safe plant operation. Here the experiments with 2400 W power levels were discussed. To start the experiment the loop was started and a steady state

was established. After achieving steady state, secondary flow in the heat exchanger was stopped completely at $t=24000$ s. Due to the inability of the liquid metal to dispense its heat, the steady state was disturbed and the temperatures of the loop began rising. Figure 3.26 (a) shows the rise in temperature at inlet and outlet of heated section during the heat sink loss experiment with loop initial power of 2400 W. Whereas Fig 3.26 (b) shows the variation of inlet and outlet temperature in the heat exchanger.

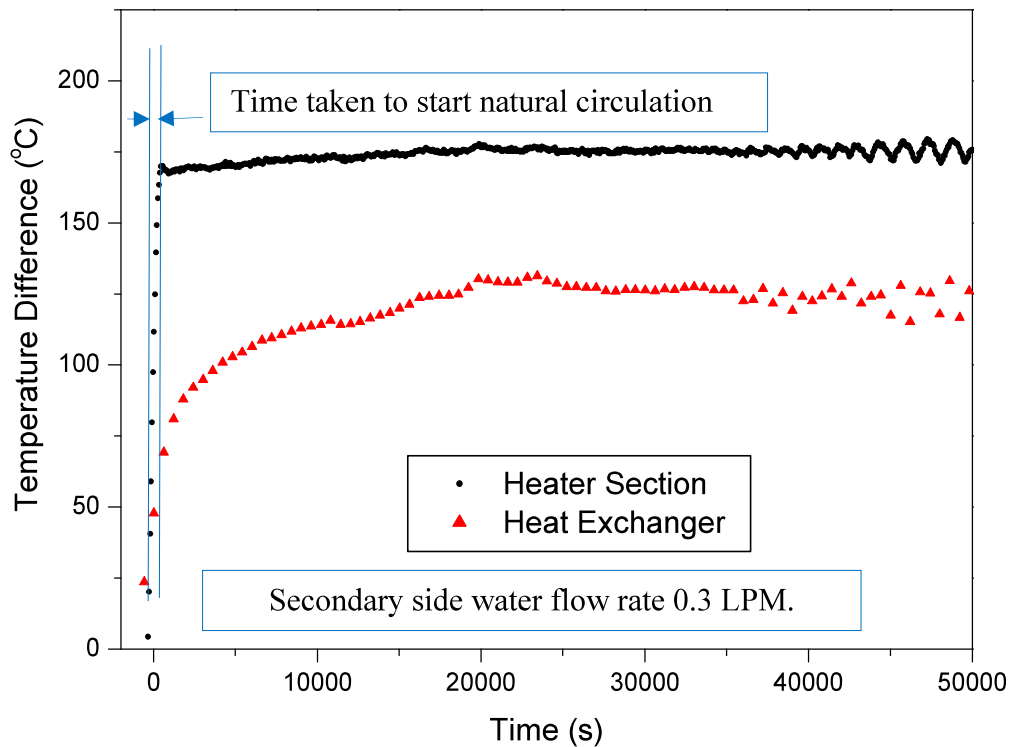


Fig 3.25 (b) Temperature difference across the heater section and heat exchanger during start-up of the loop from stagnation condition at 3000 W power.

Here despite the absence of the cooling by secondary flow, the LBE temperature difference between the inlet and outlet of the heat exchanger was maintained at significant value. To study it in detail, the temperature difference in the heater section and the heat exchanger are plotted along with the secondary side inlet and outlet temperatures during the experiments, for two power levels 1200 W and 2400 W and shown in Fig 3.27 (a) and (b). In both cases it can be seen that the temperature at inlet of the secondary side of the heat exchanger has

increased and the outlet temperature is decreased due to the stopping of the air flow. But the temperatures remained well below 100 °C, due to which the heat removal is continued although at reduced rate even for a long time and hence natural circulation in the loop is continued. It is observed that that due to the loss of heat sink the temperature of the loop increased. So this transient has prominent effect in most part of the loop.

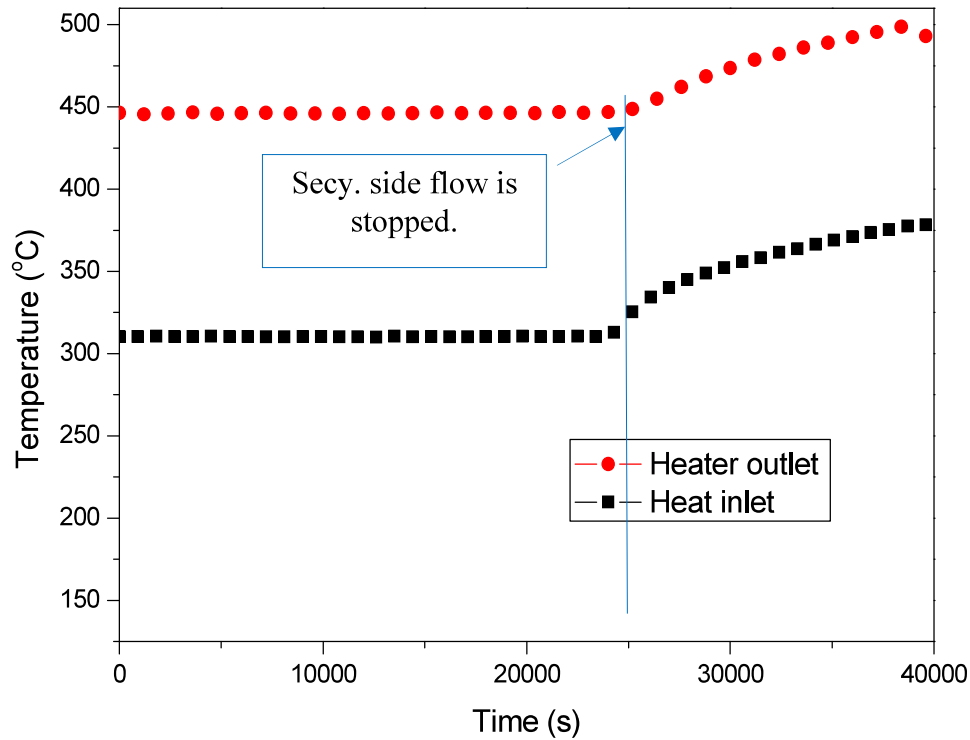


Fig. 3.26 (a). Variation of inlet and outlet temperature of heated section during the simulation of loss of heat sink with initial steady state power 2400 W.

3.7.2.3 Step change in heater power

Effect of step change in main heater power has been studied in the loop. Initially the loop was operated at 2100 W power level at steady state. The power was decreased to 1800 W for at 7000 s and stepped up back to 2100 W. The effect of this power change was shown in Fig. 3.28 in terms of change in temperature. In the heater section, the step change could be clearly seen.

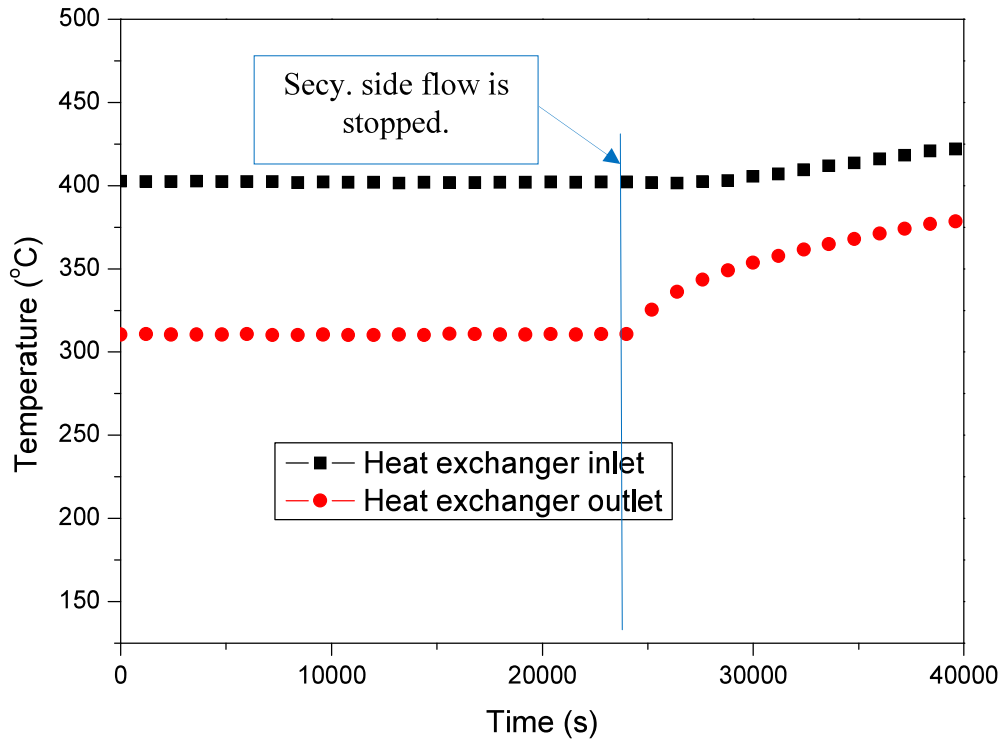


Fig. 3.26 (b). Variation of inlet and outlet temperature of heat exchanger during the simulation of loss of heat sink with initial steady state Power 2400 W.

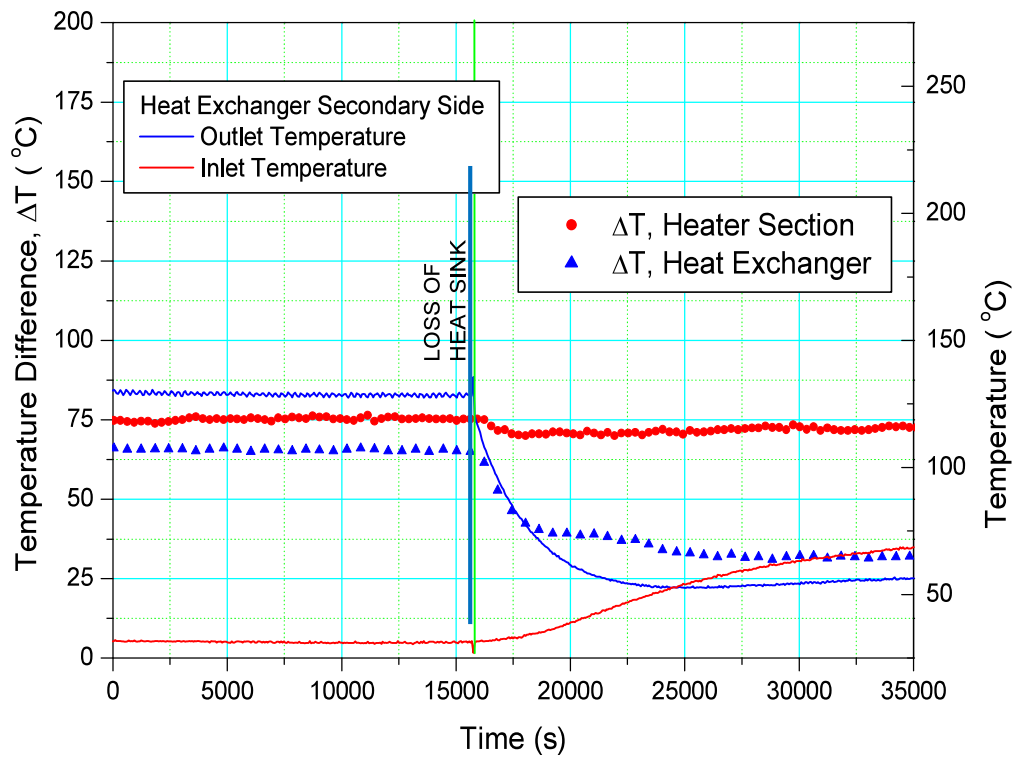


Fig. 3.27 (a) Variation of the difference of LBE inlet and outlet temperature of heated section and heat Exchanger, during the simulation of loss of heat sink with initial steady state Power 1200 W.

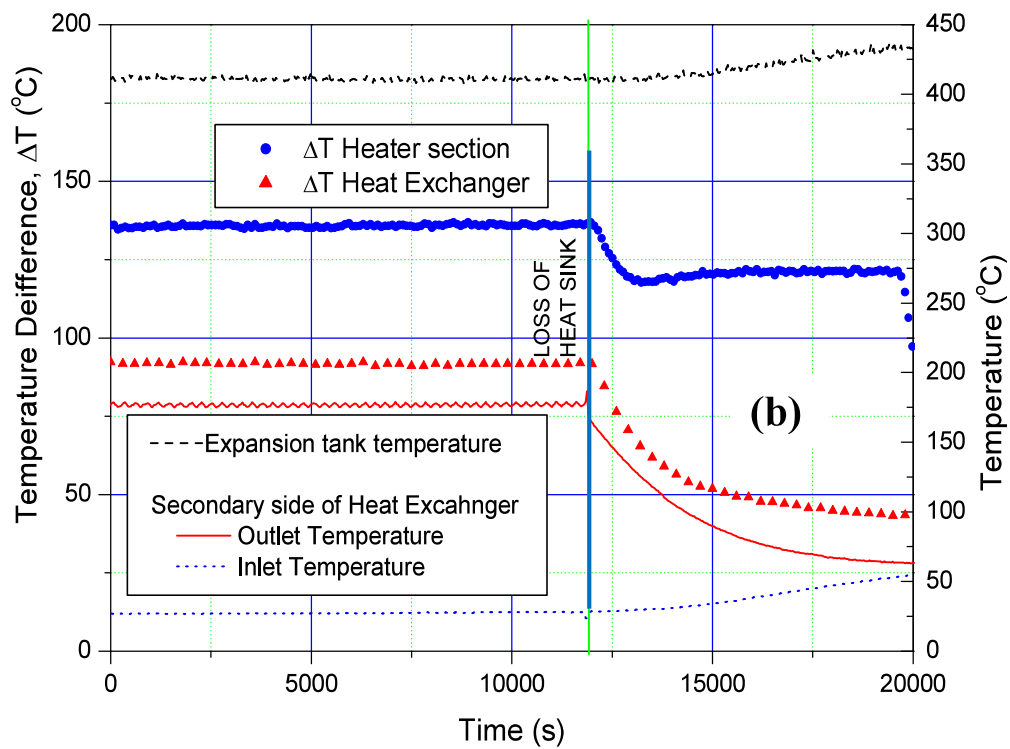


Fig. 3.27 (b) Variation of the difference of LBE inlet and outlet temperature of heated section and heat exchanger, during the simulation of loss of heat sink with initial steady state Power 2400 W.

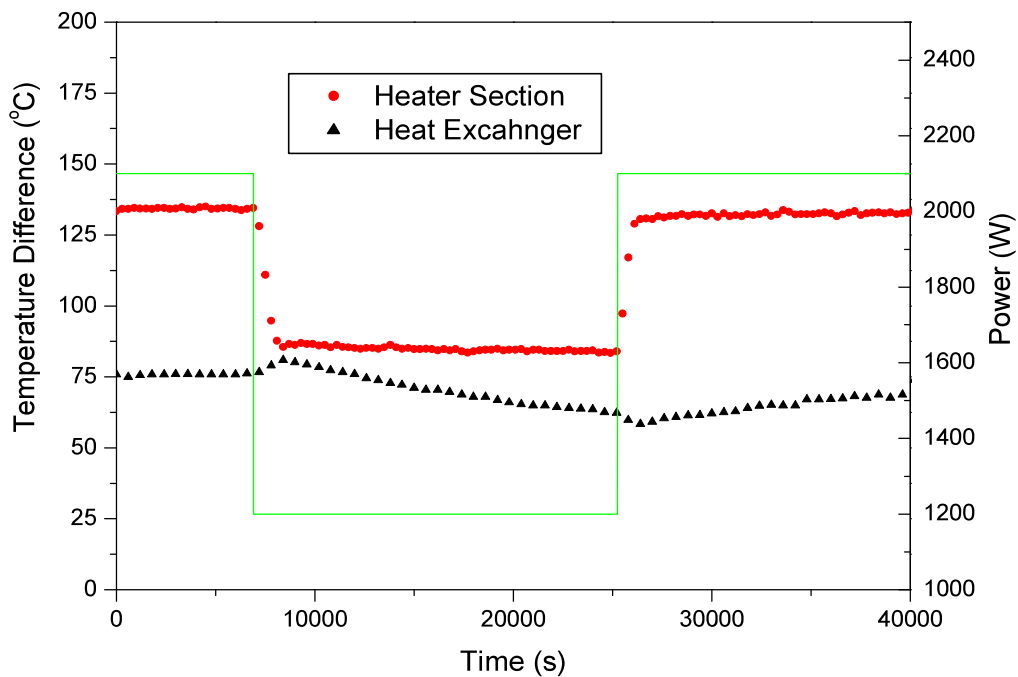


Fig. 3.28 Variation of temperature difference in LML during step change in power 2100 W-1200 W-2100 W.

The power rise leads to decrease in temperature difference across the heater section from 135 °C to 85 °C in 1270 s. It remained at this value till the power is restored to 2100 W. To reach the temperature difference 135 °C, it took 1030 s. In the heat exchanger initially the temperature difference has increased, which is due to the reduction in natural circulation flow caused by the step power reduction. But it is slowly reduced because of the reduction in temperature of LBE in the heat exchanger. When the power is restored to 2100 W the increase in the temperature difference is much slower than the heater section. This is because of the high inventory in the expansion tank which takes long time to regain the initial LBE temperature.

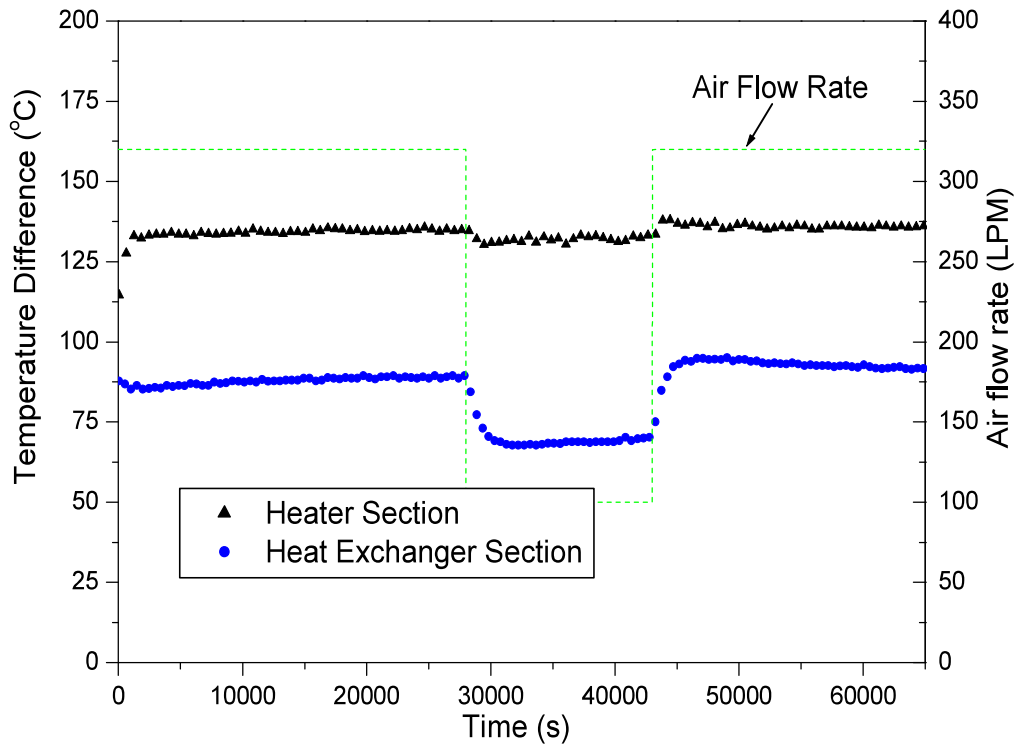


Fig 3.29 Temperature variation in the loop when secondary air flow was decreased from 320 LPM to 100 LPM with 2280 W loop power

3.7.2.4 Effect of coolant flow in heat exchanger

The effect of the variation in secondary side coolant flow rate was also studied. The variation of power and the results obtained were depicted in Fig 3.29. The air flow rate was

decreased from 320 LPM to 100 LPM and again restored to 320 LPM. The power was kept constant at 2280 W. Significant changes of heat transfer rate in the heat exchanger is seen in the form of temperature difference across the heat exchanger. While the change in temperature difference across the heater section is lower than that of heat exchanger. It can be seen that the step change in power mainly affects the temperature gradient across the heater section whereas the step change in secondary side coolant flow rate affects the temperature gradient across the heat exchanger section. In general it can be summarised that local change in heat input and output in the loop affects local temperature gradient more than the whole loop.

3.8 SUMMARY OF MAJOR FINDINGS

A loop with LBE coolant was made to generate experimental data up to 500 °C. The necessary instrumentation like oxygen sensor, level sensor, etc, were developed for smooth operation of the loop. Following were the major achievements/findings from the experimental studies,

1. Instruments for measurement of oxygen in LBE and level measurement were developed and found to be sufficient for loop operation. The chemistry control of LBE in the loop during the operation was achieved by using controlled injection of Ar+H₂ in molten LBE.
2. During steady state natural circulation experiment, data were generated for Gr_m ranging from 10¹¹ to 10¹³ and Re_{ss} range 600 to 2000.
3. A correlation, developed for steady state natural circulation single phase Newtonian fluids was compared with experimental results and found to be in good agreement with the experimental results.

4. The transient experiment conducted are, start up experiment at different power, heater trip, loss of heat sink, step change of power and the effect of secondary coolant flow variation in the heat exchanger.
5. It was seen during the start-up experiment that with loop power increase, the time required to initiate the natural circulation, decreases. The time to reach steady state mainly depends on the secondary side heat transfer conditions.
6. In the loss of heat sink experiment it was found that, the temperature of the loop rises steadily when the secondary coolant was stopped. Continuation of the natural circulation for long time in the loop was observed, even after the coolant flow secondary side was stopped. This is due to the natural cooling in the secondary side through the structural material and cooling by recirculation of the air.
7. In step change in heater power it was found that, the rise in temperature difference across the heater section was more than that of heat exchanger. But in the experiment to study the effect of the secondary coolant flow in the heat exchanger, the temperature rise in the heat exchanger during the step change of coolant flow was more prominent. From the results of these two experiments it can be concluded that the effect of step change in parameters in heaters and heat exchangers are more prominent at respective locations.

Chapter 4

EXPERIMENTAL STUDIES IN KILO TEMPERATURE LOOP

4.1 INTRODUCTION

As discussed in the previous chapter the LML could be operated only up to 500 °C due to the limitation of use of the structural materials to withstand high temperature. Experimental data were required at higher temperature for the design of CHTR, whose operating temperature is ~1000 °C. Since LML was made of SS316, maximum allowable temperature for operation was 500 °C. So another loop was required for experimental studies at higher temperature. This chapter deals with the development of a high temperature loop. Two materials were tried to make the loop Mo based alloy and Nb based alloy. Nb based alloy was found to be better for the fabrication of the loop and consequently a high temperature loop which was capable of operating above 1000 °C, Kilo Temperature Loop (KTL) was set up using this material. A number of experimental studies were carried out on LBE natural circulation in this loop which are discussed in this chapter.

4.2 DEVELOPMENTAL WORK FOR HIGH TEMPERATURE LOOP

As discussed in the chapter 2, at high temperature only Nb based alloy and Mo based alloys were compatible with molten LBE. TZM (5 % Titanium, 0.08 % Zirconium and 0.02 % Carbon with the balance Molybdenum.), a Mo based alloy was tried for development of the loop. But due to joining difficulties the loop could not be developed.

4.3 DESIGN OF THE LOOP WITH Nb-ALLOY

After carrying out the unsuccessful trials with TZM, Nb alloy i.e. Nb 1% Zr 0.1 % carbon were tried. The development of the material was carried out in Material Science Division (MSD), BARC for CHTR application. The mechanical properties at high temperature were found to be good and suitable for the loop design conditions (Tewari et al., 2003) [130].

The mechanical test results of the EB welded pieces were found to be satisfactory with the design requirement of the loop. The availability of the material and sizes were evaluated. All the joints of the loop were done by EB welding. The size of the vacuum chamber of EB welding machine also limited the size and geometry the loop. The development of the fabrication techniques were carried out jointly by NFC, MSD and Reactor Engineering Division (RED) of BARC for the Nb alloy components and the detailed design of the loop was finalised. Figure 4.1 shows the isometric view of the Kilo Temperature Loop (KTL). Due to limitation of material availability, the loop was designed in two parts, high temperature part and low temperature part. The main loop where the natural circulation of LBE takes place was made of Nb-alloy. The low temperature part which consists of the dump tank, the loop filling lines and the isolation valve were designed with SS316 material. For the mechanical design of the loop components, ASME Section VIII division I was referred. Since the components were to be designed to work at high temperature, the creep stress of Nb-alloy was taken as the maximum allowable stress at design temperature. The details of the thickness calculation of different components of the loop are given in Appendix 4.1. The flexibility analysis of the loop was also carried out to design the support system of the loop. Figure 4.2 shows the loop with supports.

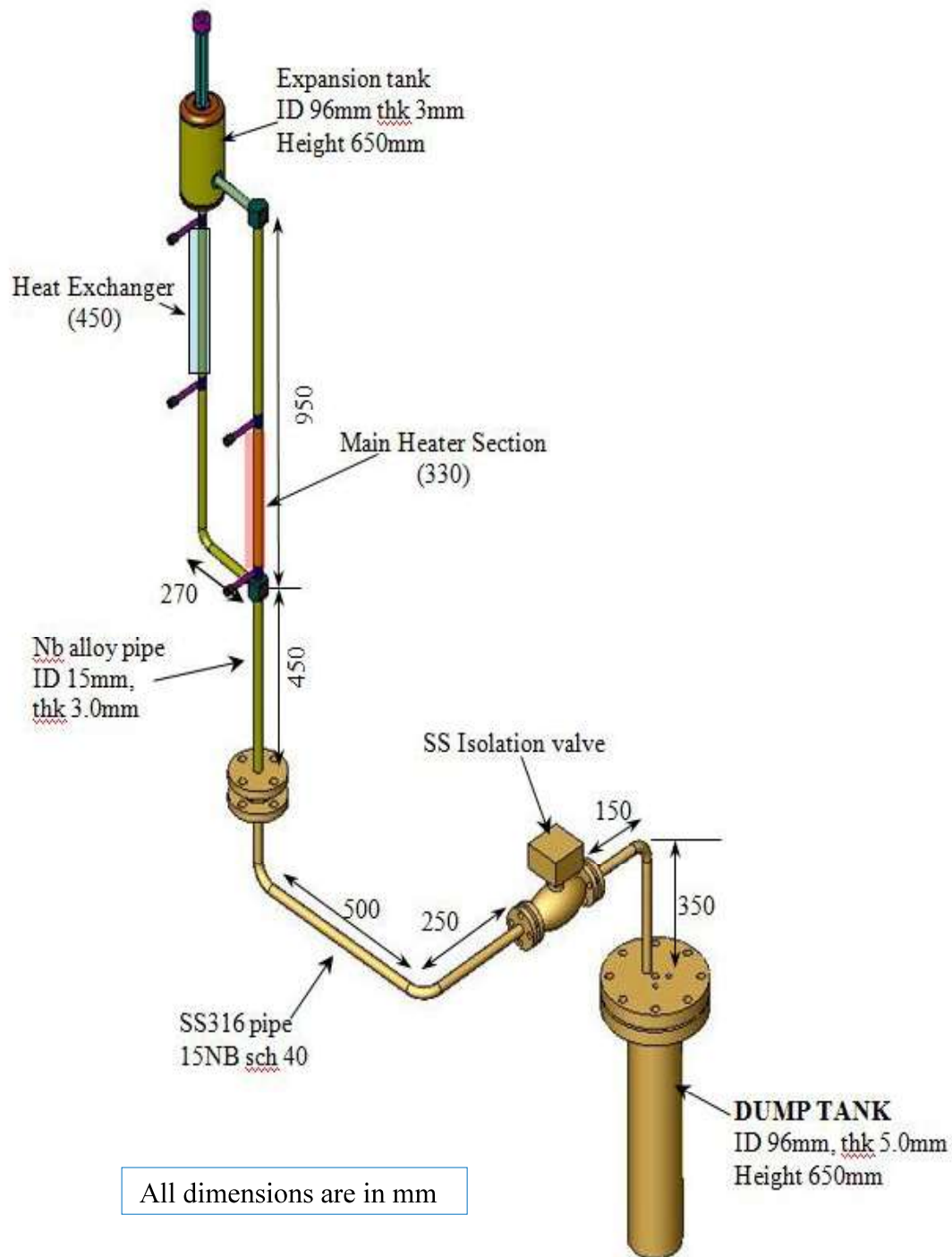


Fig 4.1. Isometric view of the KTL made jointly with NFC, Hyderabad.

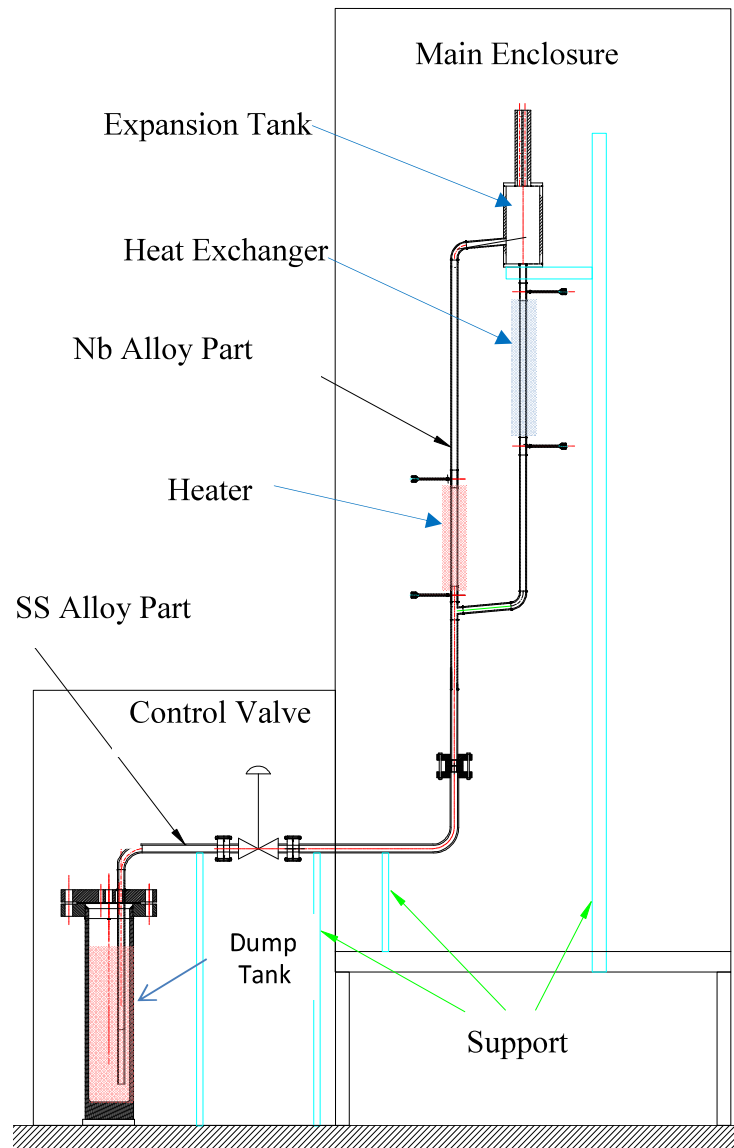


Fig 4.2 Schematic of the support of KTL

A number of trials were carried out on EB welding of different components of the loop. After the trials the Nb alloy loop components were made at NFC. The expansion tank which has internal diameter of 104 mm was made by joining number of circular rings which were again individually made from rectangular plates. The elbows and tees were specially made for ease of EB welding. The different components of the loop were shown in Fig 4.3. Since the source of the electron beam was fixed in the EB welding machine the job was to be moved as per requirement of welding. Proper jigs and fixture were developed for the loop. The procedure

and sequence of welding of the joints were developed. A stainless steel loop was made with the same geometry to finalise the welding and assembly procedure of the loop. After this the Nb alloy loop was successfully assembled as per the procedure developed.



Tank, Nozzle, Top Tube Cluster



Nozzle for thermocouple



Specially designed Elbows



Full loop assembly

Fig 4.3 KTL components and loop assembly fabricated in NFC, Hyderabad.

4.4 DESCRIPTION OF KILO TEMPERATURE LOOP (KTL)

KTL comprises of five basic parts: heater, cooler, dump tank, expansion tank and loop piping. Table 4.1 gives the main design parameters of the loop. High temperature and low temperature parts of the loop were joined with ANSI standard SS 316 flanges. Ceramic impregnated SS metallic gasket was used for sealing the flanged joints. Figure 4.4 shows the schematic of the flanged joint. The KTL has been designed to operate up to 1100 °C. The present set up does not allow forced circulation of the cooling argon gas in the secondary side because of the possibility of sudden cooling of the loop heat exchanger section if the argon flow was started abruptly. The sudden cooling of the section lead to the thermal stress generation in the joints and from the stress analysis it was found that it may cause failure of the joints at higher temperature. Moreover the oxygen impurity in the argon gas may lead to oxidation on the outer surface of the Nb alloy piping in the heat exchanger section.

Table 4.1 Design parameters of KTL

Sl. No.	Parameters	Values
1.	Fluid used	Lead Bismuth Eutectic (LBE)
2.	Fluid circulation mode	Natural circulation
3.	Line size	15 mm NB(1/2") Sch 80
4.	Centre line vertical distance between heat exchanger and heater	500 mm
5.	Total circulation length	2500 mm
6.	Loop material	Nb-1 %Zr-0.1 %C
7.	Design pressure of the loop	4 kgf/cm ²
8.	Coolant inventory	32 kg
9.	Maximum main heater power	2.0 kW
10.	Maximum operating temperature	1100 °C
11.	Loop Height	2.5 meters (approx)

So the heat exchanger in the present loop was designed as vertical tube in tube type and cooled by natural convection of argon gas in the enclosure. Figure 4.5 shows the schematic of the heat exchanger. The inner tube was the part of the primary loop and LBE was flowing through it vertically in downward direction. The outer tube was concentric to the inner tube with both ends open. So the secondary side was a vertical annular passage where argon gas in the enclosure enters from the bottom of the passage, flows through it due to natural convection and goes out through the upper opening. This way the heat from the heat exchanger was rejected inside the enclosure.

The dump tank which was made of SS 316 serves as the melt tank and holds the total inventory of LBE of the facility. It holds sufficient amount of LBE even when the loop was filled during the experiment. In case of an emergency, the LBE was required to be dumped at high temperature. The additional LBE which was kept at low temperature in the melt tank mixes with the high temperature LBE and keeps the dump tank temperature below the design limit.

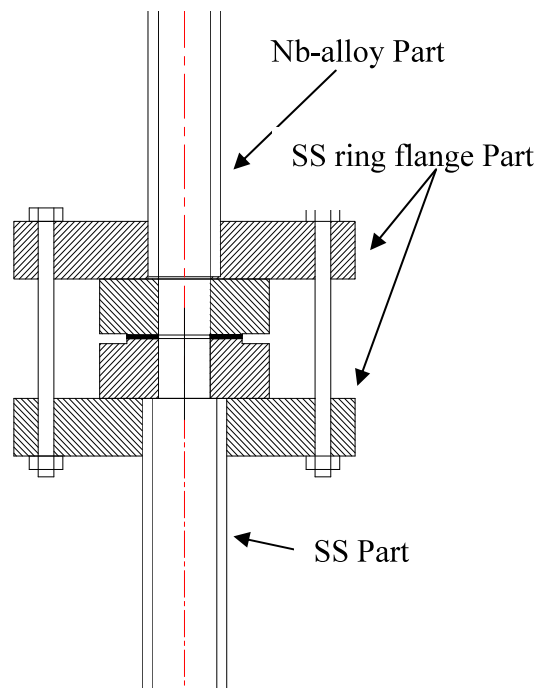


Fig 4.4 Joint between Nb alloy part and SS part of the loop.

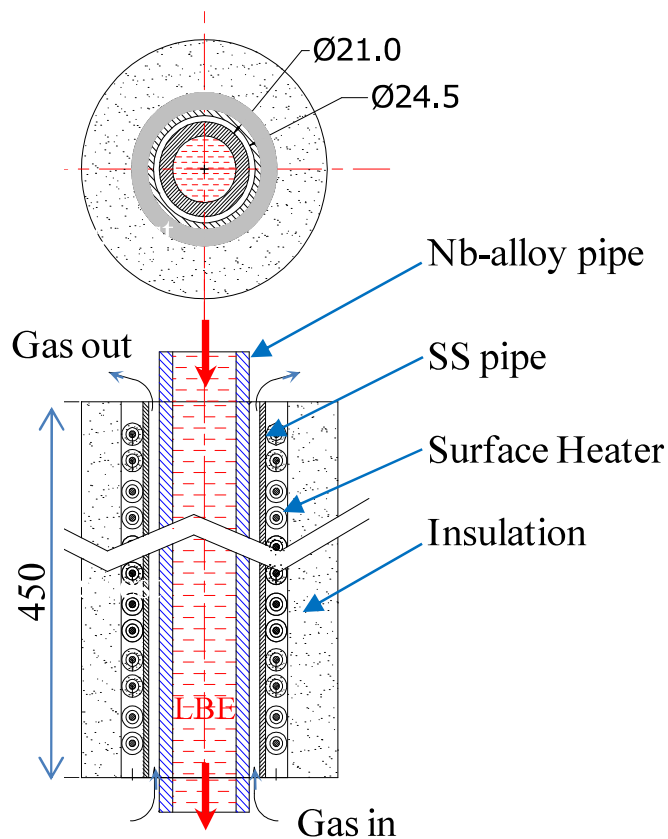


Fig. 4.5 Schematic of heat exchanger of the loop.

Argon gas inlet and outlet lines were connected for cover gas purging. The tank was connected to the main loop by a 15 NB pipe which was immersed in the LBE to a sufficient depth so that when the surface of LBE was pressurized by Ar gas, the LBE was lifted through the pipe to fill the loop. The dump tank has continuous level sensor which works on gas bubbling method as explained in chapter 3. The gas pressure and LBE temperature in the tank was also measured. The temperature controlled heaters were provided to keep the tank at required temperature. An expansion tank has been provided at the top of the loop to accommodate the volumetric expansion of the LBE. This tank consists of a discrete type LBE level sensor to monitor LBE level and thermocouples to monitor the LBE temperatures. The cover gas pressure of the tank was also monitored. Trace heaters were provided in the piping and other components of the loop such that temperatures at all locations of the loop could be controlled as and when required.

The possibility of any leakage of LBE vapour into the atmosphere was prevented by suitably designed ventilation system as shown in Fig 4.6. Control valves have been used for controlling cover gas pressure and dumping the LBE in to the dump tank remotely. The loop was successfully operated up to 1100 °C. The temperature limit of all the heaters in the low temperature section of the loop were kept at below 500 °C, so that the temperature of the section does not exceed the design limit.

The instrumentation and control of the process plays the most important role as the molten lead alloy freezes at 125 °C. K-type SS 316 Sheathed thermocouples were used for LBE temperature measurement. For the surface temperature measurement, inconel sheathed thermocouples were used. There were 25 thermocouples in the loop. Surface temperatures on piping and vessels were being monitored and power supply to the heaters was, controlled continuously. The main heater of the loop was resistance type with maximum power of 2 kW. Pressure measurement was done by remote seal type electronic transmitters. Diaphragm of these transmitters was rated up to 300 °C. These instruments sense cover gas pressure and purging gas (argon) pressure and do not face high temperature. Control valves of 1/2" size were used for controlling cover gas pressure remotely. One isolation valve of size ½" NB with band heater were used to isolate the dump tank from the loop. This open/ close type valve was controlled by solenoid valve using 24 VDC remote control. All the electronic signals transmitted from the field transmitters were sent to the central control system for further processing. Data acquisition system has been provided for data storage and analysis. Pressure measurements have been done by remote seal type electronic transmitters. These instruments sense cover gas and purging gas pressures. Beside this, the level of LBE was sensed by discrete type level probe. Figure 4.6 shows the P&I of the loop.

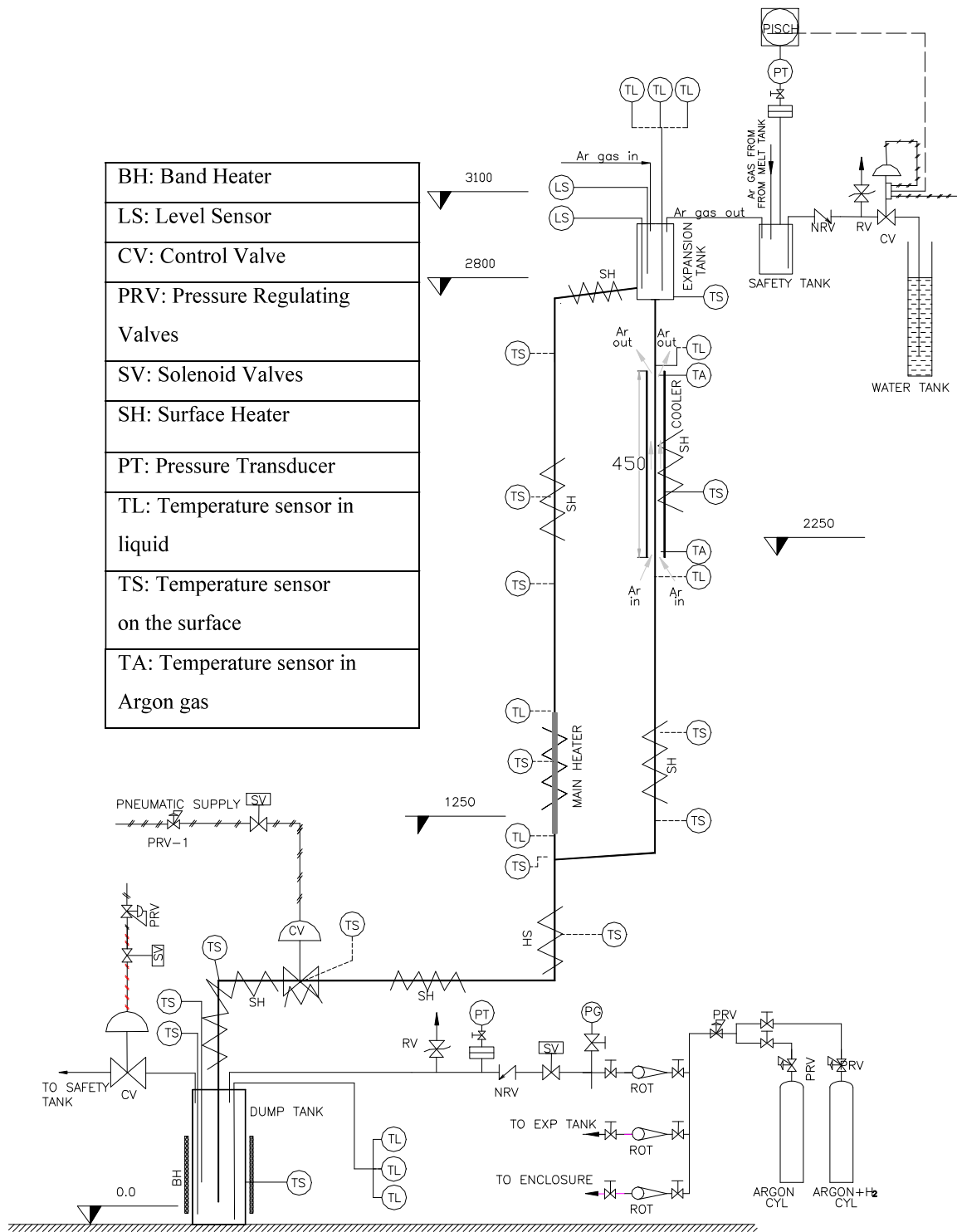


Fig 4.6 P&I diagram of KTL

4.5 ENCLOSURE FOR INERT GAS AND OXYGEN SCAVENGING SYSTEM

Nb-alloy, which was used as construction material for main loop piping and expansion tank, picks up the oxygen present in the ambient at higher temperature and gets oxidized quickly beyond 400 °C. This oxidation rate increases with temperature. So the main Nb-alloy loop was kept in an inert gas enclosure. The front side of the enclosure was provided with transparent glasses for the visibility of the loop from outside. Argon gas was purged in the enclosure with a rate of 1.0 to 3.0 LPM. This gas was used to lower the oxygen level in the enclosure. The discharged argon gas was passed through a water column which provides positive pressure to the enclosure as well as acts as scrubber to the gas to remove lead particles if any. The heat from the heat exchanger of KTL was rejected inside the enclosure by the natural convection of the inert gas. Fins were designed and provided on both sides of the walls of the enclosure for better heat transfer so that the temperature of the enclosure remains below 200 °C even at maximum power level of the KTL. Another figure of the enclosure with fins and cooling coil is given in Appendix 4.3. Figure 4.7 shows the isometric view of the enclosure with fins. Apart from fins, water cooling coils were provided at the top of the enclosure for additional cooling. Appendix 4.2 gives the details of the thermal design of the enclosure. There were six nozzles provided in the enclosure. The instrumentation tubes and wires were passed through these nozzles. The tubes were sealed by swage lock fitting. The electrical wires were mineral insulated and sealed by ceramic cements. The thermocouple wires penetrations were also sealed by ceramic cement. The enclosure was tested for leak tightness up to the pressure 300 mm water column. The low temperature part of the KTL was also enclosed in a separate enclosure made of steel with sufficient leak tightness. This enclosure is connected to the ventilation system of LML for filtration of lead vapour which may be generated due to any leakage in the dump tank

connections. The level of Pb in the water scrubber tanks was monitored periodically. The sampling of enclosure surface dust was done whenever it was required to do maintenance work inside the enclosure. Figure 4.8 shows the loop with the enclosure. Analysis has been carried out to estimate the maximum time of operation at different temperature. The analysis was done on the basis that the minimum thickness of the Nb-alloy material should be available to contain the hot LBE at maximum operating temperature and pressure. It was found that maximum thickness of the loop material which can be allowed for oxidation was 1.7mm. It was found that that with 10 ppm oxygen in argon gas the loop can be operated more than 8 months at 1000 °C, which was the sufficient time to conduct all the experiments envisaged.

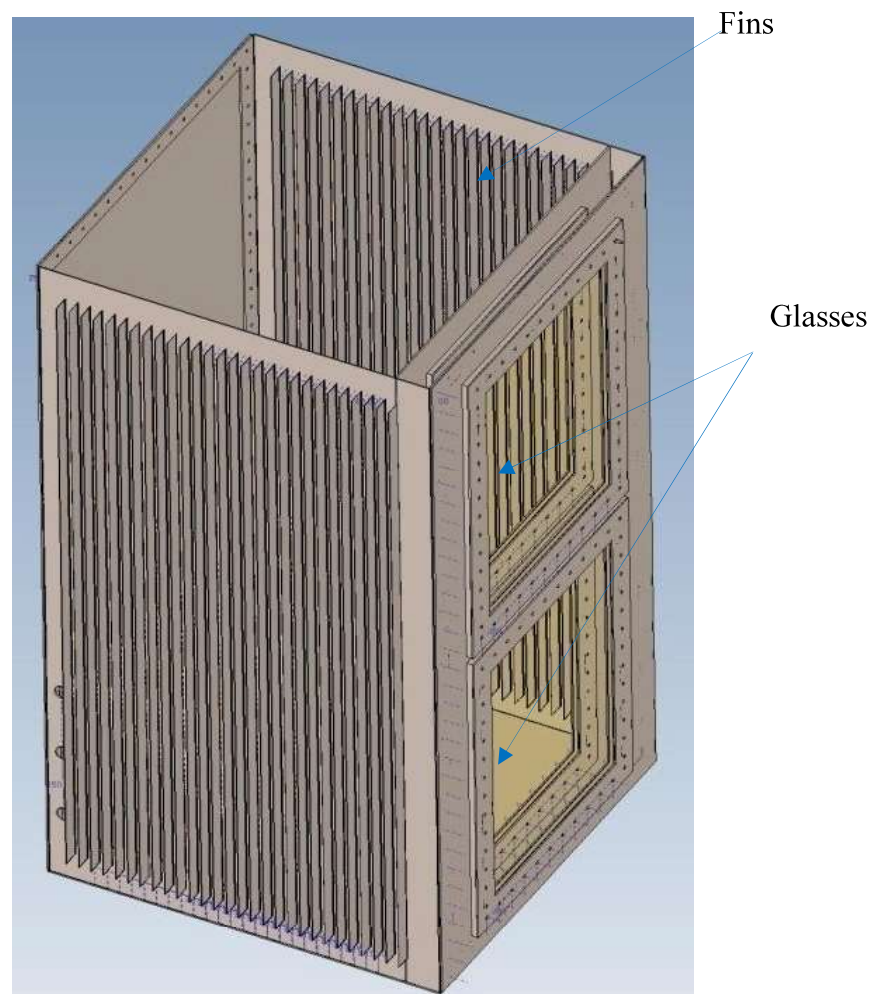


Fig 4.7 Solid model of the enclosure of KTL (top finned plate is not shown for clarity).

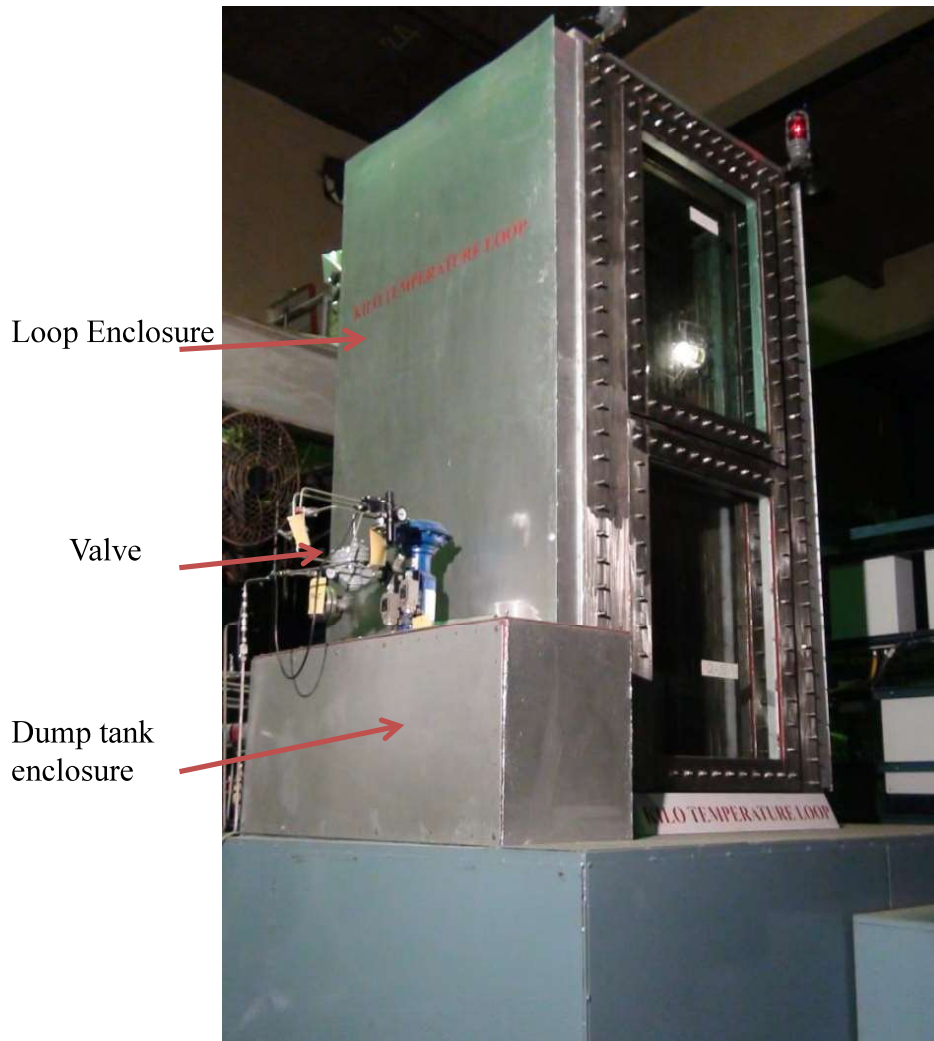


Fig 4.8 KTL facility with the enclosure

So it was decided to keep the oxygen level at 10 ppm or below. The detailed calculation of oxidation rate with different oxygen concentration and at different operating temperatures was given in Appendix 4.3. An online oxygen analyser made by TECHNOVATION[®](model OX-1) was used for the monitoring oxygen level in the enclosure. To achieve low oxygen concentration, high purity argon gas was continuously purged from the enclosure. But the required oxygen (~10ppm) level could not be achieved with the purging process. A separate circuit was designed in which the argon gas of the enclosure was re-circulated through oxygen scavenging systems. The flow diagram of the oxygen removal system was shown in Fig 4.9.

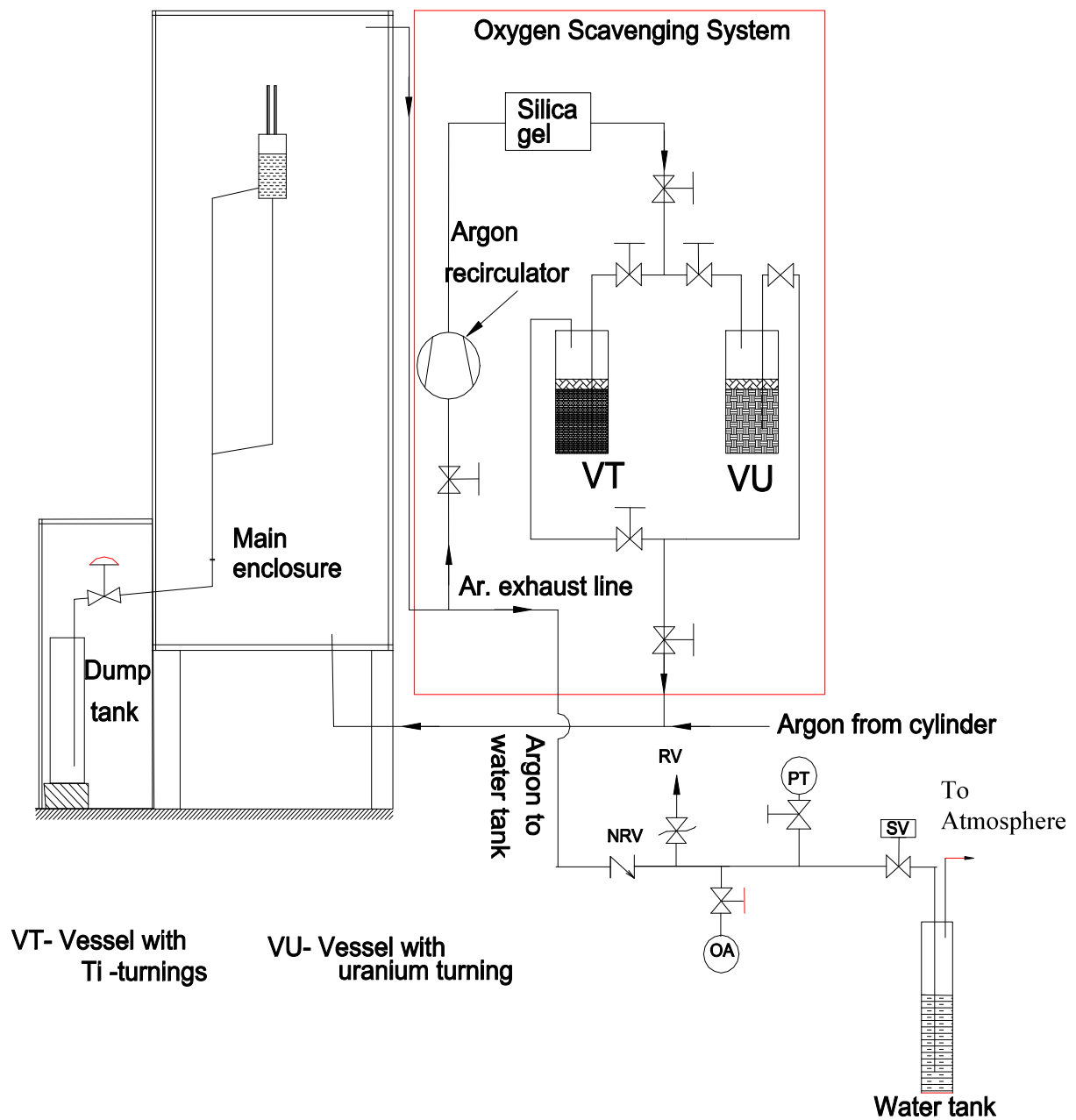


Fig 4.9 Flow sheet of oxygen scavenging system the KTL enclosure.

The oxygen was removed from the enclosure from atmospheric level to 2000 ppm by purging with argon gas. The argon gas in the enclosure was re-circulated through Titanium turning vessel (VT) at 600 °C to reduce the oxygen from 2000 to 200 ppm. To reduce from 200 ppm to 10 ppm, uranium turning at 150 °C was used. By this way, very low oxygen level has been achieved in the enclosure containing the loop. The argon gas recirculation circuit also consists of a silica gel unit to remove moisture from the gas.

4.6 LOOP OPERATING PROCEDURE

Apart from testing the loop instrumentation and other auxiliary systems as a part of commissioning, the leak test of the loop and the enclosure were carried out at rated pressure condition. The air inside the loop and the enclosure was replaced with argon gas by repeated evacuation and refilling of argon gas. This was done for at least three cycles as recommended in the LBE handbook. The oxygen concentration in the purged argon gas was then measured to ensure that the oxygen concentration is less than 10 ppm. The solid ingot of the LBE was melted in the dump tank by heating and the slag suspended in the LBE was manually removed. The operational safety guidelines as given in LBE Handbook (2007) [67] was followed during the slag removal process. The liquid LBE was then bubbled with Ar+H₂ gas to remove dissolved oxygen in the LBE. The whole loop was then heated to 250 °C. Since whole section of the Nb alloy piping are welded, care had been taken to avoid uneven heating in the piping to prevent stress generation in the piping. After attaining the required temperature at all the locations of the loop, the LBE coolant in the dump tank was then pressurized by argon gas system. Due to pressurization, molten LBE flows into the loop and subsequently fills up the loop. When the level sensor at the expansion tank detects the LBE level, the loop was automatically isolated from the dump tank by the isolation valve. After the filling of LBE, all the surface heaters were put OFF and the main heater of the loop was

put ON at certain power level. Natural circulation of the coolant in the loop starts due to heating of the coolant in the heated section and cooling of the heat exchanger. Argon in the enclosure provides natural cooling in the secondary side coolant in the heat exchanger. After losing heat in the heat exchanger, LBE re-enters the heated section through 15 mm NB pipeline, thus completing the loop. During the operation of the loop high purity argon gas was used as cover gas in the vessels. The argon gas pressure inside the enclosure and the loop were maintained at 150 mm water column higher than the atmospheric pressure to avoid ingress of air in the enclosure. When the enclosure pressure falls below 50 mm Water column, the Ar outlet line was closed automatically to prevent further drop in the pressure. Various natural circulation experimental studies were carried out in the loop from 200 °C to 1100 °C, which were described in the following section. After the experiments the LBE was dumped to the dump tank by opening the isolation valve. It was ensured that the LBE temperature in the loop was below 500 °C before the dumping. The pressure of argon gas inside the enclosure was maintained till the temperature of the loop falls below 200 °C.

4.7. RESULTS AND DISCUSSIONS

The loop was operated to study the steady state and transient behaviour of the LBE for a wide range of temperature. The details of the experiments conducted were discussed below,

4.7.1 Steady State Experiments

In the steady state experiments, the loop was allowed to reach steady state conditions at different input power levels. The power of the loop heater was varied from 200 to 1200 W. The temperatures at inlet and outlet of the heated section were recorded. Figure 4.10 (a) shows temperature rise across the heater section at different steady state heater power levels.

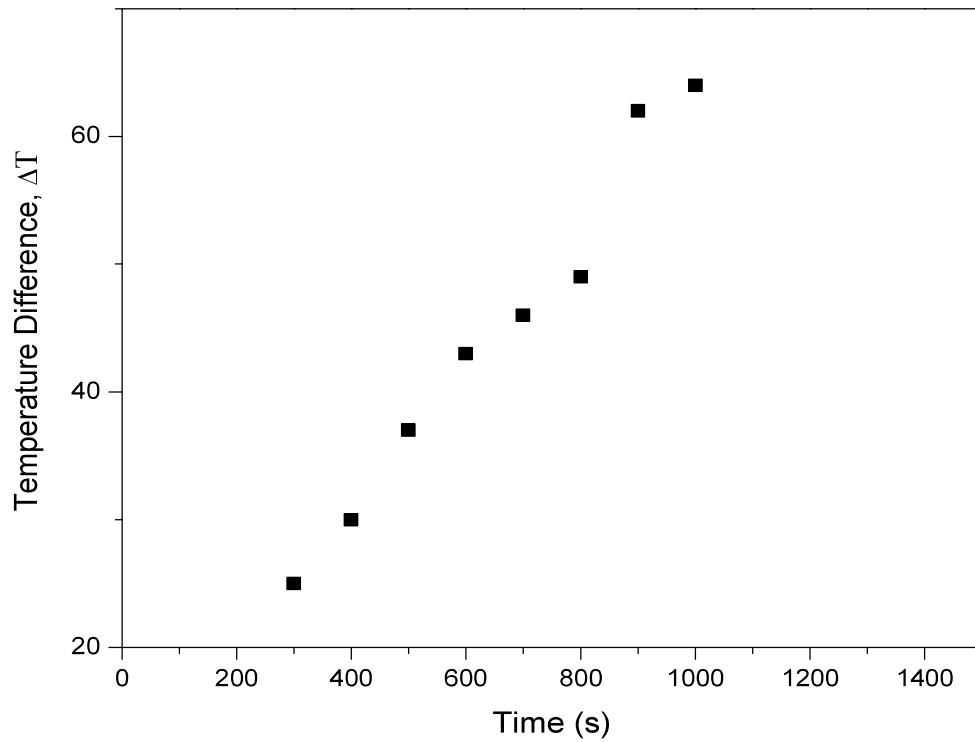


Fig 4.10 (a) Temperature rise across heated section during steady state natural circulation at different power levels.

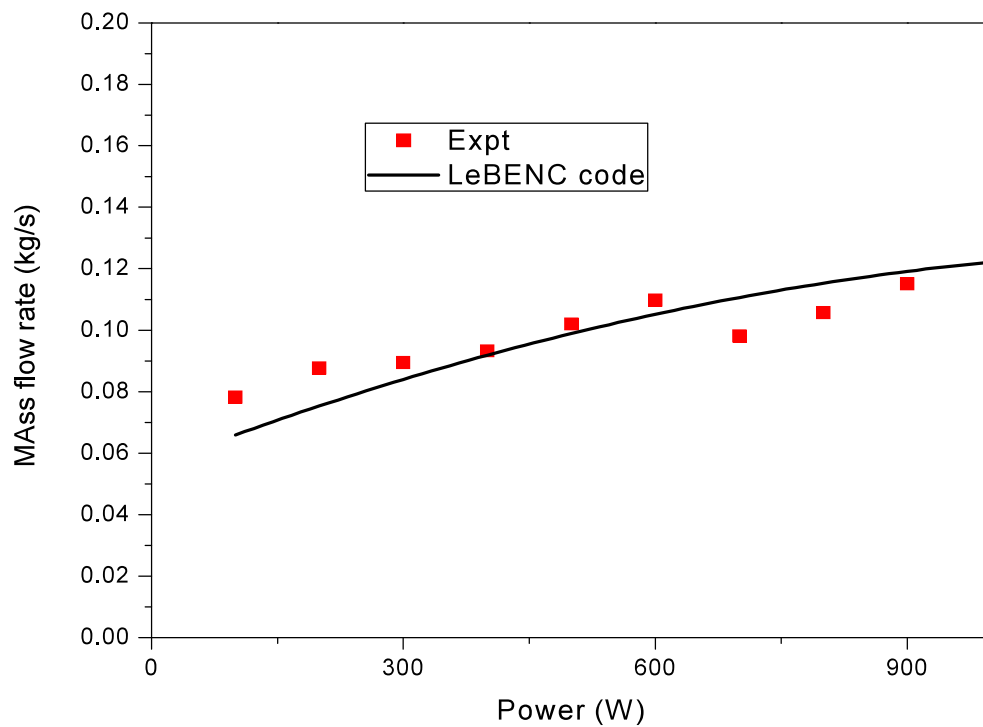


Fig 4.10(b) Mass flow rate of LBE during steady state natural circulation at different power levels.

The steady state LBE mass flow rate was found from the measured heater power and the temperature difference LBE at inlet and outlet of the heated section, i.e

$$W_{ss,LBE} = \frac{Q}{C_{p,LBE} (T_{heater,outlet} - T_{heater,inlet})} \quad (4.1)$$

Figure 4.10 (b) shows the estimated steady state LBE mass flow rates in the loop at various main heater power levels. The flow rate was found to vary from 0.075 kg/s to 0.12 kg/s for power level varying from 100 W to 900 W.

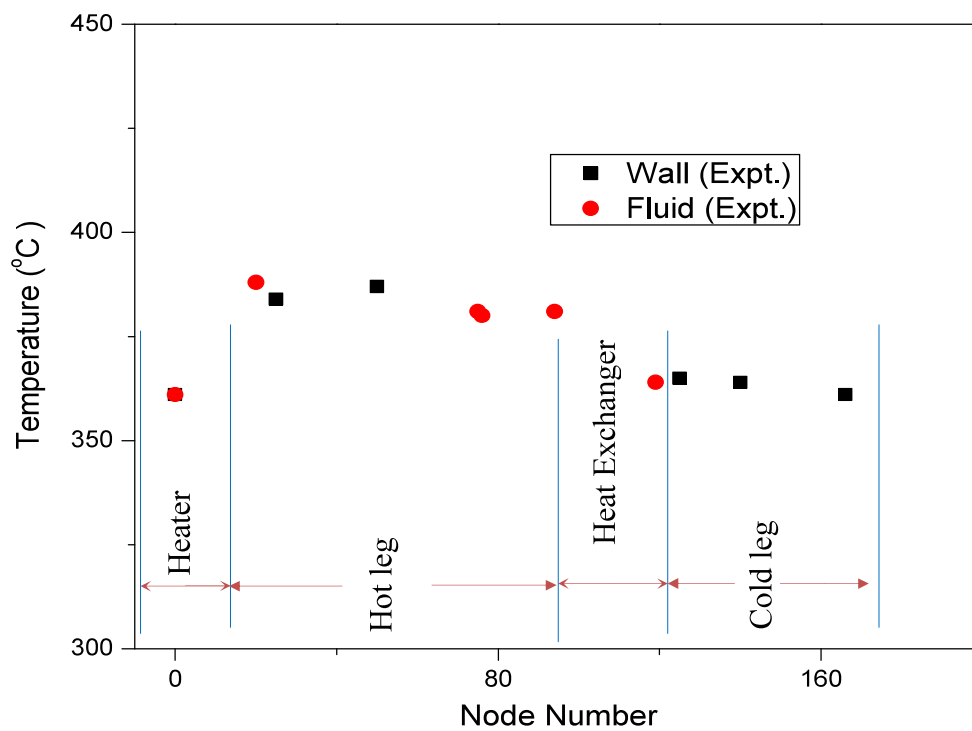


Fig. 4.11 Fluid and wall temperature distribution in the axial direction of the loop at 360 W power.

Figure 4.11 shows the steady state axial temperature distribution in the loop at loop power of 360 W. The temperature varies linearly in the heater section. The wall temperature was found to be higher than the fluid temperature in this section because the heater was put on the outer surface of the pipe and so heat flows radially into the fluid through the pipe wall thickness. There was temperature drop of 8 °C in the hot leg region due to heat loss in the

pipng through the insulation. The temperature drop in the cooler was not linear which may be due to the natural convection cooling by argon gas flowing through the narrow annulus.

4.7.2 Comparison of Steady State Natural Circulation Flow Equations with Experimental Data

As given in chapter 2, the steady state natural circulation flow rate is expressed in dimensionless form as,

$$\text{Re}_{ss} = c \left(\frac{Gr_m}{N_G} \right)^r \quad (4.2)$$

There were few correlations in the above form and were available in literature which were developed for natural circulation of single phase water. Table 4.2 gives the values of the coefficients mentioned in Eq (4.2). It can be seen from Table 4.2 that three correlations were available (Vijayan et al., 2002 [3] ; Swapnalee et al., 2011 [19]; Wang et al., 2013) [131], which cover wide range of Re. The correlation given by Vijayan (2002) [3] was derived from the momentum equation in single phase natural convection data. Swapnalee et al. (2011) [19] derived the correlation for each regime of flow, from the pressure drop correlations available in literature. The correlations developed by Wang et al. (2013) [131] was derived from CFD analysis of a closed natural circulation water loop. Pilkhwal (2007) [18] also carried out CFD analysis to predict the single phase natural circulation in a closed loop and found that the correlation given for turbulent flow regime by Wang et al. matches well with the CFD predictions and experimental data. The correlation given by Kumar et al. (2013) [20] was developed from the experimental data and valid for lower Reynolds number. It was to be noted that all the correlations were developed for single phase water as working fluid. Validity of these correlations for liquid metals was to be checked by comparing with the

experimental data. The steady state natural circulation results of the KTL, LML and other liquid metal loops collected from literature to evaluate the correlations discussed above.

Table 4.2 The values of coefficients of Eq (4.1) recommended by different authors

References	C	r	Range of validity
Vijayan et al. (2002) [3]	0.1768	0.5	Re<1100
	1.956	0.3636	Re>1100
Swapnalee et al. (2011) [19]	0.1768	0.5	Re<898
	1.216	0.387	<898<Re<3196
	1.956	0.364	Re> 3196
Wang et al. (2013) [131]	0.1653	0.493	Laminar
	0.9833	0.403	Transition
	0.8422	0.3962	Turbulent
Pilkhwal et al. (2007) [18]	0.8422	0.3962	700<Re<1250
Kumar et al. (2013) [20]	1.4092	0.3757	VHVC (736<Re<4757)
	0.40879	0.43471	VHHC (816<Re< 5758

From the liquid metal flow rates, corresponding loop power and the loop geometry parameters of the loops non-dimensionless numbers Re_{ss} , Gr_m and N_G were calculated for each loop and plotted in a single graph. The calculations were briefed in Appendix 4.3. After this analysis, the correlations given in Table 4.2 were compared with the experimental data. Figure 4.12 shows the experimental results of various liquid metal loops. The comparison of the various correlations given in Table 4.2 is also shown in the graph. It can be seen that all the correlations are matching with the experimental results within $\pm 20\%$ range with the experimental results. The error analysis of various parameters were carried out and given in

Appendix 4.5. It is found that the error of experimental values Re_{ss} is $\pm 8.7\%$. The Gr_m and N_G values has maximum error $\pm 11.2\%$ and $\pm 8.7\%$ respectively.

4.7.3 Transient Studies

Transient studies were carried out to simulate some postulated accident scenarios in the reactor. The main objective was to observe the LBE coolant behaviour during various transient conditions. The transient experimental studies include start-up of the loop from zero power conditions, heater trip and step power change.

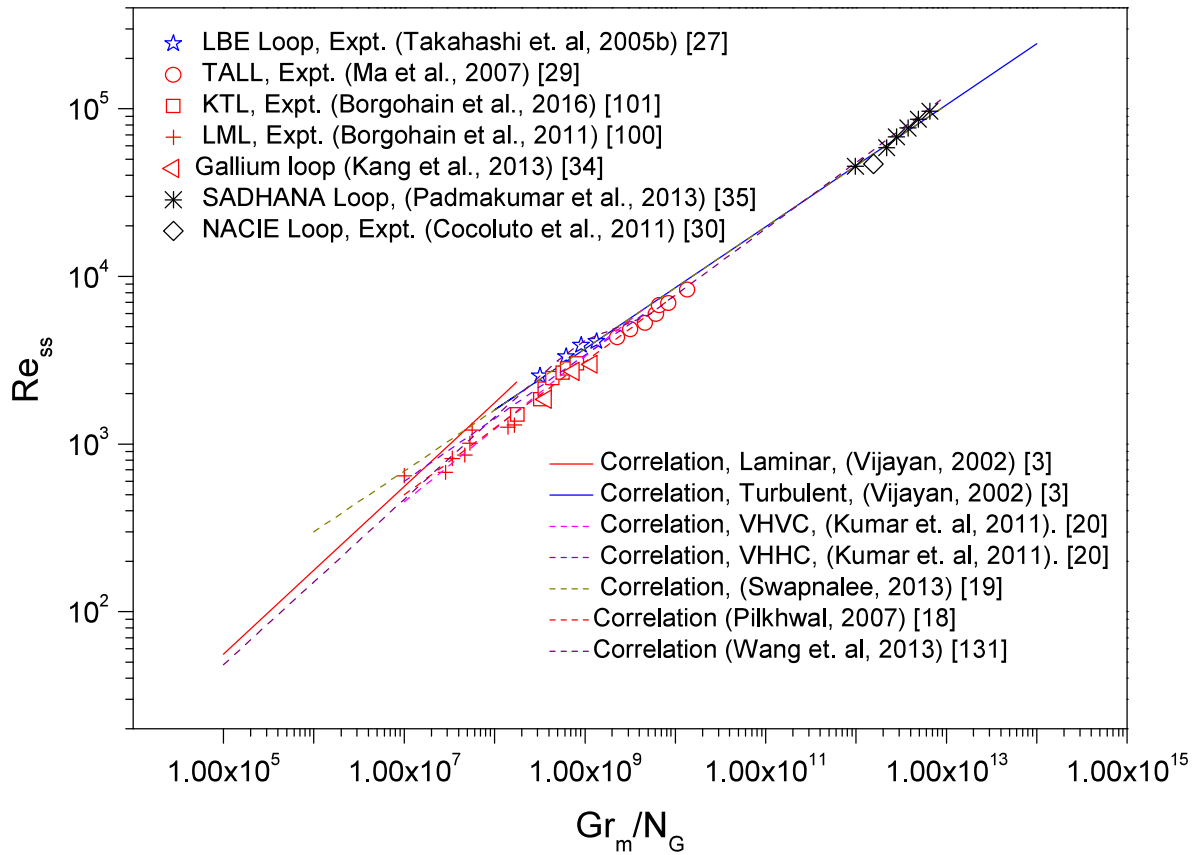


Fig 4.12 Comparison of steady state natural circulation correlations with experimental data for flow range of $100 < Re_{ss} < 10^5$.

4.7.3.1 Start-up operation

Start-up operation from main heater zero power condition for various power levels was carried out. Initially, the loop was running at steady state by natural circulation of LBE.

The main heater was put off and the cold leg temperature was slowly increased to the hot leg temperature by starting the trace heaters in the cold leg. The heat exchanger temperature in the secondary side was also increased by the trace heaters. In this way, near no flow condition was achieved by reducing the LBE temperature differences across the heated section and heat exchanger near to zero. To start the experiment, main heater power was set at certain power and the trace heaters of cold leg and heat exchanger were put off.

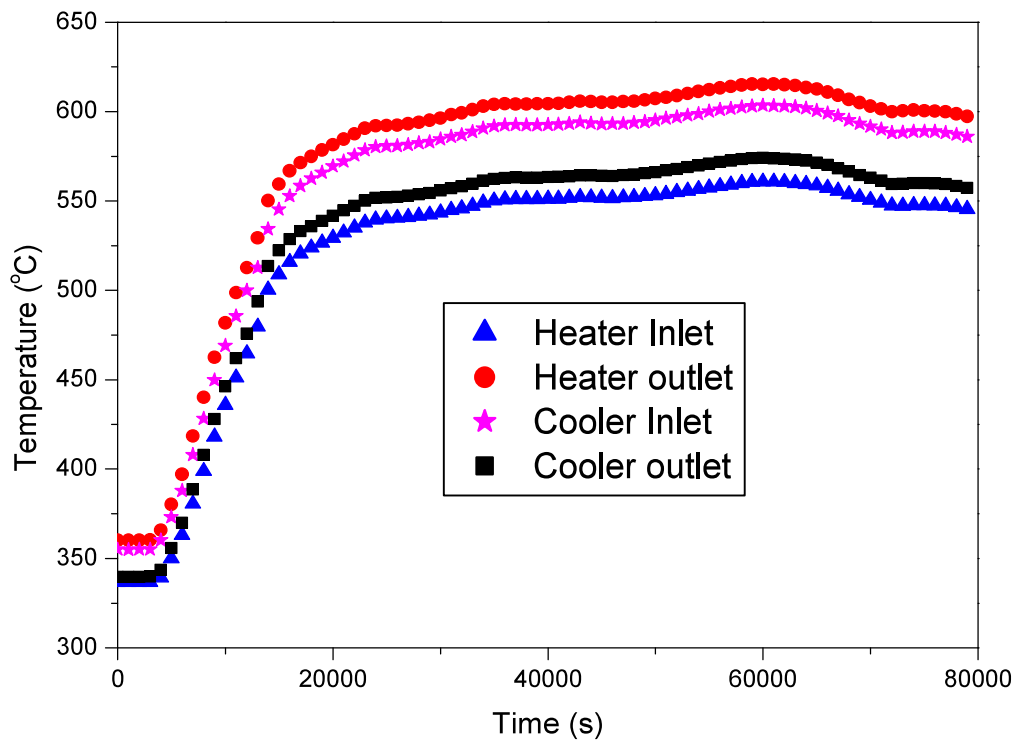


Fig 4.13 (a) Start up experimental results at 800 W and with loop avg temperature 350°C.

Figure 4.13 shows results of the experiments conducted at 800 W power and with different initial loop temperatures. It can be seen from Fig 4.13 (a) that the loop temperature slowly increases and achieves steady state in 20000 s. From Fig 4.13 (b) it can be seen that it takes around 15000 s to reach steady state. So with higher initial temperature the loop reaches steady state in less time. It can also be seen that there was no oscillation in loop temperature

in any of the results, which means instability in natural circulation was not present during the experiments.

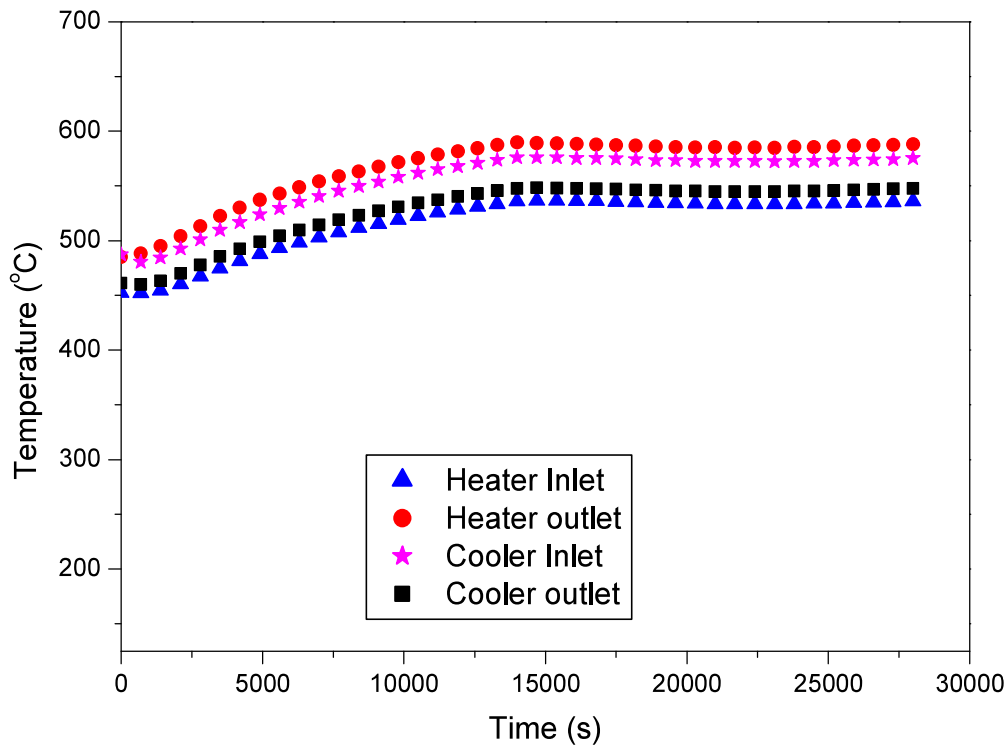


Fig 4.13 (b) Start up experimental results at 800 W and with loop average temperature 475 °C.

4.7.3.2 Loss of heat source

The loss of heat source was simulated by switching off the main heater from the steady state operation of the loop at certain power. The experiments were carried out from different initial power levels. Figure 4.14 (a) shows the case with 200 W initial loop power. Except the heat exchanger inlet temperature, other temperatures decrease after the heater trip till the end of the experiments. The temperature of the heat exchanger inlet which was also at the downstream of the expansion tank increases suddenly at 5000 s. This may be due to the stoppage of natural circulation due to the lack of driving force. The high inventory of the LBE in the expansion tank which was located just on the upstream of the heat exchanger inlet, keeps the temperature at this location higher compared to the other locations.

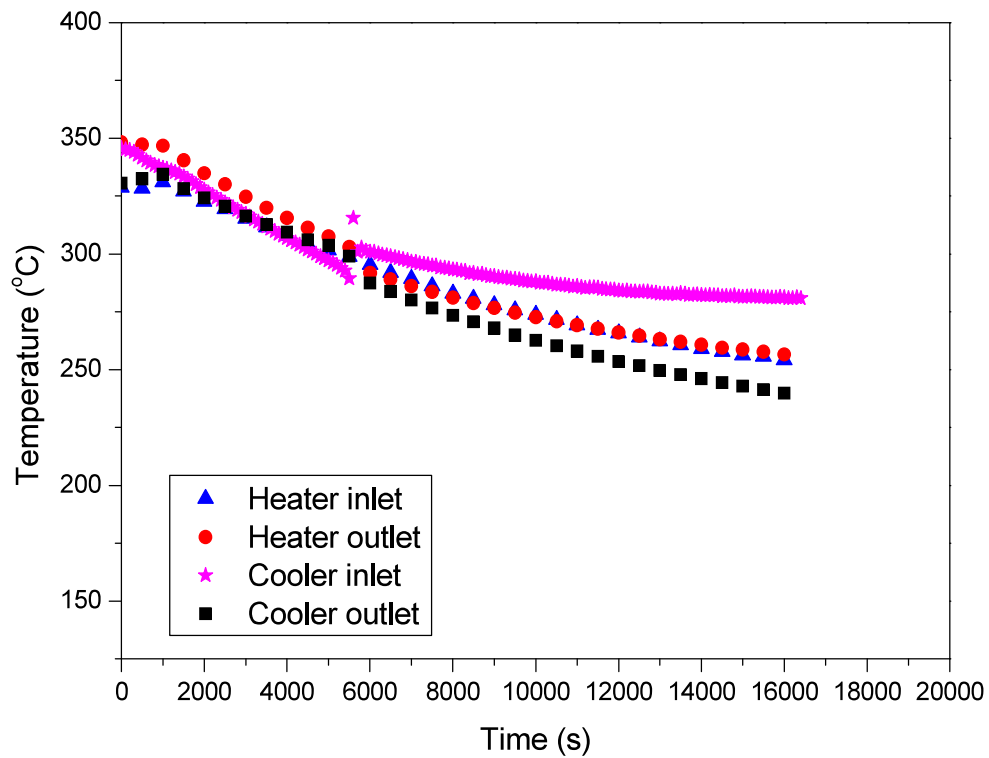


Fig 4.14 (a) Temperature variation in the loop during heater trip experiments at power 200 W.

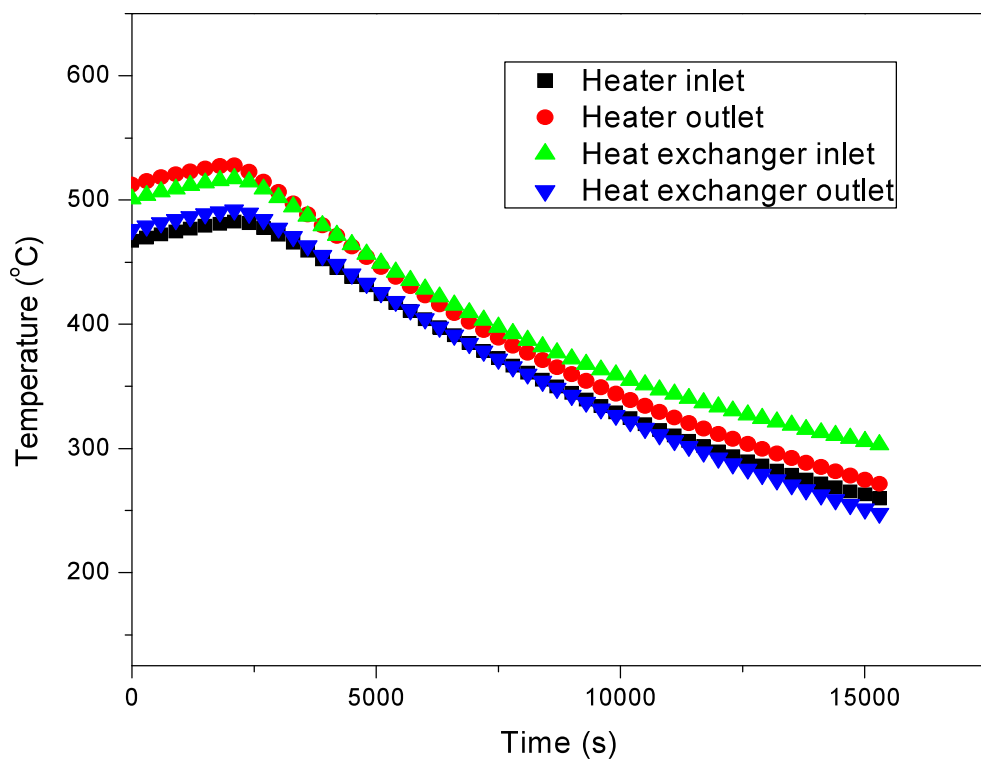


Fig 4.14 (b) Temperature variation in the loop during heater trip experiments at power 700 W.

The experiments were carried out for power levels 700 W and 1000 W also. Figure 4.14 (b) shows the loss of heat source experiment with 700 W as the initial loop power. It can be seen that at higher power the natural circulation remains active even after long duration.

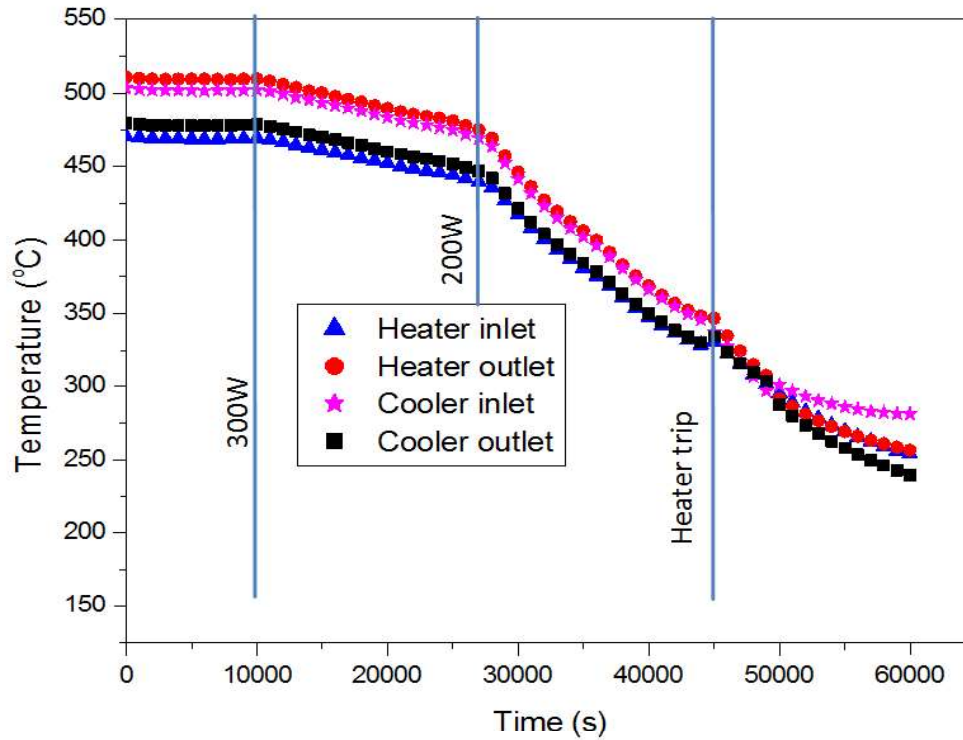


Fig. 4.15 Variation of loop temperature during step change in power 440-300-200-0 W.

4.7.3.3 Step change of heater power

Effect of step change in main heater power was studied in the loop. Figure 4.15 shows an experiment with step power change. The loop power was decreased from 440 W to 300 W. The power was then decreased to 200 W and after that the heater was tripped. Figure 4.16 shows another experiment on step power change. The loop was running at steady state with power level of 700 W. The power was increased from 700 W to 800 W. After it reaches steady state with 800 W, the heater was tripped. After 6000 s the power was reset at 800 W. The loop reaches steady state at this power after 14000 s. It can be seen that the temperature distribution was reproduced at 800 W in this experiments.

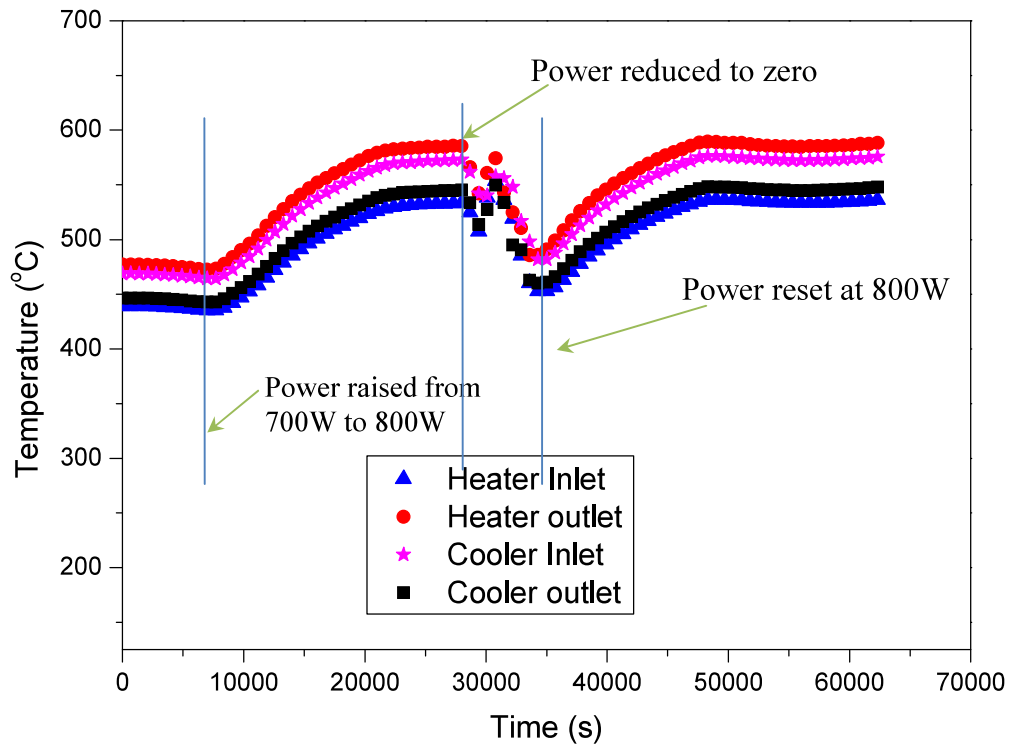


Fig. 4.16 Variation of temperatures during different power levels in the loop.

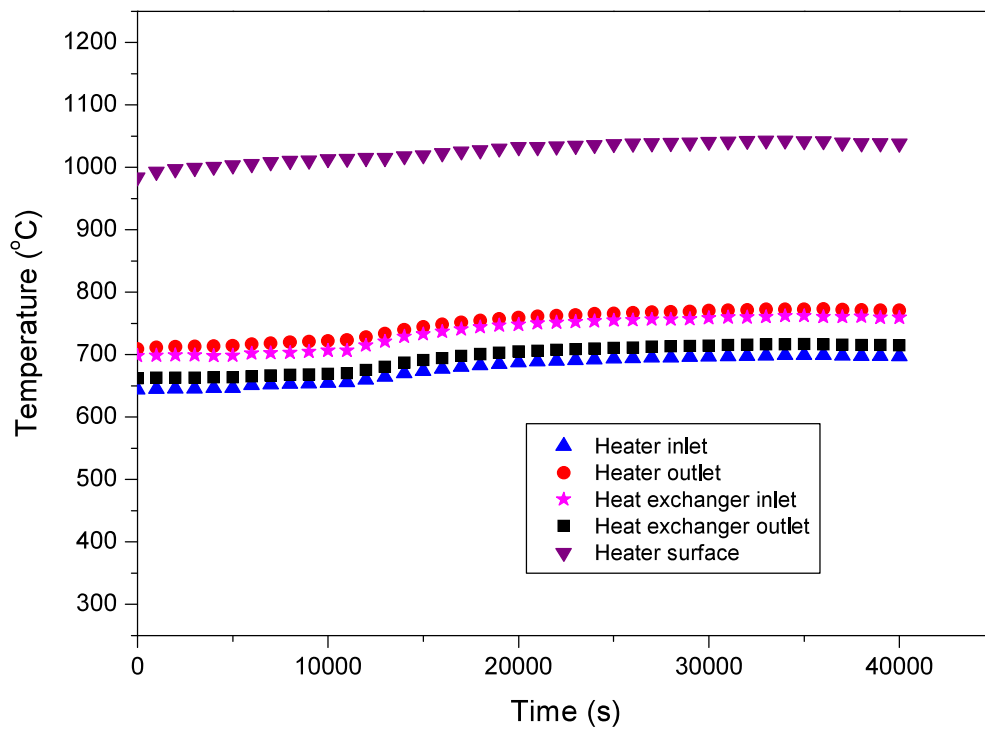


Fig. 4.17 Variation of loop temperature during step change in power from 1100 W to 1200 W.

The step power change experiments at higher power were shown in Fig 4.17. Here the maximum pipe wall temperature has reached 1060 °C during steady state and the loop was operated for 72 hours.

4.8 SUMMARY OF MAJOR FINDINGS/ACHIEVEMENTS

1. A LBE loop with maximum operating temperature of ~1100 °C was designed and fabricated. An enclosure and an oxygen scavenging system were designed to operate the loop at high temperature with negligible oxidation of the Nb alloy.
2. The natural circulation data were generated from 200 °C to 780 °C of LBE. The steady state data were evaluated at various loop temperature levels. The range of Re_{ss} is from 1500 to 3200. The temperature difference across the heater was found to be more at high operating temperature compared to low temperature at same loop power.
3. The steady state correlations available for single phase flow were compared with the experimental data of KTL, LML and other liquid metal loop data. It is found that all the correlations matches well with the experimental data within ± 20 % accuracy.
4. In transient experiments, start-up transient shows gradual rise of temperature in the loop without any oscillation. The loop took much more time to reach steady state than that of LML. This was due to the natural cooling in the secondary side of heat exchanger.

5. During loss of heat source experiment at low power, the natural circulation flow found to be stopped after certain time period. At higher power however the natural circulation continued for long duration after the power was put off.
6. During experiments with step change in power it was seen that there was smooth change in temperature in the loop without any instability.

Chapter-5

EVALUATION OF LBE HEAT TRANSFER COEFFICIENT AT DIFFERENT FLOW REGIMES

5.1 INTRODUCTION

Heat transfer process is an important aspect in the natural circulation studies (Vijayan, 2002) [3]. During natural circulation in a closed loop heat transfer can be divided into three zones, (a) main heater section where heat addition to the primary medium takes place, (b) the heat exchanger, where the heat transfer from primary medium to the secondary fluid takes place and (c) in the piping where the heat was lost through the insulation. The heater section was one of the most important part of the loop where the heat from the electrical heater was transferred to the working fluid. If we consider only the heater section of the loop, during the LBE start up from stagnant condition experiment, the following sequence of events of LBE flow can be envisaged, (i) when the main heater of the loop is started and the LBE is still at stagnant condition, the LBE in the heater section may experience free convection near the heater surface. This phenomena will be prominent if the heater section has bigger diameter compared to other parts of the loop piping. (ii) the free convection will initiate the LBE flow in the loop slowly. The bulk flow of LBE in the loop starts, which results in mixed convection in the heater section. (iii) when the bulk flow through the heater dominates over the free convection in the heater section the flow become forced convection type and may become turbulent if the flow rate is high. So LBE in the loop, especially in the heater section undergoes different flow regime during transient experiments. The different flow regimes in a vertical tube were identified by Metais and Eckert, (1964) [117] in graphical form which is given in Fig 5.1. The operating region in the heat section of KTL and LML are also

highlighted in the figure. The value of $Gr Pr \frac{d}{L}$ is calculated at the heater region of the loops.

The value of Gr is $Gr = \frac{g\beta(T_w - T_c)d^3}{\nu^2}$.

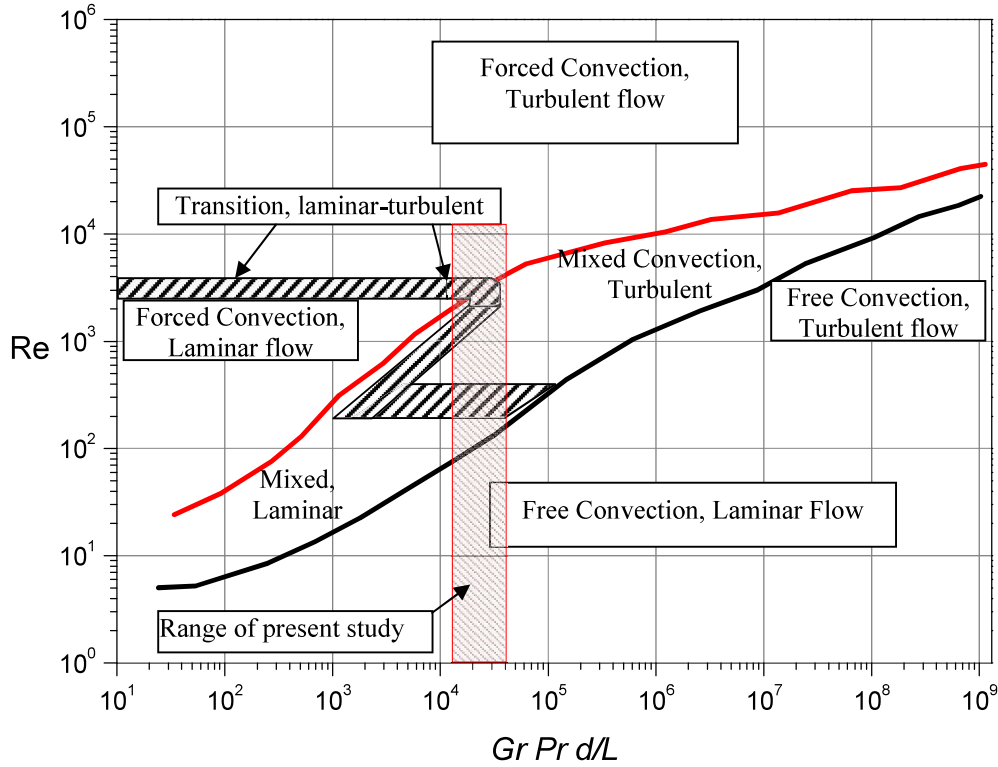


Fig 5.1 Regimes of free, mixed and forced convection flow through vertical tubes [117]

If the flow regimes changes during the experiments, the heat transfer coefficient also changes with the nature of flow. So the heat transfer coefficient is to be properly modelled in the theoretical simulation of the natural circulation. A brief literature survey was carried out on heat transfer in free convection, mixed convection and forced convection through tubes in liquid metals. The liquid metal heat transfer studies in vertical plates was found in literature (Churchil and Chu, 1975) [132], Chang et al., 2011 [133] and Sheriff and Davis, 1978) [118]. However liquid metal free convection heat transfer studies in vertical tubes were not found in literature. So CFD studies were to be carried out to find the free convection heat transfer coefficient in vertical tubes for LBE. Extensive studies have been carried out in the mixed

convection in vertical channels ([134], [120], [135], [136]). Jackson et al. (1989) [137] gives the review on the mixed convection heat transfer. However the mixed convection heat transfer studies in vertical tube with LBE were not found in literature. So it also needs CFD studies to find the heat transfer coefficient for the LBE flow. In case of forced circulation heat transfer in liquid metals including LBE, extensive studies were carried out. Both experimental data and different correlations were available in literature. However the correlations were to be assessed to find the best suitable one for the present studies. The variation of LBE heat transfer coefficients in the developing length of the heater and heat exchanger are to be considered, because of their limited heat transfer length. A correlation developed for low Prandtl number fluids [138] was found and this is to be further validated by CFD analysis for LBE application. The validation of CFD codes was required before use in liquid metal applications. The liquid metal has very low molecular Prandtl number (Pr). So modification in turbulence models, especially turbulent Prandtl number (Pr_t) was required for application in liquid metal heat transfer analysis [139]. An assessment of the correlations for finding Pr_t in liquid metals were to be carried out again to find the best one for the LBE applications.

Following sections describes about the studies and evaluation of the heat transfer coefficients for the different flow regimes of the LBE. These heat transfer correlations were used in the formulations of natural circulation equations in the subsequent chapter.

5.2 DIFFERENT FLOW REGIMES IN NATURAL CIRCULATION

5.2.1 Free Convection

Literature review revealed that the free convection studies were in liquid metal with vertical heated plates were only available. Table 5.1 shows the correlations developed from

experimental results and applicable for low Prandtl number fluids with uniform heat flux condition. The free convection heat transfer studies in vertical tube was not found in literature. A CFD analysis was required for the verification of these correlations for LBE application. Ideally for free convection in a closed loop the bulk fluid flow was zero i.e. when the fluid was in stagnation.

Table 5.1 Correlations available for free convection heat transfer for low Prandtl number fluids in vertical plate.

Reference	Correlation	Remarks
Churchil and Chu (1975) [131]	$\overline{Nu}^{1/2} = 0.825 + \frac{0.387 Ra^{1/6}}{\left[1 + \left(0.437 / Pr\right)^{9/16}\right]^{8/27}}$	This correlation is valid for wide range of Prandtl number.
Chang et al. (2011) [132]	$Nu_x = 0.732 \left(Gr_x^* Pr^2 \right)^{1/5}$	This was developed for sodium.
Sheriff and Davis (1978) [118]	$Nu_x = 0.674 \left(Gr_x^* Pr^2 \right)^{0.213}$	Valid for sodium for the range $10^6 < Gr^* < 3 \times 10^{11}$

But for ease of analysis, a range of flow starting from zero can be assumed where free convection heat transfer correlations can be applied [133]. In the present analysis the free convection regime is assumed in the range of $0 < Re < 50$, as given in Joye et al. (1989) [133].

5.2.2 Mixed Convection

The heat transfer in a vertical heated tube with liquid flowing upward varies with the free convection. Jackson et al. (1989) [137] studied the mixed convection with sodium in vertical tubes for both upward and downward flow. In the experimental studies, the radial velocity profile was similar to other fluids like water, but the temperature profile was not similar. The buoyancy effect near the wall enhanced heat transfer in upward flows whereas

detoriated the heat transfer in downward flows. Figure 5.2 shows the variation of the enhancement of the heat transfer with the buoyancy parameter Bo. Jackson et al. (1994) [120] carried out 2D CFD analysis with low Re k- ϵ turbulence model and the prediction was reasonably good but it over predicted for the downward flow. Experimental results for LBE mixed convection heat transfer could not be found. So CFD analysis was required to be carried out to find the heat transfer coefficient in LBE.

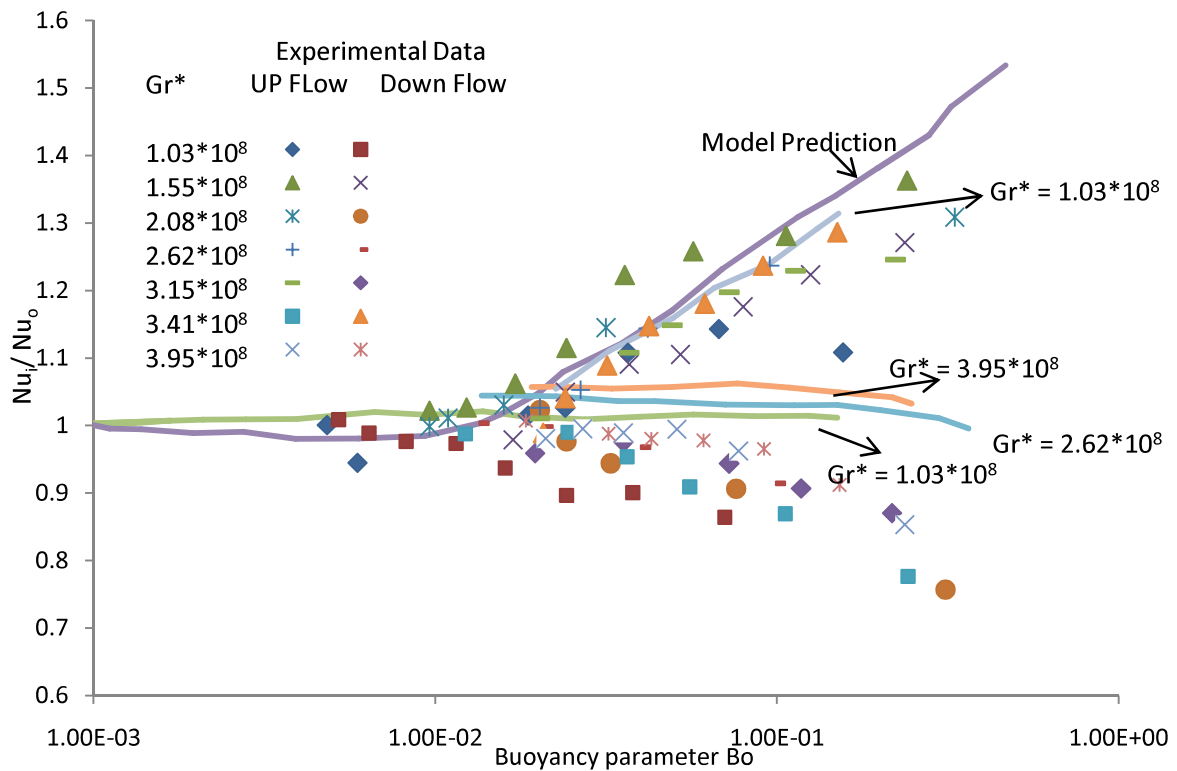


Fig 5.2 Influence of buoyancy on heat transfer to sodium [120].

5.2.3 Heat Transfer in Forced Laminar Flow

As per LBE handbook, laminar flow heat transfer in LBE in circular tube is similar to the normal fluids. So the formula, $Nu = 4.36$ should be valid for the liquid metal also. However the Nusselt number values may change in flow through vertical tubes due to the presence of gravity as discussed above. The deviation of the values depends both on the Re and Gr as shown in Fig 5.2.

5.2.4 Forced Convection Turbulent Flow

A number of experimental studies carried out on liquid metal heat transfer in turbulent flow. After a literature survey, a few correlations were selected for assessment with experimental data on LBE. Table 5.2 gives the available heat transfer correlations for liquid metals with their range of applicability.

Table 5.2: Literature review of heat transfer correlations in liquid metal flow in pipe with uniform wall heat flux

Reference	Correlations	Range of Application	Remarks
Lyon (1951) [140]	$Nu = 7.0 + 0.025 \left(\frac{Pe}{Pr} \right)^{0.8}$	$0 < Pr < 0.1$ and $4 \times 10^3 < Re < 3 \times 10^6$,	Based on analogy of turbulent momentum and energy transfer.
Lubarski and Kaufman (1955) [141]	$Nu = 0.625 Pe^{0.4}$	$0 < Pr < 0.1$ and $10^4 < Re < 10^5$,	Based on the experimental studies on various liquid metals.
Ibragimov et al. (1960) [142]	$Nu = 4.5 + 0.014 Pe^{0.8}$	$0 < Pr < 0.1$ and $10^4 < Re < 10^5$,	Experimental
Holman (1964) [129]	$Nu = 4.36 + 0.0053 Pe$	$0 < Pr < 0.1$ and $2300 < Re < 23500$,	Experimental, with LBE and mercury.
Ede (1961) [143]	$Nu = 4.36 (1 + 0.06 Gr^{0.3})$	$300 < Re < 100000$	Experimental with water and air.
Notter and Sleicher (1972) [144]	$Nu = 6.3 + 0.0167 Re^{0.85} Pr^{0.93}$	$0.004 < Pr < 0.1$ and $10^4 < Re < 10^6$,	Numerical analysis.
Kirrilov and Ushakov (2001) [145]	$Nu = 5.0 + 0.025 Pe^{0.8}$	$0 < Pr < 0.1$ and $10^4 < Re < 10^5$,	Experimental, with special measure for LBE purification.
Cheng & Tak (2006) [146]	$Nu = A + 0.018 Pe^{0.8}$ Where, $A = \begin{cases} 4.5 & Pe \leq 1000 \\ 5.4 - 9 \times 10^{-4} Pe & 1000 \leq Pe \leq 2000 \\ 3.6 & Pe \geq 2000 \end{cases}$	$Pe < 6000$	Formulations based on various correlations.

5.3 CFD APPLICATION FOR LIQUID METAL HEAT TRANSFER

Recently use of CFD in liquid metal thermal hydraulic studies is gaining acceptance for design of liquid metal cooled nuclear reactor systems. But assessment of CFD codes for liquid metal application is essential before using it for the design of system level studies. Due to the much higher surface tension and the drastically lower Prandtl number of liquid metals compared to water, the CFD modelling of liquid metal flows cannot rely on turbulence models developed and validated for water flows. Thus, a separate benchmarking of the CFD modelling for liquid metal flows was inevitable.

The most widely used turbulence models in CFD were based on eddy diffusivity concepts (e.g., $k-\epsilon$ model), which use turbulent Prandtl number to evaluate the turbulent heat transport. IAEA-TECDOC 1520 (2003) [147] provides a comprehensive report on the different CFD studies and highlights major hurdles for its application in liquid metal systems. It was emphasized that improvement in turbulence modelling and turbulent Prandtl number formulation were essential for precision results. LBE handbook (2007) also points out that careful validation of CFD codes with experimental results was necessary for liquid metal flow related analysis. There were some works on validation of CFD codes for liquid metal heat transfer prediction ([146] and [148]).

5.3.1 Turbulent Prandtl Number

In turbulent flow, the thermal eddy diffusivity ϵ_H is correlated to momentum diffusivity as below,

$$\epsilon_H = \frac{\epsilon_M}{Pr_t} \quad (5.1)$$

Where Pr_t is called turbulent Prandtl number. Reynolds analogy assumes that $\epsilon_H = \epsilon_M$, i.e. $Pr_t=1.0$. Experimental evidence indicates that $Pr_t = 0.9$ is correct for most of the conventional fluids, i.e. air, water, etc. [139]. During 1950s it was found that the experimentally

determined heat transfer coefficients for liquid metal flows falls below what would be predicted using Reynolds analogy. The possible reason was found to be the role of Pr_t in heat transfer prediction. A lot of experimental and theoretical studies were carried out to evaluate Pr_t . Reynolds (1975) [149] assessed more than 30 methods to calculate Pr_t and found that the value of Pr_t in a tube depends on molecular Prandtl number, radial distance from the wall and eddy diffusivity. It was emphasized that semi-empirical methods were more promising for the prediction of Pr_t . Gori et al. (1979) [150], carried out numerical analysis for heat transfer in low Prandtl number fluids flowing through pipes. Based on their analysis the correlations for Pr_t were specified for different Reynolds number ranges. Kays (1994) [139] assessed the present status of the Pr_t for wide range of Prandtl number. It is found that for liquid metal turbulent Prandtl number is higher than unity. In tube flow with heat transfer from the wall, the value of Pr_t varies in radial direction. Recently, Cheng and Tak (2006) [146] derived a correlation for Pr_t based on the heat transfer correlations available in literature and CFD analysis. The correlation is reported to be valid for a wide range of Peclet number. Fuchs (1973) [151] carried out experimental studies on sodium and Pr_t values were found at different radial locations. The different methods for prediction of Pr_t for liquid metal heat transfer were briefed in LBE handbook (2007) [67]. It is mentioned that semi-empirical methods were the best approach to derive turbulent Prandtl number of fluids.

However for practical application, the empirical correlations are preferred for simplicity. But care should be taken while applying those correlations, because they were developed for particular range of parameters and fluids. Some of the empirical correlations developed for Pr_t for liquid metal applications are discussed below,

Aoki (1963) [152] proposed the following correlation,

$$Pr_t = X \left[1 - \exp\left(\frac{-1}{X}\right) \right] \quad (5.2)$$

Where, $X = 0.014 \text{ Re}^{0.45} \text{Pr}^{0.2}$, Reynolds (1975) [149] proposed following correlation for liquid metal flows,

$$\text{Pr}_t = (1 + 100 \text{Pe}^{-0.5}) \left[\frac{1}{1 + 120 \text{Re}^{-0.5}} - 0.15 \right] \quad (5.3)$$

Gori et al. (1979) [150] carried out numerical analysis for low Prandtl number fluids by using one equation (k) turbulence model near wall region and a two-equation (k- ϵ) turbulence model in the core region. From the analysis, they recommended that the Eq. (5.2) and Eq. (5.3) can be used for $40,000 < \text{Re} < 170,000$. For $170,000 < \text{Re} < 260,000$, the following correlation was proposed,

$$\text{Pr}_t = 0.85 + \frac{0.005}{\text{Pr}} \quad (5.4)$$

The above correlation was derived by Jischa and Rieke (1979) [153] based on the modelling of transport equations for turbulent kinetic energy, turbulent heat flux and turbulent mass flux. For $260,000 < \text{Re} < 400,000$, $\text{Pr}_t = 0.85$ was recommended. Cheng and Tak (2006) [146] developed a correlation for Pr_t , based on the evaluation of various heat transfer correlations for liquid metal flow and CFD analysis, which was given as,

$$\text{Pr}_t = \begin{cases} 4.12 & \text{for } \text{Pe} \leq 1000 \\ \frac{0.01 \text{Pe}}{[0.018 \text{Pe}^{0.8} - (7 - A)]^{1.25}} & \text{for } 1000 \leq \text{Pe} \leq 6000 \end{cases} \quad (5.5)$$

Where, A is given in Table 5.2.

5.3.2 Turbulence Models and Mesh Distribution

As it can be seen from Eq. (5.1) that ϵ_H is mainly calculated from ϵ_M . So it is important to analyse whether the turbulent momentum diffusivity, ϵ_M is calculated by turbulence models are correct or not. For Reynolds number up to 10000, which includes free convection, mixed convection and forced convection were solved by using low Re-turbulence

model as done by Jackson et al. (1988). For $Re > 10000$, four turbulence models which were available in PHOENICS-3.6 have been taken for the evaluation: a) standard k- ϵ model, which is the most widely used for turbulent CFD analysis. b) RNG (ReNormalised Group) k- ϵ model, which takes into account of the small scale turbulence by expressing them in terms of larger scale motions and modified viscosity. c) Chen and Kim modified k- ϵ turbulence model which improves dynamic response of ϵ -equation by introducing an additional time scale in the equation and d) LVEL (Length-VELocity) model, which is a zero equation turbulence model and a unique feature of PHOENICS. Equilibrium log-law wall functions were used to provide near-wall boundary conditions for the mean-flow and turbulence transport equations. The RNG k- ϵ turbulence model in PHOENICS is based on “Renormalized Group” theory and was proposed by Yakhot and Orszag (1986) [154]. In this model an inverse effective Prandtl number is used to calculate the effective thermal conductivity. The inverse effective Prandtl number varies with μ_{mol}/μ_{eff} , which is consistent with experimental evidence and takes care of turbulent heat transfer. There is no need to modify the turbulent Prandtl number because the model itself takes care of the turbulent heat transfer. It is reported that this model works well across a broad range of molecular Prandtl numbers, from liquid metals to paraffin oils. There were few literatures ([155] and [45]) where this model has been applied to LBE heat transfer studies. So an assessment of this model was also carried out. Mesh distribution was another factor to be considered carefully during CFD analysis. Here, 2-dimensional structured grid was used in cylindrical coordinate. The mesh density near the tube wall is important for the turbulent model applications. For low Re turbulence model, the y_1^+ is kept lower than 5. For high Reynolds number flow, as the wall function used is equilibrium log law function, the mesh density near the wall is kept so that $30 < y_1^+ < 130$ [156]. This requirement was met by adjusting the mesh numbers near the wall at different flow rate.

5.3.3 Evaluation of Nusselt number from PHOENICS Results

To compare the CFD results with empirical heat transfer correlations, Nusselt number was calculated from the temperature distribution obtained by the CFD analysis. The Nusselt number for fully developed region was calculated from the PHOENICS results as described below,

$$Nu = \frac{\bar{h}d}{k} \quad (5.6)$$

Where \bar{h} is the average heat transfer coefficient, and

$$\bar{h} = \frac{q''}{T_w - T_m} \quad (5.7)$$

Where q'' is the heat flux at the inner surface of the wall. T_w is the inner surface wall temperature of the tube and T_m was found as [157],

$$T_m = \frac{\sum Tu(2\pi r)dr}{\sum u(2\pi r)dr} \quad (5.8)$$

5.3.4 Thermo-physical Properties of Lead Bismuth Eutectic

The thermo-physical properties for the analysis were calculated from the equations as given in LBE Handbook (2007) [67]. Care has been taken to maintain the fluid temperature within the range of application of the properties.

5.3.5 Heat Transfer in Developing Flow

The flow in the heater and heat exchanger was assumed as the developing flow. The Nusselt number varies along the axial direction appreciably in this regions. For simultaneously hydro-dynamically and thermally developing liquid metal flow in pipe a correlation was given by Chen and Chiou (1981) [158] for calculating the local Nusselt number in developing flow with constant wall heat flux and is given below,

$$\frac{Nu_x}{Nu_\infty} = 0.88 + \frac{2.4}{x/d_h} - \frac{1.25}{\left(x/d_h\right)^2} \quad (5.9)$$

The range of applicability of the above correlation is $Pr \leq 0.03$ and $2 \leq x/d_h \leq 35$.

Where Nu_∞ is the Nusselt number for fully developed flow and to be evaluated based on the flow regime.

5.4 HEAT TRANSFER FORMULATIONS IN DIFFERENT PARTS OF THE LOOPS

KTL and LML were rectangular shaped closed loops with three major heat transfer sections such as heater section, piping (hot leg and cold leg) and heat exchanger. The convective heat transfer modes in LBE will be different in different sections of the loops. Following sections brief on the heat transfer in the different sections,

5.4.1 Heater Section

In KTL the heater section was vertical and the flow was in upward direction. The heat was added to the loop through the heater section pipe walls. During transient experiments different modes of convective heat transfer i.e. free convection, mixed convection and forced convection will be experienced in this section. In LML the heater was immersion type and was modelled as the heat source in the energy equation. The heat transfer coefficient need not to be defined to simulate the heat transfer from the heater to LBE in LML. However the heat loss through the heater section was to be modelled.

5.4.2 Piping

In the piping the heat transfer was mainly due to the heat loss through the insulation. This heat transfer rate was much less than that takes place in heater section and in the heat exchanger (less than 15%). So the gravitational effect on the heat transfer was negligible

here. The correlations for heat transfer coefficient which were developed without considering gravitational effect can be used in the piping.

5.4.3 Heat Exchanger

In LML the heat exchanger was in horizontal position, so the gravitational effect may not significant as in the vertical position. Shannon and Depew [159] (1968) shown that the gravitational effect on the heat transfer is not significant if $Ra^{0.25}/Nu_o < 2$. For low flow where this condition was satisfied the correlation from Ede (1961), given in Table 5.2 was used. For higher flow rate the correlation suggested by Holman (1964) [129], was used for the heat transfer coefficient calculation in the heat exchanger. In KTL however the heat exchanger was in vertical position. The effect of gravity has also favourable effect on the heat transfer as it assist the downward flow of the cooled LBE near the wall. Like in vertical heater, here also the three modes of convective heat transfer could be experienced. The heat transfer enhancement phenomena is similar to the vertical heated up ward flow conditions [120]. So based on this assumption, same heat transfer correlations derived for the vertical heated section were used to find the LBE heat transfer coefficient in the heat exchanger of KTL.

5.5 RESULTS AND DISCUSSIONS

For the analysis a circular tube with the geometry, thermal and flow conditions described in Table 5.3 was considered. The inlet temperature was kept at 500 °C. Figure 5.3 shows the 2D axi-symmetric mesh considered for the CFD analysis. A wall with thickness of 1.0 mm was considered.

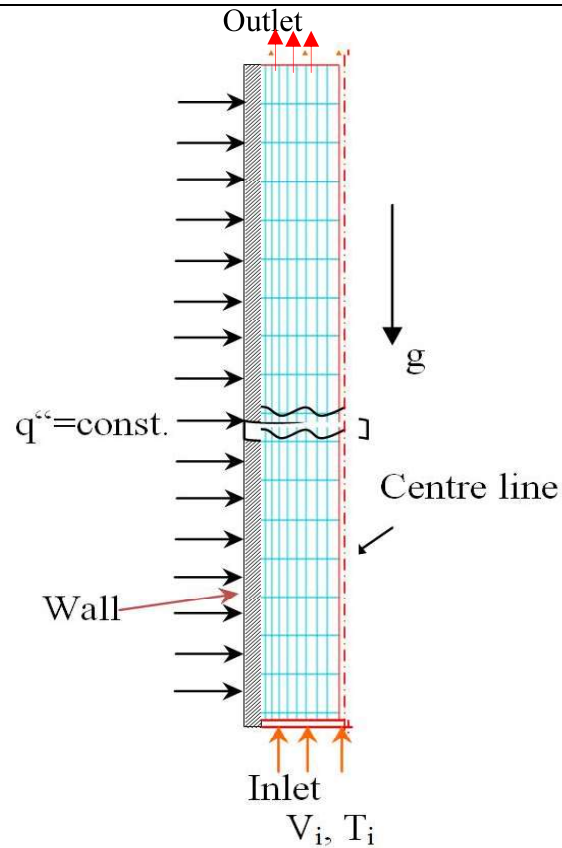


Fig. 5.3 2D axis-symmetric section of a tube with mesh distribution

Table 5.3: Parameters for the LBE heat transfer analysis

Parameters	Values
Coolant	LBE
Tube diameter/length (m)	0.02/2.0
Inlet Temperature ($^{\circ}\text{C}$)	773
Reynolds Number	5.0×10^4 to 4.5×10^5
Wall heat flux (W/m^2)	2.0×10^5
y_1^+	3-130

The boundary condition of constant heat flux was imposed on the outer surface of the tube wall. The velocity and thermal boundary layers were developed as the flow proceeds towards downstream of the heater section.

5.5.1 Free Convection

As we discussed above the free convection heat transfer correlations were available for vertical surfaces only. So CFD analysis was required to find the heat transfer in the vertical heated tube with molten LBE flow. For CFD analysis an axi-symmetry geometry of a vertical tube is considered as shown in Fig 5.3 where the flow is mainly due to the buoyancy force caused by heating at the tube wall surface. The inlet and outlet condition was defined as the constant pressure boundary conditions, due to which the flow direction may be either forward or backward across the inlet and outlet. The buoyancy force was defined by Grashof number. The Nusselt number which is mainly the function of the Gr and increases with the value of Gr. The Nusselt number variation was plotted with heat flux and the comparison is done with the correlations developed for vertical plates and mentioned in Table 5.1. Figure 5.4 shows the result. It can be seen that the prediction of the CFD code was much higher (>50%) than the correlations given in Table 5.1.

The validation of the CFD results could not be done directly, because the experimental results with free convection in vertical tubes could not be found in literature. So an effort was made to compare the results with the results of the mixed convection studies given by Jackson et al. (1994) [120]. He compared the enhancement of the heat transfer with the buoyancy factor, Bo. Bo is a function of modified Gr and inversely proportional to Reynolds number and Nusselt number. So, higher Bo means the higher dominance of buoyancy effect. At higher values of Bo, the free convection results should be comparable to the mixed convection data. A comparison of free convection results were compared with the mixed convection data from Jackson et al. (1994) [120] in Figure 5.5.

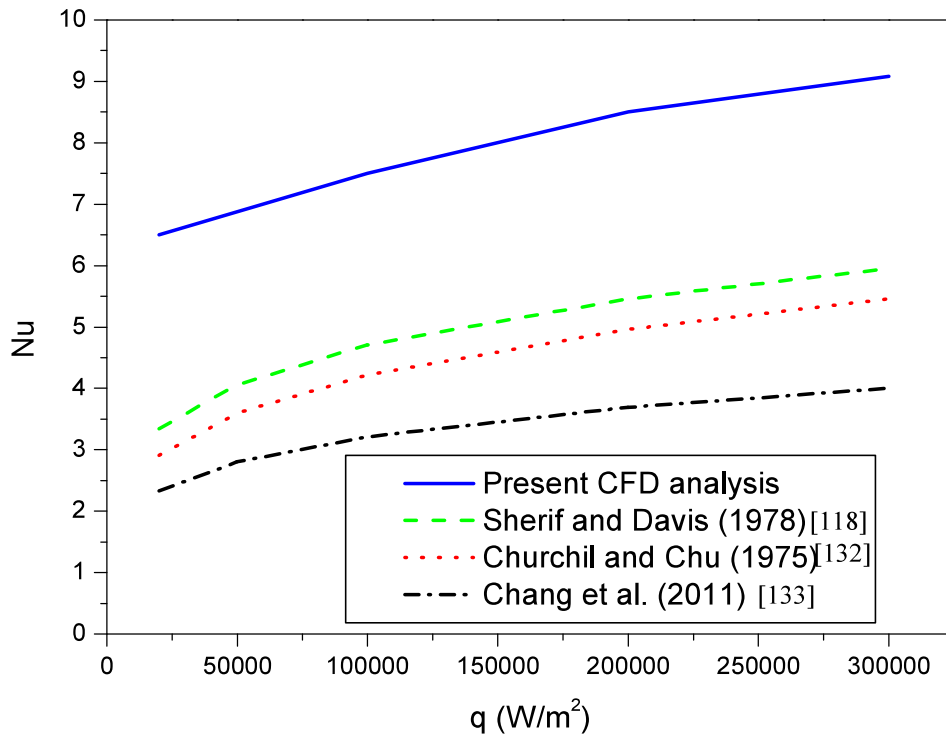


Fig 5.4 Prediction of CFD results for free convection heat transfer and comparison with correlations developed for vertical heated surfaces.

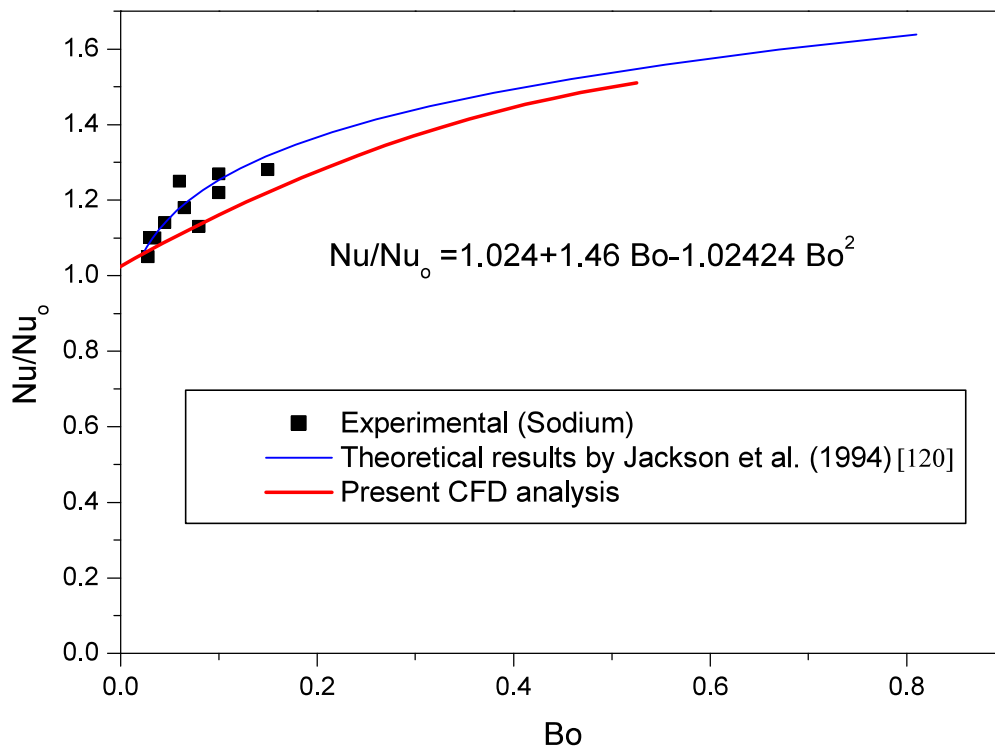


Fig 5.5 The prediction of free convection heat transfer and comparison with the data for mixed convection [120].

As expected the present free convection CFD results shows lower values compared to the mixed convection data. However the free convection values were showing similar trends and only 10% lower than the mixed convection data at high Bo values. The prediction of the CFD code thus can be assumed as reasonable. From the CFD results a correlation was developed with Bo as the function from Fig 5.5, which was given as,

$$\frac{Nu}{Nu_o} = 1.024 + 1.46Bo - 1.02424Bo^2 \quad (5.10)$$

where $Nu_o = 4.36$

To apply this correlation, it was assumed that a very small amount of bulk flow with $Re < 50$, exists in the convection. Such a low flow may exists during start up experiments in the liquid metal loops.

5.5.2 Mixed Convection

The effect of gravity on heat transfer in LBE in vertical tube at low Reynolds number range (i. e. $50 < Re < 4000$) was studied. It was found that the gravitational effect was prominent at low Reynolds number and becomes less effective as the value of Re increases. Figure 5.6 shows the simulation results of the heat transfer analysis by CFD. The comparison of the CFD results with the prediction of the correlation of Holman (1964) [142] and the formula $Nu = 4.36$ is shown in the figure. In the laminar flow range the gravitational effect was prominent and it enhances the heat transfer. As the value of Re increases, the difference between the formula and the Holman's correlation, also increases because the flow becomes turbulent at higher Reynolds number. For mixed convection heat transfer the experimental results were available for sodium and mercury. For LBE the experimental results could not be found. So CFD analysis was carried out for studies of mixed convection in vertical tube with LBE. CFD analysis was carried out for different wall heat flux at low flow to vary Bo.

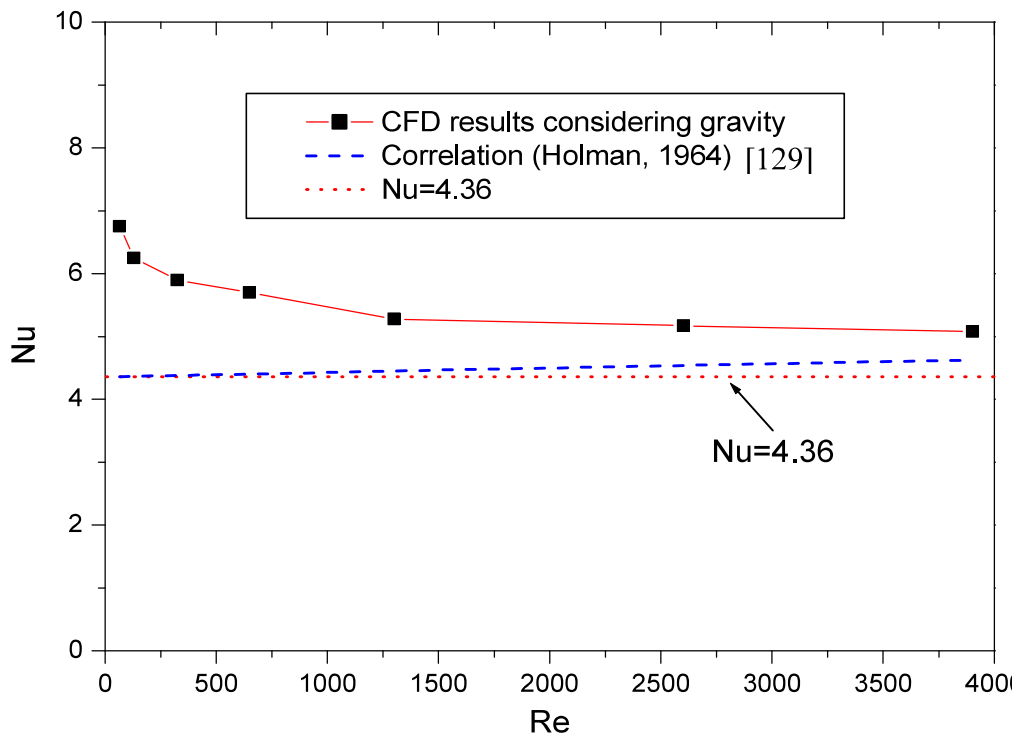


Fig 5.6 Variation of Nusselt number with Reynolds number for the range $50 < Re < 4000$.

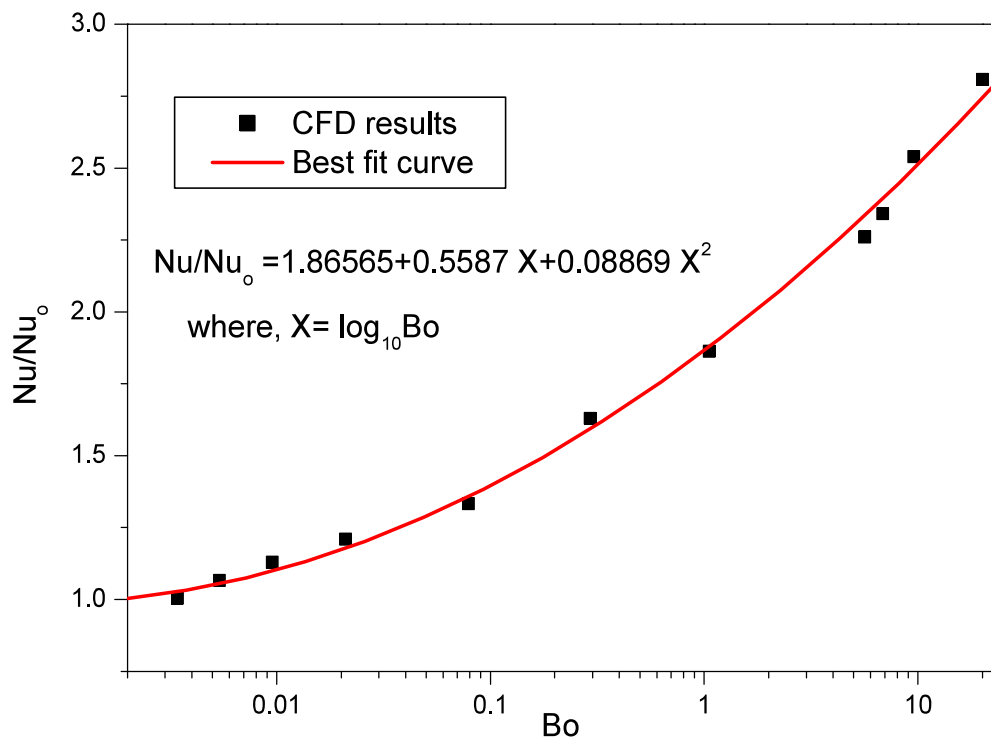


Fig 5.7 CFD results of the buoyancy aided mixed convection with LBE

The variation of the enhancement factor with Bo was predicted. Figure 5.7 shows the results of the CFD analysis. The best fit curve of the prediction gives the following correlation,

$$\frac{Nu}{Nu_o} = 1.8656 + 0.5587Bo - 0.08869Bo^2 \quad (5.11)$$

where $X = \log_{10}Bo$ and $Nu_o = 4.36 + 0.0053Pe$

This correlation can be used in the range of $50 < Re < 4000$.

5.5.3 Forced Convection

The CFD prediction of the Nusselt number for the flow range $4000 < Re < 10000$ with and without gravitational effect was shown in Fig 5.8. It can be seen that as the Re increases the gravitational effect diminishes. For this flow range three correlations were assessed and found that the correlation by Kirrilov and Ushakov (2001) [145] fits well with the CFD results. So the following correlation was taken for the Re range $4000 < Re < 10000$.

$$Nu = 5.0 + 0.025Pe^{0.8} \quad (5.12)$$

5.5.4 Heat Transfer Analysis at Higher Reynolds Number

As discussed in Section 5.2.4, there were a number of heat transfer correlations available for liquid metals in flow range, $Re > 10000$. Figure 5.9 depicts variation of Nusselt number as a function of Peclet Number using various heat transfer correlations given in Table 5.2. The correlations were assessed by comparing experimental results from Seban (1950) [160], Johnson et. al. (1954) [161] and Lubarski (1951) [162]. The correlation given by Lyon (1951) [140] over predicts the experimental data, with $Pr_t = 1.0$, while with $Pr_t = 3.0$ as shown Fig 5.9, it under predicts. So the influence of Pr_t on heat transfer coefficients can be observed. The correlation from Kirrilov and Ushakov (2001) [145] also over predicts the experimental results.

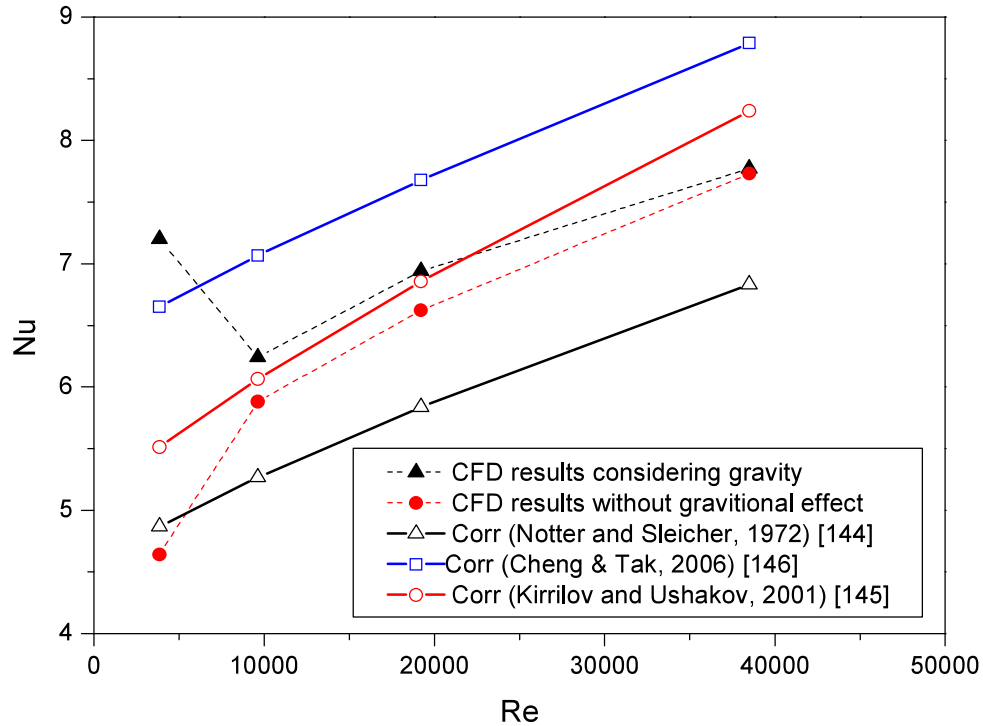


Fig 5.8 CFD results of LBE heat transfer in vertical tube for flow range $4000 < Re < 38500$.

It is to be noted that the correlation was developed from the results of experimental studies with pure sodium, whose thermo-physical properties were different from lead bismuth eutectic. The correlation of Notter & Sleicher (1972) [144] over predicts the experimental data by 10% up to $Pe=1500$. At higher flow the correlation predicts well, as shown in Fig. 5.9. This correlation has been used in LBE handbook (2007) [67] for assessment of other correlations for liquid metal applications. The correlation proposed by Cheng & Tak (2006) [146] under predicts the experimental results in whole flow range. The correlation suggested by Lubarsky and Kaufman (1955) [141] predicts well the experimental results up to Peclet number 2000. It should be noted that this correlation was developed from the results from twenty experimental studies. The working fluids of these studies include sodium, lead-bismuth and mercury. The correlation suggested by Lubarsky and Kaufman (1955) [141] under predicts the experimental results at higher flow. The correlation recommended by

Ibragimov et al. (1960) [142] also under predicts the experimental results. As mentioned in the literature the possible reason was that the correlation developed was without control of impurity and oxygen in the liquid metal during the experiments.

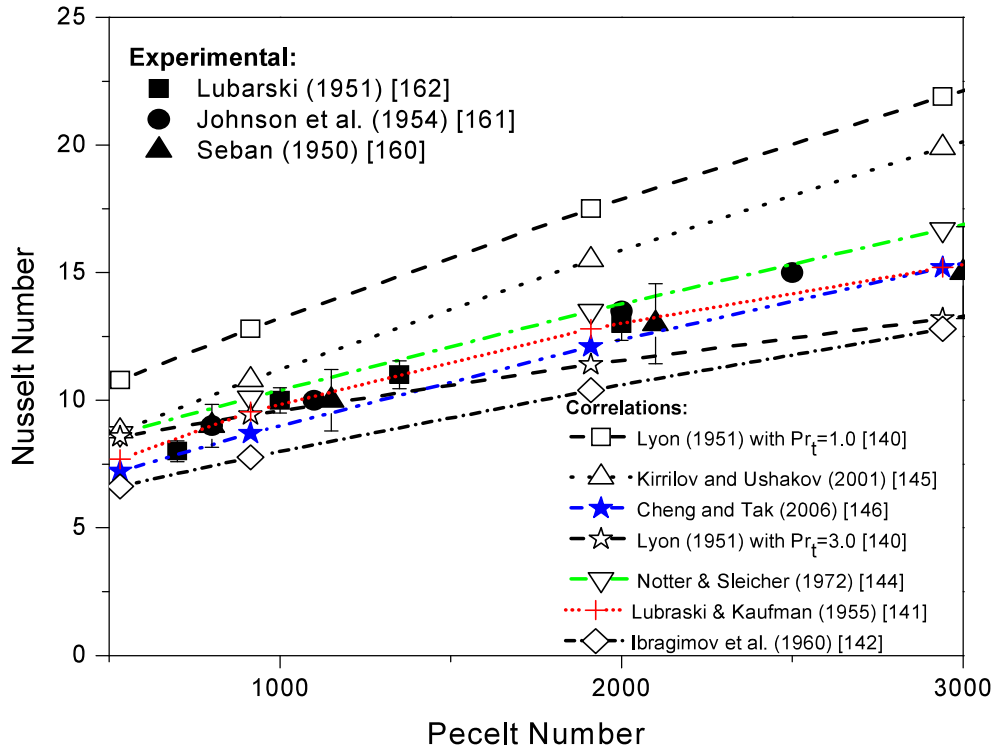


Fig 5.9 Comparison of liquid metal heat transfer correlations with experimental results.

His objective was to study the heat transfer performance of liquid metal in industrial environment. Since in the present studies, the flow range of LBE is less than $Pe = 2000$, the correlation given by Lubarsky and Kaufman (1955) [141] is found to be best to the experimental results and hence selected for further assessment of CFD analysis. Following sections give the details of the results of the analysis.

5.5.4.1 Effect of mesh size

For higher Reynolds number flow analysis also the mesh size was to be properly selected for correct results. The geometry was discretised with structured mesh as shown in

Figure 5.3. For discretising the domain, the guide lines suggested by NEA report (2007) [163] were followed.

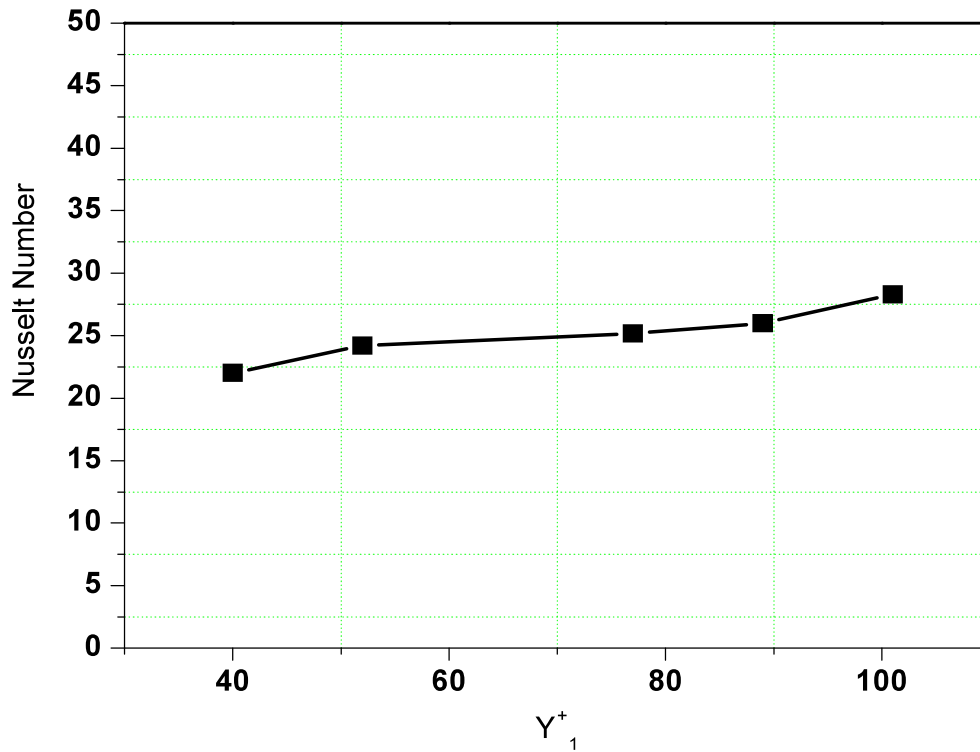


Fig 5.10 Variation of fully developed Nusselt Number with y_1^+ with k- ϵ turbulence model.

As per PHOENICS user manual (2005) [156] for k- ϵ based turbulence model application the value of y_1^+ should be maintained between 30 and 500. However since log law wall function was used for turbulence modelling y_1^+ was maintained between 30 and 120. Figure 5.10 shows the variation of Nusselt number with y_1^+ for inlet velocity of 2 m/s. Standard k- ϵ model was used for the analysis. It was seen that prediction of Nu in the range of $40 < y_1^+ < 80$ was unaffected by variation of y_1^+ . For further analysis the range of y_1^+ was kept in between 40 and 80 for all the flow velocities by changing the mesh size near the wall.

5.5.4.2 Turbulent Prandtl number effect

The turbulent Prandtl number varies with flow rate of the liquid metal. The various correlations for Pr_t were given by Eq. (5.2) to Eq. (5.5). Figure 5.11 shows the variation of turbulent Prandtl number with Peclet number by the above mentioned correlations. The correlation proposed by Cheng & Tak (2006) [146] covers entire range of Peclet number shown in the graph, while Reynolds (1975) [149] and Aoki (1968) [152] correlations were valid up to the Peclet number 2000. Beyond $Pe=2000$ the correlation from Jischa and Rieke (1979) [153] was valid. The Cheng and Tak (2006) [146] correlation for Pr_t was derived from empirical heat transfer correlations and results of CFD analysis.

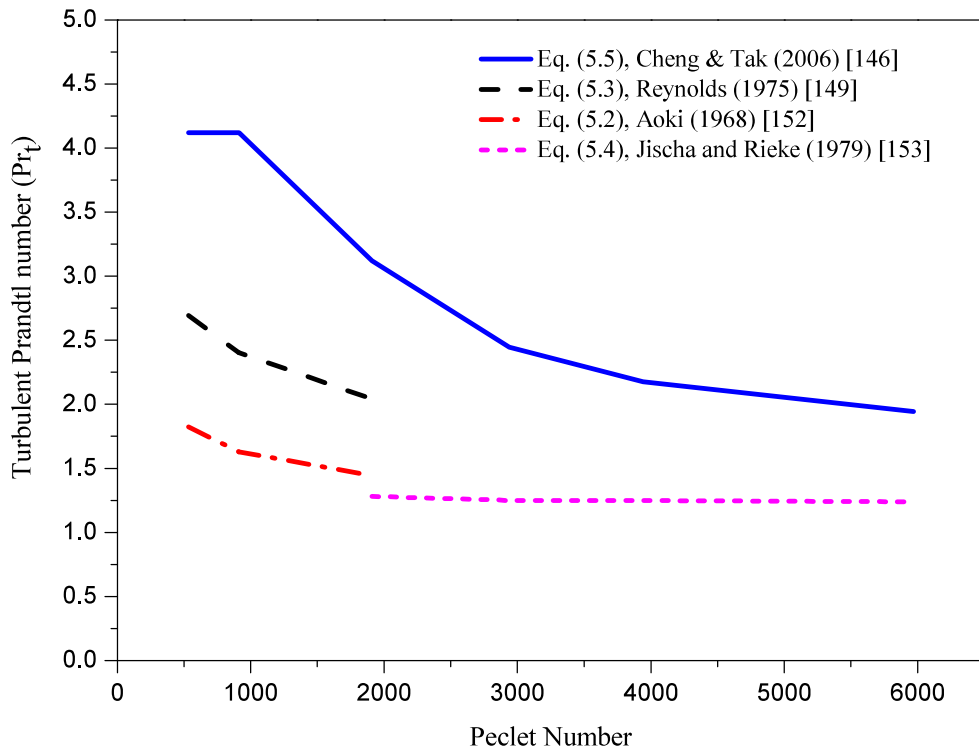


Fig 5.11 Variation of turbulent Prandtl Number with Peclet Number for liquid metal.

The value of A in Eq. (5.5) which was defined in Table 5.2, was used to fit the various regime of Peclet number. The non-linear equation of A makes the Pr_t variation not so smooth, as in the case of other two correlations. It can be seen from Figure 5.11 that the Pr_t calculated

by Eq. (5.2) is lower than Eq. (5.3), but trend of variation of Pr_t with Pe , by both equations were similar. Gori et al. (1979) [151] suggested the correlation from Jischa and Rieke (1979) [154] for higher Pe values ($Pe > 2000$). The prediction of the correlation is shown in shown in Fig 5.11. This correlation was suggested for high Pe range because at high Pe , turbulence plays dominant role in heat transfer as compared to molecular conduction. So the variation of Pr_t with Pe was not significant.

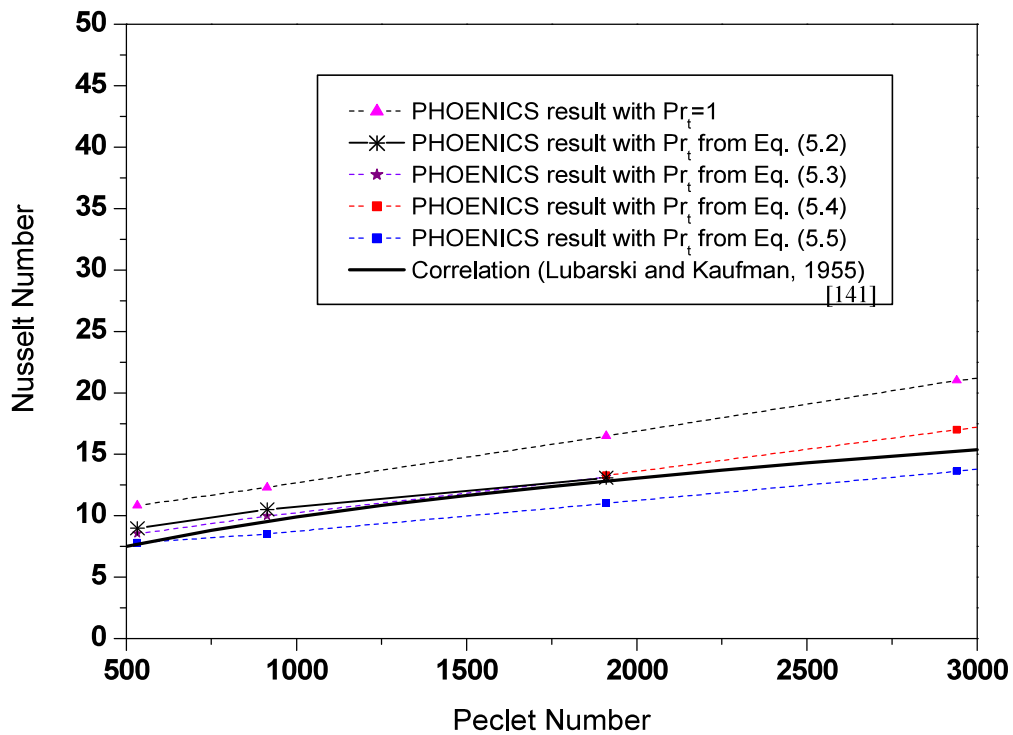


Fig. 5.12 Comparison of CFD prediction using standard $k-\epsilon$ model for different Pr_t with empirical correlation for Nusselt number.

To study the effect of turbulent Prandtl number on the heat transfer prediction using CFD, the Nusselt number for fully developed flow has been calculated for different flow rates. The turbulent Prandtl numbers estimated by Eqs. (5.2) to (5.5) were used in the standard $k-\epsilon$ turbulence model in PHOENICS code. Figure 5.12 shows the predicted variation of Nusselt number with Peclet number. For comparison, the Nusselt number estimated by the correlation of Lubarski and Kauffman (1955) [141] is also given in Fig 5.12. It can be seen

that with $Pr_t=1.0$, the CFD analysis over predicts Nusselt number. In case of liquid metal, thermal conductivity is much higher than that for air or water. The molecular conduction is higher than convective heat transfer near the wall. The turbulent thermal diffusivity plays a lesser role here. So as seen from Eq. (5.1) when $Pr_t = 1.0$, $\epsilon_H=\epsilon_M$, which means ϵ_H is overestimated in case of liquid metals. This results in higher prediction of heat transfer as seen in Figure 5.12. But, as per Eqs. (5.2) to (5.5), which were developed especially for liquid metals, Pr_t is always greater than one and can be seen in Figure 5.11. This makes $\epsilon_H<\epsilon_M$ and different values of Pr_t at various values of Pe regulate ϵ_H . From Figure 5.12, it can be seen that Pr_t calculated from Eqs. (5.2) to (5.4) give best conformation with correlations. The analysis with Pr_t from Eq. (5.5) under predicts the Lubarski and Kauffman correlation by 15% beyond $Pe=800$, which may be due to the value of Pr_t calculated by the equation is high which suppresses ϵ_H as per Eq. (5.1). From the above analysis it can be seen that up to $Pe=2000$, the Nusselt number, predicted by CFD analysis with the Pr_t values calculated from Eq (5.2) and Eq (5.3), match well with the correlation from Lubarsky and Kaufman (1955) [141].

5.5.4.3 Effect of turbulence models

The selection of turbulence model is also important for prediction of heat transfer. As discussed in Section 5.3.2, four turbulence models were selected for the analysis. Figure 5.13 shows the prediction of the Nusselt number using various turbulence models. The Pr_t values for this analysis were calculated from Eqs. (5.2) and (5.4). The values of Pr_t were incorporated in all the turbulence models except RNG k- ϵ model. In RNG k- ϵ model, the turbulent heat transfer was accounted by calculating effective Prandtl number, which in turn varies with turbulent viscosity and molecular Prandtl number (LBE Handbook, 2007).

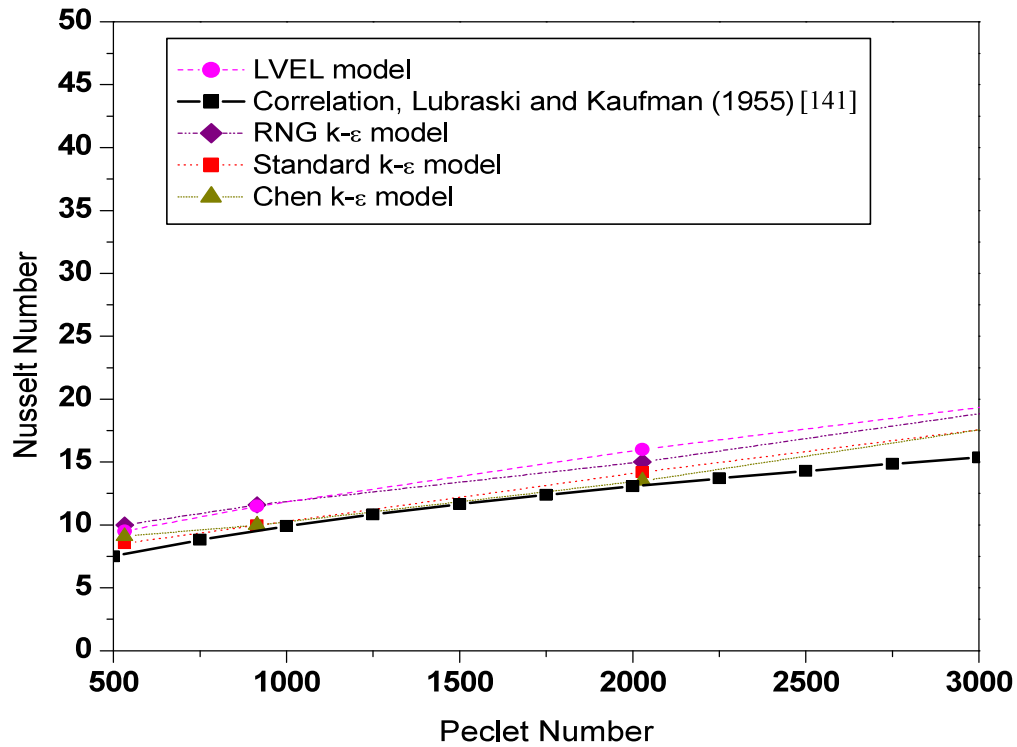


Fig. 5.13. Comparison of CFD prediction using different turbulence models with empirical correlations for Nusselt number.

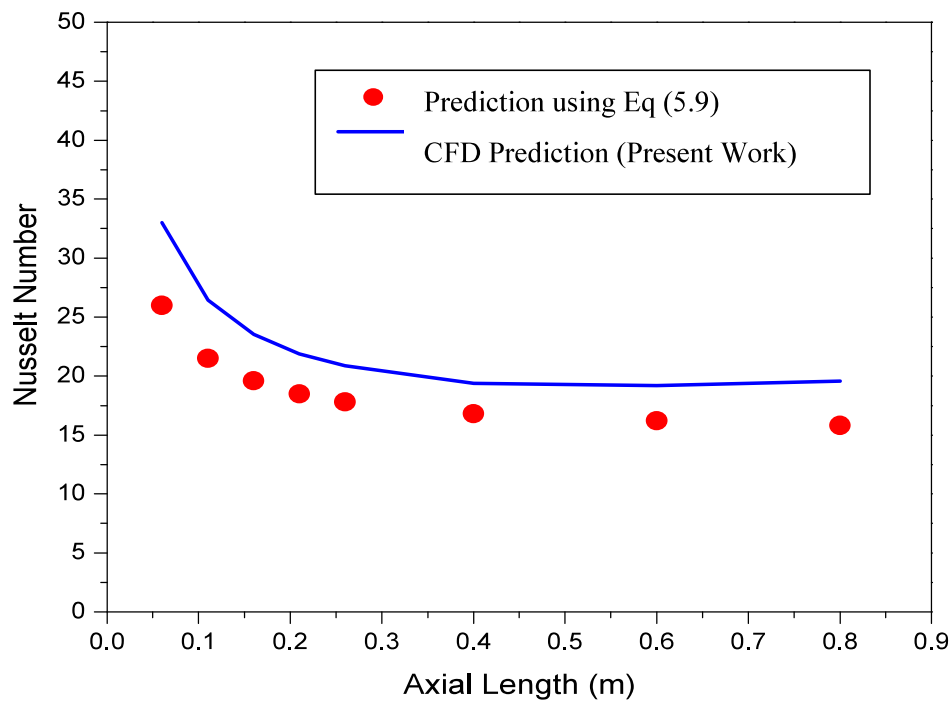


Figure 5.14. Variation of local Nusselt number along the axial distance.

The analysis using RNG k- ϵ turbulence model over predicts the Lubarsky and Kaufman (1955) [141] correlation by 10% at Peclet number 3000. Both standard k- ϵ model and Chen k- ϵ model with modified Pr_t shows good matches with the correlation by Lubarsky and Kaufman (1955) [141] up to $Pe = 2000$. So the correlation from Lubarsky and Kaufman (1955) [141] was selected for calculating Nusselt number for $500 < Pe < 2000$.

5.5.4.4 Developing length

It is well known that the local Nusselt number varies in the entry length due to the developing boundary layer. As shown in Figure 5.14, up to 0.5 m from the entrance the Nusselt number variation was very clear. Beyond this length the Nusselt number becomes steady, which means the flow was fully developed. It can be seen that at 0.1m length the local Nusselt number was 1.7 times higher than the developed flow. It can further be seen that the CFD results over predicts the correlation given by Eq. (5.9) through the tube length but this deviation is less than 10 %. The calculation was carried out with the inlet velocity $v=2$ m/s and with k- ϵ model. The Pr_t used in the CFD analysis was calculated from Eqs. (5.3) and (5.4).

5.6 SUMMARY OF MAJOR FINDINGS

1. Heat transfer correlations in LBE is found for different flow regimes (a) Free convection (b) mixed convection and (c) forced convection. The existing heat transfer correlations in liquid metals are reviewed and assessed for present applications. For free convection and mixed convection with $50 < Re < 4000$, heat transfer correlations for LBE were not available. So correlations were generated from CFD analysis for this ranges of flow. For other flow ranges (i.e. $Re > 4000$) the existing correlations were assessed and best fitted correlations with experimental results (available from

literature) and CFD results are selected for use in the theoretical analysis of the LBE natural circulation.

2. The application of general purpose CFD codes like PHOENICS in liquid metal heat transfer analysis requires that the turbulent Prandtl number is to be modified. Few correlations were found in literature on turbulent Prandtl number (Pr_t). After assessment, the correlation from Aoki (1963) [152] for $500 < Pe < 2000$ and Jischa and Reiki (1979) [153] for $2000 < Pe < 6000$ were selected for the present studies. For $Pe < 500$, $Pr_t = 4.12$ is taken as given by Cheng and Tak (2006) [146].
3. Based on the assessment and CFD analysis different correlations were recommended which are given in Table 5.4.

Table 5.4 Heat Transfer correlations used for fully developed flow

Correlations	Range	Remarks
$\frac{Nu}{Nu_o} = 1.024 + 1.46Bo - 1.02424Bo^2$ where, $Nu_o = 5.0 + 0.025Pe^{0.8}$	Free convection for $Re < 50$,	Developed from present CFD analysis
$\frac{Nu}{Nu_o} = 1.8656 + 0.5587X - 0.08869X^2$ where $X = \log_{10}Bo$ and $Nu_o = 4.36 + 0.0053Pe^*$	Mixed convection for $50 < Re < 4000$	Developed from present CFD analysis
$Nu = 5.0 + 0.025Pe^{0.8}$	for $4000 < Re < 10000$	Correlation from Kirrilov and Ushakov (2001) [145]
$Nu = 6.3 + 0.0167Re^{0.85}Pr^{0.93}$	for $Re > 10000$	Correlation from Notter and Sleicher (1972) [144]

Except for the free convection regime, the correlation for developing flow as given in Eq. (5.9) was used in the heater and cooler sections to find the axially varying heat transfer coefficient.

Chapter 6

DEVELOPMENT OF COMPUTER CODE LeBENC

6.1 INTRODUCTION

The literature survey carried out on liquid metal natural circulation revealed that the system codes were generally used for water based system analysis. Since no system codes were available in hand for the LBE system analysis, a code was needed to be developed. The code should be able to analyse the steady state and transient natural circulation flow of LBE in a closed loop, considering all the parameters which may affect the natural circulation flow of LBE at high temperature. A 1 D computer code was developed based on the formulation given by Vijayan et al. (2001) [11]. The code was developed to simulate the LML and consequently upgraded to simulate the KTL also. Following sections give the details of the code, analysis and validation with experimental data of LML and KTL.

6.2. NUMERICAL CODE, LeBENC

A code named LeBENC (Lead Bismuth Eutectic Natural Circulation) has been developed to predict the behaviour of liquid metal loop under natural circulation. The code has the ability to, (a) handle non-uniform diameter loops, (b) different working fluid in primary and secondary side of the loop, (c) handle trace heating and surface heat loss from the walls to ambient (d) axial conduction through liquid metal and the pipe wall and (e) simulate both steady state as well as transient natural circulation flow. LeBENC is a one dimensional finite difference code, developed to study the steady state and transient behaviour of liquid metal natural circulation loop.

6.2.1 Mathematical Formulation of LeBENC Code for LML

This section provides an overview of the theoretical formulation and solution procedure used in the code LeBENC. The 1-D governing equations were discussed below. Since this was a closed loop with incompressible fluid, the mass flow rate is independent of the locations in the loop and is only a function of time. So the continuity equation was not considered for the analysis. The momentum equation solves the natural circulation flow rate by equating the mainly the buoyancy head and the total pressure drop in the loop. Energy equation takes account of the heat energy transfer in the loop. Fluid axial conduction is considered in the energy equation as it might play an important role in LBE loop. Axial conduction of the solid wall was also solved by considering the axial conduction equation. The code was validated with experimental results of single phase water natural circulation loop [164].

6.2.1.1 Momentum equation for fluid

Assuming Boussinesq approximation to be valid, the momentum equation, for 1-D incompressible flow neglecting pressure work and viscous dissipation, for ‘ith’ pipe section can be written as,

$$\frac{\Delta x_i}{A_{in}} \frac{dW}{dt} = \rho g \Delta z_i - \frac{f_i \Delta x_i}{D_{in,i}} \left(\frac{W}{2\rho_0 A_{in,i}^2} \right) - k_i \left(\frac{W^2}{2\rho_0 A_{in,i}^2} \right) - \Delta p_i - \Delta p_{acc,i} \quad (6.1)$$

In the buoyancy term, the density ρ was given by the following equation which is valid over small temperature ranges,

$$\rho = \rho_0 [1 - \beta(T - T_0)] \quad (6.2)$$

The summation of acceleration pressure drop and static pressure drop in a closed loop becomes zero. Therefore, Eq. (6.1) can be written as,

$$\oint \frac{\Delta x_i}{A_i} \frac{dW}{dt} = \rho_0 g \beta \oint T_i \Delta z_i - \oint \frac{f_i \Delta x_i}{D_i} \left(\frac{W^2}{2\rho_0 A_i^2} \right) - \oint k_i \left(\frac{W^2}{2\rho_0 A_i^2} \right) \quad (6.3)$$

6.2.1.2 Energy equation for fluid

$$\frac{\partial T}{\partial t} - \alpha \frac{\partial^2 T}{\partial x^2} + \frac{W}{A\rho_0} \frac{\partial T}{\partial x} = \begin{cases} \frac{-h_{in}(T - T_{wi})}{D\rho_0 Cp} + \frac{q\xi_h}{\rho_0 Cp A} & \text{Heated section} \\ \frac{-h_{in}(T - T_{wi})}{D\rho_0 Cp} & \text{pipe and heat exchanger} \end{cases} \quad (6.4)$$

It can be noted that the second term of the right hand side of the equation was for the heat source (immersion heater) in the heated section of the loop.

6.2.1.3 Conduction equation for the wall

Heat loss from the pipe wall was considered in writing conduction equation for the pipe wall.

$$\frac{\partial T_w}{\partial t} - \alpha_w \frac{\partial^2 T_w}{\partial x^2} = \begin{cases} \frac{4h_{in}(T_w - T_i)}{\rho_w Cp_w} \left(\frac{D_{in}}{D_o^2 - D_{in}^2} \right) - \frac{4h_a(T_w - T_a^n)}{\rho_w Cp_w} \left(\frac{D_{in}}{D_o^2 - D_{in}^2} \right) & \text{For heater and pipe} \\ \frac{4h_{in}(T_w - T_i)}{\rho_w Cp_w} \left(\frac{D_{in}}{D_o^2 - D_{in}^2} \right) - \frac{4h_s(T_w - T_s^n)}{\rho_w Cp_w} \left(\frac{D_{in}}{D_o^2 - D_{in}^2} \right) & \text{For heat exchanger} \end{cases} \quad (6.5)$$

The thermal conduction resistance across the pipe wall thickness is not considered in the equation.

6.2.2 Discretization of the Governing Equations

Out of several possible ways to discretize the governing equations, the implicit method for discretizing the momentum equation and the explicit method for discretizing energy equation for fluid as well as conduction equation for wall were used.

6.2.2.1 Discretization of momentum equation

The implicit scheme for discretizing momentum equation was used as shown below,

$$\sum_{i=1}^N \frac{\Delta x_i}{A_i} \frac{W^{n+1} - W^n}{\Delta t} = \rho_0 g \beta \oint T_i^{n+1} \Delta z_i - \sum_{i=1}^N \left(\frac{f_i \Delta x_i}{D_i} + k_i \right) \left(\frac{W^{n+1}}{2 \rho_0 A_{in,i}^2} \right) \quad (6.6)$$

Temperature integral $\oint T_i^{n+1} \Delta z_i$ in the above equation, was evaluated by using the Trapezoidal rule. Eq (6.6) can be written after simplification as,

$$W^{n+1} = W^n - \left(\frac{C_2}{C_1} \Delta t \right) W^{n+1} |W^{n+1}| + \left(\frac{C_3}{C_1} \Delta t \right) \sum_{i=1}^N T_i^{n+1} \Delta z_i \quad (6.7)$$

Where C_1 , C_2 and C_3 were given by,

$$\left. \begin{aligned} C_1 &= \sum_{i=1}^N \frac{\Delta x_i}{A_{in,i}} \\ C_2 &= \sum_{i=1}^N \left(\frac{f_i \Delta x_i}{D_{in}} + k_i \right) \left(\frac{1}{2 \rho_0 A_{in}^2} \right) \\ C_3 &= \rho_0 g \beta \end{aligned} \right\} \quad (6.8)$$

For solving the momentum equation T_i^{n+1} was taken from the energy equation.

6.2.2.2 Discretization of energy equation

For energy equation, first order explicit upwind scheme and central difference scheme was used to discretize the convective term and the diffusion term respectively. The discretized energy balance equation for ' i^{th} ' node of the fluid in the heater section can be written as follows,

$$\frac{T_i^{n+1} - T_i^n}{\Delta t} = \alpha \left(\frac{T_{i+1}^n - 2T_i^n + 2T_{i-1}^n}{\Delta x_i^2} \right) - \frac{W}{\rho_0 A_{in,i}} \left(\frac{T_i^n - T_{i-1}^n}{\Delta x_i} \right) - \frac{4h_{in,i}}{D_{in,i} \rho_0 Cp} (T_i^n - T_{w,i}^{n+1}) + \frac{q\zeta_h}{\rho_0 Cp A_{in,i}} \quad (6.9a)$$

for heater section

$$\frac{T_i^{n+1} - T_i^n}{\Delta t} = \alpha \left(\frac{T_{i+1}^n - 2T_i^n + 2T_{i-1}^n}{\Delta x_i^2} \right) - \frac{W}{\rho_0 A_{in,i}} \left(\frac{T_i^n - T_{i-1}^n}{\Delta x_i} \right) - \frac{4h_{in,i}}{D_{in,i} \rho_0 Cp} (T_i^n - T_{w,i}^{n+1}) \quad (6.9b)$$

for heat exchanger and pipe

After some algebraic manipulations, the above equation can be written as,

$$T_i^{n+1} = a_{i+1}^n T_{i+1}^n + a_i^n T_i^n + a_{i-1}^n T_{i-1}^n + b_i^{n+1} \quad (6.10)$$

The values of coefficients in Eq. (6.10) were given in Table 6.1,

Again, the coefficients of T_i^{n+1} , T_{i-1}^n and T_{i+1}^n were all positive but that of T_i^n can become negative. Therefore the limiting time step to keep the coefficient positive was expressed as, for $W > 0$

$$\Delta t = \frac{1}{\left(\frac{2\alpha}{\Delta x_i^2} + \frac{W^n}{\rho_0 A_{m,i} \Delta x_i} + \frac{4h_{m,i}}{\rho_0 Cp D_{m,i}} \right)} \quad (6.11)$$

for $W < 0$

$$\Delta t = \frac{1}{\left(\frac{2\alpha}{\Delta x_i^2} - \frac{W^n}{\rho_0 A_{m,i} \Delta x_i} + \frac{4h_{m,i}}{\rho_0 Cp D_{m,i}} \right)} \quad (6.12)$$

It is to be noted that time step was function of mass flow rate. Therefore, time step is to be recalculated for each new time level.

6.2.2.3 Discretization of conduction equation for the wall

Discretized energy balance equation for ' i^{th} ' node of wall can be written as

$$\left(\frac{T_{w,i}^{n+1} - T_{w,i}^n}{\Delta t} \right) = \alpha_w \frac{(T_{w,i+1}^n - 2T_{w,i}^n + T_{w,i-1}^n)}{\Delta x_i^2} - \frac{4h_{m,i}(T_{w,i}^n - T_i^n)}{\rho_w Cp_w} \left(\frac{D_{m,i}}{D_{o,i}^2 - D_{m,i}^2} \right) - \frac{4h_o(T_{w,i}^n - T_o^n)}{\rho_w Cp_w} \left(\frac{D_{m,i}}{D_{o,i}^2 - D_{m,i}^2} \right) \quad (6.13)$$

After some algebraic simplifications above equation can be written as

$$T_{w,i}^{n+1} = a_{w,i+1}^n T_{w,i+1}^n + a_{w,i}^n T_{w,i}^n + a_{w,i-1}^n T_{w,i-1}^n + b_{w,i}^n \quad (6.14)$$

The values of coefficients in Eq. (6.14) were given in Table 6.1,

Table 6.1 Values of the coefficients in Eq. (6.10) and Eq. (6.14)

Coefficient		Energy Equation [Eq. (6.10)]		Wall conductions Equation [Eq. (6.14)]
		W>0	W<0	
$a_{i+1}^n, a_{w,i+1}^n *$		Fo_i^n	$Fo_i^n - Co_i^n$	$Fo_{w,i}^n$
$a_i^n, a_{w,i}^n *$	Heater section	$1 - 2Fo_{w,i} - Co_i^n - \frac{4h_m \Delta t}{\rho_0 Cp D_{m,i}}$	$1 - 2Fo_{w,i} + Co_i^n - \frac{4h_m \Delta t}{\rho_0 Cp D_{m,i}}$	$1 - 2Fo_{w,i} - \frac{4h_m}{\rho_w Cp_w} \frac{D_{m,i} \Delta t}{(D_{o,i}^2 - D_{m,i}^2)} - \frac{4h_a}{\rho_w Cp_w} \frac{D_{o,i} \Delta t}{(D_{o,i}^2 - D_{m,i}^2)}$
	Piping	$1 - 2Fo_{w,i} - Co_i^n - \frac{4h_m \Delta t}{\rho_0 Cp D_{m,i}}$	$1 - 2Fo_{w,i} + Co_i^n - \frac{4h_m \Delta t}{\rho_0 Cp D_{m,i}}$	$1 - 2Fo_{w,i} - \frac{4h_m}{\rho_w Cp_w} \frac{D_{m,i} \Delta t}{(D_{o,i}^2 - D_{m,i}^2)} - \frac{4h_a}{\rho_w Cp_w} \frac{D_{o,i} \Delta t}{(D_{o,i}^2 - D_{m,i}^2)}$
	Heat exchanger	$1 - 2Fo_{w,i} - Co_i^n - \frac{4h_m \Delta t}{\rho_0 Cp D_{m,i}}$	$1 - 2Fo_{w,i} + Co_i^n - \frac{4h_m \Delta t}{\rho_0 Cp D_{m,i}}$	$1 - 2Fo_{w,i} - \frac{4h_m}{\rho_w Cp_w} \frac{D_{m,i} \Delta t}{(D_{o,i}^2 - D_{m,i}^2)} - \frac{4h_s}{\rho_w Cp_w} \frac{D_{o,i} \Delta t}{(D_{o,i}^2 - D_{m,i}^2)}$
$a_{i-1}^n, a_{w,i-1}^n *$		$Fo_i^n + Co_i^n$	Fo_i^n	$Fo_{w,i}^n$
$b_i^n, b_{w,i}^{n+1} *$	Heater section	$\frac{4h_m \Delta t T_{w,i+1}^{n+1}}{\rho_0 Cp D_{m,i}} - \frac{q \xi_h}{\rho_0 Cp A_{in}} \Delta t$		$\frac{4h_m}{\rho_w Cp_w} \frac{D_{m,i}}{(D_{o,i}^2 - D_{m,i}^2)} T_i^n + \frac{4h_a}{\rho_w Cp_w} \frac{D_{o,i}}{(D_{o,i}^2 - D_{m,i}^2)} T_{o,i}^n$
	Piping	$\frac{4h_m \Delta t T_{w,i+1}^{n+1}}{\rho_0 Cp D_{m,i}}$		$\frac{4h_m}{\rho_w Cp_w} \frac{D_{m,i} \Delta t}{(D_{o,i}^2 - D_{m,i}^2)} T_i^n + \frac{4h_a}{\rho_w Cp_w} \frac{D_{o,i} \Delta t}{(D_{o,i}^2 - D_{m,i}^2)} T_{o,i}^n$
	Heat exchanger	$\frac{4h_m \Delta t T_{w,i+1}^{n+1}}{\rho_0 Cp D_{m,i}}$		$\frac{4h_m}{\rho_w Cp_w} \frac{D_{m,i} \Delta t}{(D_{o,i}^2 - D_{m,i}^2)} T_i^n + \frac{4h_s}{\rho_w Cp_w} \frac{D_{o,i} \Delta t}{(D_{o,i}^2 - D_{m,i}^2)} T_{o,i}^n$

*coefficients for Eq (6.14)

The coefficients of $T_{w,i}^{n+1}$, $T_{w,i-1}^n$ and $T_{w,i+1}^n$ were all positive but that of $T_{w,i}^n$ may become negative depending on the chosen time step. Therefore the limiting time step to keep the coefficient $T_{w,i}^n$ of positive was expressed as,

$$\Delta t = \left(2 \frac{\alpha_w}{\Delta x_i^2} + \frac{4h_{in,i}}{\rho_w C p_w} \frac{D_{in,i}}{(D_{o,i}^2 - D_{in,i}^2)} + \frac{4h_o}{\rho_w C p_w} \frac{D_{in,i}}{(D_{o,i}^2 - D_{in,i}^2)} \right)^{-1} \quad (6.15)$$

The minimum of the time steps, as calculated by Eq. (6.11), Eq. (6.12) and Eq. (6.15), was taken for calculation in each time level.

Fo_i^n and Co_i^n were Fourier number and Courant number respectively calculated at n^{th} time level and were given by,

$$Fo_i^n = \frac{\alpha \Delta t}{\Delta x_i^2}, \quad Fo_{w,i}^n = \frac{\alpha_w \Delta t}{\Delta x_i^2}, \quad Co_i^n = \frac{W^n \Delta t}{\rho_0 A_{in,i} \Delta x_i} \quad (6.16)$$

6.2.3 Solution Procedure Adopted in the Code

For convenience in calculation, the length of the node in wall and fluid were taken equal. These nonlinear and coupled equations were then solved iteratively using the procedure mentioned below.

- 1) The minimum of the time steps as calculated from Eq. (6.11) or Eq. (6.12) and Eq. (6.15) was taken for calculation.
- 2) Discretized wall conduction equation i.e., Eq. (6.14) was solved explicitly using above time step to obtain $T_{w,i}^{n+1}$.
- 3) Using $T_{w,i}^{n+1}$ in discretized energy balance equation for fluid i.e., Eq. (6.10), nodal fluid temperature at new time level (i.e., T_i^{n+1}) was obtained.

- 4) Temperature integral $\oint T_i^{n+1} \Delta z_i$ in momentum balance equation i.e., in Eq. (6.7), was evaluated by using the Trapezoidal rule.
- 5) Flow rate at new time level i.e., W^{n+1} was obtained by solving discretized momentum equation i.e., Eq. (6.7).
- 6) Step (1) to (5) was repeated until steady state was achieved.

6.2.4 Discretization of LML

The whole loop was discretised into 14 segments and 280 nodes. The discretisation of the simplified geometry of the loop was shown in Fig. 6.1. Table 6.2 shows the details of the main loop components and sizes.

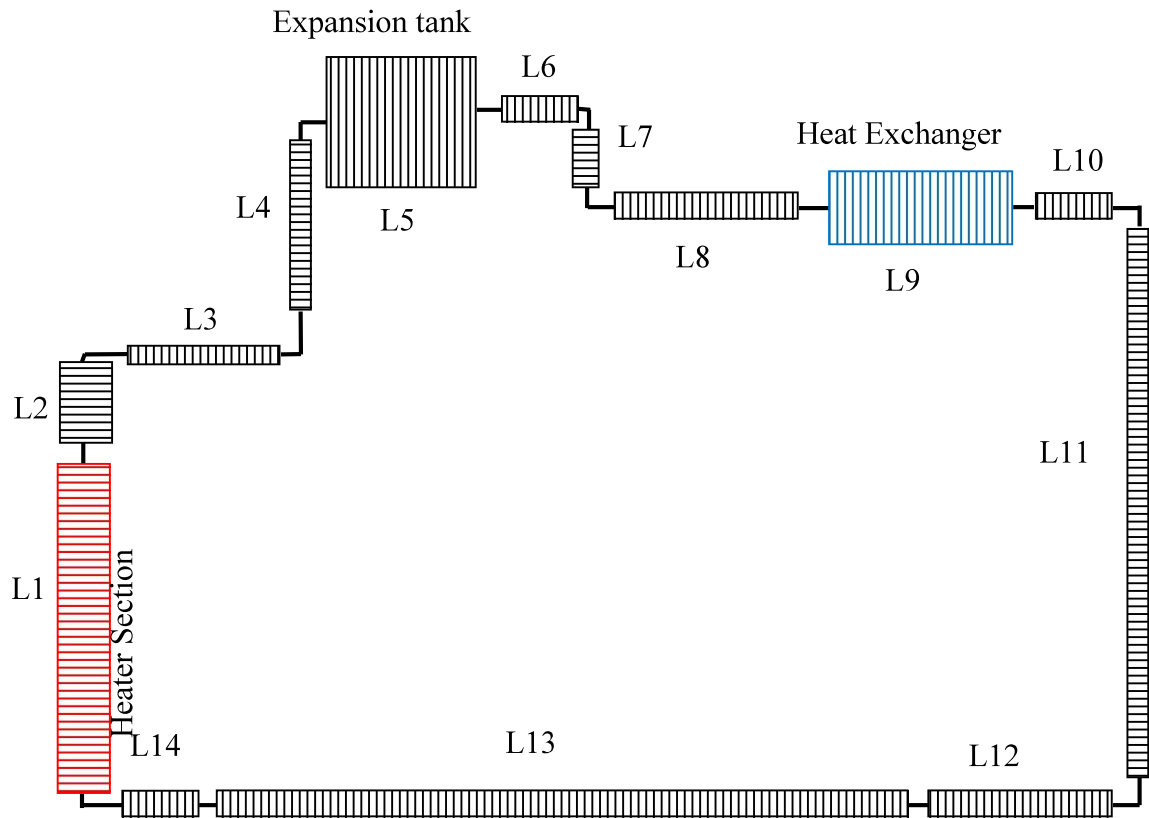


Fig. 6.1 Discretisation of the Loop geometry for analysis using LeBENC code

Thermo physical properties of LBE were taken from LBE handbook (2007) [67]. Temperature dependent properties were calculated at each time step by incorporating recommended correlations of the properties in the code. The properties of piping material, was taken from Incropera and Dewitt (1996) [157] which were also temperature dependent.

Table 6.2 Loop parameters used in the code (Fig 6.1)

Segment	Part details	Length (mm)
L1	Heated section, 75NB sch 80 pipe	800
L2	75NB sch 80 pipe	100
L3	15NB sch 80 pipe	200
L4	15NB sch 80 pipe	450
L5	Expansion tank, 200NB sch 80 pipe	350
L6	15NB sch 80 pipe	200
L7	15NB sch 80 pipe	300
L8	15NB sch 80 pipe	325
L9	Heat Exchanger, Primary side :NB, sch 80	500
L10	15NB sch 80 pipe	200
L11	15NB sch 80 pipe	1050
L12	15NB sch 80 pipe	350
L13	15NB sch 80 pipe	1150
L14	15NB sch 80 pipe	350

6.2.5 Constitutive Equations

Since molten lead bismuth is Newtonian fluid so the hydraulic loss coefficients validated with water is applicable for molten LBE also [59]. The hydraulic resistance

correlations given in the Handbook by Idelchik (1988) [165] were used. The hydraulic loss coefficients in the loop were calculated using the correlations given in Table 6.3.

Table 6.3 Correlations for pressure loss coefficients used in the LeBENC analysis

Pressure losses	Correlations	Range of application
Frictional losses	$f = \frac{64}{Re}$	$Re < 2000$ and $\bar{\Delta} \leq \bar{\Delta}_{lim}$
	$f = \frac{0.316}{Re^{0.25}}$	$4000 \leq Re \leq 10^5$ and $\bar{\Delta} \leq \bar{\Delta}_{lim}$
	$f = 4.4 Re^{-0.595} \exp\left(-\frac{0.00275}{\bar{\Delta}}\right)$	For $Re_o < Re < Re_1$
	$f = (f_2 - f^*) \exp\left\{-\left[0.0017(Re_2 - Re)\right]^2\right\} + f^*$ Where $f^* = 0.032$, $f_2 = 7.244 Re^{-0.649}$ for $\bar{\Delta} \leq 0.007$ $f^* = 0.0758 - \frac{0.0109}{\bar{\Delta}^{0.286}}$, $f_2 = \frac{0.145}{\bar{\Delta}^{-0.244}}$ for $\bar{\Delta} > 0.007$	For $Re_1 < Re < Re_2$
	$f = \frac{1}{\left[2 \log(2.51 / Re \sqrt{f + \bar{\Delta} / 3.7})\right]^2}$	For $Re > Re_2$
Local Losses	$k = \left(1 - \frac{A_o}{A_1}\right)^2$	Sudden expansion
	$k = 0.5 \left(1 - \frac{A_o}{A_1}\right)$	Sudden Contraction

The local pressure loss coefficients at the elbows were also calculated from correlations and the graphical data given by Idelchik et al. (1988) [164]. The effect of roughness on pressure drop depends on the flow rate also. The limiting value of roughness below which the surface can be treated as smooth, was given as (Idelchik, 1988) [164],

$$\overline{\Delta}_{\text{lim}} = \frac{18 \times \log \text{Re} - 16.4}{\text{Re}} \quad (6.17)$$

The surface roughness may cause the departure of the frictional pressure drop coefficient from Hagen-Poiseulle law beyond a certain flow rate. This limiting value was given by Re_o . Similarly the change of flow from laminar to transition was given by Re_1 and the transition to turbulent was given by Re_2 . The correlations to find the limiting Reynolds numbers were given below,

$$\text{Re}_o = 754 \exp\left(\frac{0.0065}{\overline{\Delta}}\right), \quad \text{Re}_1 = 1160 \left(\frac{1}{\overline{\Delta}}\right)^{0.11} \quad \text{and} \quad \text{Re}_2 = 2090 \left(\frac{1}{\overline{\Delta}}\right)^{0.0635}$$

The heat transfer coefficients in LBE in the heat exchanger and the piping was calculated from the following correlation suggested by Holman (1964) [129],

$$\text{Nu} = 4.36 + 0.0053 \text{ Pe} \quad (6.18)$$

6.3 FORMULATION OF LEBENC CODE FOR KTL

6.3.1 Mathematical Formulation of LeBENC Code for KTL

The primary side of KTL is a closed loop whereas, the secondary side of the KTL is an open loop where the argon gas is driven by natural convection. So the LeBENC code had to be modified to handle two loops in series. The details of the governing equations were given below,

6.3.1.1 Momentum equation for fluid

As explained above 1D momentum equation can be written as given in Eq (6.1), assuming Boussinesq approximation to be valid, incompressible flow and neglecting viscous dissipation. In buoyancy term, the density ρ was given by the Eq (6.2), which is valid over small temperature ranges. The summation of acceleration pressure drop and static pressure drop in a closed loop becomes zero.

So, for primary side,

$$\sum_i \frac{\Delta x_{i,1}}{A_{i,1}} \frac{dW_1}{dt} = \rho_{0,LBE} g \beta_{LBE} \oint T_{i,1} \Delta z_{i,1} - \sum_{i=1}^{N_1} \frac{f_{i,1} \Delta x_{i,1}}{D_{i,1}} \left(\frac{W_1^2}{2\rho_{0,LBE} A_{i,1}^2} \right) - \sum_{i=1}^{N_1} k_{i,1} \left(\frac{W_1^2}{2\rho_{0,LBE} A_{i,1}^2} \right) \quad (6.19)$$

In the secondary side though the loop was not closed, the acceleration pressure drop was neglected because the heat exchanger height was small and argon gas flow rate was also low.

Therefore, the momentum equation can be written as,

$$\frac{\Delta x_{i,2}}{A_{i,2}} \frac{dW_2}{dt} + \frac{W_2^2}{A^2} \frac{\Delta v}{\Delta x} = -\frac{\Delta p}{\Delta x_i} - \left(\frac{f \Delta x_{i,2}}{D_{i,2}} + k_{i,2} \right) \frac{W_2^2}{2\rho_{Ar}} - g \int \rho \Delta z \quad (6.20)$$

The term $\frac{W_2^2}{A^2} \frac{\Delta v}{\Delta x}$ is non zero for an open loop, the effect of the term on natural convection

flow of argon gas was studied with steady state conditions and found that this term has negligible effect on the argon flow. The details of the analysis is given in the Appendix 6.1.

So the term is neglected in further analysis. So Eq (6.20) becomes,

$$\sum_i \frac{\Delta x_{i,2}}{A_{i,2}} \frac{dW_2}{dt} = \rho_{0,Ar} g \beta_{Ar} \sum_{i=1}^{N_2} T_{i,2} \Delta z_{i,2} - \sum_{i=1}^{N_2} \frac{f_{i,2} \Delta x_{i,2}}{D_{i,2}} \left(\frac{W_2^2}{2\rho_{0,Ar} A_{i,2}^2} \right) - \sum_{i=1}^{N_2} k_{i,2} \left(\frac{W_2^2}{2\rho_{0,Ar} A_{i,2}^2} \right) \quad (6.21)$$

6.3.1.2 Energy equation for fluid

Similarly,

$$\frac{\partial T_1}{\partial t} - \alpha_1 \frac{\partial^2 T_1}{\partial x^2} + \frac{W_1}{A_1 \rho_{0,LBE}} \left(\frac{\partial T_1}{\partial x_1} \right) = \frac{-4h_{in,1}(T_1 - T_w)}{\rho_{0,LBE} D_1 C p_{LBE}} \quad \text{primary side} \quad (6.22)$$

$$\frac{\partial T_2}{\partial t} - \alpha_2 \frac{\partial^2 T_2}{\partial x_2^2} + \frac{W_2}{A_2 \rho_{0,Ar}} \left(\frac{\partial T_2}{\partial x_2} \right) = \frac{-4h_{in,2}(T_2 - T_w)}{\rho_{0,Ar} C p_{Ar}} \frac{D_{s,1}}{D_{s,2}^2 - D_{s,1}^2} \quad \text{secondary side} \quad (6.23)$$

The second term in the Eq (6.23) is negligible for argon gas. However, this term is still computed because same set of equations are solved for both LBE and argon gas.

6.3.1.3 Conduction equation for the wall

The wall conduction equation for the pipe is as given below,

$$\frac{\partial T_w}{\partial t} - \alpha_w \frac{\partial^2 T_w}{\partial x^2} = \begin{cases} -\frac{4h_i(T_w - T)}{\rho_w C p_w} \left(\frac{D_i}{(D_o^2 - D_i^2)} \right) - \frac{4h_{Ar}(T_w - T_{encl})}{\rho_w C p_w} \left(\frac{D_o}{(D_o^2 - D_i^2)} \right) + \frac{4q}{\rho_w C p_w} \left(\frac{D_o}{(D_o^2 - D_i^2)} \right) & \text{For heater} \\ -\frac{4h_i(T_w - T)}{\rho_w C p_w} \left(\frac{D_i}{(D_o^2 - D_i^2)} \right) - \frac{4h_{Ar}(T_w - T_{encl})}{\rho_w C p_w} \left(\frac{D_o}{(D_o^2 - D_i^2)} \right) & \text{For piping} \\ -\frac{4h_i(T_w - T)}{\rho_w C p_w} \left(\frac{D_i}{(D_o^2 - D_i^2)} \right) - \frac{4h_2(T_w - T_2)}{\rho_w C p_w} \left(\frac{D_o}{(D_o^2 - D_i^2)} \right) & \text{For Heat exchanger} \end{cases} \quad (6.24)$$

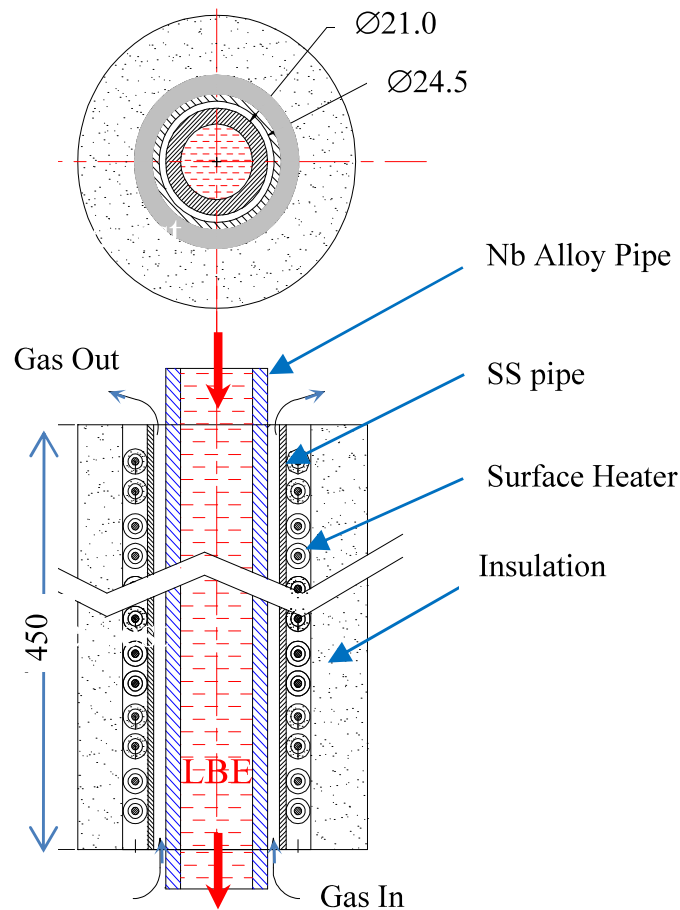
The time step for the secondary side was calculated as

$$\Delta t = \frac{1}{\frac{2\alpha}{\Delta x_i^2} + \frac{W_{Ar}^n}{\rho_{0,Ar} \Delta x_i} + \frac{4h_{Ar,i} D_{s,1}}{\rho_{0,Ar} C p_{Ar} (D_{s,2}^2 - D_{s,1}^2)}} \quad (6.25)$$

So the time step was calculated as the minimum value found from Eq (6.11), (6.12), (6.15) and (6.25).

6.3.2 Modelling of Heat Exchanger

The KTL has been designed to operate up to 1100 °C. The present set up does not allow forced circulation of the argon gas coolant on the secondary side because of the possibility of sudden cooling of the loop heat exchanger section during abrupt flow of argon gas, which may lead to the generation of large thermal stress in the piping and cause loop failure. So the heat exchanger in the present loop was designed as vertical tube in tube type and cooled by natural convection of argon gas of the enclosure.



(a) Schematic of Heat Exchanger

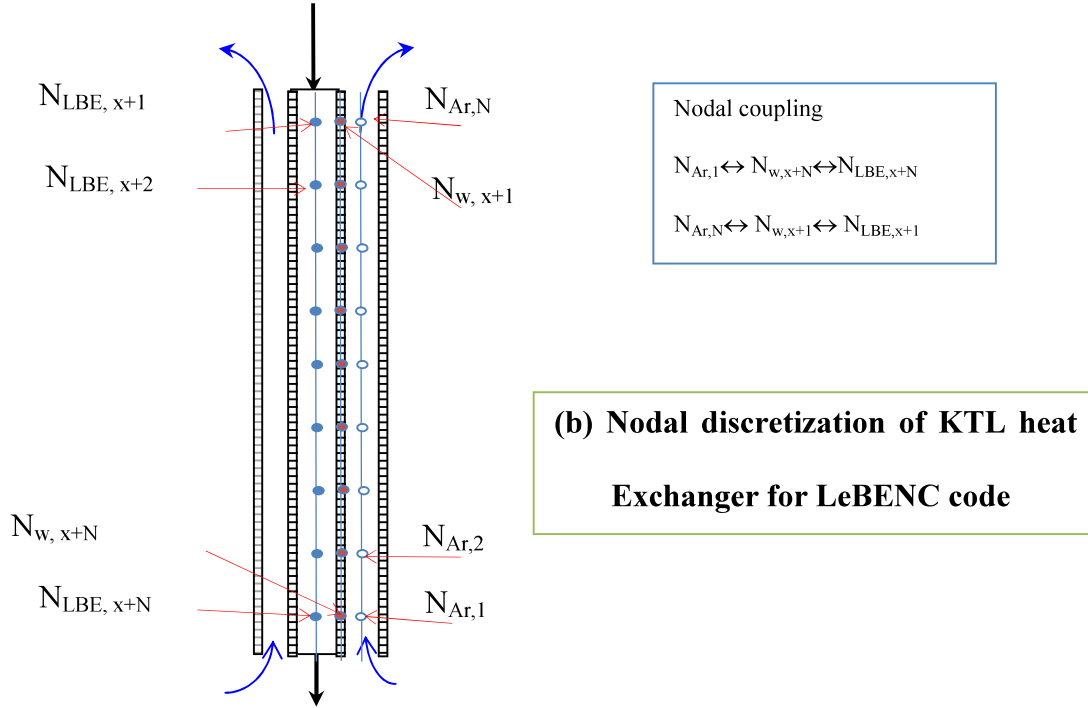


Fig 6.2 Schematic of the heat exchanger and nodal discretization for LeBENC code.

Figure 6.2 (a) shows the schematic of the heat exchanger. The inner tube was part of the primary loop and LBE was flowing through it vertically downward. The outer tube was concentric to the inner tube with both ends open. So the secondary side was a vertical annular passage where argon gas in the enclosure enters from the bottom of the passage, flows through it due to natural circulation and goes out through the upper opening. This way the heat from the heat exchanger was rejected inside the enclosure.

6.3.2.1 Nodal discretisation and coupling of the primary and secondary side parameters

The flow of argon gas in the secondary side depends on the primary loop temperature. So for transient cases the argon flow rate and inlet temperature of the argon gas also varies with time. The governing equations for natural circulation in the primary and secondary side of the heat exchangers as well as the wall conduction equation are to be solved as coupled equations. As the flow directions of the fluids in the heat exchanger were in opposite

direction, the nodes in both sides of the heat exchangers were to be connected accordingly, i.e. as shown in 6.2 (b) $N_{LBE, x+1}$ node at the entry in the primary side of heat exchanger was to be connected to the exit node, $N_{Ar,1}$ of the secondary side and so on.

6.3.2.2 Finding inlet temperature of argon gas in the secondary side of the heat exchanger of KTL

The argon gas from the exit of the heat exchanger rejects heat inside the enclosure. The heat loss from the piping also heats up the argon gas in the enclosure. The enclosure wall contains fins on the both sides to reject the heat to the ambient by passive way. When the loop was set at a certain power level, the heat accumulates in the enclosure and the enclosure temperature increases till it reaches steady state condition. Figure 6.3 shows the heat balance of the KTL with enclosure system. The inlet temperature of the argon gas in the heat exchanger also changes with time. The inlet temperature of the argon gas can be estimated as given in the following procedure.

The rate of accumulation of heat in the enclosure at any instant is given as,

$$\Delta Q = Q_{loop,loss} - Q_{ambient,loss} \quad (6.26)$$

Where,

$$Q_{loop,loss} = Q_{piping,loss} + Q_{hx,loss}$$

$$Q_{ambient,loss} = U_{encl} A_{encl} (T_{encl} - T_{ambient})$$

$$Q_{piping,loss} = h_a A_{piping} (T_w - T_{encl})$$

$$Q_{hx,loss} = h_{hx} A_{hx} (T_{Ar,in} - T_{Ar,out})$$

To find the heat loss through the enclosure finned wall the overall heat transfer coefficient U_{encl} was calculated using the natural convection heat transfer correlation from Churchill and Chu (1975) [132].

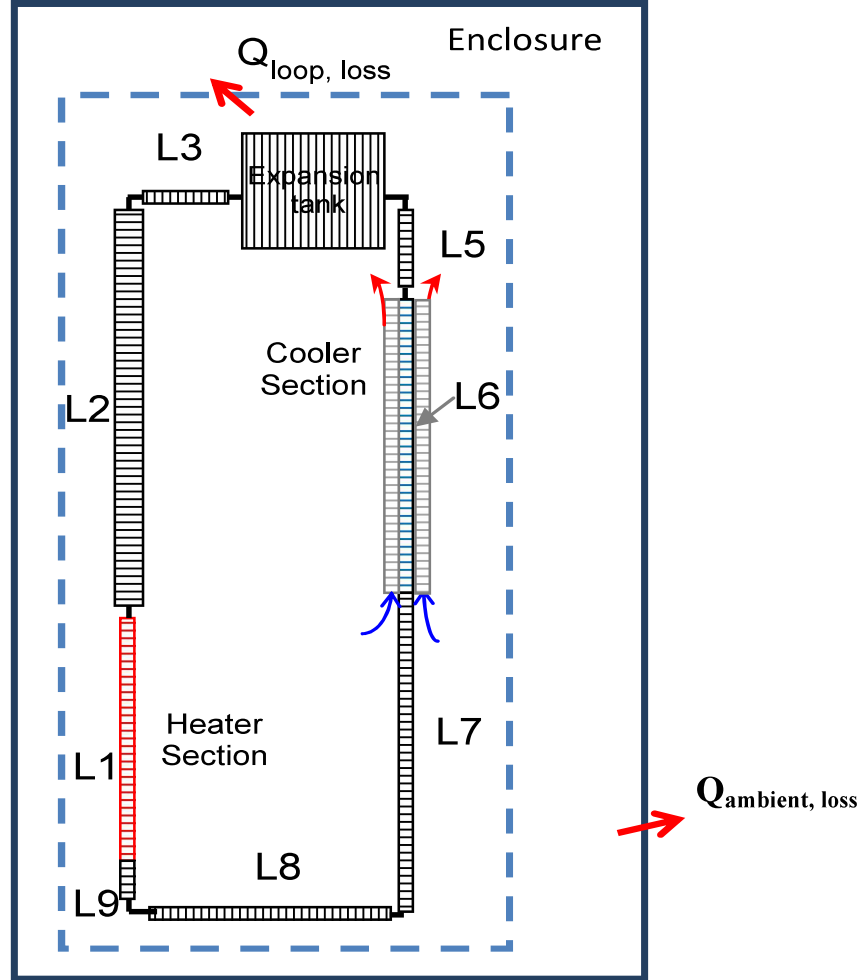


Fig. 6.3 Discretisation of the KTL main loop geometry for analysis using LeBENC code

The A_{encl} was the effective finned surface area of the wall of the enclosure. h_{Ar} was calculated based on the heat loss through the insulation from the piping per unit length. The calculation procedure of h_{Ar} was given in Chapter 3. The variation in temperature of the enclosure was calculated from the rate of accumulation of heat ΔQ in the enclosure. The

calculated enclosure temperature was used in the Eq (6.21) for the prediction of loop temperature and argon flow rate.

6.3.3 Discretization of the Governing Equations and the Loop

The discretisation process of the equations for KTL was same as mentioned in above section 4.0. The implicit method was used for discretizing the momentum equation. Implicit central difference scheme was used for the conductance equation. The whole loop was discretised into 9 segments and 165 nodes. The discretisation of the simplified geometry of the loop was shown in Fig. 6.3. In the heat exchanger the secondary side was assumed as the single segment and discretised with equal number of nodes as the primary side segment. Temperature dependent properties were calculated in each time step by incorporating recommended correlations of the properties in the code. The properties of piping material, Nb-alloy was taken from Distefano and Chitwood (2001) [166]. The local hydraulic loss coefficients in various components and piping were calculated from Idelchik et al. (1988) [164] and used in the code for analysis of the loop. The properties of argon gas were taken from Incropera and Dewitt (1996) [157] which were temperature dependent. The heat transfer coefficients in LBE in the heater section and the heat exchanger was calculated from the correlations given in Table 5.2, as found in Chapter 5.

The heat transfer correlation used for argon for natural convection in annular space with both ends open was given as [167] ,

$$Nu' = 0.29 (Ra)^{0.27} \text{ for } 10^3 < Ra < 10^8 \quad (6.27)$$

6.4 VALIDATION OF LEBENC CODE WITH LML

6.4.1 Steady State Analysis

In steady state analysis the LeBENC code was used to predict the natural circulation mass flow rate at a certain power level. With a set loop power and given heat transfer conditions in the secondary side of the heat exchanger, the code was run for sufficient time till the steady state condition was reached. The steady state natural circulation flow predicted by the code was expressed in terms of the non-dimensionalised numbers as given in Eq (4.2) of Chapter 4. Figure 6.4 shows the results of the comparison with the experimental results. The prediction conforms well to the experimental results.

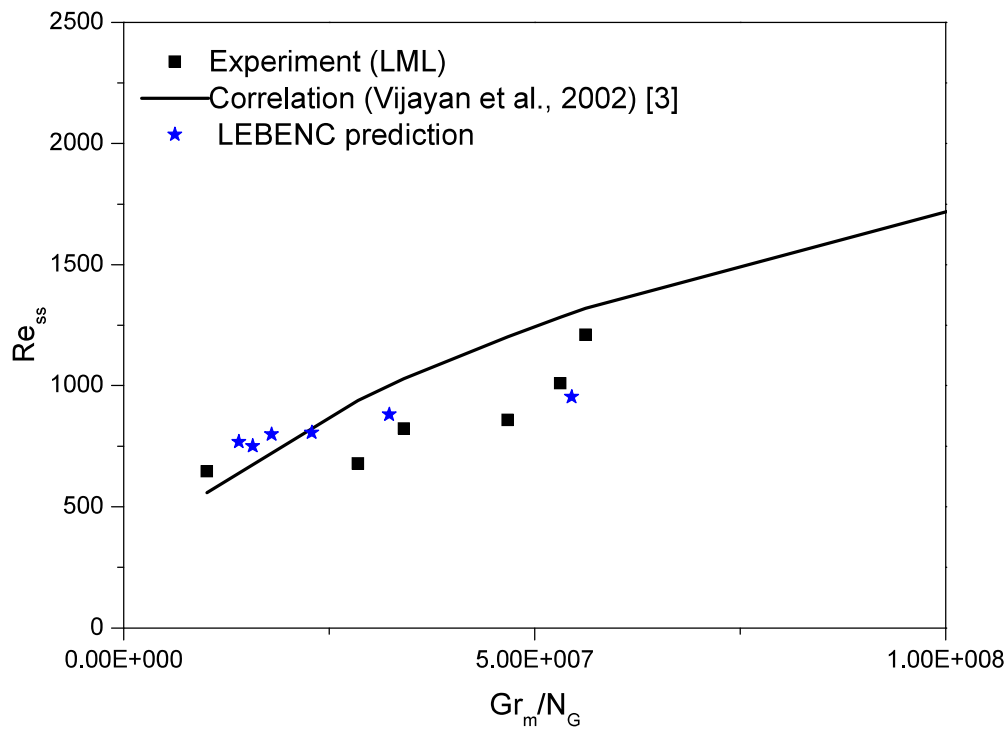


Fig 6.4 Steady state natural circulation prediction by LeBENC code and comparison with experimental data of LML.

Figure 6.5 shows the comparison with the experimental results with (a) air and (b) water as the secondary side coolants at same power of 2400 W. Here the code predicts well for both

the coolants. Figure 6.6 (a) shows the prediction of the code with low loop power (900 W) with air as the secondary side coolant. The code was also used to predict the steady state axial temperature distribution at high loop power. Figure 6.6 (b) shows the result for 4500 W power case with water as the secondary side coolant

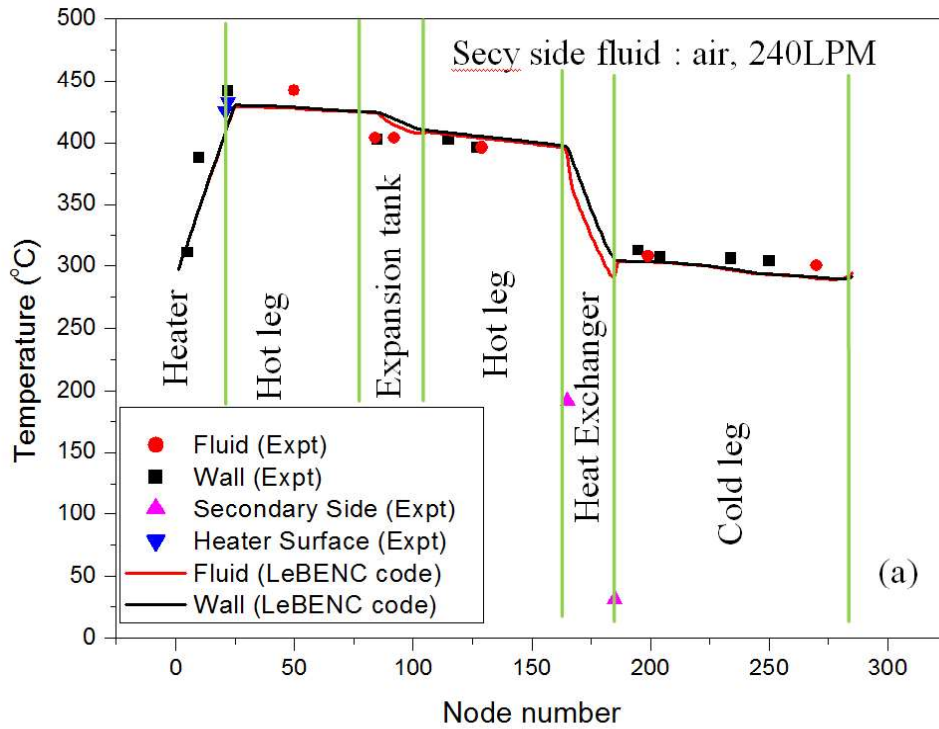


Fig. 6.5 (a) Steady state temperature distribution along the length of the loop at main heater power= 2400 W with air as the secondary side fluid.

6.4.2 Transient Analysis

6.4.2.1 Start-up experiment

In this transient experiment simulation the initial conditions i. e. the axial temperature distributions, loop power, secondary side calculated heat transfer coefficient and secondary coolant temperatures were given as input and the code was run for sufficient time till the natural circulation reaches the steady state. Figure 6.7 shows the start-up simulation results for 1200 W power with air as the secondary side coolant. It could be seen that the LeBENC predictions are matching well with the experimental results. Figure 6.8 shows the simulation

of start up experiment at power 2400 W and with air as the secondary side coolant. The prediction of the results were found to be matching well with the experimental results except during the initial period. The 3D nature of the expansion tank and thermal inertia of various structures like, supports and flanges make it difficult to simulate the heat transfer at the initial period by the 1D code.

6.4.2.2 Loss of heat sink

In this simulation steady state natural circulation was obtained by running the code for sufficient time. Then the heat transfer coefficient was reduced to zero in the secondary side of the heat exchanger. Figure 6.9 shows the variation of temperature along the heater inlet and outlet for the loop power 1200 W. It can be seen that the prediction matches well with the experimental results. There was sudden rise in the temperature mainly due to the decrease in the heat transfer coefficient to zero. But the experimental results show slow rise in the temperature which may be due to the rejection of heat in the heat exchanger secondary side and inlet and outlet piping. This could not be simulated accurately in the LeBENC code. Here the heat sink loss experiment is simulated by assuming two conditions (a) with secondary side heat transfer coefficient to zero and with (b) a calculated heat transfer coefficient which is found to be $25 \text{ W/m}^2\text{°C}$. This was calculated by assuming natural convection in stagnant air in the secondary side with the average experimental values of LBE temperature and air temperatures. In the first case the LBE temperature difference across the heat exchanger ($\Delta T_{\text{LBE,HX}}$) is decreased drastically as expected. But the value of $\Delta T_{\text{LBE,HX}}$ still remained at $\sim 10 \text{ °C}$. This is due to the cooling by axial conduction of the heat exchanger structure material. With the second case, LeBENC predicts well the experimental data.

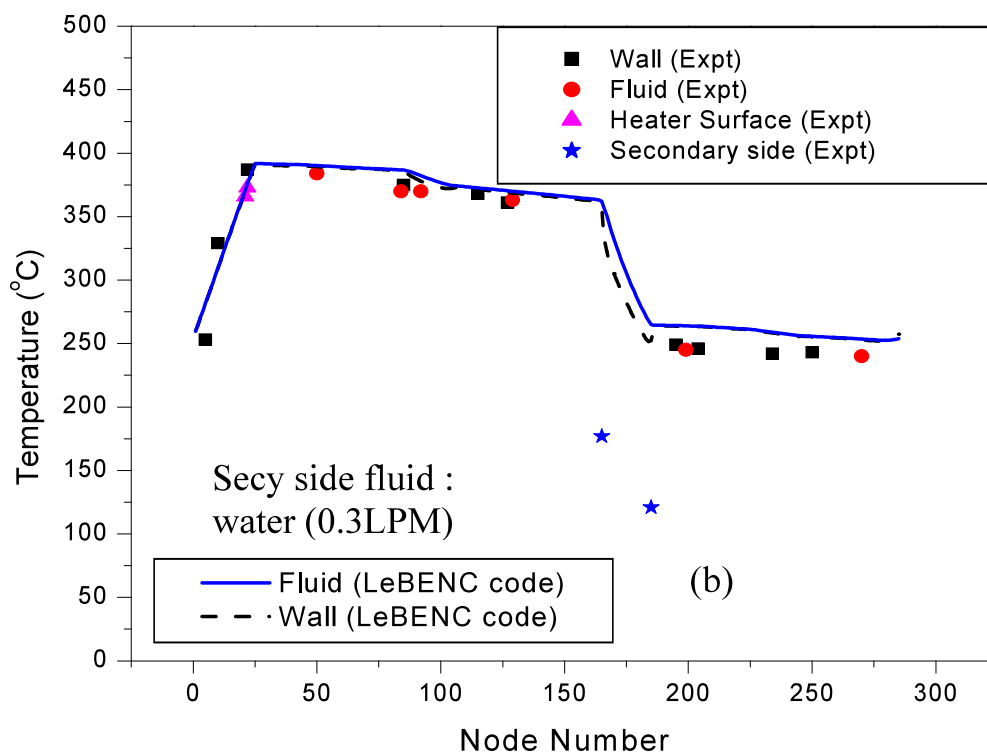


Fig. 6.5 (b) Steady state temperature distribution along the length of the loop at main heater power 2400 W with water as the secondary side fluid.

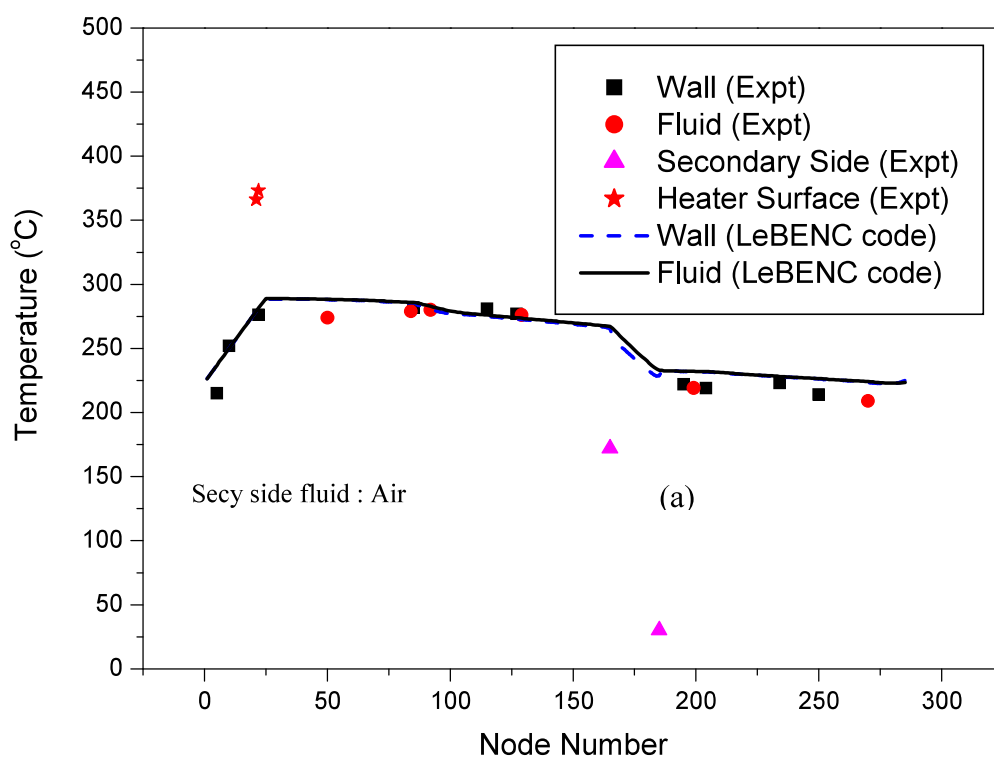


Fig 6.6 (a) Steady state axial temperature distribution of the loop at 900 W power.

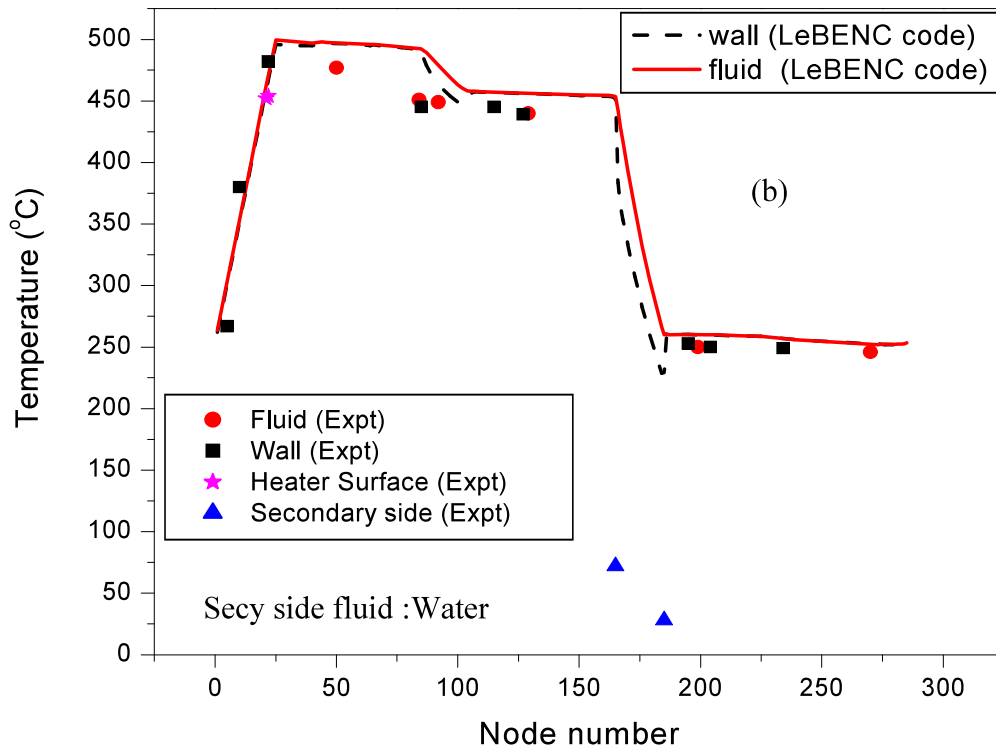


Fig 6.6 (b) Steady state axial temperature distribution in LML at 4500 W power.

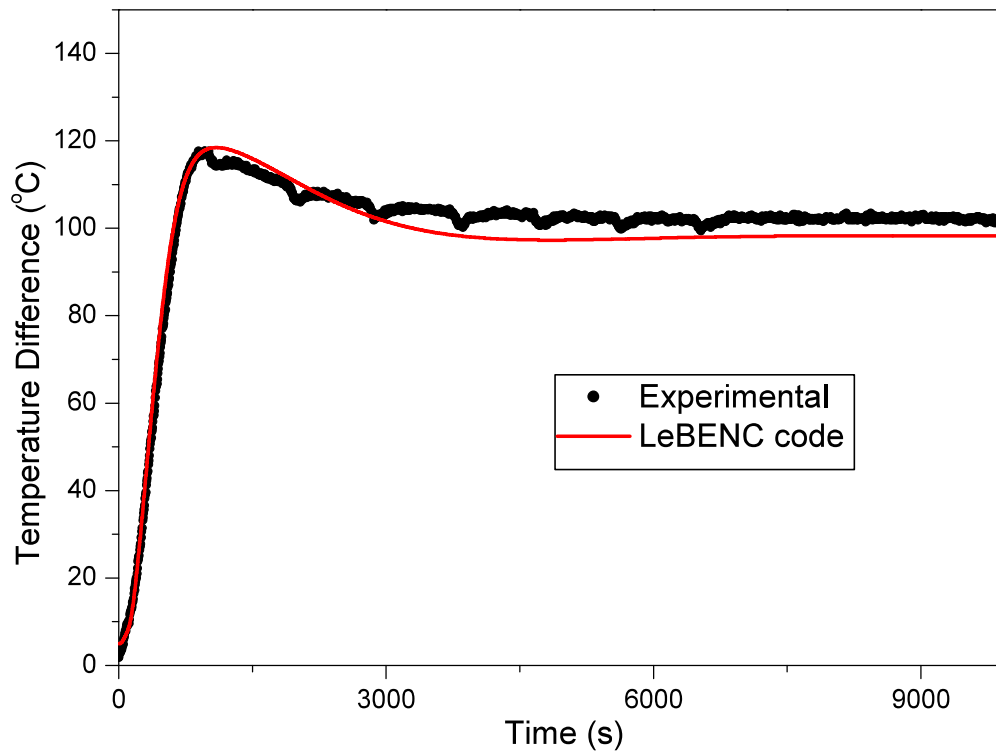


Fig. 6.7 Simulation of start-up experiment in LML at power 1200 W.

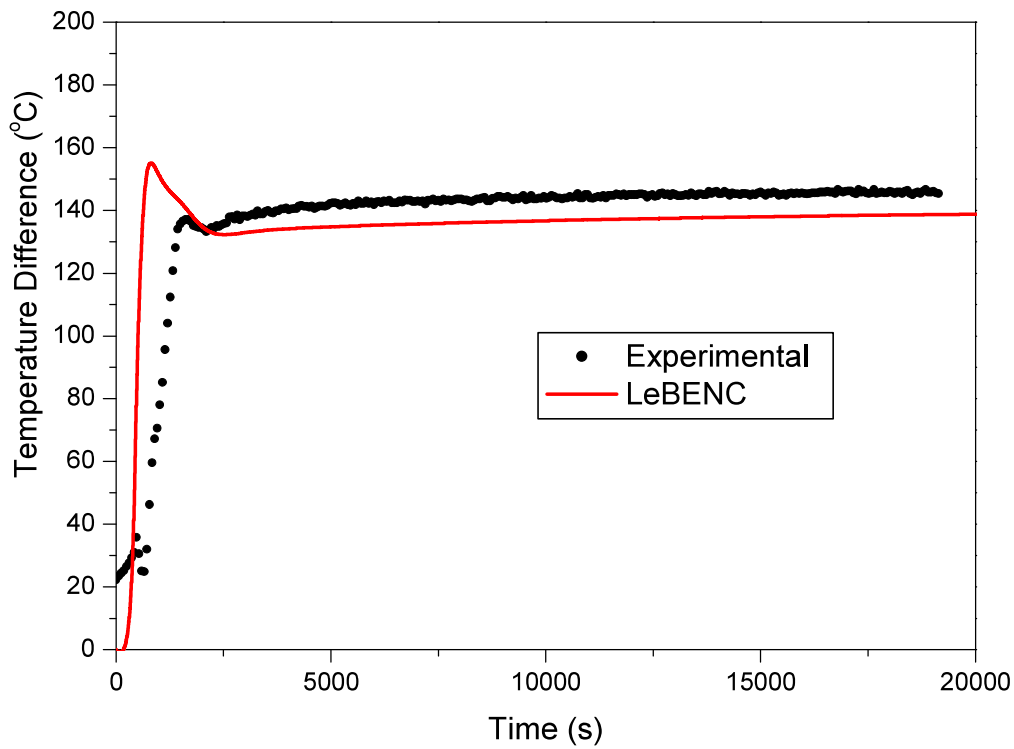


Fig 6.8 Simulation of start-up experiment in LML at 2400 W power.

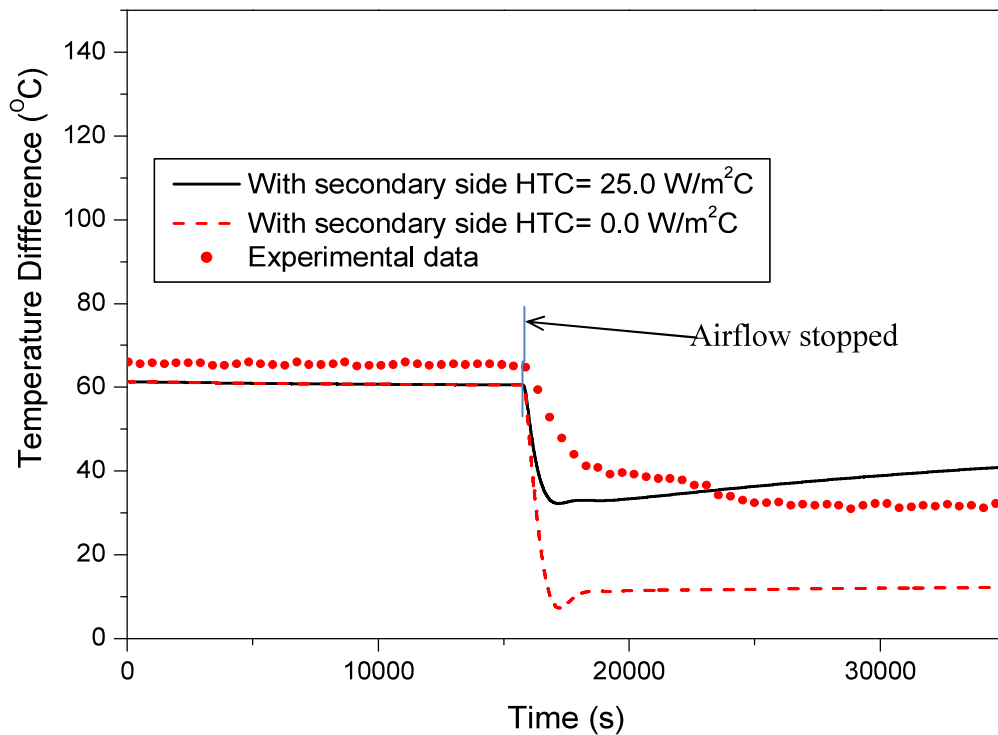


Fig. 6.9. Comparison of the LeBENC prediction with the experimental data of the variation of temperature difference across the heat exchanger during the simulation of Loss of Heat Sink with initial steady state Power 1200 W.

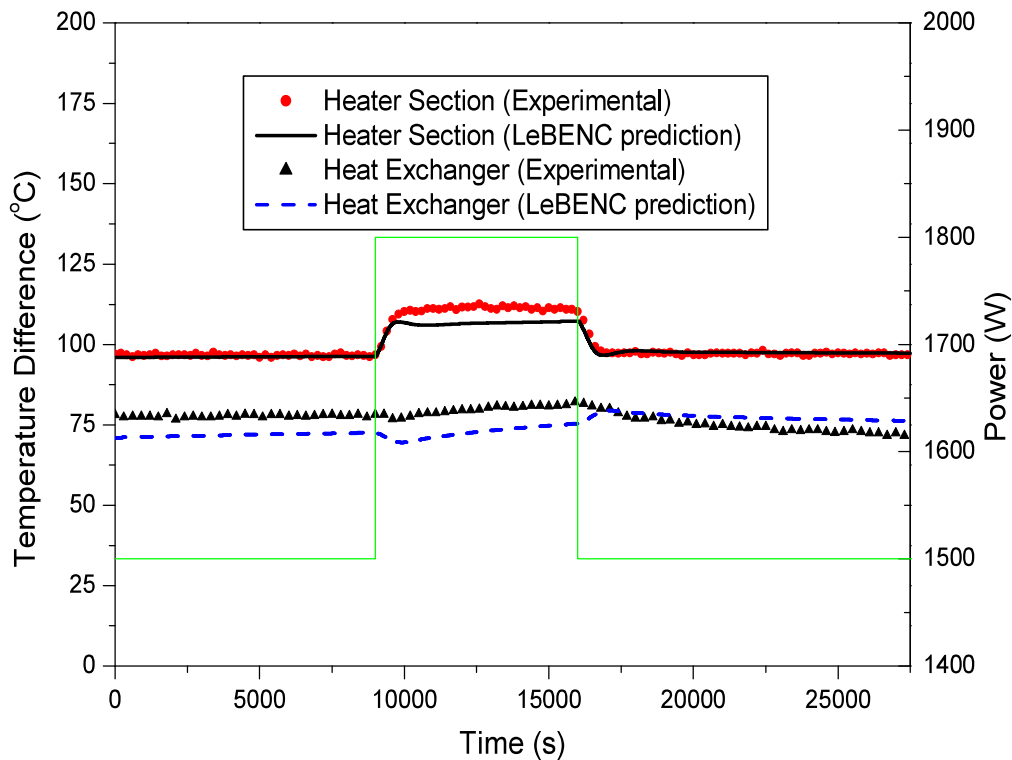


Fig. 6.10 Comparison of the LeBENC prediction with the experimental data of the variation of temperature difference across the heater section and the heat exchanger during the step change in power experiment.

6.4.2.3 Effect of the step change in power

In this simulation, the code was run with rated power and boundary conditions of the loop matching with the experimental conditions. The code was programmed to raise the loop power as per the experimental study keeping the secondary conditions same and after certain time, the loop power was decreased to the original power. Figure 6.10 shows the comparison of the LeBENC prediction with the experimental data of the power step experiments 2100-1200-2100 W. It can be seen that the LeBENC code under predicts the experimental results in the heater section especially during the power step up conditions. However the maximum deviation was less than 10%. In the heat exchanger the secondary side heat transfer coefficient varies with temperature and this could not be simulated in the LeBENC code. This led to deviation of the secondary side predictions from the experimental results, as shown in Fig 6.10. However this deviation is also less than 10 %.

6.4.2.4 Effect of change in the secondary coolant flow rate

This experiment was also simulated by running the code at rated power for sufficient time to reach steady state and the coolant flow rate variation was simulated by changing the heat transfer coefficient and the secondary side average temperature. Figure 6.11 shows the simulation with the loop rated power of 1500 W with step change in air flow rate 200-320-200 LPM. The deviation of the LeBENC prediction of the experimental results are less than 10%.

6.5 VALIDATION OF LeBENC WITH KTL EXPERIMENTAL DATA

6.5.1 Steady State Analysis

The LeBENC code was modified as discussed above, to simulate the natural circulation in main loop part of KTL. The code was run with simulated boundary conditions for sufficient time at a power level to reach steady state. The predicted steady state temperature distribution in the loop and mass flow rate were compared to experimental data. This steady state natural circulation simulation were carried out at different power levels and the results are shown in Fig 6.12. Figure 6.12 (a) shows the variation of temperature difference ΔT with power. It can be seen that the LeBENC prediction was fairly good with experimental results with maximum deviation of 12.5%. Figure 6.12 (b) shows the variation of the mass flow rate with power. LeBENC code predictions conforms well with the calculated experimental results.

Figure 6.13 shows predicted and measured steady state inlet temperature at different power levels. As the power increases the inlet temperature of the heater section, which was the lowest temperature of LBE in the main part of circulating loop, increases slowly first then increases at higher rate with increasing power levels in the loop.

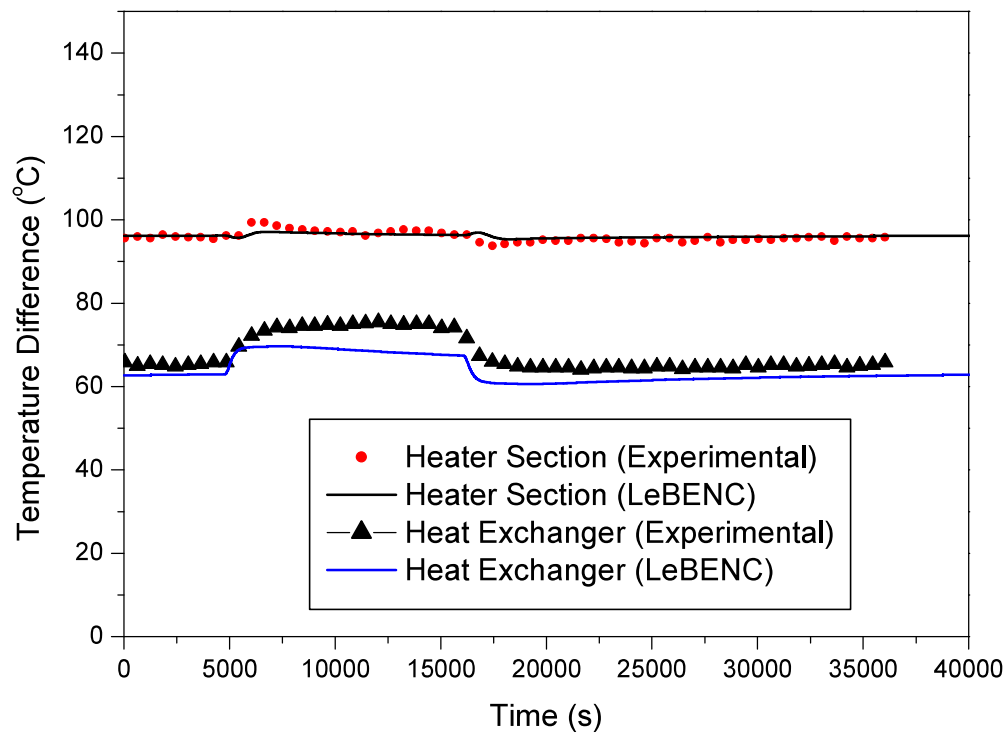


Fig 6.11 Variation in temperature differences across the heater section and the heat exchanger of LML with step change in secondary air flow 200-320-200 LPM with 1500 W.

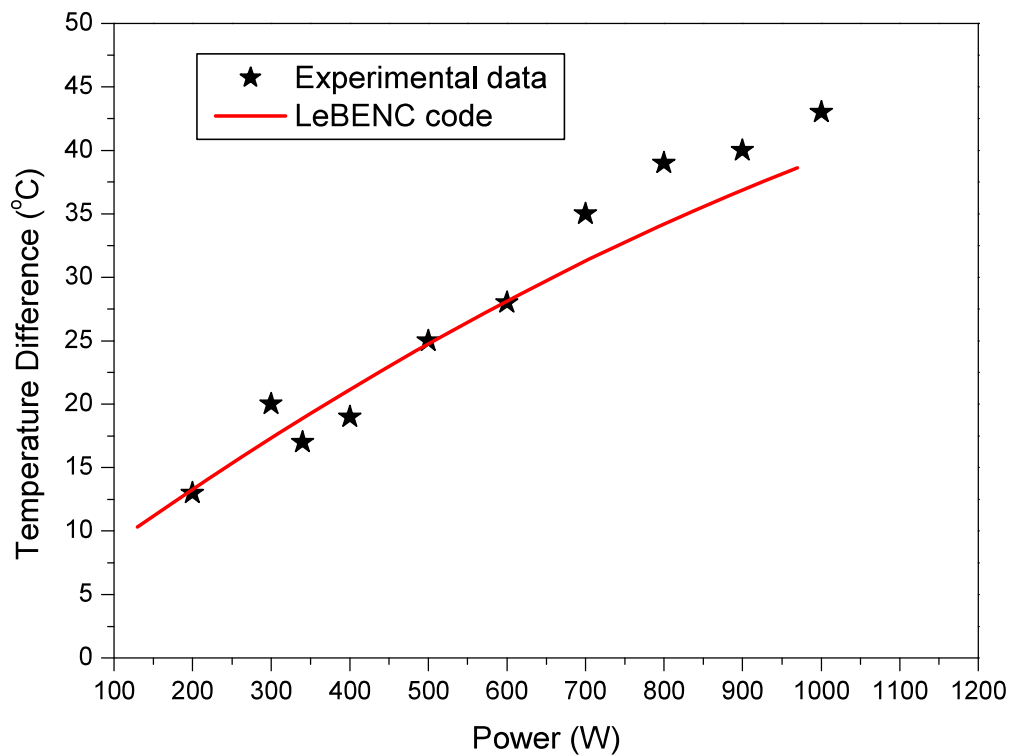


Fig 6.12 (a) Temperature rise across heated section during steady state natural circulation results at different power levels.

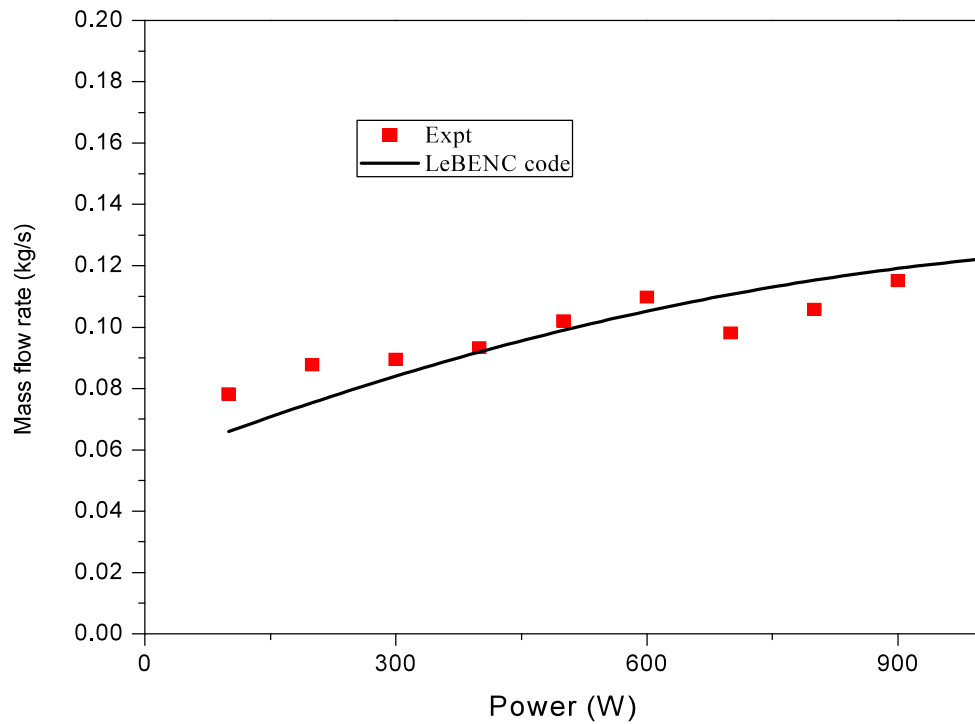


Fig 6.12 (b) Calculated steady state natural circulation LBE mass flow rate in LML at different power levels.

The code predicts well the experimental results of the inlet temperature. Figure 6.14 shows the comparison of the code prediction for the steady state axial temperature distribution in the loop at power 360 W with experimental data. The temperature varies linearly in the heater section. As expected, the wall temperature was found to be higher than the fluid temperature in this section because the heat transfer was taking place from the outer surface of the pipe through the wall thickness to the inside LBE. In the heat exchanger the temperature drop was not linear which was due to the natural convection cooling by argon gas flowing through the narrow annulus in the secondary side. The overall prediction of LeBENC code conforms well to the experimental results with less than 5% deviation.

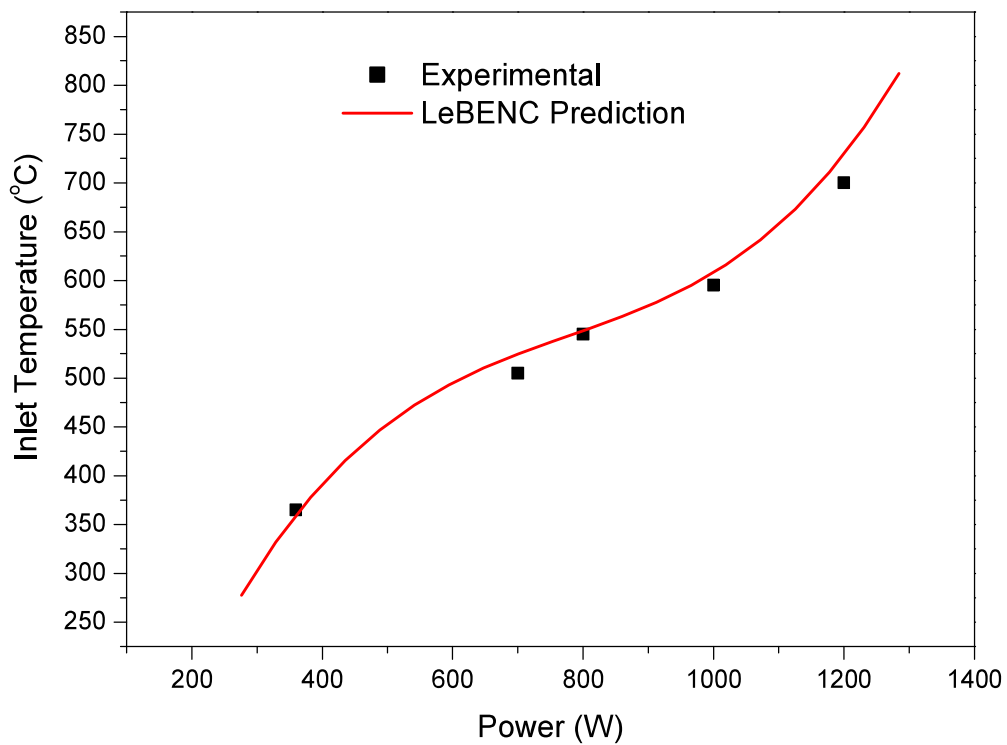


Fig. 6.13 Variation of main heater section inlet temperature of LBE at different steady state power levels.

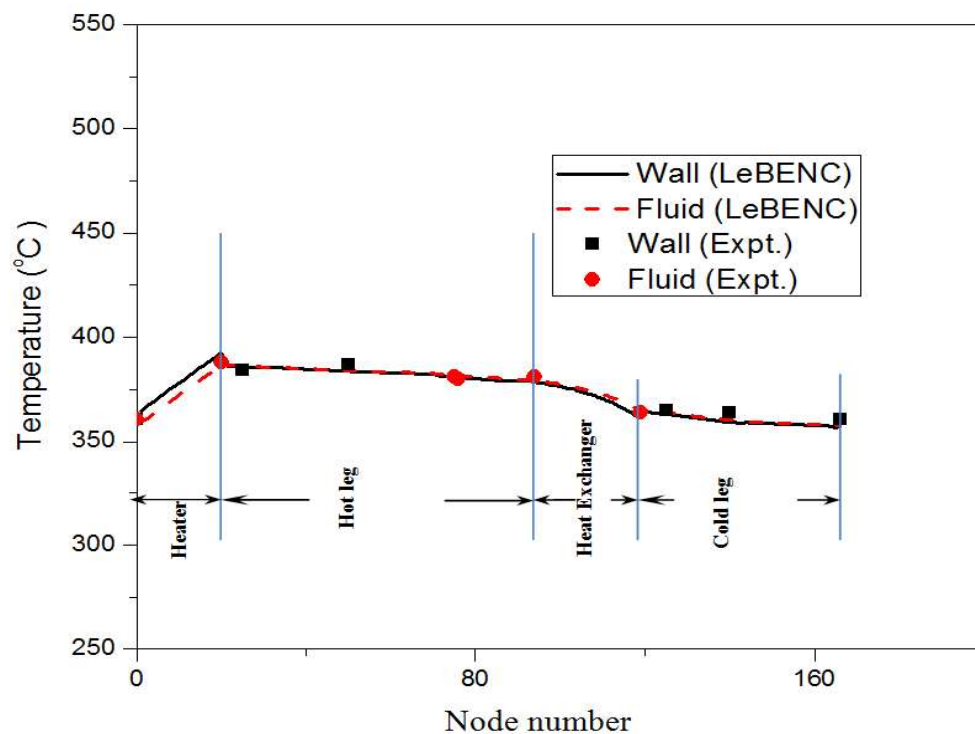


Fig. 6.14 Fluid and wall temperature distribution in the axial direction of the loop at 360 W power.

6.5.2 Transient Studies

Simulation of the transient experiments in KTL was also carried out with the LeBENC code. Following sections give the details of the theoretical studies carried out.

6.5.2.1 Start-up simulation test

In the start up experiment simulation, the initial temperature distribution of LBE in the loop, argon inlet temperature and the main heater power was taken from the experimental data as input for the code. The code was run for sufficient time till it reaches steady state.

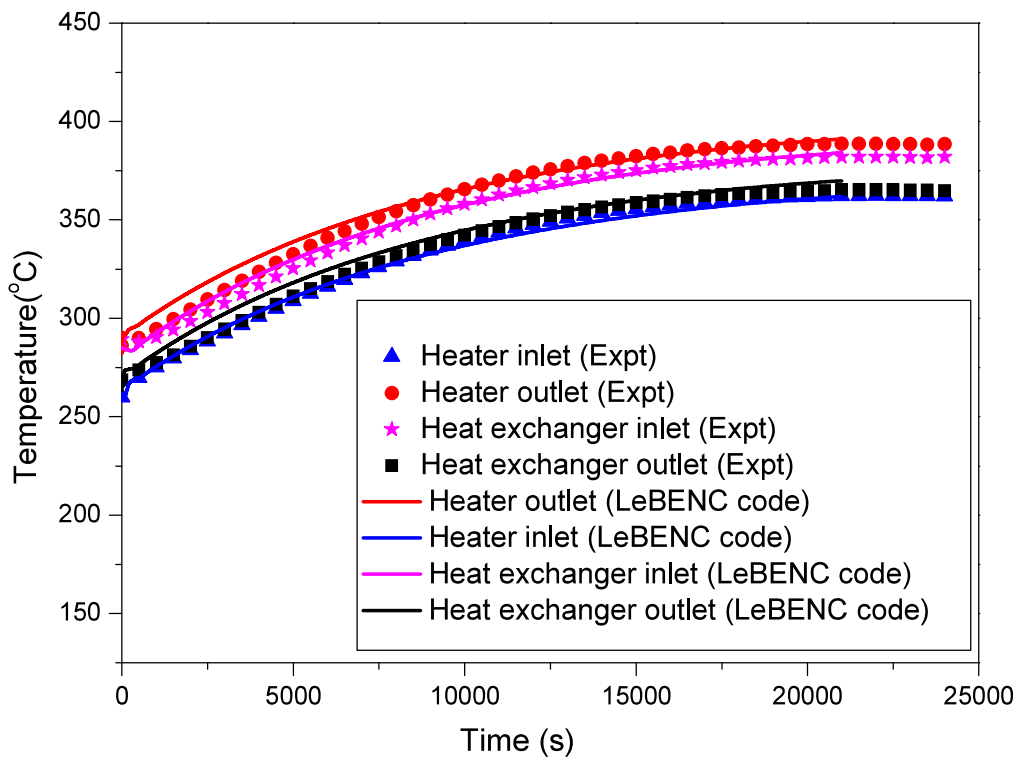


Fig. 6.15 (a) Temperature variation during start-up experiment of the loop from zero power condition to 360 W power level.

Figures 6.15 (a) and Fig 6.15 (b) show the simulation of two more start up experiments at two different power levels. The prediction of the code matches well with the experimental data.

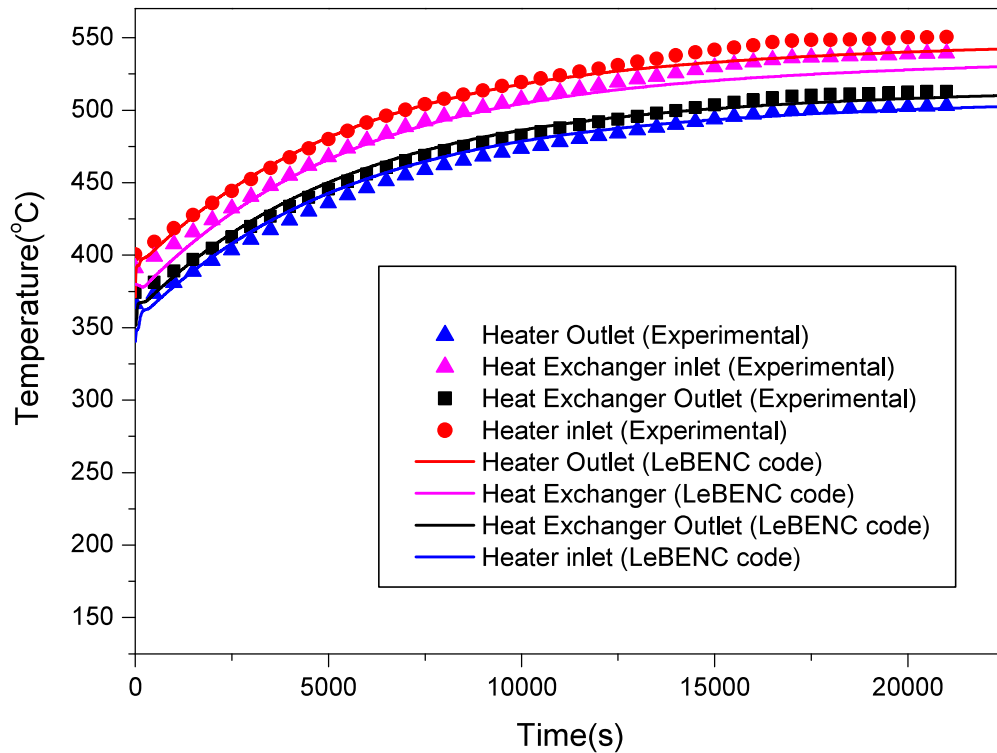


Fig. 6.15 (b) Temperature variation during start-up experiment of the loop from zero power condition to 700 W power level.

6.5.2.2 Loss of heat source

In this experiment, the code was run sufficient time with rated power to reach steady state, then the loss of heat source was simulated by instantly reducing the main heater power to zero. Figure 6.16 shows the loss of heat sink experiment with 1000 W as the initial main heater power. The comparison of the prediction of LeBENC code with experimental data was also shown in the graph. It can be seen from that the temperature variation with time as predicted by the code was linear compared to the experimental results. This may be due to the simplification of the loop geometry to simulate by the 1 D code.

6.5.2.3 Step change of heater power

In this simulation the code was programmed to change the main heater power after reaching steady state with initial set power level.

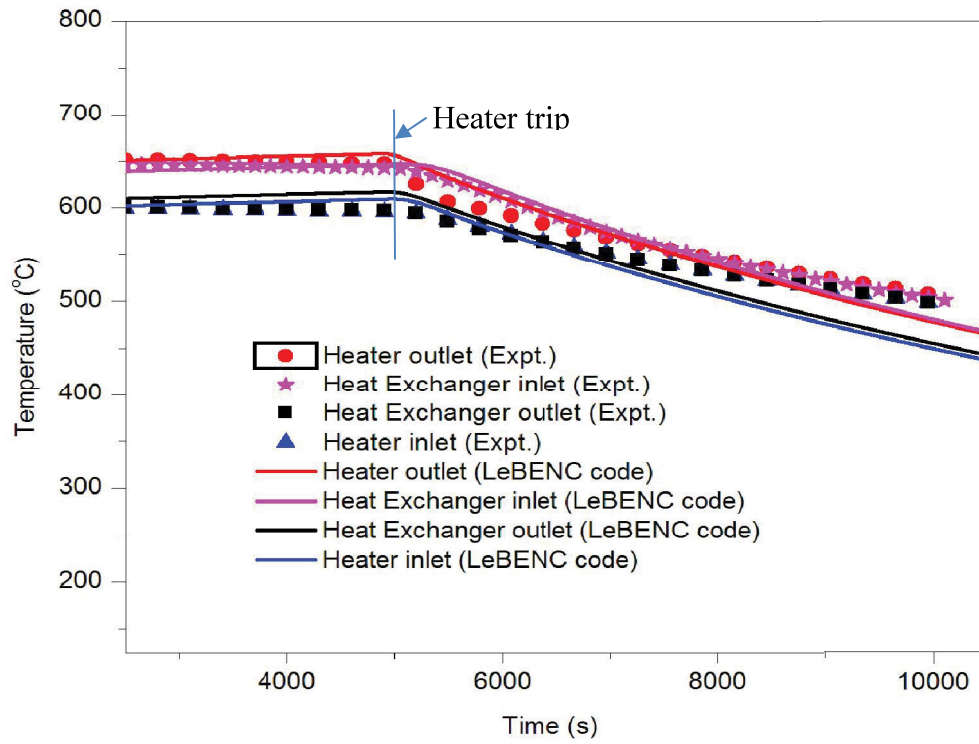


Fig 6.16 Temperature variation in the loop during loss of heat sink with initial power 1000 W.

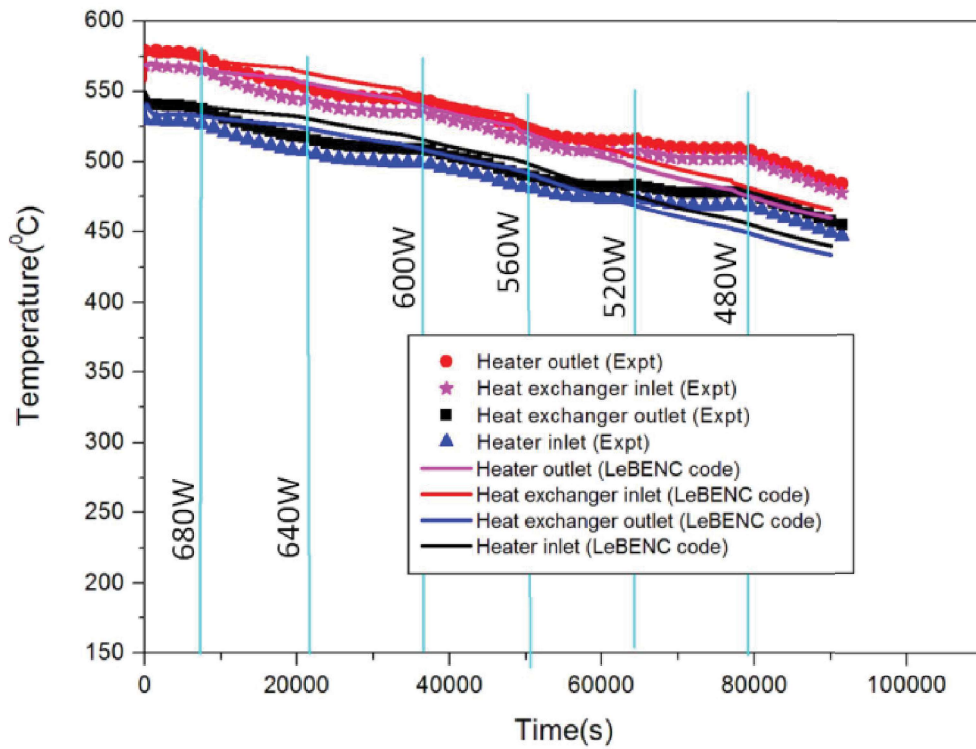


Fig. 6.17 Variation of loop temperature during step change in power from 720 W to 480 W in step of 40 W.

Figure 6.17 shows the variation of temperature when the main heater power was decreased from 680 W to 480 W in step of 40 W at certain time interval. The entire experiment was simulated using LeBENC code and the prediction was found to be good in comparison with the experimental data. Figure 6.18 shows the step power change simulation at very high temperature ($\sim 780^\circ\text{C}$). The deviation of the simulation results from the experimental results was found to be less than 12%.

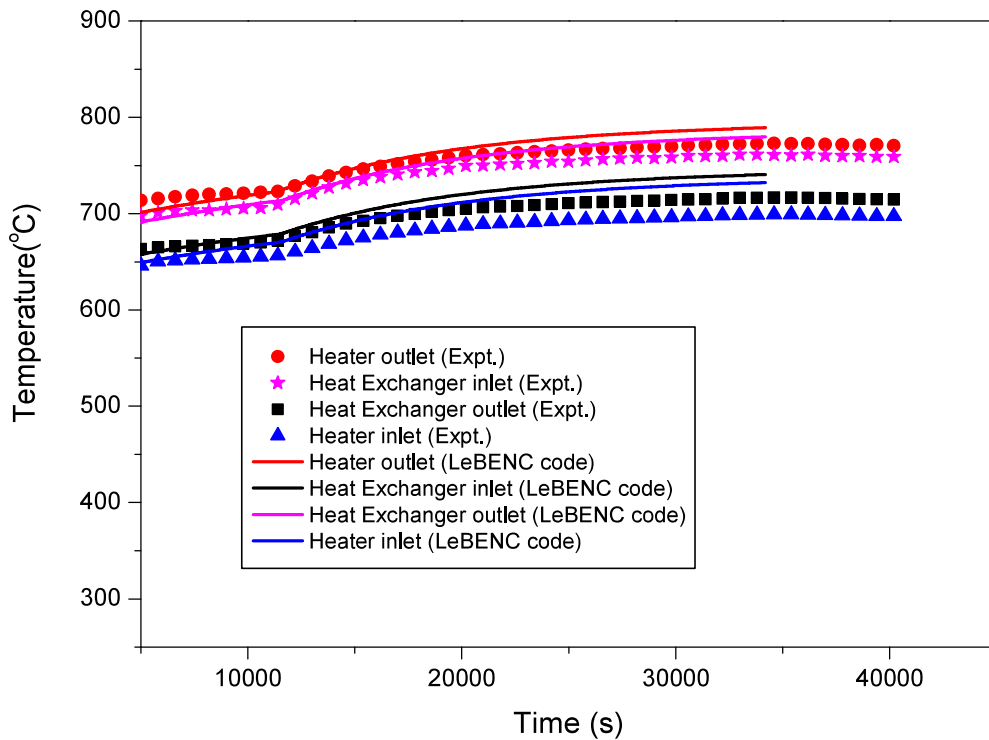


Fig. 6.18 Variation of loop temperature during step change in power from 1100 W to 1200 W.

6.6 SUMMARY OF MAJOR FINDINGS

1. A 1D computer code was developed for natural circulation studies of LBE at high temperature considering different parameters which may affect the natural circulation flow.

2. The code was used to simulate the steady state and transient experiments of LML and KTL and validated the predictions with the experimental data extensively. The simulation was carried for the temperature range of 200 °C to 780 °C.
3. For steady state natural circulation the code predicted well the experimental results of the both loop LML and KTL with the deviation less than 15 %. The wall temperature and fluid temperature were predicted well at different loop power levels.
4. During transient analysis, in case of high power experiments or higher step change in power or higher flow rate change in secondary coolant the code prediction deviated from the experimental results more than the experiments involving lower value of the corresponding parameters.
5. However the maximum deviation of the transient simulation results from the experimental results were less than 15% for whole temperature range of 200 °C to 780 °C.

Chapter-7

EFFECT OF VARIOUS PARAMETERS ON LBE NATURAL CIRCULATION

7.1 INTRODUCTION

The natural circulation in LBE may be affected by several factors. The various factors were axial conduction, heat loss in the piping, heat transfer coefficients, frictional pressure drop due to roughness of the piping surface, etc. This chapter gives the discussion on the various factors and evaluation of the effects of the parameters on the performance on the natural circulation of LBE. The code LeBENC, which was developed and validated extensively with the experimental loops LML and KTL was used for the evaluation.

7.2 DIFFERENT PARAMETERS WHICH MAY AFFECT NATURAL CIRCULATION OF LBE

The different parameters considered in the present analysis are,

- (a) Axial conduction of LBE in the loop
- (b) Effect of loop piping heat loss
- (c) Heat transfer coefficients in LBE and in the secondary side, and
- (d) Effect of piping surface roughness.

The effect of axial conduction on natural circulation is an important aspect as liquid metal has high thermal conductivity compared to water. Sabharwall et al. (2012) [39] carried out analysis considering axial conduction on natural circulation and found the limiting Reynolds number beyond which the effect of the axial conduction becomes negligible. Gargin and

Turker (2011) [123] carried out numerical studies on axial conduction effect on laminar duct flows and found that beyond $Pe=10$, the axial conduction effect was negligible. However a comprehensive analysis was required on the effect of axial conduction on the natural circulation of LBE.

Studies on the effect of heat loss in the piping on the natural circulation were not found in literature. This may be due to the fact that most of the studies reported in literature were on the water based loops and the operating temperature was significantly lower than the liquid metal loops. So the heat loss through piping of the water based loop was not significant as compared with the heat removed in the heat exchanger. Since the natural circulation driving head mainly depends on the vertical height difference between the centres of the heater and the heat exchanger, the heat loss in the piping may lead to change in the effective height difference and may affect natural circulation flow rate. Moreover the average loop temperature will also decrease with the increase in the heat losses. Since LeBENC code can handle the heat loss in the piping, the code can be used to study the effect of the heat loss on the natural circulation.

The effect of heat transfer coefficients in heater and heat exchanger are also important especially during transient flow conditions. For example, during start up experiments as discussed in Chapter 5, LBE experiences different flow regimes with time in the heater and heat exchanger sections, i. e. free convection, mixed convection and forced convection to reach steady state flowing condition. The heat transfer correlations were different for each flow regimes. The effect of LBE heat transfer coefficient on the natural circulation flow was to be studied with the code to predict the uncertainty on the theoretical results because of assuming constant heat transfer coefficient in the LBE medium. The studies on the effect of

the secondary side boundary conditions on the natural circulation are also important. In KTL the secondary side was cooled by the natural circulation of the argon gas. If the secondary side boundary conditions are taken as forced convection with constant heat transfer coefficient, the prediction will not be accurate. This can be further analysed with the code LeBENC. Since LBE is corrosive at high temperature, it may make the surface rough by corrosion. This may eventually increase the frictional pressure drop in the loop and in turn it may affect the natural circulation flow rate. This study is not found in literature so far. The details of the formulation on frictional pressure drop due to roughness are given in section 6.2.5 in Chapter 6. The formulations were included in LeBENC code and so parametric studies can be carried out to study the effect of surface roughness on the natural circulation of LBE. Theoretical studies were carried out using the code LeBENC on each of the above parameter. Following section gives the details of the analysis,

7.3 RESULTS OF THE PARAMETRIC ANALYSIS AND DISCUSSION

7.3.1 Effect of Thermal Conduction of LBE

LeBENC code was run simulating the steady state condition with different loop power levels in the LML and KTL. Figure 6.5 and Fig 6.6 in Chapter 6, show the steady state axial temperature distribution in the loop and the comparison with the experimental results. It can be seen that the variation of the temperature distribution was linear except at the inlet and outlets of the heater and the heat exchangers of the loop where the gradient in temperature are not so sharp. This may be due to the axial conduction effect in LBE. The axial conduction may be more prominent at very low flow, i.e. at low power levels. So natural circulation studies were carried out at low power range (10 to 500W loop power) in LML, using LeBENC code. The heat loss in the piping was not considered in the study to get more clear picture of the axial conduction effect. The results are discussed in the following sections.

7.3.1.1 Axial temperature variation

Figure 7.1 shows the results of the analysis at different power of the loop. It can be seen that lower the loop power, more prominent was the reduction in the sharpness of the axial temperature distribution at the inlets and outlets of the heater and the heat exchanger.

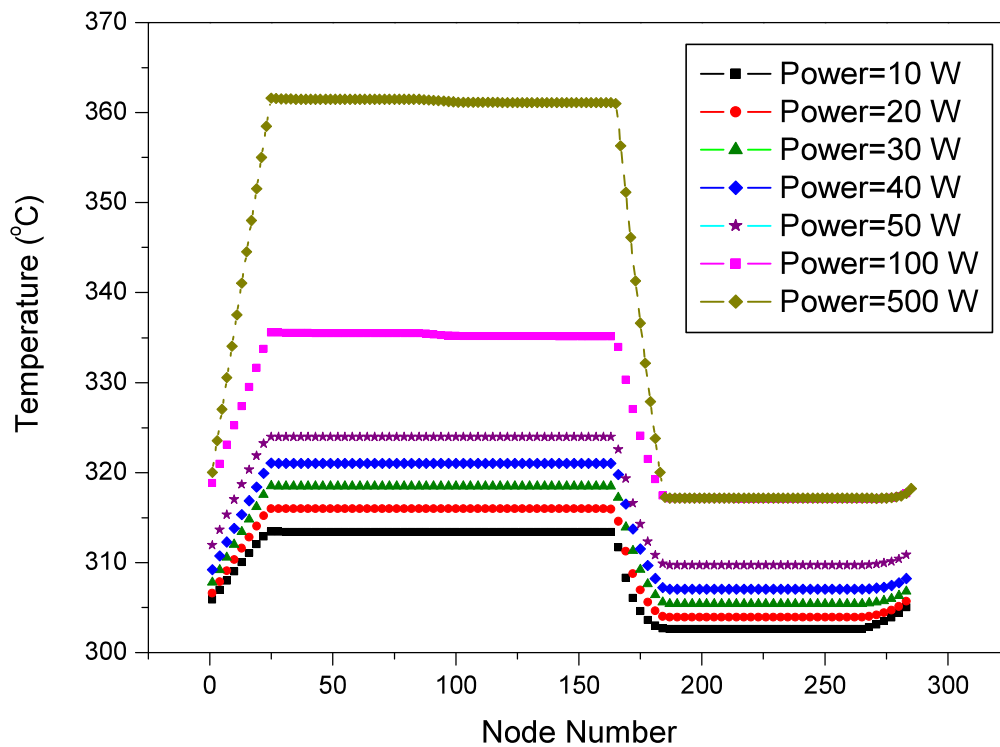


Fig 7.1. Prediction of axial temperature distribution of LBE at different power levels.

Another analysis was carried out to ensure that this effect was due to the axial conduction. In this analysis two cases were run with water and LBE as the working fluids in LML using the code LeBENC. Figure 7.2 shows that with water, the temperature gradients are sharper than that of LBE. So it can be concluded that the reduction in the temperature gradients are due to the axial conduction and its effect is prominent at very low power. The difference in loop temperature between the two cases was because of the lower thermal conductivity of water which reduces the heat transfer in the heat exchanger thereby increasing the loop temperature.

Another case was run with thermal conductivity $k=10 \times k_{LBE}$. In this case the temperature profile was found to be similar to that obtained with LBE.

As per Gargin and Turker (2011) [123] the axial conduction effect was prominent up to $Pe=10$. The Peclet number of the loops calculated on the basis of steady state Reynolds number (Re_{ss}) and found that the experiments carried out was in the range of $2.5 < Pe < 15$ for LML and $8.0 < Pe < 37$ in KTL. It was found that for both the loops the axial conduction effect on axial temperature distribution were prominent up to $Pe=10$ approximately. So it can be concluded that the limit of Peclet number found by Girgin and Turker (2011) [123] for axial conduction effect was also applicable for the LBE natural circulation loops.

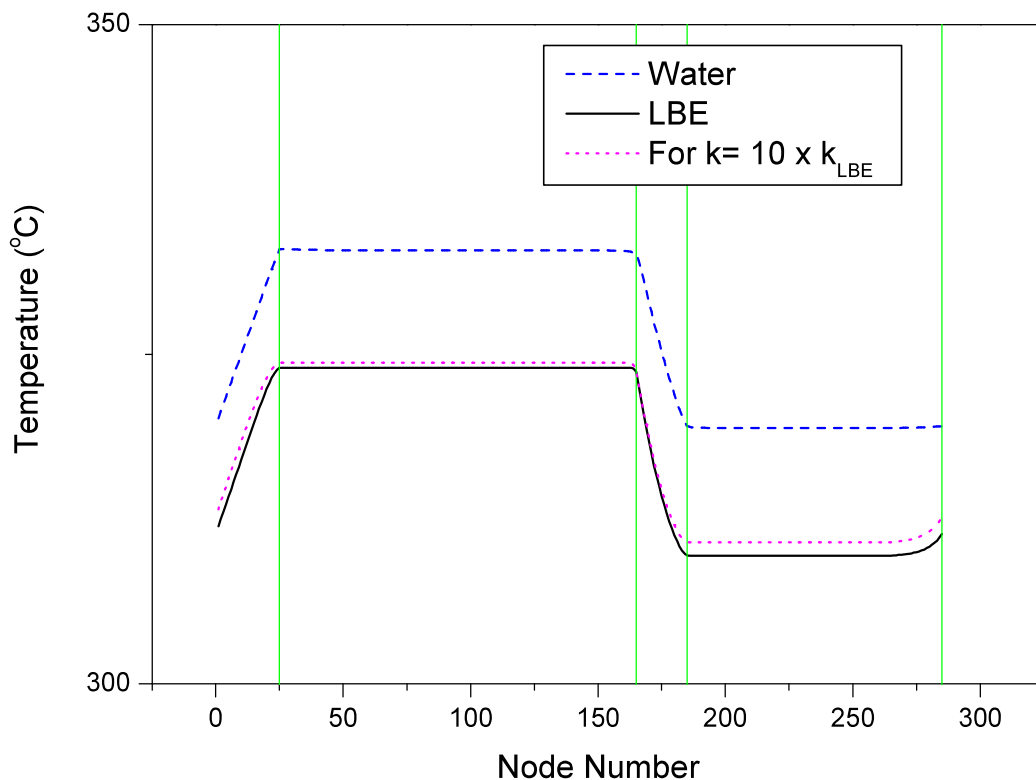


Fig 7.2 Prediction of axial temperature distribution of water and LBE at 50 W power level.

7.3.1.2 Effect on natural circulation flow rate

Steady state natural circulation analysis was carried out by varying axial thermal conductivity of LBE at different power levels. The contribution of conduction and convection terms for thermal energy transport in the loop were calculated for LML at different power. Three power levels were considered, 20 W, 100 W and 900 W. It was found that the thermal energy transport by conduction term is less than 0.2% of the convection term in all the cases. So the effect of thermal conductivity on natural circulation is negligible. Transient studies were also carried out to find the effect of thermal conductivity on the temperature variation with time. The LeBENC code was run to simulate the start-up experiment with 700 W power in KTL and three different values of thermal conductivities, $k = k_{LBE}/10$, $k = k_{LBE}$, and $k = 10 \times k_{LBE}$ were considered. Figure 7.3 shows the result of the analysis. The corresponding Peclet numbers are, $Pe=250$, 25 and 2.5.

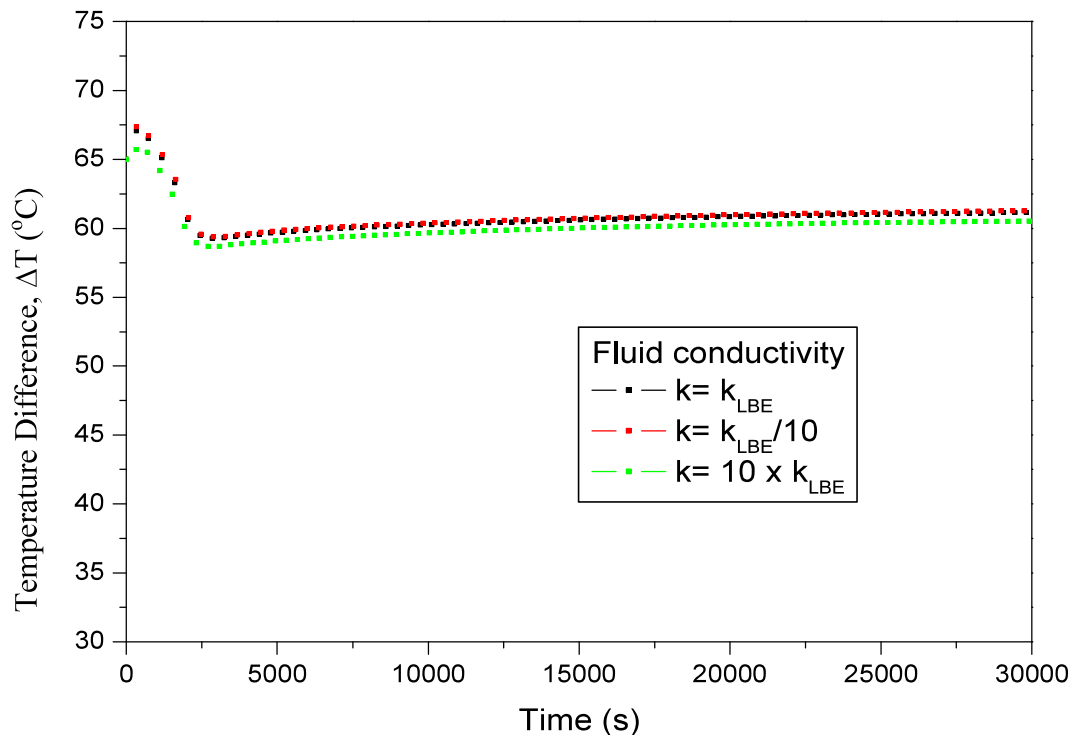


Fig 7.3 Prediction of variation of temperature difference across the heater in KTL during start up experiment at 700 W power with different thermal conductivities of the working fluid.

It can be seen that the effect of the axial conduction was negligible on the theoretical result of the start up experiments. So it can be concluded that the effect of thermal conductivity on the LBE natural circulation is not significant.

7.3.1.3 Effect of radial thermal conduction of LBE on natural convection

In the above sections the heat loss in the piping was assumed to be zero to study the effect of axial conduction. If the heat loss in the piping is considered, thermal conductivity of LBE may play important role on the temperature variation along the length. Since the specific heat of LBE is much less than normal fluid like water, the increase in heat loss due to higher radial conduction may lead to high heat loss in the piping. The higher heat loss may affect the natural circulation to a great extent. This is studied with the loop geometry of LML using LeBENC code. A case was analysed where the heat loss in the cold leg was put to zero. The heat loss in the heater section, hot leg and heat removal in the heat exchanger were considered. With this condition the effective vertical distance between the heater and cooler will be more and the results will be distinguishable at different conditions. With loop power 900 W, steady state natural circulation was simulated by setting thermal conductivity of LBE to three values, $k = k_{LBE}$, $k_{LBE}/10$ and $10 \times k_{LBE}$. Figure 7.4 shows the buoyancy head developed in the three cases. It could be seen that with $k = k_{LBE}/10$, the buoyancy head developed is lowest and hence the natural circulation flow rate. In this case the heat loss in the piping is reduced due to lower radial thermal conduction through the LBE to the piping. With $k = 10 \times k_{LBE}$, the increase in thermal buoyancy head is marginal. With increasing $k = k_{LBE}$, the thermal resistance at outer surface of the piping becomes controlling parameter for heat transfer. So further increase in K_{LBE} will not affect the heat loss any more.

7.3.2 Effect of Surface Roughness of the Piping

The effect of the surface roughness on the natural circulation was studied. Three cases have been studied for start-up experiment at 700 W in KTL. Case (a) considering the smooth surface, (b) surface roughness factor $\bar{\Delta}=0.027$, for oxidized surface and (c) $\bar{\Delta}=0.1$ for scaled surface. The corresponding pressure drop coefficients were calculated using the correlations given in Table 6.2 in chapter 6. Figure 7.5 shows the prediction of the LeBENC code for the three cases and comparison with the experimental results.

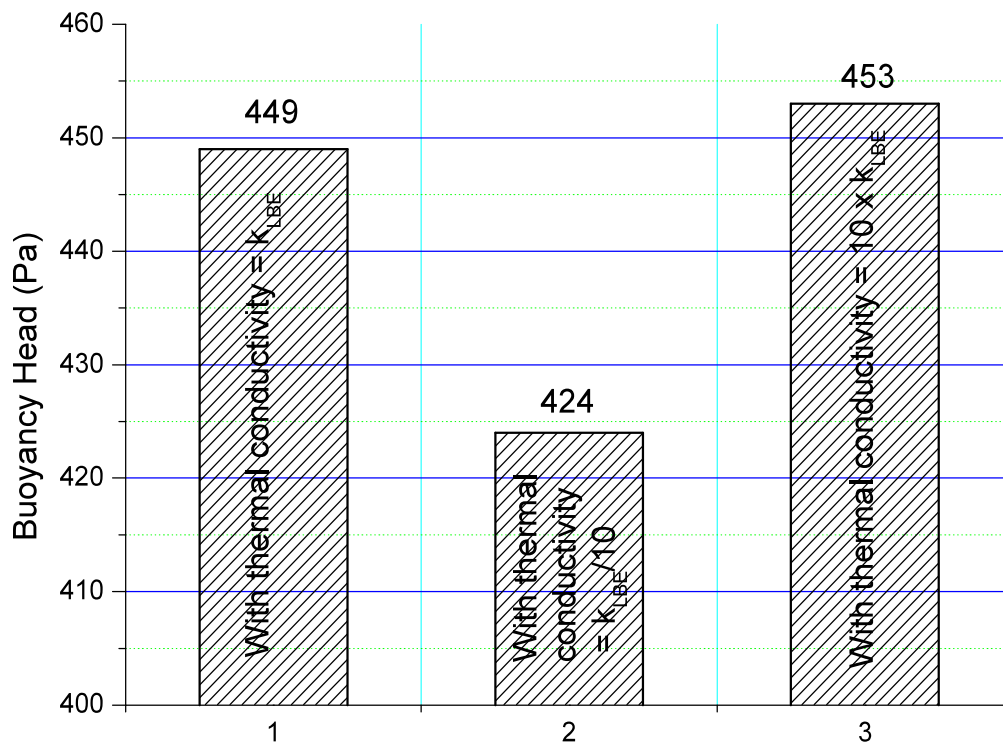


Fig 7.4 Buoyancy head developed at different thermal conductivities of LBE with heat loss in the piping.

It can be seen that the effect of roughness was negligible on the natural circulation of LBE. It should be noted that the maximum Reynolds number of LBE during the studies in the loop was calculated as 6000. In this flow range the roughness effect may not play a great role on the natural circulation. The effect of pipe surface roughness on the steady state natural circulation results was also studied and found to be negligible.

7.3.3 Effect of Heat Transfer Coefficients

The heat transfer coefficients (both in primary and the secondary sides) in the loop decide the heat transfer rate in the heater section and the heat exchanger in a loop. This may mainly affect the prediction of the transient experimental results. To study this two cases have been analysed using the code LeBENC,

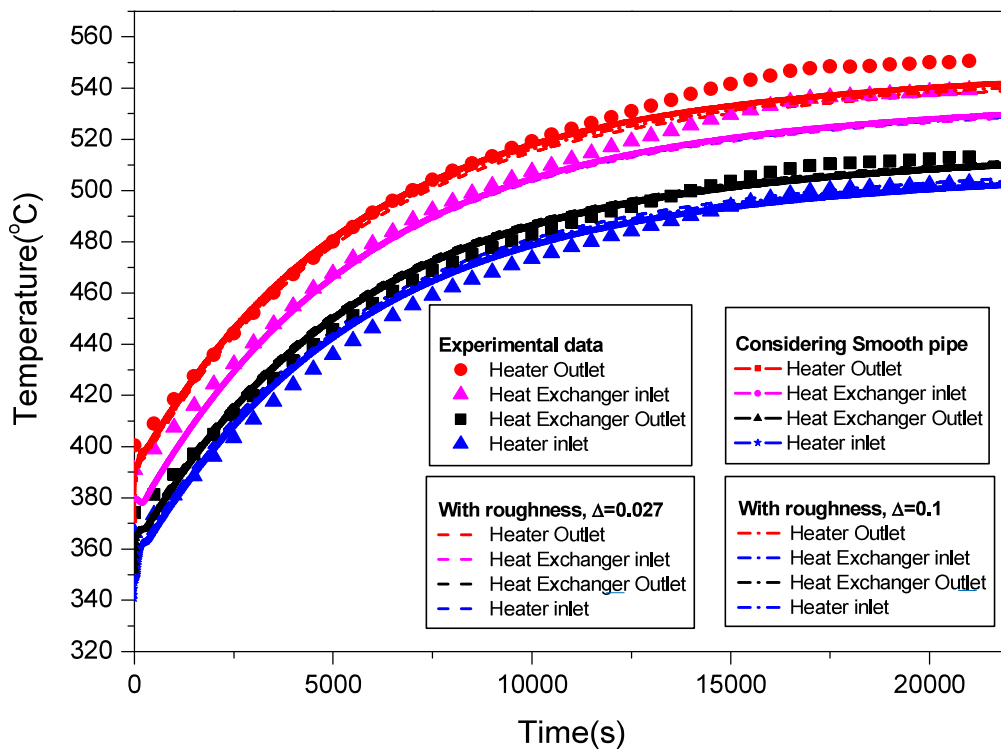


Fig 7.5 LeBENC predictions on the effect of pipe surface roughness on the natural circulation of LBE during start-up experiment at 700 W power in KTL.

(a) Effect of primary side heat transfer coefficient

(b) Effect of secondary side heat transfer coefficient

(a) Effect of primary heat transfer coefficient

As discussed in Chapter 5, the heat transfer coefficient changes depending on the flow regimes prevailing in the heater and the heat exchanger. In case of transient simulation, like

start up experiment the flow passes through different regimes. A start-up case has been studied in KTL geometry, with power level 700 W in the main heater and constant heat transfer coefficients and temperature in the secondary side. The secondary side boundary conditions are maintained at constant value during the simulation so that the effect of the primary side heat transfer coefficient can be clearly visible. Here also two cases have been studied, (i) Varying heat transfer coefficient in heater and heat exchanger with the variation of flow regime as discussed in chapter 5, and (ii) With constant heat transfer coefficient by assuming laminar flow and without gravitational effect, i.e. finding the heat transfer coefficient by using the formula $Nu=4.36$. LeBENC code was run for both the cases. Figure 7. 6 shows the prediction of temperature variation in the loop for both the cases. It can be seen that the effect of heat transfer coefficient was not significant on the temperature variation in the loop. Figure 7.7 shows the variation of the average temperature difference between the wall surface and the fluid ($\Delta T_{w, LBE}$), in the heater section of KTL during start up experiments at 700 W power. The value of $\Delta T_{w, LBE}$ decreases marginally with increasing heat transfer coefficient. The loop temperature variation is a function of different factors like, thermal inertia of the loop, secondary side heat transfer coefficients, etc. The contribution of the LBE heat transfer coefficient may be not significant on the transient behaviour of the loop. Though there was variation of heat transfer coefficient in the loop, its effect could not be seen on the loop temperature variation.

(b) Effect of secondary side heat transfer coefficient

The secondary side heat transfer coefficient may play major role on the natural circulation behaviour of the loop. In the heat exchanger the primary side heat transfer is much more than the secondary side if the secondary side coolant is gas or air. So the secondary side heat

transfer coefficient will be the controlling parameter for the heat transfer in the heat exchanger.

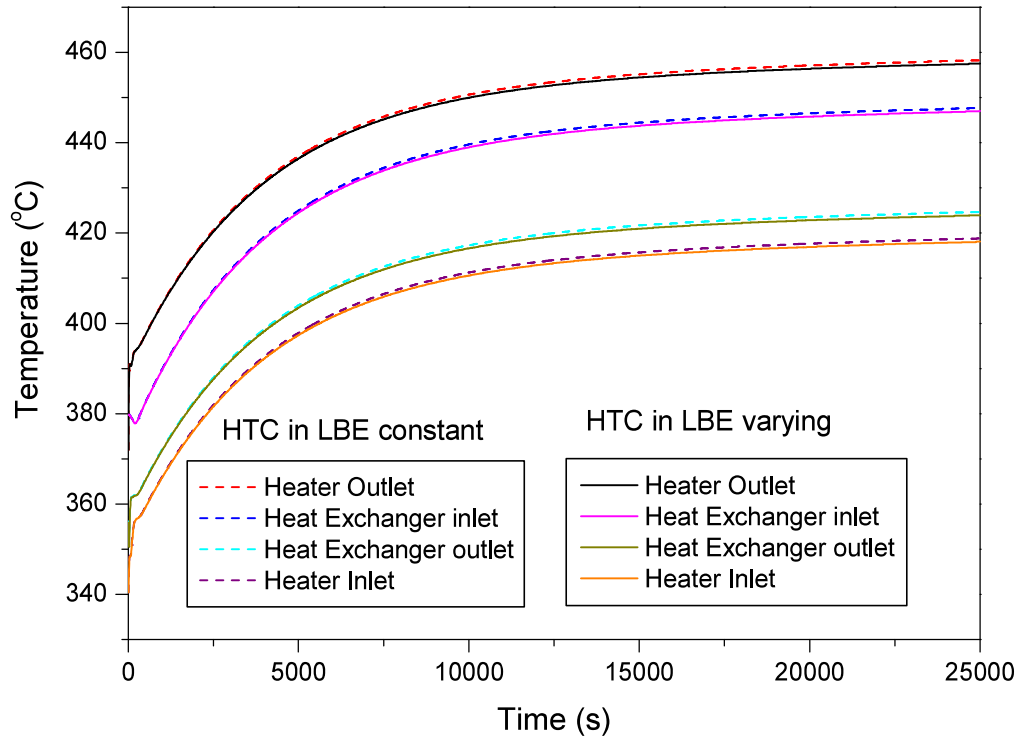


Fig 7.6 Effect of LBE heat transfer coefficients on the temperature variation with time during start up experiments at 700 W power in KTL.

Here also two cases has been studied for the start up experiment with 900 W power in KTL. LeBENC code was used to simulate two boundary conditions (a) constant heat transfer coefficient and temperature in the secondary side of the heat exchanger and (b) natural cooling by argon gas in the secondary side. Figure 7.8 shows the results of the analysis. It can be seen that with case (a) boundary condition, the LeBENC predicts the time required to achieve steady state 7000 s, which was less than the time given by experiments. case (b) boundary condition, the prediction of the time was more accurate. In the case (b) the heat transfer coefficient as well as the inlet temperature of the secondary side argon changes slowly as the temperature of the LBE increases in the primary side.

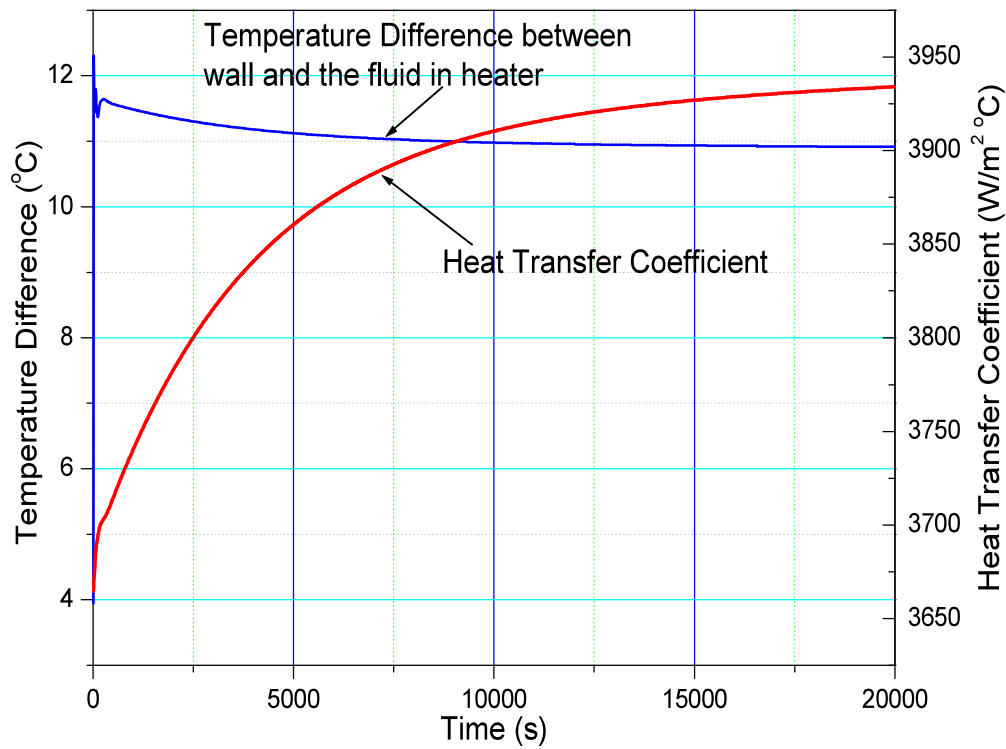


Fig 7.7 Effect of LBE heat transfer coefficients on the temperature difference between average wall and fluid temperatures in the heater section of KTL

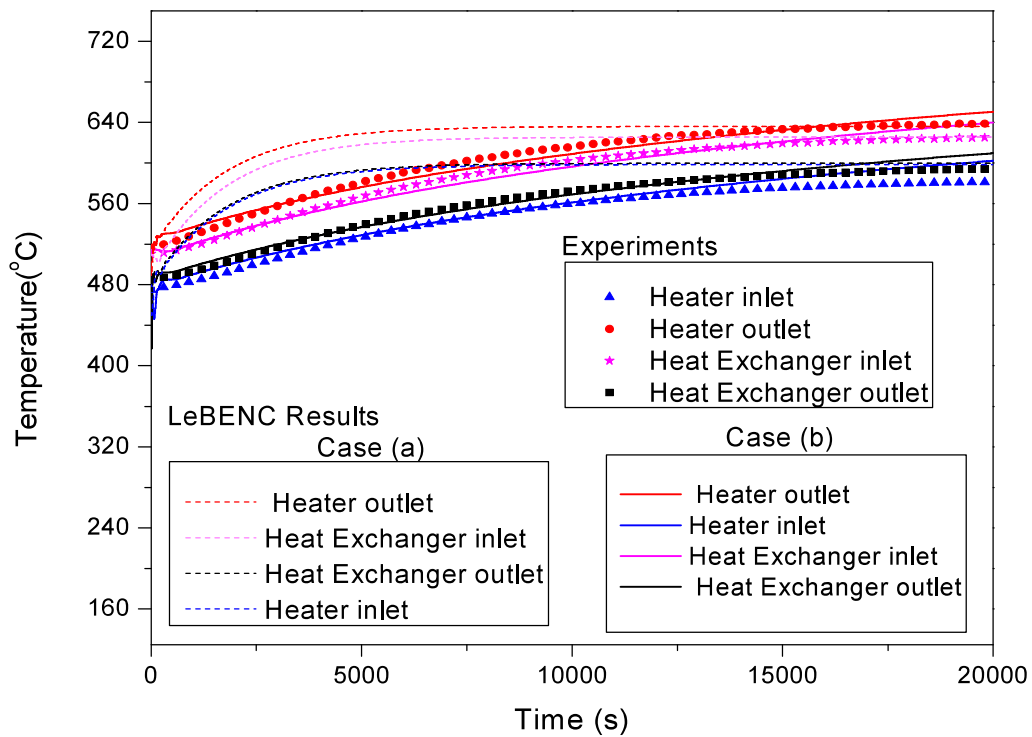


Fig. 7.8 Start-up at 900 W power and comparison with LeBENC data considering different boundary conditions at the secondary side.

With This may slow down the process to reach steady state in the primary loop as it happened during the experiment. So it can be seen that the secondary side heat transfer boundary conditions have significant effect on the natural circulation behaviour of the loop.

7.3.4 Effect of Heat Loss in Piping

Heat loss through the piping is inevitable in high temperature loops. The LBE temperature may be very sensitive on the rate of heat loss in the loop due to the low specific heat of LBE. LeBENC code was used to study the heat loss effect on natural circulation of LBE in closed loops. The details of the modelling of the heat loss in the piping were discussed in chapter 3. To study this, start-up cases have been simulated using LeBENC for 900 W power level with four cases, (a) the heat loss in the whole piping, (b) heat loss in the hot leg only, (c) heat loss in the cold leg (d) no heat loss in the piping. Figure 7.9 show the results of the analysis. It can be seen that the minimum temperature difference across the heater section is found for case (b). The condition of heat loss in the hot leg only results in higher effective vertical distance between the heater section and heat exchanger in LML. This results in the lower requirement of ΔT across the heater section for a particular heater power level. The maximum temperature difference across the heater section is found with the case (d), where the heat loss only through cold leg results lowering of effective vertical distance between the heater and the heat exchanger. Figure 7.10 shows the buoyancy head developed in all the four cases. The buoyancy head developed in the two cases, case (a) and case (d) are similar. This is due to the similar amount of heat loss in the cold leg and hot leg makes the effective height difference between the heater and the heat exchanger, same as that of without heat loss case.

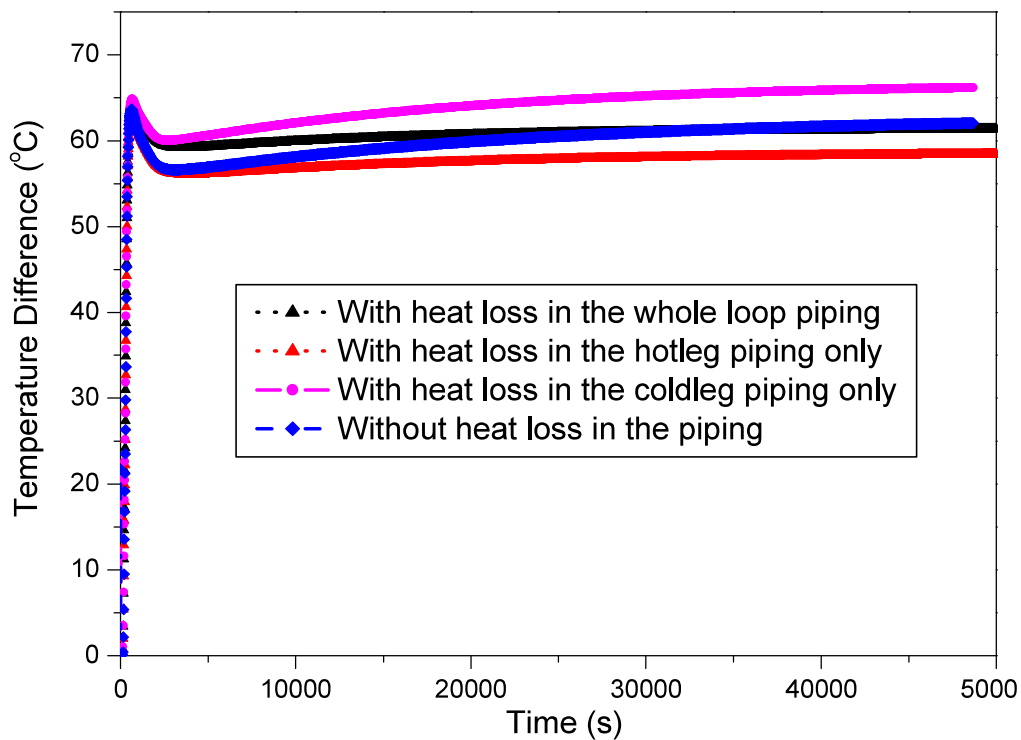


Fig 7.9 Variation of temperature difference across the heater section during start up experiment simulation at 900 W in LML with different heat loss conditions in the piping.

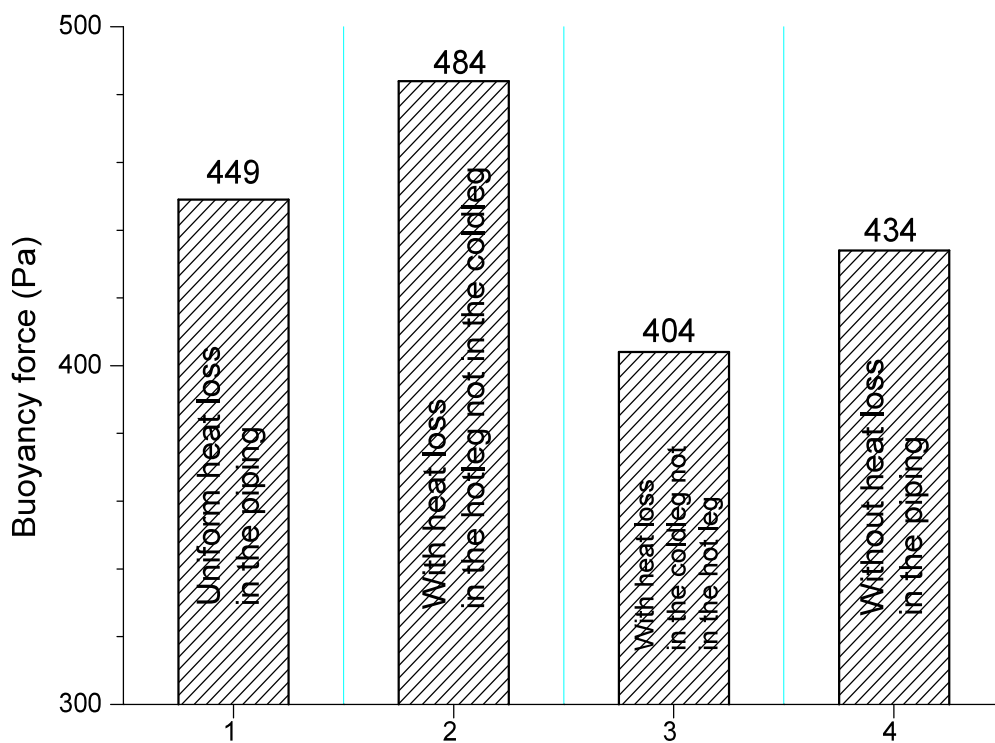


Fig 7.10 Prediction of buoyancy head developed in the LML at 900 W power at various conditions of heat loss in the piping.

In case (a), the heat loss in the hot leg piping increased the effective height for buoyancy head whereas in case (c) effective height was reduced due to the heat loss in the cold leg of LML. So the buoyancy heads also changed accordingly. Figure 7.11 shows the LBE mass flow rate predicted for all the cases. The variation of mass flow rate is similar to that of the buoyancy head developed.

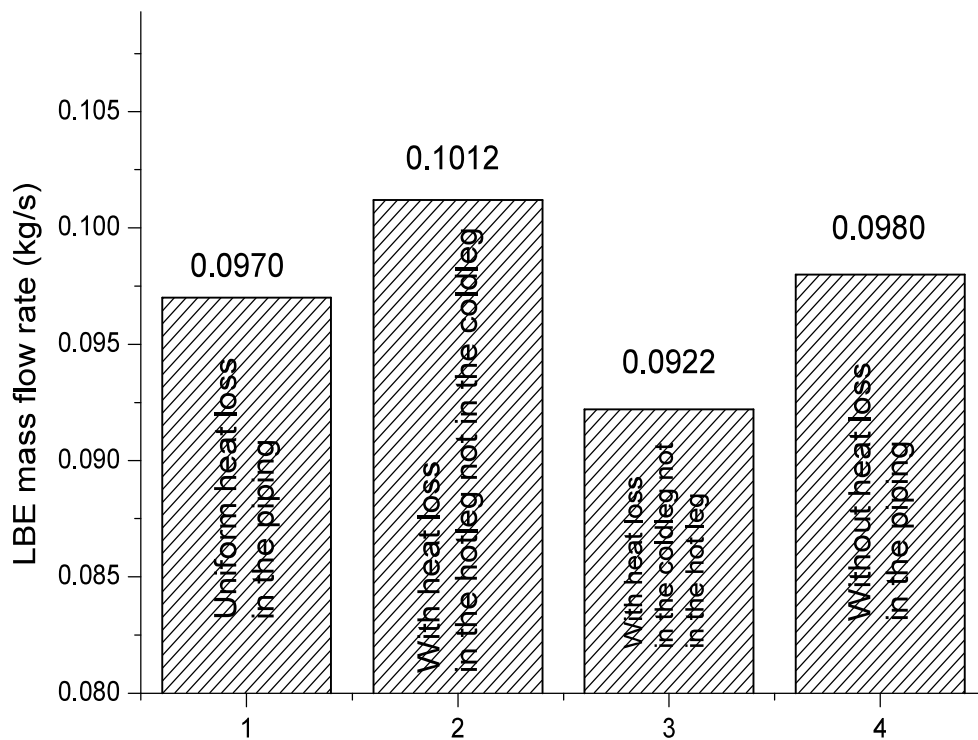


Fig 7.11 Prediction of LBE mass flow rate in the LML at 900 W power at various conditions of heat loss in the piping.

7.4 SUMMARY OF MAJOR FINDINGS

1. LeBENC code which was validated extensively with the experimental results of LML and KTL has been used to study the effect of different parameters on natural circulation of LBE in closed loops.

2. The axial conduction effect of LBE was mainly found on the axial temperature distribution in the loop. It was found that the effect remains prominent up to $Pe = 10$. The effect on the natural circulation flow rate was found to be negligible. For transient temperature distribution also the effect of axial conduction was found to be negligible.
3. The effect of surface roughness was found to be negligible for both steady state and transient natural circulation flow rate. This was due to very low flow rate of LBE which causes thick viscous sub layer covering the rough wall surfaces.
4. The effect of the variation of primary side heat transfer coefficient due to the changing flow regimes was found to be negligible on the natural circulation of LBE. This could be due to the high heat transfer coefficient in the LBE and the change in LBE heat transfer has no significant effect on the overall natural circulation behaviour in the loop. However the secondary side heat transfer conditions were found to have significant effect on the natural circulation behaviour. This was due to the cooling by gas in the secondary side, which has lower heat transfer coefficient (~50 times lower than the LBE side heat transfer coefficient).
5. The extent on the influence of the heat loss in the piping on the natural circulation flow rate in a closed loop depends on the proportion of heat loss in the hot leg and cold leg. This decides the effective vertical height between heater and the heat exchanger and the buoyancy head developed is varied accordingly.

Chapter-8

SUMMARY AND SCOPE FOR FUTURE WORK

8.1 INTRODUCTION

Natural circulation on Lead Bismuth Eutectic (LBE) was carried out in the present work. The summary of the work and the conclusions drawn from the results of the studies can be divided into three sections

1. Experimental work on natural circulation of LBE in two loops, Liquid Metal Loop (LML) and Kilo Temperature Loop (KTL).
2. Development of computer code LeBENC and its validation.
3. Studies on the effect of different parameters on LBE natural circulation.

8.2 EXPERIMENTAL WORK ON NATURAL CIRCULATION OF LBE IN TWO LOOPS, LML AND KTL

Experimental studies were carried out to generate the LBE natural circulation data relevant to Compact High Temperature Reactor (CHTR) design. For this work, two LBE loops were constructed based on the knowledge gained from literature review. LML was developed to operate up to 500 °C. The instrumentation essential for operation of the loops were also developed. The LBE chemistry was maintained by active oxygen control technique. KTL was designed, fabricated commissioned with Nb-alloy as structural material to conduct the experiments at higher temperature (> 500 °C). The loop was kept in an inert gas enclosure to avoid oxidation of the Nb-alloy at higher temperature. The oxygen concentration in the

argon gas enclosure was maintained below 10 ppm with the help of a specially developed oxygen scavenging system. Natural circulation data were generated in both the loops for Gr_m range 10^{11} to 10^{13} and Re_{ss} range 600 to 3200. The experiments were conducted in the temperature range 200 °C to 780 °C.

The steady state natural circulation experimental results of liquid metal loops reported in literature were analysed and the data were converted to non-dimensionalised form so that inter-comparison of the data from different loops can be compared. The natural circulation correlations developed from the experimental data of water based loops were compared with the liquid metal experimental data and maximum deviation were found to be within 20.0%. Transient experiments were carried in the two loops to simulate different postulated events in CHTR. The transient experiment conducted are, start up experiment at different power, heater trip, loss of heat sink, step change of power and the effect of secondary coolant flow variation in the heat exchanger. Among the experiments, it was found that the start up experiments causes largest temperature gradient in the loop. It was also observed that the time to initiate natural circulation decreases with increasing power levels.

In the loss of heat sink experiments the natural circulation was found to be sustained during entire duration of the experiment but at reduced rate of flow. During the step change in power experiment the step change in temperature is more in the heater section than other part of the loop. In the step change of secondary coolant flow rate experiment, the step change in LBE temperature distribution is more prominent in the heat exchanger than in the heater section. But in the loss of heat sink experiment the change in temperature could be seen at all part of the loop. During entire experimental studies no instability of the LBE was observed.

8.3 DEVELOPMENT OF COMPUTER CODE LeBENC AND ITS VALIDATION

The literature survey revealed that the system codes were generally used for natural circulation in closed loops. Since there was no system code available in house, which can handle LBE systems, a computer code had to be developed for theoretical analysis. The required features of the code was assessed to analyse LBE systems at high temperature. Since the LBE flow varies in the loop especially during the transient experiments, the heat transfer coefficient will also change with the flow rate. The heat transfer coefficients at different flow regimes, free convection, mixed convection and forced convection were evaluated by CFD analysis. These correlations were used during theoretical analysis of the LBE natural circulation. A computer code named LeBENC (Lead Bismuth Eutectic Natural Circulation) was developed. The momentum equation was solved to find the natural circulation flow rate by equating mainly the buoyancy head and the total pressure drop in the loop. Energy equation takes into account of the heat transfer in the loop. Fluid axial conduction was considered in the energy equation as it might play an important role in LBE loop. Conduction equation for the solid wall was also solved by considering 1-D axial conduction equation. The code was extensively validated with the experimental results of LML and KTL.

8.4 STUDIES ON THE EFFECT OF DIFFERENT PARAMETERS ON LBE NATURAL CIRCULATION

The effect of different parameters on the LBE natural circulation in a closed loop at high temperature were studied using the code LeBENC. The parameters studied are, heat loss in the piping, thermal conduction in LBE, roughness of the pipe surface and the heat transfer coefficients of LBE. The heat loss in the piping decreases the loop temperature. The effect of

heat loss on buoyancy head developed in the loop is found to be significant if the heat loss causes the change in the effective height between the heater section and the heat exchanger. The axial conduction effect on the axial temperature distribution in the loop was found to be significant up to $Pe \approx 10$, which was in accordance with Gargin and Turker (2011) [123]. But the mass flow rate was found to be unaffected by the axial conduction of LBE. It was found that the pipe surface roughness and heat transfer coefficient of LBE have no significant effect on the LBE natural circulation in the range of Reynolds number studied.

8.5 SUGGESTIONS FOR FUTURE WORK

8.5.1 Experimental Studies

The natural circulation experimental studies were carried out up to 780°C only. Further generation of natural circulation data in KTL could be done at ~1000°C and beyond. This will help to design CHTR for normal operating and accidental conditions. The mass flow rate in KTL and LML could not be measured because of the unavailability of the instruments for low flow rate measurement at high temperature. Experimental studies are required for different orientation of the cooler and heater arrangements (i.e. HHHC, HHVC, VHHC and VHVC) in the loop. The experiments on the natural circulation stability in the various orientation are essential for the validation of stability codes for liquid metal systems.

8.5.2 Computational Studies

3D analysis of the loop considering the structural material are to be carried out to simulate the multidimensional heat transfer in the structural material of the loop. CFD codes could be used for the analysis. The analysis could be done for the prediction of both steady state and transient natural circulation. The coupling of LeBENC code with CFD codes could

result in an efficient tool to study the transients in natural circulation loops. The piping of the loop can be modelled with LeBENC code and the bigger components of the loops like heater section, cooler section and expansion tank could be simulated with 3D CFD codes.

8.5.3 Stability Analysis

Stability analysis is important to characterise a natural circulation loop. The stability analysis of a non uniform diameter loop considering the axial conduction of LBE, the thermal inertia of structural material and heat loss in the piping is important for getting better insight of liquid metal natural circulation system. The results of the analysis could be validated extensively with the experimental results.

Appendix- 4.1

Calculation of wall thickness of KTL components

Expansion tank:

As it was informed by NFC, Hyderabad the maximum wall thickness of the expansion tank can be maintained by 3 mm only due to the limitation in fabrication of the plates and tubes required for the different components of the loop. The mechanical design was checked for the designed pressure.

Expansion Tank:

Wall thickness= 3.0 mm , Tank OD/ID =114.0 mm/108.0 mm

Since $d/t = 36.0 > 20.0$, the thin shell formula can be applied

The Hoop stress developed is,

$$\sigma = pd/2t \quad (A4.1.1)$$

Assuming $p=4.5$ bar, the stress developed is, $\sigma = 4.5 \times 108.0/(2 \times 3.0) = 8.1$ MPa < 20 MPa,

This creep value at 1200 °C is 20 MPa, as per Wojick (2001) [168].

Nb-alloy Piping:

The size of the piping of the main loop was OD/ID=21/15 mm, thickness 3.0 mm. Using the thickness formula for pressure vessel from ASME VIII div 1,

$$t = \frac{PR}{SE + 0.6P} \quad (A4.1.2)$$

Where $P=0.45$ MPa

S = Allowable stress=20 MPa , E = Joint Efficiency= 1.0 for seamless pipe

R = Internal Radius =0.0075 m

So the minimum thickness required, from the above equation was found to be ~0.2mm, which was less than the existing pipe thickness (3.00 mm). So the design was safe.

SS Piping:

Since the SS section was designed for lower temperature ($\sim 300^\circ\text{C}$), the creep was not considered in the design. The size of the piping of the main loop was OD/ID=21/15 mm, thickness 3.0mm. Using Eq. (A4.1.2), we could find out the minimum thickness required for the dump tank. Inserting the following values in the equation,

Where $P=0.45\text{ MPa}$

$S = \text{Allowable stress} = 14.5\text{ MPa}$ (From ASME Section II) at 510°C

$E = \text{Joint Efficiency} = 1.0$ for seamless pipe

$R = \text{Internal Radius} = 0.00788\text{ m}$

So the minimum thickness required, from the above equation was found to be $\sim 0.25\text{mm}$, which was less than the existing pipe thickness (2.77 mm). So the design was safe.

Dump tank:

As per the ASME code, the dimension of the dump tank of the loop was OD/ID=120.0/142.0 mm, thickness 11.0mm. Using Eq. (A4.1.2), we could find out the minimum thickness required for the dump tank. Inserting the following values in the equation,

$P=0.45\text{ MPa}$

$S = \text{Allowable stress} = 14.5\text{ MPa}$ (From ASME Section II) at 510°C

$E = \text{Joint Efficiency} = 1.0$ for seamless pipe

$R = \text{Internal Radius} = 0.060\text{ m}$

the minimum thickness required was found to be $\sim 3.5\text{ mm}$, which was less than the existing pipe thickness (11.0 mm). So the design was safe.

Appendix 4.2

Heat transfer analysis of the enclosure of KTL

The enclosure of KTL was mainly designed to provide inert gas condition to the loop so that the loop can be operated at higher temperature without oxidation of the loop material. During the operation the heat of the loop was rejected inside the enclosure. This heat is to be ultimately rejected outside effectively to avoid temperature rise in the enclosure. To remove heat, two sides of the enclosure were provided with fins and additionally with a water cooling coil at the top. Figure A4.2.1 shows the schematic of the enclosure.

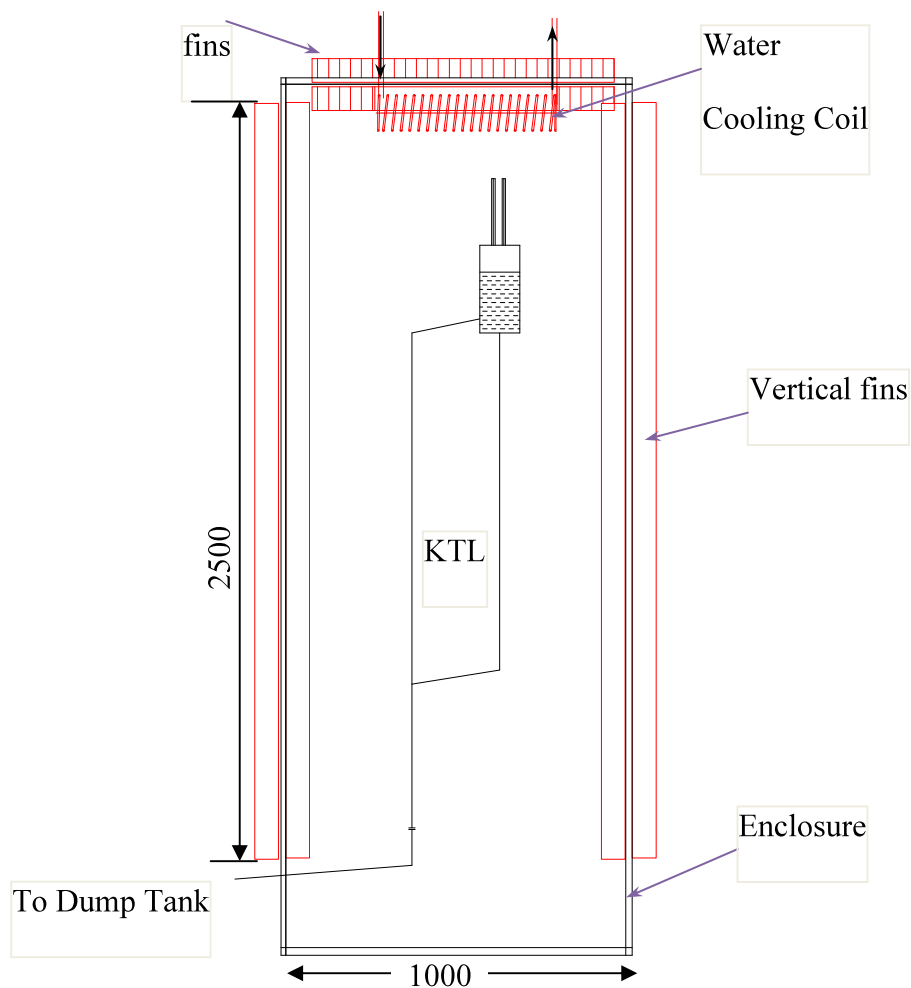


Fig A4.2.1 Schematic of the KTL enclosure showing fins and cooling coil

The heat of the loop was rejected inside the enclosure. The heat was to be rejected outside effectively to avoid temperature rise in the enclosure. To remove heat, two sides of the enclosure were provided with fins. The fins were provided on the both inner and outer surfaces. Here the calculation of the fin effectiveness and the temperature distribution in the enclosure are discussed. Since the heat was rejected by natural convection from the outer surfaces of the enclosure. The heat transfer can be estimated by using Churchill and Chu correlation, as given below,

$$\overline{Nu} = \left\{ 0.825 + \frac{0.387 Ra_L^{1/6}}{\left[1 + \left(0.492 / Pr \right)^{9/16} \right]^{8/27}} \right\}^2 \quad (A4.2.1)$$

Assuming $Pr=0.7$ and calculating Ra as 5.69×10^9 for a typical case of $T_w=150^\circ\text{C}$ and $T_\infty=30^\circ\text{C}$. Here the T_w and T_∞ were the enclosure wall temperature and the ambient temperature respectively. We get the average convective heat transfer coefficient as,

$$h_{\text{conv}} = 4.5 \text{ W/m}^2\text{K}$$

The equivalent heat transfer due to radiation, assuming 150°C as wall temperature,

$$h_{\text{rad}} = \varepsilon \sigma (T_w + T_\infty) (T_w^2 + T_\infty^2) \quad (A4.2.2)$$

So the total heat transfer coefficient was, $h = h_{\text{conv}} + h_{\text{rad}} = 11 \text{ W/m}^2\text{K}$

Effectiveness of the fins

For rectangular plate the effectiveness is given by,

$$\phi = \frac{\tanh mL}{mL} \quad (A4.2.3)$$

Where $m = \sqrt{\frac{\zeta h}{AK}}$, ($\zeta = 2 \times L + t$, $A = w \times H$, $H = 2.5 \text{ m}$) (Fig A4.2.2)

The values of effectiveness with respect to fin height is given in Fig 4.2.3,

It was seen that in the range of height considered (0.01 to 0.05 m) the effectiveness remain almost same. The fin height could be increased further but due to the problem of welding at the fin base the fin height was kept 50 mm. The pitch was again decided for the convenience of welding.

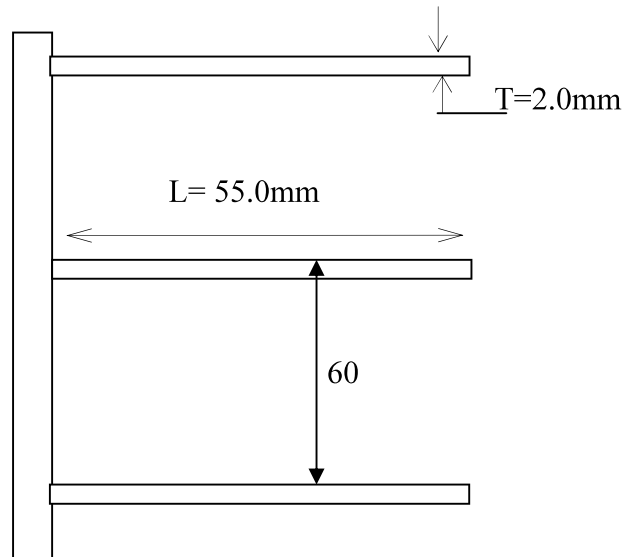


Fig A4.2.2 Fin schematic for the calculation of effectiveness

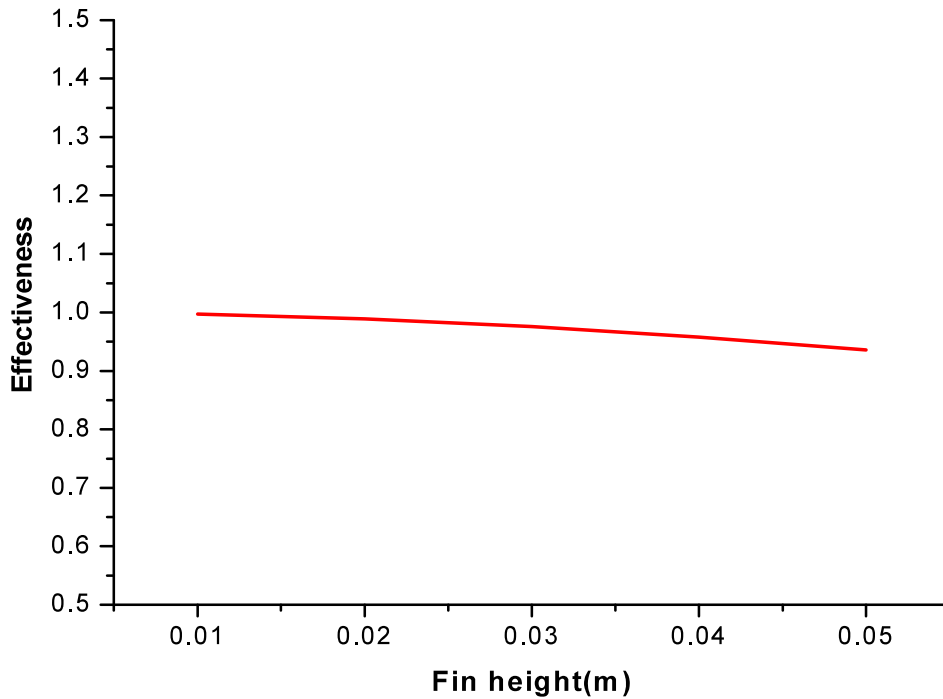


Fig A4.2.3 Calculated fin effectiveness variation with fin height

The heat transfer across the finned surface:

The heat was transferred through wall with fins on the both side as shown in the Fig A4.2.4.

As shown in the Figure,

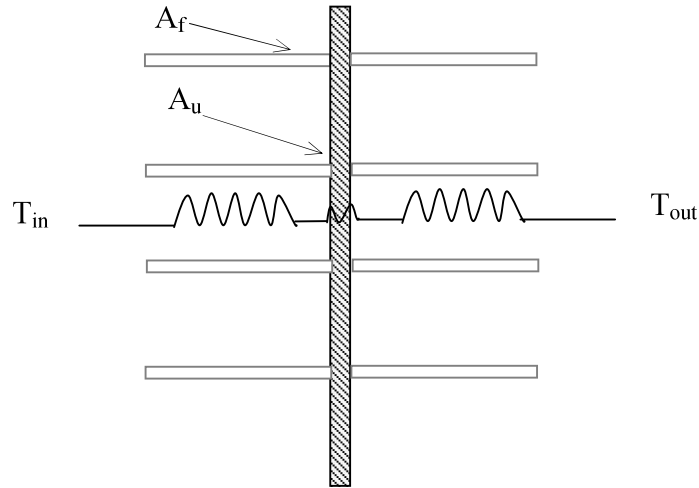


Fig A4.2.4 Schematic of the fins for the calculation of overall heat transfer

$$A_f = \text{Finned surface area} = (2xL + t) \times H = (2 \times 0.05 + 0.02) \times 2.5 = 0.3 \text{ m}^2 \text{ per pitch}$$

$$A_u = \text{Un-finned surface area} = (p - t) \times H = (0.06 - 0.002) \times 2.5 = 0.145 \text{ m}^2 \text{ per pitch}$$

$$A = \text{Base Area} = H \times W = 2.5 \times 0.06$$

$$= 0.15 \text{ m}^2 \text{ per pitch,}$$

The heat transfer in the inner finned surface is given by,

$$Q = (\phi_1 A_f + A_u) h_{in} (T_{in} - T_{wi}), \quad (\text{A4.2.4})$$

$$T_{in} - T_{wi} = \frac{Q}{[\phi_1 A_f + A_u] h_{in}} \quad (\text{A4.2.5})$$

Where

ϕ_1 = Effectiveness of inner finned surface area.

T_{wi} = Inner fin base temperature.

Considering

a) Geometry of the inner fins and outer fins are same,

and b) Outer and inner heat transfer coefficients are same

The overall heat transfer coefficient of the finned wall can be given as,

$$\frac{1}{U} = \frac{2A}{(\phi_1 A_f + A_u)h} + \frac{w_w}{K_w} \quad (A4.2.6)$$

Inserting the values, we get, $U=15.1\text{W/m}^2\text{K}$, for 4000 W case. This value is calculated iteratively for different power levels.

This overall heat transfer coefficient was used for CFD analysis,

CFD of analysis of the KTL enclosure

PHOENICS was used for the analysis. A quarter symmetry of the square enclosure was used for the analysis. The heat source in the analysis was simulated as a cuboids with the height equal to the heat exchanger of the loop and centrally located in the enclosure. The CFD model of the enclosure was shown in figure A4.2.5 (a). Only left and right surfaces (finned surface) were considered as heat conducting surfaces. The front, bottom and back surfaces were considered to be adiabatic. This assumption gives conservative results. Four cases have been studied as given in Table A4.3.1. Fig A4.2.5 (b) gives the results of the CFD analysis for a case. Table A4.2.2 gives the maximum temperatures of the analysed cases.

Table A4.2.1 Cases Considered for CFD analysis

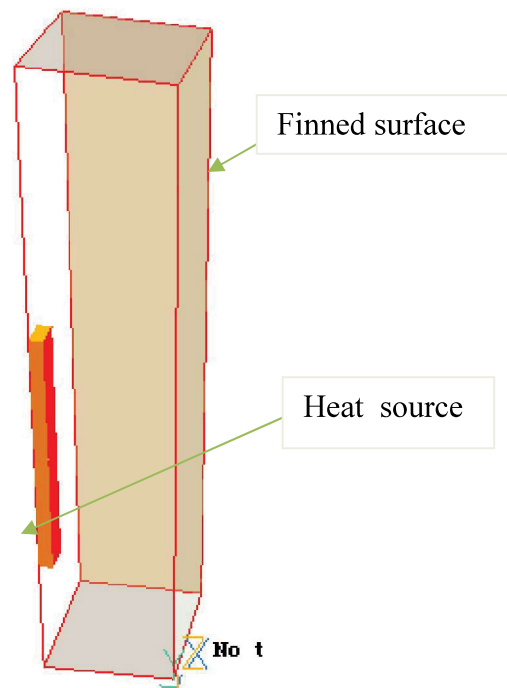
Case No	Cases
1	Heat transfer only through the two sides of finned surfaces
2	Heat transfer through the two sides of finned surfaces, top and bottom bare surfaces (no fin)
3	Heat transfer through the two sides of finned surfaces, top finned and bottom bare surfaces
4	Heat transfer through the two sides of finned surfaces, top and bottom bare surfaces with water cooling coil on the top.

Table A4.2.2 Summary of the results of CFD analysis,

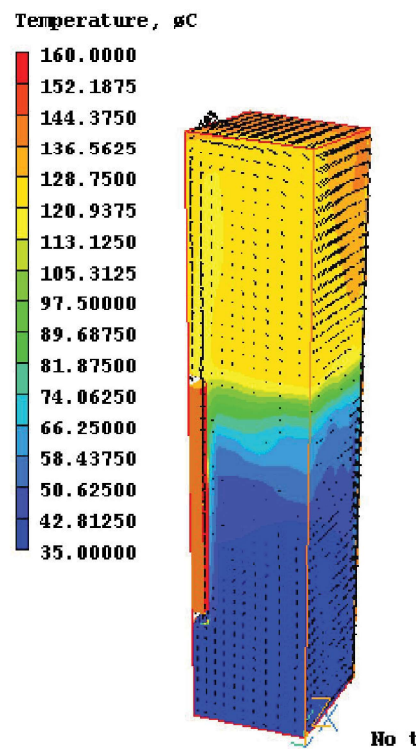
Case No	Maximum Temperature (°C)	
	Top Surface	Side surfaces
1	155	140
2	142	120
3	130	95
4	85	72

Table A4.2.3 Summary of the results of CFD analysis for case 3

Power	Maximum Temperature (°C)	
	Top Surface	Side surfaces
1000	78	54
2000	103	70.
3000	130	95
4000	150	99



(a) The 1/4th symmetric 3D model for the CFD analysis



b) case-3 with 4000 W power

Fig A4.2.5 CFD modelling and the results of a typical case

Appendix 4.3

OXIDATION OF THE NIOBIUM AT HIGH TEMPERATURE

This appendix consists of the findings from literature survey on the oxidation of Niobium in air and low oxygen concentration (from 10 ppm to 1000 ppm) and the calculation of the oxidation rate of the Nb-alloy at different oxygen concentration in air and at different temperatures. Kofstad and Espevik (1965) [169] studied on the oxidation rate of Nb-1Zr alloy in presence of air at different temperature. It was found that from 400°C the oxidation process picks up and around 550°C it becomes significant. Delgrosso et al. (2000) [170] carried out oxidation test in air, at 1 % and 5 % oxygen. At 1 % (10000 ppm) and at 650 °C the oxidation rate was calculated as 0.475 mg/cm²hr. Distefano and Chitwood (2001) [165] tried to plot the variation of oxidation rate with entire range of oxygen pressure. In the range of oxygen pressure 10⁻² to 10² Pa, the plot was based on the indirect interpretation from various sources. Unfortunately our oxygen level in the enclosure region fell in this range. This region shows reversal of the oxidation rate and the data for this region is limited.

After comparing the results with some discrete values, found from the literatures, it was found that the plot over predicts the oxidation rate. Distefano et al. (2000) [170] observed that the oxidation rate was lower in case of argon gas medium, than the vacuum conditions. So when we use this data for the analysis for our KTL the results will be conservative. Based on the above mentioned literature studies a graph has been plotted for temperature 1000 °C and 650 °C. The oxygen range was 10 ppm to 10000 ppm. As per the mechanical design analysis the expansion tank will be the most sensitive to thickness reduction. As mentioned in Appendix 4.1 the Hoop stress at design pressure was 8.1 MPa. The corresponding required thickness was found to be 1.3mm. The thickness of the tank was

3.0 mm. So maximum 1.7 mm can be allowed for the oxidation. With the data of oxidation plotted in Fig A4.3.1, the number of hours required to oxidise the available thickness (1.7 mm) of Niobium was calculated for 650 °C and 1000 °C.

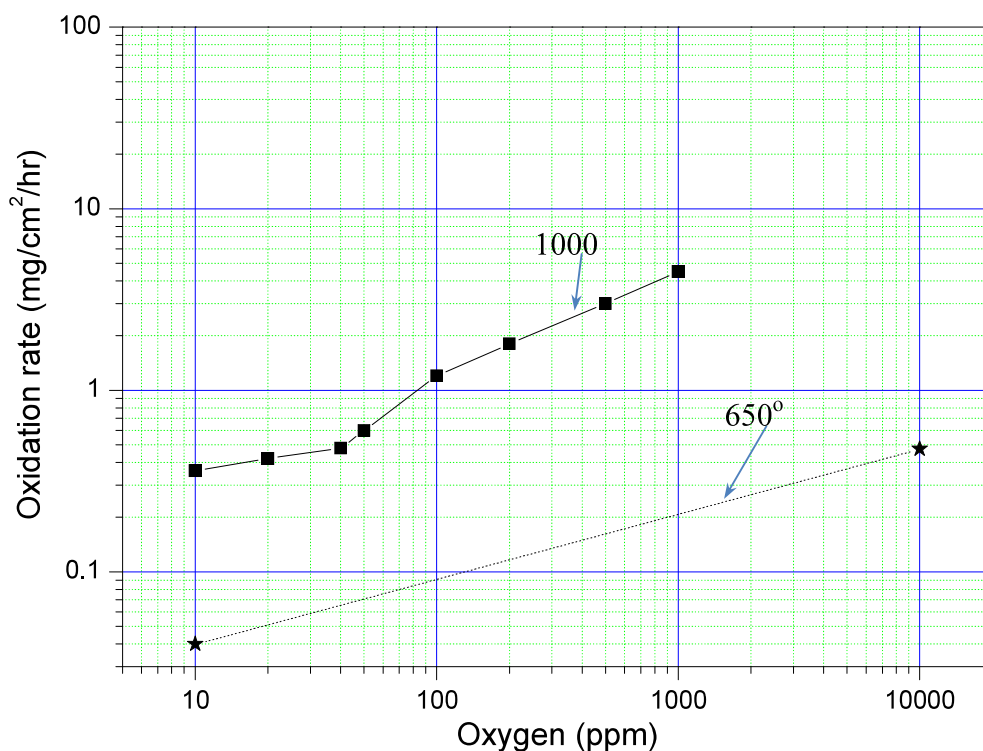


Fig. A4.3.1. The calculated oxidation rate at 650 °C and 1000 °C with different oxygen concentration

For intermediate temperatures the values were found by linear interpolation. Figure A4.3.2 (a) shows the result for 650 to 900 °C and Fig A4.3.2 (b) shows the results for 1000°C. It should be noted that the values for 1000 °C was calculated based on the data generated in vacuum condition, where oxidation rate was higher than the argon medium. The values are also tabulated in Table A4.3.1.

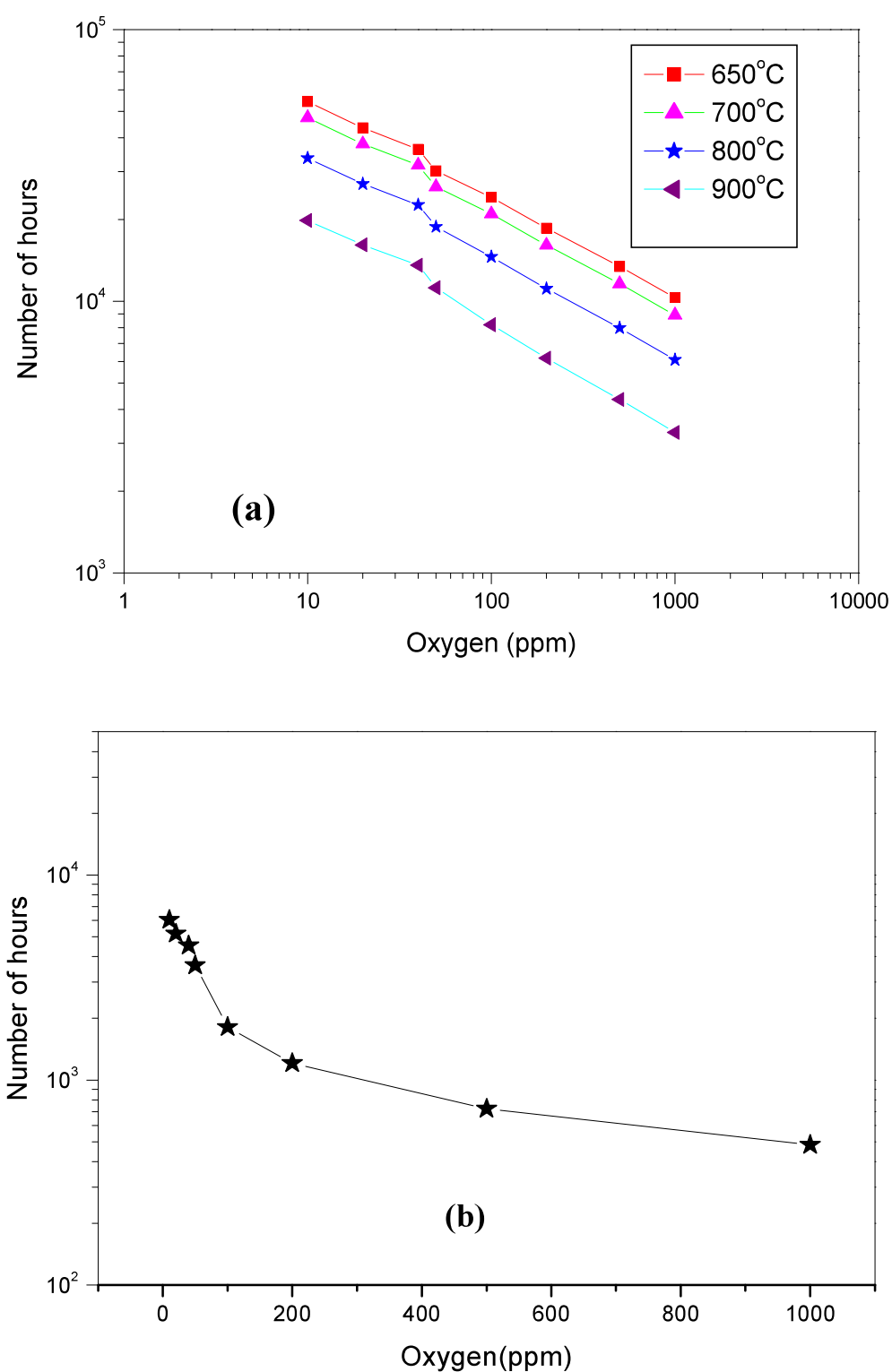


Fig. A4.3.2 Maximum number of hours considering thickness of 1.7mm Nb oxidation with varying oxygen concentration for (a) temperature range 650-900°C (b) at 1000°C.

If it is considered that the minimum loop life is 4000 hours, the loop can be run at or below 40 ppm for operating temperature up to 1000 °C. For 900 °C the maximum oxygen limit is 500 ppm. For temperature 800°C and below, with maximum oxygen limit is 1000 ppm for safe operation of the loop. Table A4.3.1 shows the results of the calculations which were based on the experimental data from DiStefano et al. (2000) [171]. It can be seen that with 10 ppm oxygen in argon gas the loop can be operated more than 8 months at 1000 °C, which was sufficient time to conduct all the envisaged experiments. So it was decided to keep the oxygen level at 10 ppm or below.

Table A4.3.1. The number of hours required for oxidation of 1.7 mm thick Nb with varying oxygen concentration for different temperatures.

Oxygen (ppm)	Temperature (°C)					
↓	650	700	800	900	1000	1100
10	54361.94	47458.84	33652.63	19846.42	6040.22	3562.18
20	43489.55	38016.38	27070.03	16123.68	5177.33	3083.76
40	36241.29	31711.13	22650.81	13590.49	4530.16	2718.10
50	30201.08	26404.37	18810.96	11217.54	3624.13	2161.18
100	24160.86	20968.18	14582.81	8197.44	1812.06	1018.62
200	18585.28	16102.82	11137.89	6172.97	1208.04	669.54
500	13422.70	11608.72	7980.75	4352.79	724.83	395.33
1000	10305.58	8902.39	6096.00	3289.61	483.22	260.76

Appendix 4.4

CALCULATION OF NON-DIMENSIONLISED NUMBERS OF DIFFERENT LIQUID METAL LOOPS

To compare the steady state natural circulation of different liquid metal loops, the individual loops thermal hydraulic characteristics were to be expressed in non-dimensional numbers. Vijayan (2002) [3] showed that for steady state natural circulation, the flow in single phase uniform or non-uniform diameter natural circulation loops can be expressed as,

$$\text{Re}_{ss} = c \left(\frac{Gr_m}{N_G} \right)^p \quad (\text{A4.4.1})$$

Where, $\text{Re}_{ss} = \frac{D_r W_{ss}}{A_r \mu}$, $D_r = \frac{1}{L_t} \sum_{i=1}^N D_i L_i$, $A_r = \frac{1}{L_t} \sum_{i=1}^N A_i L_i$, $L_t = \sum_{i=1}^N L_i$

and $Gr_m = \frac{D_r^3 \rho_o^2 \beta g Q_h \Delta Z_c}{A_r \mu^3 C_p}$

N_G is a geometric parameter of the loop and defined as,

$$N_G = \frac{L_t}{D_r} \sum_{i=1}^N \left(\frac{\bar{l}_{eff}}{D^{1+b} A^{2-b}} \right)_i \quad (\text{A4.4.2})$$

Where, $\left(\bar{l}_{eff} \right)_i = \left(L_{eff} \right)_i / L_t$, $\left(L_{eff} \right)_i = L_{ei} + L_i$, $k_i = \frac{f_i L_{ei}}{D_r}$, $\bar{A}_i = \frac{A_i}{A_r}$, $\bar{D}_i = \frac{D_i}{D_r}$, $\bar{L}_i = \frac{L_i}{H}$,

$$c = \left(\frac{2}{a} \right)^{1/(3-b)} \quad \text{and} \quad p = 1/(3-b)$$

The schematic of different liquid metal loops which were considered for the present analysis are shown in Figure A4.4.1 to Fig A4.4.5 along with their major dimensions. The pressure drop coefficient of the heater rod bundles in the loops were calculated by using the

appropriate correlations available in the literature. The values of the constants 'a' and 'b' depend on the nature of the flow. For laminar flow, $a=1$ and $b=64$. For turbulent flow, $a=0.316$ and $b=0.25$, if Blasius friction factor correlation was used. L_{ei} was the equivalent length to absorb the local loss coefficient k_i .

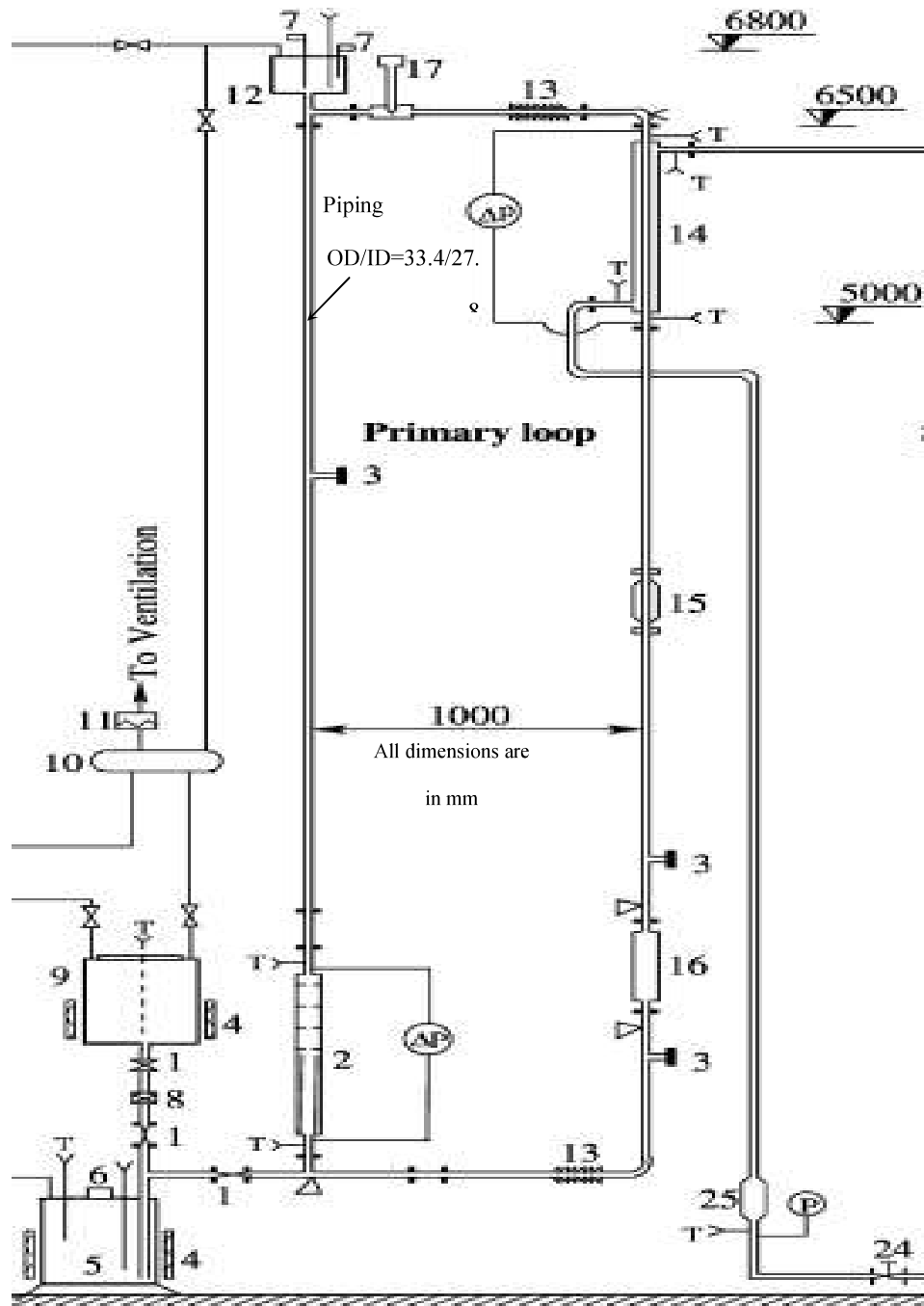


Fig A4.4.1 Schematic of TALL facility [36]

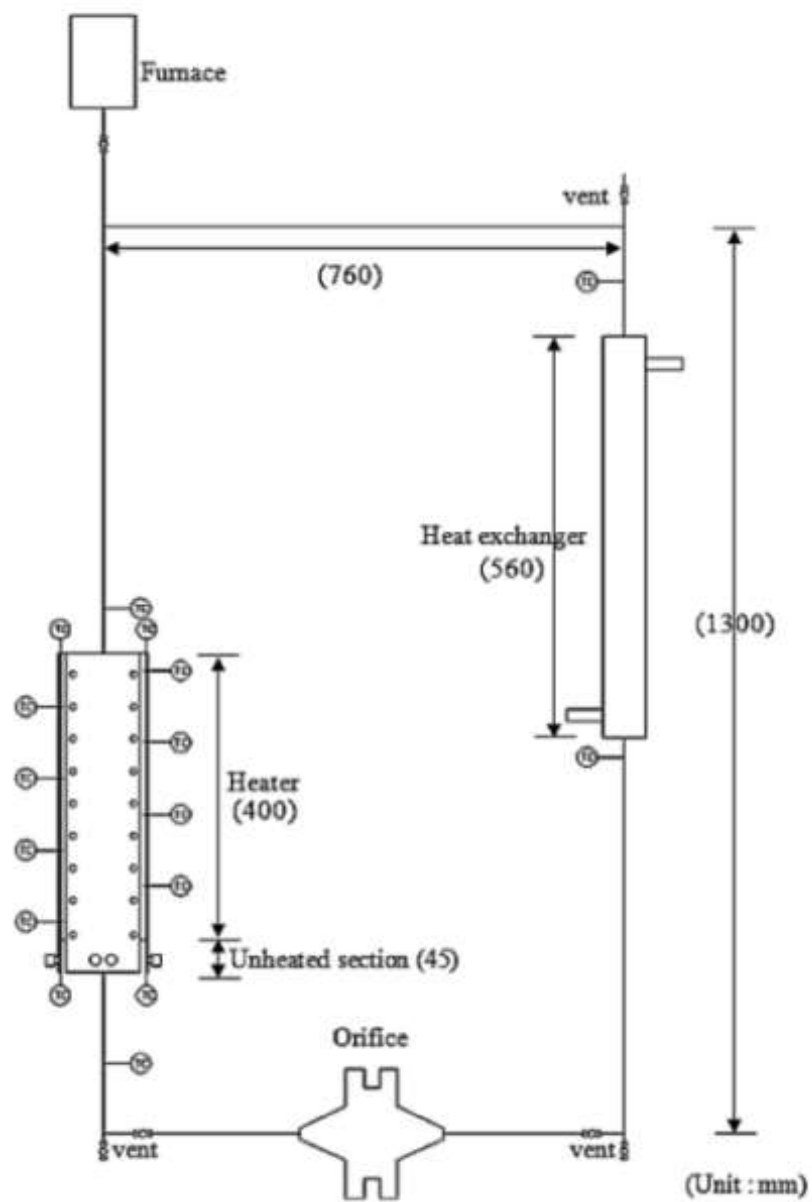


Fig A4.4.2 Schematic of Gallium Loop [34]

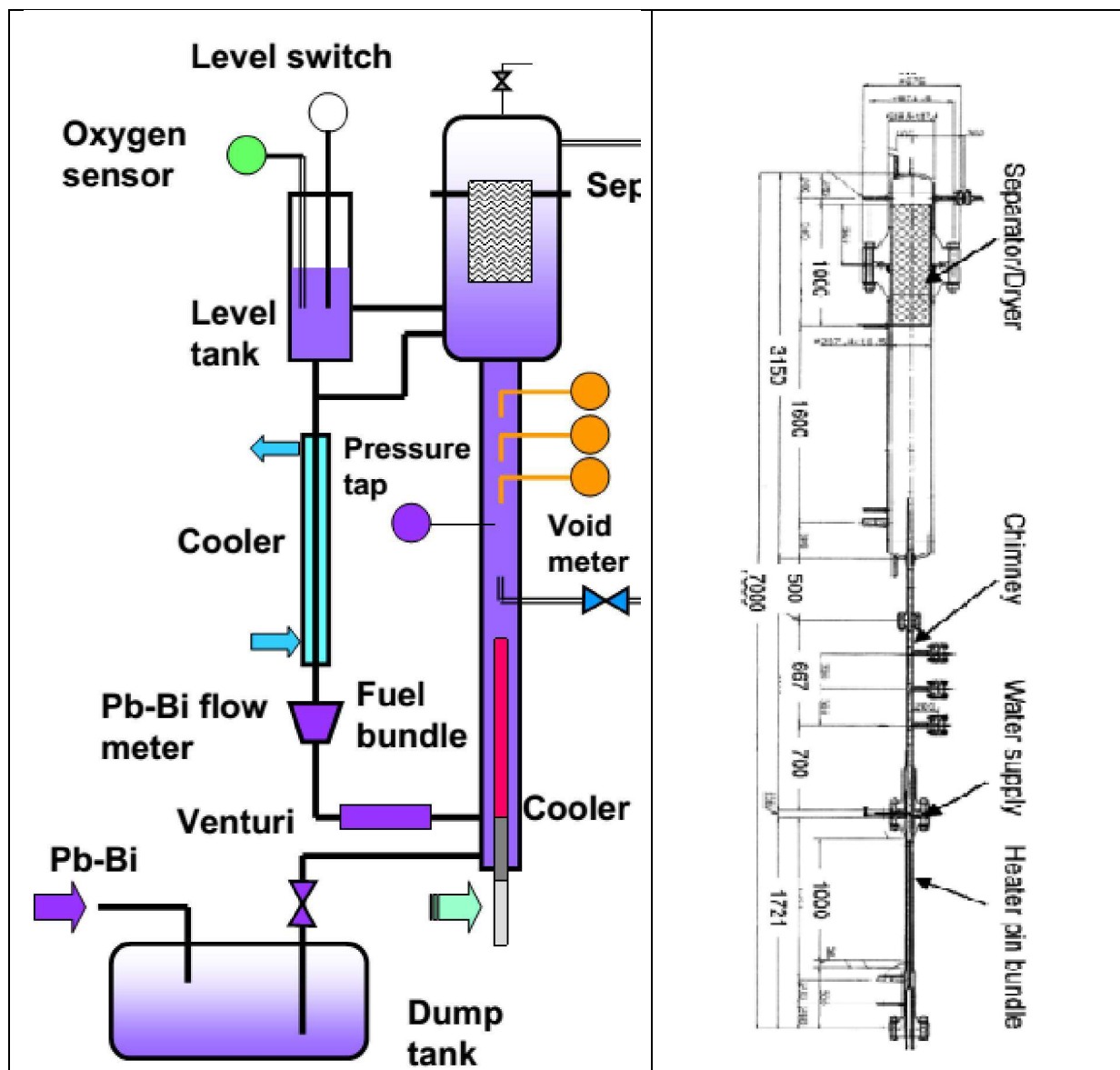


Fig A4.4.3 Schematic of LBE loop [27]

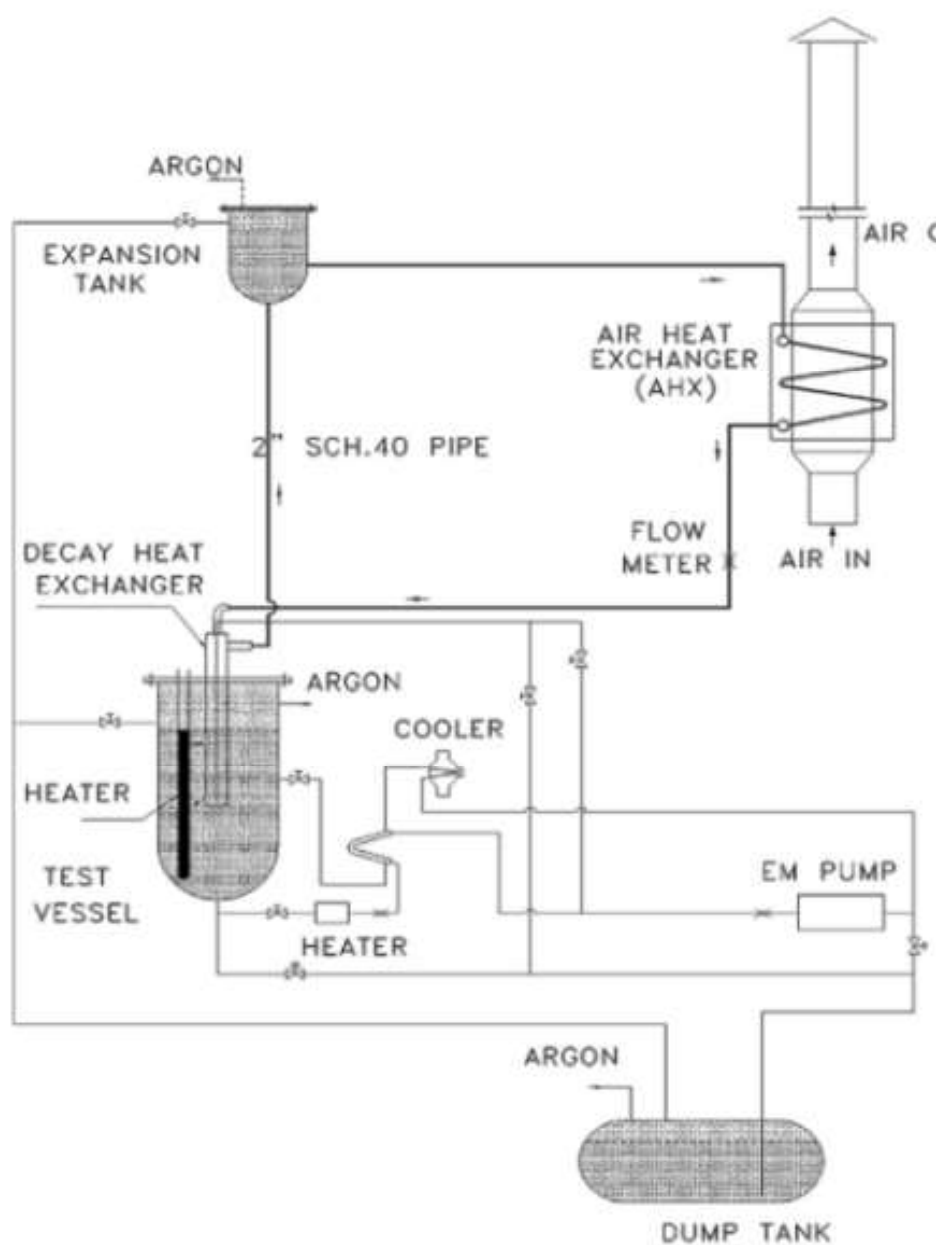


Fig A4.4.4 Schematic of SADHANA loop [35]

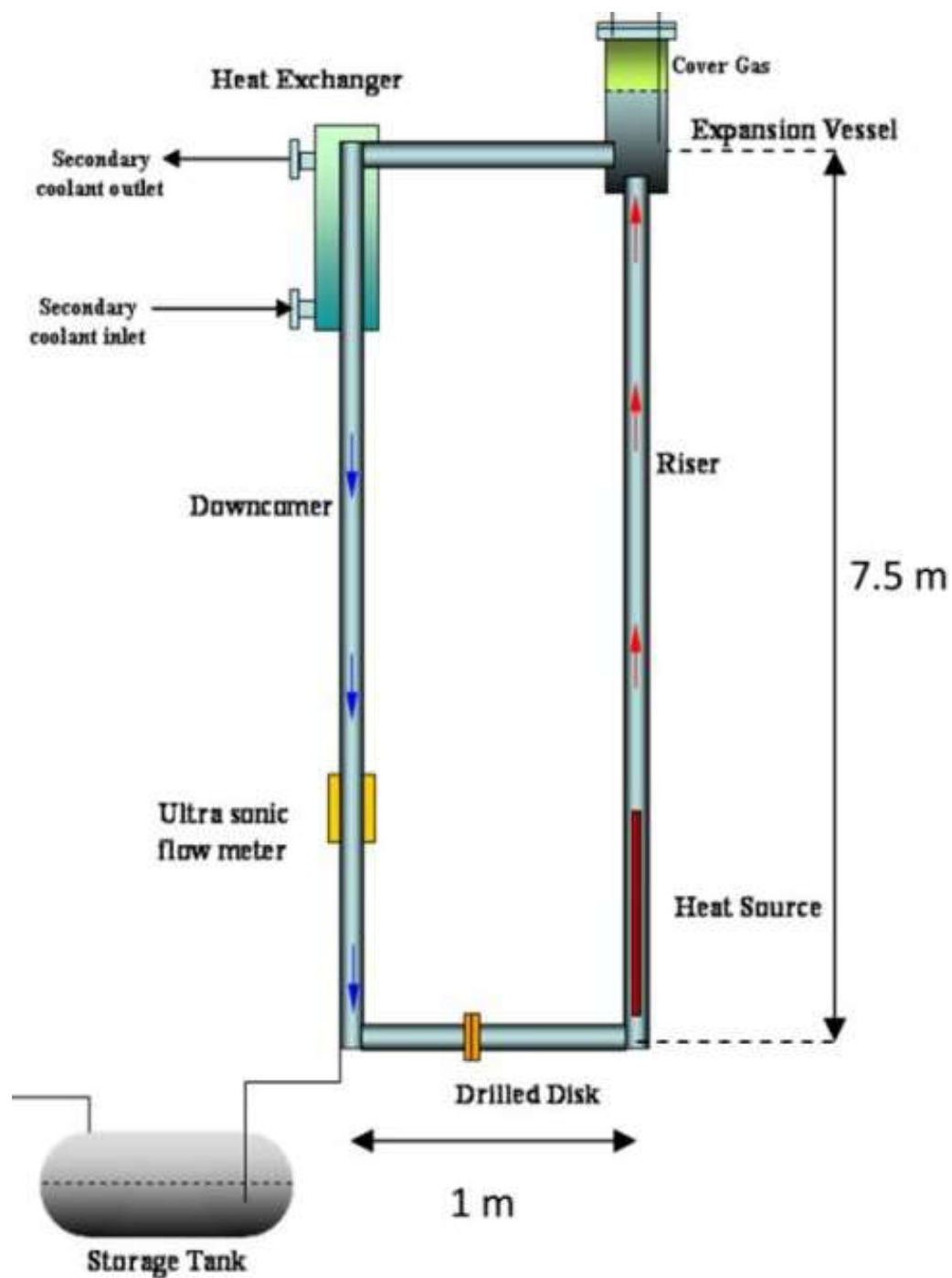


Fig A4.4.5 (a) Schematic of NACIE loop [30]

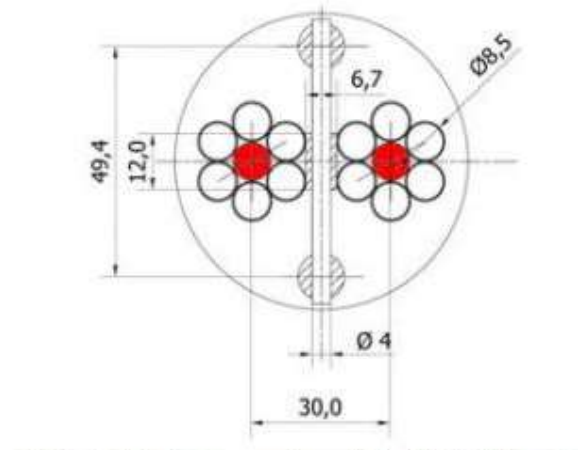


Fig A4.4.5 (b) Cross-section and view of the NACIE heater rod bundle [30]

The schematic of the LML and KTL are not shown here, as they are already discussed extensively in chapter 3 and chapter 4. The pressure drop coefficients and the hydraulic diameter of different parts of each loop were calculated using appropriate correlations to find the geometry parameter N_G for each loop. The LBE loops TALL, NACIE and the LBE loop reported by Takahashi et al.(2005b) have heater sections consisting of heater rod bundles with spacers. These sections of the loop are characterised by the correlations suggested by the respective literatures.

Table A4.4.1 shows the major parameters of the loop and the range of calculated dimensionless parameters for individual loops. The range of parameters corresponds to the range of operating heater power levels of each loop.

Table A4.4.1 Details of the natural circulation liquid metal loops and operating range

Design parameters	TALL (Ma et al., 2007) [29]	LBE loop (Takahashi et al., 2005) [28]	Gallium Loop (Kang et al., 2011) [34]	SADHAN A (Padmakumar et al., 2013) [35]	NACIE (Cocculuto et al., 2011) [30]	LML (Present work)	KTL (Present work)
Max. operating Temperature(°C)	500	550	450	500	550	500	1100
Height between the thermal centres, m	5.5	2.0	1.3	19.5	6.125	0.475	0.45
Piping size (ID), mm	27.8	29.9	8.5	52.5	62.7	14.0	15.0
Total Length (Lt), m	13.4	11.64	4.12	39.63	16.8	6.7	2.379
$D_r = \frac{1}{L_t} \sum_{i=1}^N D_i L_i$ (mm)	28.17	34.85	8.5	65.58	64.98	29.63	20.86
Range of N_G (Eq 4.4.2)	3300-34700	12600-13470	560-565	4077-4275	800-875	63000-125000	1617-2525
Range of Gr_m (Eq 4.4.1)	7×10^{13} - 5×10^{14}	10^{13} - 5×10^{13}	5.0×10^{11} - 1.0×10^{12}	10^{16} - 10^{17}	1.3×10^{15} - 2×10^{15}	10^{12} - 10^{13}	10^{11} - 10^{13}
Range of Re_{ss}	4000-10000	2000-4000	2500-4000	>10000	>10000	600-1500	1200-4000

The values of Re_{ss} are plotted with respect to the Gr_m/N_G in Fig 4.18 in Chapter 4.

Table A4.4.2 Steady State Natural circulation experimental data used for the analysis

Sl No	Loop	Ref	Power (W)	Mass flow rate* (kg/s)
1	TALL	Ma et al., 2007 [29]	3000 4500 6000 8000 10000 11500 14250	0.25 0.28 0.30 0.34 0.38 0.4 0.44
2	LBE loop	Takahashi et al., 2005 [28]	1000 2000 3000 4500	0.46 0.60 0.70 0.80
3	Gallium Loop	Kang et al., 2011 [34]	1000 2000 3000	0.023 0.034 0.0375
4	SADHANA	Padmakumar et al., 2013 [35]	2.25×10^5 2.80×10^5 3.20×10^5 3.60×10^5 4.10×10^5 4.25×10^5	1.09 1.24 1.31 1.39 1.45 1.475
5	NACIE	Cocculuto et al., 2011[30]	2.25×10^4	5.4
6	LML	Present work	900 1500 1800 2400 3300 4200 4920	0.095 0.108 0.115 0.121 0.125 0.129 0.133
7	KTL	Present work	100 300 400 500 600 700 800 1200	0.057 0.078 0.087 0.089 0.093 0.102 0.109 0.115

* The mass flow rates in SADHANA, LML and KTL are calculated by balancing heat across the heater section.

Appendix 4.5

ERROR ANALYSIS

The error analysis is carried out to find the uncertainty in experimental values and derived parameters. The measured variables are temperature, power and secondary side coolant flow rate for the single phase LBE loops considered in the present work.

The uncertainty in thermo-physical parameters are taken from LBE handbook (2007) [67].

Table A4.3.1 gives the uncertainties of different primary parameters considered in the analysis.

Table A4.3.1 Error of different primary parameters considered in the analysis

SI No.	Parameters	Error (%)
1	Temperature (T)	±0.5
2	Heater Power (Q _h)	±1.0
3	Secondary side flow rate (Q _s)	±2.0
Thermo-physical properties of LBE		
4	Density (ρ)	±0.7
5	Specific heat (C _p)	±7.0
6	Viscosity (μ)	±5.0
7	Thermal conductivity (K)	±5.0

The error in measured parameters can be estimated as follows,

1. LBE temperature differences across the heater or heat exchanger,

$$\Delta T_{diff} = \sqrt{(\Delta T_{out})^2 + (\Delta T_{in})^2}$$

Considering, $\Delta T_{out} = \Delta T_{in} = \Delta T = \pm 0.5\%$

$$\Delta T_{diff} = \sqrt{2} \Delta T = \pm 0.705\%$$

2. LBE mass flow rate, \dot{m}

LBE mass flow rate is derived from the energy balance in the heater section,

$$\dot{m} = \frac{Q}{C_p T_{diff}}$$

Error in mass flow rate calculation can be found as,

$$\frac{\Delta \dot{m}}{\dot{m}} = \sqrt{\left(\frac{\Delta Q_h}{Q_h}\right)^2 + \left(\frac{\Delta C_p}{C_p}\right)^2 + \left(\frac{\Delta T_{diff}}{T_{diff}}\right)^2}$$

$$\frac{\Delta \dot{m}}{\dot{m}} = \sqrt{(1.0)^2 + (7.0)^2 + (0.705)^2} = \pm 7.1\%$$

3. The modified Grashof number Gr_m in Eq (2.1) can be calculated as,

$$\frac{\Delta Gr_m}{Gr_m} = \sqrt{2\left(\frac{\Delta \rho}{\rho}\right)^2 + \left(\frac{\Delta C_p}{C_p}\right)^2 + \left(\frac{\Delta Q_h}{Q_h}\right)^2 + 3\left(\frac{\Delta \mu}{\mu}\right)^2}$$

$$\frac{\Delta Gr_m}{Gr_m} = \sqrt{2(0.7)^2 + (7.0)^2 + (1.0)^2 + 3(5.0)^2} = \pm 11.2\%$$

4. The experimental value of Re_{ss} as given in Eq (2.1) can be calculated as,

$$\frac{\Delta Re_{ss}}{Re_{ss}} = \sqrt{(5.0)^2 + (7.1)^2} = \pm 8.7\%$$

5. The error in heat transfer rate at the secondary side of heat exchanger can be calculated as,

$$\frac{\Delta Q_s}{Q_s} = \sqrt{\left(\frac{\Delta W_s}{W_s}\right)^2 + 2\left(\frac{\Delta T_{diff}}{T_{diff}}\right)^2}$$

$$\frac{\Delta Q_s}{Q_s} = \sqrt{(2.0)^2 + 2(0.705)^2} = \pm 2.12\%$$

6. The error in Log Mean Temperature Difference (LMTD) in the heat exchanger of LML can be approximated as,

$$\frac{\Delta T_{ln}}{T_{ln}} = 4 \frac{\Delta T}{T} = 4 \times 0.5 = 2.0\%$$

7. The error in calculation of overall heat transfer coefficient can be done as follows,

$$\frac{\Delta U_o}{U_o} = \sqrt{\left(\frac{\Delta Q_s}{Q_s}\right)^2 + \left(\frac{\Delta T_{ln}}{T_{ln}}\right)^2}$$

$$\frac{\Delta U_o}{U_o} = \sqrt{(2.12)^2 + (2.0)^2} = \pm 2.91\%$$

So the error range of different parameters can be summarised as follows,

Table A4.5.2 Error range of different parameters

Sl No	Parameter	Symbol	Error
1	Temperature difference	$\frac{\Delta T_{diff}}{T_{diff}}$	$\pm 0.705\%$
2	Mass flow rate	$\frac{\Delta \dot{m}}{\dot{m}}$	$\pm 7.1\%$
3	Gr_m	$\frac{\Delta Gr_m}{Gr_m}$	$\pm 11.2\%$
4	Re_{ss}	$\frac{\Delta Re_{ss}}{Re_{ss}}$	$\pm 8.7\%$
6	Overall HTC in the secondary side of HX	$\frac{\Delta U_o}{U_o}$	$\pm 2.91\%$

Appendix 6.1

Effect of acceleration pressure drop in the secondary side of KTL

6.1.0 INTRODUCTION

In Chapter 4 the description of KTL and the experimental studies carried out were given. The secondary side of the heat exchanger in KTL is an open loop with argon flowing through the annular space by natural convection to cool the LBE. The assumptions considered to solve the governing equations in a closed loop may not be applicable here. So separate analysis is required to check the validity of the assumptions in the open loop. Especially the acceleration pressure drop in an open loop may not be negligible as in the closed loop. In this section an open loop section in the form of vertical circular pipe is considered for the analysis. Let us consider an open loop as shown in Fig. A6.1.1 with a heated length of L_h and unheated lengths of L_i and L_o at the inlet and outlet of the heated section respectively.

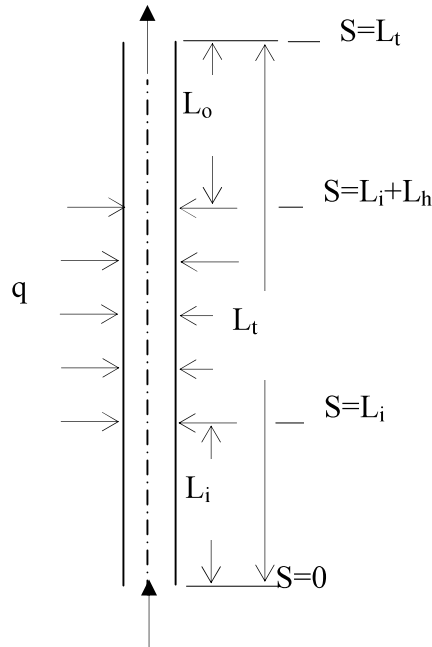


Fig. A6.1.1: Simple open loop Natural circulation section considered for analysis

The unheated lengths are insulated and the heat flux is specified. In addition, the inlet temperature T_i and fluid density at the inlet ρ_i are specified. The conservation equation of mass is given by.

$$\frac{\partial W}{\partial x} = 0 \quad (\text{A6.1.1})$$

Note that the above equation assumes incompressible flow, which is adequate for air flow where velocities are expected to be very low. Incompressible assumption is adequate for Mach number less than 0.2. The momentum conservation equation for a pipe segment of length Δs , can be written as,

$$\frac{1}{A} \frac{\partial W}{\partial t} + \frac{1}{A^2} \frac{\partial (W^2 v)}{\partial x} + \frac{\partial p}{\partial x} + \left(\frac{f}{DA^2} + \frac{K}{A^2 \Delta x} \right) \frac{W^2}{2\rho} + \rho g \sin \theta = 0 \quad (\text{A6.1.2})$$

As per Eq. (1), the mass flow rate is independent of the location in the loop, but is a function of time. In view of this, Eq. (2) can be rewritten as

$$\frac{1}{A} \frac{dW}{dt} + \frac{W^2}{A^2} \frac{dv}{dx} + \frac{dp}{dx} + \left(\frac{f}{DA^2} + \frac{K}{A^2 \Delta x} \right) \frac{W^2}{2\rho} + \rho g \sin \theta = 0 \quad (\text{A6.1.3})$$

It may be noted that for gases, the 2nd term may not be negligible. Equation (6.1.3) can now be integrated over the inlet and outlet of the open loop assuming fluid properties to be constant except density in the buoyancy force term. Integrating, one obtains,

$$\frac{1}{A} \frac{dW}{dt} \int_{s=i}^o dx + \frac{W^2}{A^2} \int_{s=i}^o \partial v + \int_{s=i}^o \partial p + \left(\frac{f \int_i^o dx}{DA^2} + \frac{K}{A^2} \right) \frac{W^2}{2\rho} + g \int_i^o \rho dx \sin \theta = 0 \quad (\text{A6.1.4})$$

Assuming Boussinesq approximation to be valid, the density in the buoyancy force term can be expressed as

$$\rho = \rho_0 [1 - \beta(T - T_0)] \quad (\text{A6.1.5})$$

Where the reference value can be the mean temperature or the inlet temperature. Noting that $dx \sin \theta = dz$, Eq. (4) can be integrated to obtain,

$$\frac{L_t}{A} \frac{dW}{dt} + \frac{W^2}{A^2} (v_o - v_i) + (p_o - p_i) + \left(\frac{fL_t}{DA^2} + \frac{K}{A^2} \right) \frac{W^2}{2\rho} + g\rho_o \int_i^o [1 - \beta(T - T_o)] dz = 0 \quad (\text{A6.1.6})$$

Where H is the height of the loop. In the present case, $H=L_t$. Replacing the loss coefficient K by an equivalent length, L_e , and noting that $p_i = p_o + \rho_o gH$, we obtain,

$$\frac{L_t}{A} \frac{dW}{dt} + \left(\frac{W}{A} \right)^2 (v_o - v_i) + \left(\frac{f(L_{eff})_t}{DA^2} \right) \frac{W^2}{2\rho_o} - g\rho_o \beta \int_i^o T dz + g\rho_o \beta T_o H = 0 \quad (\text{A6.1.7})$$

Where $(L_{eff})_t = L_t + L_{eff}$. The friction coefficient can be expressed as

$$f = \frac{p}{\text{Re}^b} \quad (\text{A6.1.8})$$

Using Eq. (A6.1.8) in Eq. (A6.1.7), we obtain,

$$\frac{L_t}{A} \frac{dW}{dt} + \left(\frac{W}{A} \right)^2 (v_o - v_i) + \left(\frac{(L_{eff})_t}{D^{1+b} A^{2-b}} \right) \frac{p \mu^b W^{2-b}}{2\rho_o} - g\rho_o \beta \int_i^o T dz + g\rho_o \beta T_o H = 0 \quad (\text{A6.1.9})$$

The energy equation for the open loop can be written as

$$\frac{\partial T}{\partial t} + \frac{w}{A\rho_o} \frac{\partial T}{\partial x} = \begin{cases} \frac{4q''}{D\rho_o Cp} & \text{heater for } L_i < x \leq L_i + L_h \\ 0 & \text{pipes for } 0 < x \leq L_i \text{ and } L_h < x \leq L_t \end{cases} \quad (\text{A6.1.10})$$

Generally, to enhance the flow rate often a tall riser (i.e. the height above the heated section, L_o in this case) is employed.

6.2. STEADY STATE PERFORMANCE

The steady state governing equations can be obtained by dropping the time derivatives from the momentum and energy equations. The resultant equations are given by

$$\left(\frac{W}{A}\right)^2 (v_o - v_i) + \left(\frac{(L_{eff})_t}{D^{1+b} A^{2-b}}\right) \frac{p\mu^b W^{2-b}}{2\rho_0} - g\rho_0\beta \int_i^o T dz + g\rho_0\beta T_o H = 0 \quad (A6.1.11)$$

$$\frac{dT}{dx} = \begin{cases} \frac{4q'' A}{DWCp} & \text{heater for } L_t < x \leq L_i + L_h \\ 0 & \text{pipes for } 0 < x \leq L_i \text{ and } L_h < x \leq L_t \end{cases} \quad (A6.1.12)$$

Steady state temperature distribution in the heater can be obtained as

Using the boundary condition, at $x=L_i$, $T=T_i$ in Eq (A6.1.12) we get

$$T = T_i + \frac{4q'' A}{DWCp} (x - L_i) \quad (A6.1.13)$$

The temperature at the exit of the heater is obtained as

$$T_o = T_i + \frac{4q'' A}{DWCp} (L_h - L_i) \quad (A6.1.14)$$

Now the temperature integral in Eq. (6.1.11) can be obtained as

$$-g\rho_0\beta \int_i^o T dz = -g\rho_0\beta T_i z_i - g\rho_0\beta \int_{z_i}^{z_h} \left[T_i + \frac{4q'' A}{DWCp} (z - z_i) \right] dz - g\rho_0\beta T_o (z_o - z_h) \quad (A6.1.15)$$

After integrating and simplification we get,

$$-g\rho_0\beta \int_i^o T dz = -g\rho_0\beta \left\{ T_i (H - L_o) + L_h \frac{4q'' A}{DWCp} \left[\frac{(z_h + z_i)}{2} - z_i \right] + T_o L_o \right\} \quad (A6.1.16)$$

Using this in Eq. (A6.1.11) and after further simplification, we obtain,

$$\left(\frac{W}{A}\right)^2 (v_o - v_i) + \left(\frac{(L_{eff})_t}{D^{1+b} A^{2-b}}\right) \frac{p\mu^b W^{2-b}}{2\rho_0} = g\rho_0\beta (T_o - T_i) \left(H - L_o - \left(\frac{L_h}{2} \right) \right) \quad (A6.1.17)$$

Since $H=L_i+L_h+L_o$, we obtain

$$\left(\frac{W}{A}\right)^2 (v_o - v_i) + \left(\frac{(L_{eff})_t}{D^{1+b} A^{2-b}}\right) \frac{p\mu^b W^{2-b}}{2\rho_0} = g\rho_0\beta (T_o - T_i) \left[L_i + \left(\frac{L_h}{2} \right) \right] \quad (A6.1.18)$$

Since $T_o - T_i = Q_h / WCp$ the above equation can be rewritten as

$$\frac{(v_o - v_i)}{A^2} W^3 + \left(\frac{(L_{eff})_t}{D^{1+b} A^{2-b}} \right)_i \frac{p \mu^b W^{3-b}}{2 \rho_0} = g \rho_o \beta \frac{Q_h}{Cp} \left[L_i + \left(\frac{L_h}{2} \right) \right] \quad (A6.1.19)$$

If the acceleration term is negligible, then

$$W = \left[\frac{2 \rho_0^2 \beta g Q_h \Delta z_c D^{1+b} A^{2-b}}{p C p \mu^b (L_{eff})_t} \right]^{\frac{1}{3-b}} \quad (A6.1.20)$$

The Eq. (A6.1.19) is solved numerically by Newton-Raphson method with the initial guess of W found from Eq (A6.1.20). The temperature dependent properties are taken from Jaques (1988) [172]. The results of the analysis is shown in Fig. A6.1.2.

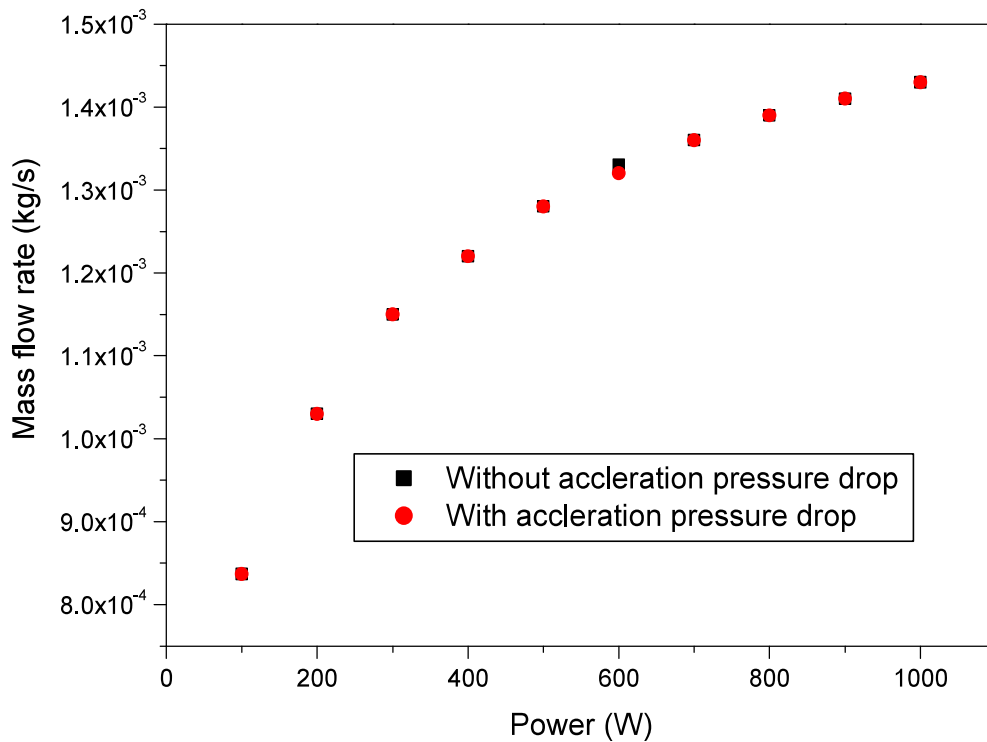


Fig A6.1.2 Natural circulation mass flow rate considering acceleration pressure drop and without acceleration pressure drop

The steady state mass flow rate, W is found for different power levels. It can be seen that the mass flow rate of argon gas increases with the power. It can be seen that the acceleration pressure drop has negligible effect on the argon gas flow rate. This is may be due to the low

flow rate of argon gas with low vertical height of the heated section. So the assumption that acceleration pressure drop is negligible on the natural circulation taken in case of the closed loop is also valid for the open loop in the secondary side of the KTL.

REFERENCES

- [1] GIF Annual Report, 2014, <http://www.gen-4.org/PDFs/GIF-2014-Annual-Report.pdf>.
- [2] Dulera I. V., Sinha R. K., 2008; High temperature reactor, J. Nuclear Materials, Vo 383, Issues 1-2, 15, 183-188.
- [3] Vijayan P.K., 2002; Experimental observations on the general trends of the steady state and stability behaviour of single-phase natural circulation loops, Nuclear Engineering and Design 215, 139–152.
- [4] Bunker, M. E. (Winter–Spring 1983). "Early Reactors From Fermi's Water Boiler to Novel Power Prototypes" ,Los Alamos Science. Los Alamos National Laboratory: 128.
- [5] IAEA TECDOC- 1531, Fast reactor database 2006.
- [6] Velusamy K., Chellapandi P., Chetal S. C. And Baldev Raj, 2010; Overview of pool hydraulic design of Indian prototype fast breeder reactor, Sadhana Vol. 35, Part 2, April 2010, 97–128.
- [7] Sienicki J. J. and Moisseytsev A.V., 2005; SSTAR Lead-Cooled, Small Modular Fast Reactor for Deployment at Remote Sites-System Thermal Hydraulic Development, Proceedings of ICAPP '06, Seoul Korea, May 15-19, 2005.
- [8] Zvirin, Y., Jeuck, P. III, Sullivan, C.W., Duffey, R.B., 1981. J. Heat Transf. 103, 645–652.
- [9] Mertol, A., Greif, R., 1985. A review of natural circulation loops. In: Kakac, S., Aung, W.
- [10] Greif, R., 1988. Natural circulation loops. J. Heat Transf. 110, 1243–1258.

-
- [11] Vijayan P.K., Bhojwani V.K., Bade M.H., Sharma M., Nayak A.K., Saha D. and Sinha R.K., 2001, Investigations on the effect of heater and heat exchanger orientation on the steady state, transient and stability behaviour of single phase natural circulation in a rectangular loop, BARC/2001/E/034, 2001.
- [12] Welander, P., 1967, On the oscillatory instability of a differentially heated fluid loop, *J. Fluid Mech.* 29, 17–30.
- [13] Creveling, H.F., De Paz, J.F., Baladi, J.Y., Schoenhals, R.J., 1975, Stability characteristics of a single-phase free convection loop, *J. Fluid Mech.* 67, 65–84.
- [14] Chen, K., 1983, On the Oscillatory Instability of Closed-Loop Thermosyphons, ASME paper 83-WA/HT-93.
- [15] Bau, H.H., Torrance, K.E., 1981, Transient and steady behaviour of an open, symmetrically-heated, free convection loop, *Int. J. Heat Mass Transf.* 24, 597–609.
- [16] Huang, B.J., Zelaya, R., 1988, Heat transfer behavior of a rectangular thermosyphon loop, *J. Heat Transf.* 110, 487–493.
- [17] Vijayan, P.K., Date, A.W., 1992, The limits of conditional stability for single-phase natural circulation with throughflow in a figure-of-eight loop, *Nucl. Eng. Des.* 136, 361–380.
- [18] Pilkhwal, D.S., Ambrosini, W., Forgone, N., Vijayan, P.K., Saha, D., Ferrari, J.C., 2007; Analysis of the unstable behaviour of a single phase natural circulation loop with one dimensional and computational fluid dynamics models. *Ann. Nucl. Energy* 34, 339–355.
- [19] Swapnalee, B. T., Vijayan, P. K., 2011; A generalized flow equation for single phase natural circulation loops obeying multiple friction laws, *International Journal of Heat and Mass transfer*, 54, 2618-2629.

-
- [20] Kumar N., Doshi J.B., Vijayan P.K., 2011, Investigations on the role of mixed convection and wall friction factor in single-phase natural circulation loop dynamics, *Annals of Nuclear Energy* 38, 2247–2270.
- [21] Chato, J.C., 1963, Natural Convection Flows in Parallel-Channel Systems, *J. Heat Transf.* 85, 339–345.
- [22] Sanders J, 1988; Stability of Single-Phase Natural Circulation With Inverted U-Tube Steam Generators. *J. Heat Transfer.* 110, 735–742.
- [23] Vijayan, P.K., Mehta, S.K., Date, A.W., 1991. *Int. J. Heat Mass Transf.* 34, 2219–2230.
- [24] Cicchini, G., 1975. Esperienze di instabilita nella circolazione naturale monofase, degree thesis in nuclear engineering, Universita degli Studi ‘‘La Sapienza’’.
- [25] Nishihara, T., 1997. Oscillatory instability of a single-phase natural circulation loop, *NURETH-8*, Kyoto, Japan, Sept. 30–Oct. 4, 1997.
- [26] Vijayan, P.K., Austregesilo, H., 1994, Scaling laws for single-phase natural circulation loops, *Nucl. Eng. Des.* 152, 331–347.
- [27] Takahashi M, Sofue H., Iguchi T., Matsumoto M., Huang F, Pramono Y., Matsuzawa T. and Uchida S., 2005a, Study on Pb-Bi natural circulation phenomena, *Progress in Nuclear Energy*, 47, 1-4, 553-560.
- [28] Takahashi M, Sofue H., Iguchi T., Pramono Y., Huang F, Novitrian, Matsumoto M., Matsuzawa T. and Uchida S., 2005b, Study on Pb-Bi-Water direct contact boiling two-phase flow and heat transfer, *Progress in Nuclear Energy*, 47, 1-4, 569-576.
- [29] Ma W., Karbojian A., Sehgal B. R., 2007, Experimental study on natural circulation and its stability in a heavy liquid metal loop, *J. Nuclear engineering and design.* 237, 1838-1847.

-
- [30] Coccoluto G., Gaggini P., Labanti V., Tarantino M., Ambrosini W., Forgione N., Napoli A., Oriolo F., 2011; “Heavy liquid metal natural circulation in a one-dimensional loop”, *Nuclear Engineering and Design* 241, 1301–1309.
- [31] Piazza I. Di, Angelucci M., Marinari R., Tarantino M., Forgione N., 2016; Heat transfer on HLM cooled wire-spaced fuel pin bundle simulator in the NACIE-UP facility, *Nuclear Engineering and Design* 300, pp 256–267.
- [32] Cho J. H., Batta A., Casamassima V., Cheng X., Choi Y. J., Hwang I. S., Lim J., Meloni P., Nitti F. S., Dedul V., Kuznetsov V., Komlev O., Jaeger W., Sedov A., Kim J. H., Puspitarini D., 2011; Benchmarking of thermal hydraulic loop models for Lead-Alloy Cooled Advanced Nuclear Energy System (LACANES), phase-I: Isothermal steady state forced convection, *Journal of Nuclear Materials*, Volume 415, Issue 3, 31 August 2011, Pages 404–414.
- [33] Agostini P., Bertacci G., Gherardi G., Bianchi F., Meloni P., Nicolini D., Ambrosini W., Forgione F., Fruttuoso G. and Oriolo F., 2002; Natural Circulation of Lead-Bismuth in a One-Dimensional Loop: Experiments and Code Predictions, 10th International Conference on Nuclear Engineering, Volume 2, Arlington, Virginia, USA, April 14–18, 2002.
- [34] Kang S., Ha K., Kim H. T., Kim J. H. and Bang I. C., 2013, An experimental study on natural convection heat transfer of liquid gallium in a rectangular loop, *International Journal of Heat and Mass Transfer* 66, 192–199.
- [35] Padmakumar, G., Vinod, V., Pandey, G.K., Krishnakumar, S., Chandramouli, S., Vijaykumar, G., Rajendra Prasad, R., Mourya, R.K., Madankumar, P., Shanmugasundaram, M., Ramakrishnan, V., Meikandamurthy, C., Rajan, K.K., 2013. SADHANA facility for simulation of natural convection in the SGDHR system of PFBR. *J. Prog. Nucl. Energ.* 66, 99–107.

-
- [36] Ma, W., Bubelis, E., Karbojian, A., Sehgal, B. R. and Coddington, P., 2006, “Transient experiments from the thermal-hydraulic ADS lead bismuth loop (TALL) and comparative TRAC/AAA analysis”, J. Nuclear engineering and design. 236, 1422-1444.
- [37] Wu, Q., Sienichi, J.J., 2003. Stability analysis on single-phase natural circulation in Argonne lead loop facility. Nucl. Eng. Des. 224, 23e32.
- [38] Barone G., Forgione N., Martelli D., Delnevo A., 2012, Pretest Analysis of thermal-hydraulic behaviour of the NACIE facility for the characterisation of a fuel pin bundle, ENEA Report No RdS/2012/058.
- [39] Sabharwall, P., Yoo, Y.J., Wu, Q., Sienicki, J.J., 2012. Natural circulation and linear stability analysis for liquid-metal reactors with the effect of fluid axial conduction. Nucl. Technol. 178 (3), 298-317
- [40] Batra C., 2013; Thermal-Hydraulic Analysis of Fast Breeder Reactor: Protected Loss of Flow (PLOF) Transient, Proceedings 22nd International conference on Nuclear Energy for New Europe, Sep 9-12, 2013, Bled-Slovenia.
- [41] Shao Y., 2011; TRACE Analysis for Transient Thermal-hydraulics of A Heavy Liquid Metal Cooled System, Master Thesis, School of Engineering Sciences, Department of Physics, Div. Nuclear Power Safety ,Stockholm.
- [42] Tenchine, D., Baviere, R., Bazin, P., Ducros, F., Geffraye, G., Kadri, D., Perdu, F., Pialla, D., Rameau, B., Tauveron, N., 2012. Status of CATHARE code for sodium cooled fast reactors. Nuclear Eng. Des. 245, 140–152.
- [43] Velusamy K., Natesan K., Selvaraj P., Chellapandi P., Chetal S. C., Sundarajan T., Suyamabazahan S., 2006, CFD studies in the prediction of thermal striping in an LMFBF, CFD4NRS, Garching, Munich, 5-7 Sept, 2006.

-
- [44] Naphade P., Borgohain A., Raj R. T. K., Maheshwari N. K., 2013; Experimental and CFD Study on Natural circulation Phenomenon in Lead Bismuth Eutectic Loop, J. Procedia Engineering, vol 64, p 936-945.
- [45] Tarantino M., Grandis S. De, Benamati G., Oriolo F., 2008; Natural circulation in a liquid metal one-dimensional loop, 376, 409-414.
- [46] Tenchine D., Baviere R., Bazin P., Ducros F., Geffraye G., Kadri D., Perdu F., Piella D., Rameau B., Tauveron N., 2012; Status of CATHARE code for sodium cooled fast reactors", Nuclear Engineering and Design 245 pp 140– 152.
- [47] Vasile A., 2012; Modelling and simulation thermal hydraulics of FRs, IAEA Seminar on Fast Reactors, Bariloche, Argentina, 1 – 5 October 2012.
- [48] Kumayev V. Y., Lebezov A. A. and Alexeev V.V., 2005, "Development and application Of MASKA-LM code for calculation of thermal hydraulics and mass transfer of lead cooled fast reactors", Proceed. 11th International Topical Meeting on Nuclear Reactor Thermal-Hydraulics (NURETH-11) Avignon, France.
- [49] Cheng, X., Cahalan, J.E., Finch, P.J, 2004, Safety analysis of an accelerator driven test facility, Nucl. Eng. Des. 229, 289-306.
- [50] Davis, C.B., 2003. Thermal-hydraulic analyses of transients in an actinide burner reactor cooled by forced convection of lead–bismuth. Nucl. Eng. Des. 224, 149–160.
- [51] Albright, D.C., Bari, R.A., 1978. Primary pipe rupture accident analysis for Clinch River Breeder Reactor. Nucl. Technol. 39 (3), 225–257.
- [52] Mohr, D., Feldman, E.E., 1981; "A dynamic behaviour of the EBR-II plant during natural convection with NATDEMO code", In: Agrawal, A.K., Guppy, J.G. (Eds.), Decay Heat Removal and Natural Convection in FBRs. Hemisphere Pub, New York.
- [53] Vaidyanathan, G., Kasinathan, N., Velusamy, K., 2010; Dynamic model of fast breeder test reactor", Ann. Nucl. Energy 37, 450–462.

- [54] Durham, M.E., 1976; Influence of Reactor Design on Establishment of Natural Circulation in a Pool-type LMFBF, . J. Br. Nucl. Energy Soc. 15, 305–310.
- [55] Hung, T.C. and Dhir, V.K., 1990, Decay heat removal in the sodium advanced fast reactor with the MDSNP code, Nucl. Technol. 91 (1), 51–60.
- [56] Yamano, H., Tobita, Y., Fujita, S., 2009. A three-dimensional neutronics and thermo-hydraulics simulation of core disruptive accident in sodium-cooled fast reactor. Nucl. Eng. Des. 239, 1673–1681.
- [57] Rajakumar A, Velusamy K, Vaidyanathan G, "Thermo-hydraulic analysis of LMFBF plenum". Proc. 9th Natl. Heat and Mass Transfer Conf., IISc. Bangalore, HMT-30-87, 1987.
- [58] Kumar Ashok M, 1990, THYC-3D, A computer code for thermal hydraulic analysis, Proc. 4th Int. Conf. on Simulation Methods in Nuclear Engineering, Montreal.
- [59] Kutalteladze S. S., Borishanskii V. M., Novikov I.I and Fedynskii O. S., 1958; Liquid Metal Heat Transfer Media, Atomic Press.
- [60] Beauchamp F., Morier O., Brissonneau L., Courouau J. L., Chabert C., Reyne F., 2010, A review of lead-bismuth alloy purification systems with regard to the latest results achieved on STELLA loop, Proceedings Workshop on Technology and components of Accelerator Development Systems, Kalshrue, Germany.
- [61] Fazio C., Ricapito I., Scaddozzo G., Benamati G., 2003, Corrosion behaviour of steels and refractory metals and tensile features of steels exposed to flowing PbBi in the LECOR loop, Journal of Nuclear Materials 318 (2003) 325–332.
- [62] Hosemann P., Thau H. T., Johnson A. L., Maloy S.A., Li N, 2008; Corrosion of ODS steels in lead–bismuth eutectic”, Journal of Nuclear Materials 373, 246–253.

-
- [63] Kikuchi K., 2009, ADS development in Japan, Proceedings on the Workshop on Applications of High Intensity Proton Accelerators October 19-21, 2009 Fermi National Accelerator Laboratory, Batavia, IL, USA.
- [64] Mikiyori O., Tatsuya M., Teruaki K. and Kin-ya K., 2003, MES lead bismuth forced circulation loop and test results, Proceedings of the 11th international conference on nuclear engineering, ICONE-11, Tokyo, Japan, 2003.
- [65] Carsten S., Wedemeyer O. , Konys J., 2011; Gas/liquid oxygen-transfer to flowing lead alloys, Nuclear Engineering and Design 241 (2011) 1310–1318.
- [66] Kirchner T., Bortoli Y., Cadiou A., Foucher Y., Stutzmann J. S., Auger T., Dai Y., Dementjev S., Geissmann K., Glasbrenner H., Groschel F., Heinrich F., Kohlik K., von Holzen G., Perret Ch., Viol D., 2003, LiSoR, a liquid metal loop for material investigation under irradiation, J. Nucl. Materials, Vol 318, p 70-83.
- [67] OECD/NEA Nuclear Science Committee, Working Group on Lead-bismuth Eutectic, Handbook on Lead-bismuth Eutectic Alloy and Lead Properties, Materials Compatibility, Thermal-hydraulics and Technologies, ISBN 978-92-64-99002-9, 2007 Edition.
- [68] Cinotti L., 2012, Coolants for FBR: Lead, Proceedings IAEA Workshop on Fast Reactor Science and Technology, CNEA Bariloche, Argentina October 1 – 5, 2012.
- [69] Cho C., Cho C., Kim J., Lee W., Tae Yung Song T. Y., 2006, Fabrication and Shakedown Testing of a Lead-Bismuth Corrosion Test Loop, Transactions of the Korean Nuclear Society Autumn Meeting, Gyeongju, Korea, November 2-3, 2006.
- [70] Abraham D.P. , Leibowitz L., Maroni V. A., McDevitt S. M., Raraz A. G., 2000; Corrosion of Structural Materials by Lead-Based Reactor Coolants, Report: ANL/CMT/CP-103107.

-
- [71] Takahashi M., Sekimoto H., Ishikawa K., Sawada N., Suzuki T., Hata K., Yoshida S., Qiu S., Yano T., Imai M., 2002; Experimental Studies on Flow Technology and Steel Corrosion of Lead-bismuth, Proceedings of ICONE 10, No. 22226, Arlington, Virginia, USA, April 10-14, 2002.
- [72] Wu Y., Huang Q., Zhu Z., Gao S., Song Y., 2012; R&D of DRAGON Series Lithium-Lead Loops for Material and Blanket Technology Testing, Fusion Science and Technology, Vol. 62 No 1, p 272-275.
- [73] Wu Y., Bai Y., Song Y., Huang Q., Zhao Z., Song G., Hu L., Jiang J., 2014, Design and R&D Progress of China Lead-Based Reactor, Proceedings on 22nd International Conference on Nuclear Engineering (ICONE-22), Prague, Czech Republic.
- [74] Technical Report, National centre for Fusion and Technologies, 2009. Source: http://www.technofusion.org/documents/TF_Report_ENG.pdf.
- [75] Pawel S. J., 2014; Liquid Metal Compatibility” ORNL, Fusion Reactor Materials Program, June 30, 2014, DOE/ER-0313/56, Vol. 56.
- [76] Knebel J. U. and Fazio C., 2003 Studies on heavy liquid metal thermal-hydraulics: Existing test facilities and test programs, IAEA-TECDOC 1520.
- [77] Loewen E. P. and Tokuhiko A. T., 2003; Status of Research and Development of the Lead-Alloy- Cooled Fast Reactor, J. Nuclear Science and Technology, Vol. 40, No. 8, p. 614–627.
- [78] Abdulla S., Liu X., Anderson M., Bonazza R., Corradini M and Cho D., Interfacial Transport Phenomena and Stability in Liquid-Metal/Water Systems: Scaling Considerations., source: www.iaea.org/inis/collection/NCLCollectionStore/_.../33015186.pdf.
- [79] Schulenberg T., Cheng X, Stieglitz R., 2005; Thermal-Hydraulics of Lead Bismuth for Accelerator Driven Systems, The 11 International Topical Meeting on Nuclear Reactor

-
- Thermal-Hydraulics (NURETH-11) Paper: 159, Popes' Palace Conference Center, Avignon, France, October 2-6, 2005.
- [80] Smolentsev S., Li F. C., Morley N., Ueki Y., Abdou M., Sketchley T., 2013, "Construction and initial operation of MHD PbLi facility at UCLA", *Fusion Engineering and Design* 88, 317–326.
- [81] Uda N., Miyazawa¹ A., Inoue S., Yamaoka N., Horiike H., Miyazaki K., 2001, Forced Convection Heat Transfer and Temperature Fluctuations of Lithium Under Transverse Magnetic Fields, *J. Nuclear Science and Technology*, Vol. 38, No. 11, P. 936–943 (November 2001).
- [82] Tanaka T. J., Bauer F. J., Lutz T. J., McDonald J. M., Nygren R. E., Troncosa K. P., Ulrickson M. A., Youchison D. L., 2004; Liquid metal integrated test system (LIMITS), *Fusion Engineering and Design*, Volume 72, 1–3, November 2004, Pages 83–92.
- [83] Bandini G., Polidori M., Meloni P., Tarantino M., Piazza I. D., 2015, RELAP5 and SIMMER-III code assessment on CIRCE decay heat removal experiments, *Nuclear Engineering and Design* 281, 39–50.
- [84] OECD/NEA Report, 2011; Experimental Facilities for Sodium Fast Reactor Safety Studies". Report: NEA/CSNI/R(2010)12.
- [85] Toshinobu S. and Hiroyuki O., 2014; Studies on accelerator-driven system in JAEA, *J. Plasma and Fusion Research*, Vol 9, No 3.
- [86] Gabriele F. D. and Kosek L., 2013, "Oxygen Monitoring in the Natural Convection Loop Colonri I" 21st International Conference on Nuclear Engineering Chengdu, China, Volume 1.
- [87] Gabriele F. S., Amore S., Scaiola C., Arato E., Giuranno D., Novakovic R. and Ricci E., 2014, "Corrosion behaviour of 12Cr-ODS steel in molten lead", *Nuclear Engineering and Design* 280, 69–75.

-
- [88] Xu Mi, 2007; Fast Reactor Technology R&D Activities in China, Nuclear Engineering and Technology, Vol.39 No.3, 2007.
- [89] Scheuermann C. M.; Mass Transfer in a 1370oC Lithium Thermal-Convection Loop, NASA Report : NASA TM-X2986.
- [90] DeVan J. H., DiStefano J. R. and Jansen D. H., 1966; Compatibility of boiling alkali Metals with refractory alloys Metals and Ceramics Div. Ann. Progr. Rept. June30, 1966, ORNL-3970, pp.176-77.
- [91] Bryhan A. J. and Chan R. C., 1993; Fabricating Niobium Test Loops for SP-100 space reactor", J. Minerals, Metals and Materials Society. Vol 45, Issue 6, pp 50-53.
- [92] Rowekamp D. J., 2013; A Compact, Convective Flow NaK Test Loop for Material Exposure Contained in an Argon Atmosphere, Masters Thesis, University of Tennessee, Knoxville, USA.
- [93] Harrison R. W., 1970; Advanced Refractory Alloy Corrosion Loop Programme, Quarterly Report No 19.
- [94] Hvasta M., Nollet B. K., Anderson M. H. and Allen T. R., 2010, High Temperature Liquid metal Compatibility Testing, 19th Topical Meeting on Fusion Energy, 7-11 Nov, 2010.
- [95] Valerino A., Wood J. C. and Reznik J. F., 1968; SNAP-8 simulator loop and mechanical design, NASA report TM-X1515, 1968.
- [96] Haga K., 1983; Natural Convection Sodium Boiling Experiments in 37-Pin Bundle Geometry, J. Nucl. Sc. and Tech., 20[11], pp. 902-914.
- [97] Gnadt P. A., Anderson A.H., Clapp N.E. and Montgomery B. H., 1979; THORS-A High-Temperature Sodium Test Facility Rated at 2. 0MW, International meeting on Fast reactor safety technology, August 19-23,1979.

- [98] Annual Report, 2010, University of Latvia.
- [99] Noborio K., Yamamoto Y., Park C., Takeuchi Y. and Konishi S., 2011; High Temperature Operation of LiPb Loop", *Fusion Science And Technology*, Vol. 60.
- [100] Borgohain A., Jaiswal B. K., Maheshwari N. K., Vijayan P. K., Saha D. and Sinha R. K., 2011; Natural Circulation Studies in a Lead Bismuth Eutectic Loop, *J. Progress in Nuclear Energy*, Volume 53, Issue 4, Pages 308-319.
- [101] Borgohain A., Srivastava A.K., Jana S. S., Maheshwari N. K., Kulkarni R. D., Vijayan P. K., Tewari R., Maruthi Ram A., Jha S. K., 2016; Natural circulation studies in a LBE loop for a wide range of temperature, *Nuclear Engineering and Design*, Volume 300, p 358–375.
- [102] Cathcart J. V. and Manly W. D., 1956; The Mass Transfer Properties of Various Metals and Alloys in Liquid Lead, *Corrosion* 12, 43-47.
- [103] ANL website: <http://www.ne.anl.gov/facilities/argonne-liquid-metal-experiment/>
- [104] Sheir, L. L., R.A. Jarman, G.T. Burstein (eds.), 1994; *Metal/Environment Reactions, Corrosion*, Chapter 2.9.
- [105] Gerasimov, V., A. Monakhov (1983), *Corrosion of reactor materials*, Nuclear Engineering Materials, MIR1983.
- [106] Gorynin, V., G.P. Karzov, V.G. Markov V.A. Yakovlev, 1999; Structural Materials for Atomic Reactors with Liquid Metal Heat-transfer Agents in the Form of Lead or Lead-bismuth Alloy, *Metal Science and Heat Treatment*, Vol. 41, No 9-10, pp. 384-388.
- [107] Gorynin, V., G.P. Karzov, V.G. Markov, V.S. Lavrukhin V.A. Yakovlev, 1998; Structural Materials for Power Plants with Heavy Liquid Metals as Coolants, *Proceedings of the Conference Heavy Liquid Metals Coolants in Nuclear Technologie (HCLM-98)*, Volume 1, p. 120, Obninsk.

-
- [108] Yachmenyov, G.S., A.Ye. Rusanov, et al., 1998; Problems of Structural Materials' Corrosion in Lead-bismuth Coolant. The Problem of Technology of the Heavy Liquid Metal Coolants (Lead, Lead-bismuth)", HLMC-98, pp. 133.
- [109] Weisenburger, A., G. Müller, A. Heinzl, V. Engelko, A. Rusanov, 2005; EUROCCORR 2005.
- [110] Shmatko, B.A., N.I. Loginov, A.E. Rusanov, A.L. Shimkevich (1998), "Concept of Heavy Coolant Technology Without Oxygen", Proceedings of the Meeting on Problems of Structural Materials Corrosion in Lead-bismuth Coolant, Heavy Liquid Metal Coolants in Nuclear Technology (HLMC-98), Obninsk, Russia, 5-9 October 1999, pp. 683-685.
- [111] Park, J.J., Butt D. P. , Beard C. A. 2000, Review of liquid metal corrosion issues for potential containment materials for liquid lead and lead bismuth eutectic spallation targets as a neutron source, Nuclear Engineering and Design, Vol. 196, pp. 315-325.
- [112] Simakov, A.A., P.N. Martynov, R.S. Askhadullin, V.N. Leonov, V.S. Tsykunov, G.V. Gulevskiy, A.I. Chaban (2003), "Development and Experimental Operations of Mass-exchange Apparatuses for Guaranteeing the Assigned Oxygen Regime in the Heavy Liquid Metal Coolant", Proceedings of the Fast Neutrons Reactors Conference, Obninsk, Russian Federation, 8-12 December (in Russian).
- [113] WHO, WHO Task Group, Environmental Health Criteria for Lead – Environmental Aspects, ISBN 92 4 154285 3, World Health Organization, Geneva (1989).
- [114] Lyon, R.N., "Liquid Metal Handbook", NAVEXOS, Government Printing Office, Washington D.C. (1952).
- [115] Morita K., Maschek W., Flad M., Yamano H. and Tobita Y., 2006; Thermo physical Properties of Lead-Bismuth Eutectic Alloy in Reactor Safety Analyses, Journal of Nucl. Sc. Tech. (43), No. 5, 2006, pp. 526–536.

-
- [116] Misale M., Ruffino P., Frogheri M., 2000, "The influence of the thermal capacity and axial conduction over a single-phase natural circulation loop: 2-D numerical study", *J. Heat and Mass Transfer*, 36, 533-539.
- [117] Metais B. and E. R. G. and Eckert, Forced, mixed and free convection regions, *ASME J. Heat Heat Transfer*, Vol 86, pp. 295-296.
- [118] Sheriff, N., Davies, N.W., 1979; Liquid metal natural convection from plane surfaces: a review including recent sodium measurements, *Int. J. Heat Fluid Flow*, 1 4, pp 149–154.
- [119] Joye, D. D., Bushinsky, J. P. and Saylor, P. E. 1989. Mixed convection heat transfer at high Grashof number in a vertical tube. *Ind. Eng. Chem. Research*, 28, 1899-1903
- [120] Jackson J. D., Axcell B. P. and Walton A., 1994, Mixed-Convection Heat Transfer to Sodium in a Vertical Pipe, *J. Experimental Heat Transfer: A Journal of Thermal Energy Generation, Transport, Storage, and Conversion*, 7:1, 71-90.
- [121] Joye D. D., 1996; Comparison of aiding and opposing mixed convection heat transfer in a vertical tube with Grashof number variation, *Int. J. Heat and Fluid Flow* 17: 96-101.
- [122] Ambrosini W., D'Auria F., Pennati A., Ferreri J. C., 2001, Numerical Effects in The Prediction of Single-Phase Natural Circulation Stability, *UIT 2001 Conference*, Modena, Itali, 25-27 Jan, 2001.
- [123] Girgin I. and Turker M., 2011, Axial Heat Conduction in Laminar Duct Flows, *Journal of Naval Science and Engineering*, , Vol.7, No.2, pp. 30-45.
- [124] Nayak A. K. , Vijayan P. K. , Saha D. , Venkat Raj V. , Aritomi M., 1998 Adequacy of Power-to-volume Scaling Philosophy to Simulate Natural Circulation in Integral Test Facilities, *Journal of Nuclear Science and Technology*, Vol 35, issue 10.

-
- [125] Wu, X., Ma, J., Jiang, Y., Fu, B., Hang, W., Zhang, J., Li, N., 2006. Instrumentation of YSZ Oxygen Sensor Calibration in Liquid Lead Bismuth Eutectic. accessed at: IEE explorer <http://ieeexplore.ieee.org/stamp/stamp.jsp?arnumber=401464945>.
- [126] Orlov, Y.I., 1998. The main impurities and their condition in the PbBi coolant, contract SSC RF IPPE/CEADRN-DER 5010 6 8 B049630, Substage 2.1, Obninsk.
- [127] Samsonov, G.V., 1982. The Oxide Handbook, second ed. IFI/Plenum, New York
- [128] Borgohain A., Maheshwari N. K., Vijayan P. K. , Saha D., Sinha R. K., 2008. Development of high temperature oxygen sensor for lead bismuth eutectic. In: Proc. Discussion Meet on Electro Analytical Techniques & Their Applications, ISEAC, Munnar, Kerala, Feb 25 to 28, 2008.
- [129] Holman K. L., "A theoretical investigation of heat transfer to fluids in laminar flow in tubes " (1964). Retrospective Theses and Dissertations. 2991. Iowa State University.
- [130] Tewari R., Vishwanadh B., Srivastava D., Dey G. K., Vaibhav K., Jha S. K., Mirji K. V., Prakash B. and Saibaba N., 2011; Development Of Nb-1% Zr-0.1%C Alloy As Structural Components For CHTR, BARC/2011/E/020.
- [131] Wang, J. Y.;Chuang,T.J.; Ferng, Y. M.:CFD investigating flow and heat transfer characteristics in a natural circulation loop. *Annals of Nuclear Energy* 58 (2013) 65 –71.
- [132] Churchill S. W. and Chu H. H. S., 1975; Correlating Equations for Laminar and Turbulent Free Convection From a Horizontal Cylinders, *Int. J. Heat Mass Transfer*, 18, 1049.
- [133] Chang, K.C., Akins, R.G., Burris, L., Bankoff, S.G., 1964; Free convection of a low Prandtl number fluid in contact with a uniformly heated vertical plate, Argonne National Laboratory, ANL-6835.

-
- [134] Joye D. D., Joseph P. B. and Paul E. S., 1989, S., Mixed Convection Heat Transfer at High Grashof Number in a Vertical Tube, *Ind. Eng. Chem. Res.*, 28, 1899-1903.
- [135] Sun T. R. and Todreas N. E., 1988; Energy Transfer Mechanisms in LMR Rod Bundles Under Mixed Convection Conditions, *Nuclear Engineering and Design* 108, pp 343-357.
- [136] Martinotti C. C., F. Bassenghi, S. Bna, G. Bornia, S. Manservisi and R. Scardovelli, 2011; Effects Of Buoyancy On Mixed Turbulent Heat Transfer To Heavy Liquid Metals In Vertical Annuli, XXIX Congresso UIT sulla Trasmissione del Calore, Torino, 20-22 Giugno.
- [137] Jackson J. D., Cotton M. A. and Axcell B. P., 1989; Studies of Mixed Convection in Vertical Tubes, *Int. J. Heat Fluid Flow*, vol. 10, pp. 2-15.
- [138] Chen C. J. and Chiou J.S., Laminar and Turbulent Heat Transfer in the Pipe Entrance Region for Liquid Metals”, *International Journal of Heat and Mass Transfer*, Vol. 24, 1981, pp. 1179-1189.
- [139] Kays W. M., 1994; Turbulent Prandtl number—where are we, *J. Heat Transfer* vol 116, 1994, pp 284–295.
- [140] Lyon R. N., 1951; Liquid Metal Heat Transfer Coefficients, *Chem. Engg. Progr.*, vol. 47 (2), 1951, pp. 75-79.
- [141] Lubarski B., Kaufman S. J., 1955; Review of Experimental Investigations of Liquid Metal Heat Transfer”, *NACA Technical Note*, TN-3336, 1955.
- [142] Ibragimov M., Subbotin V. I., Ushakov P. A., 1960; Investigation of heat transfer in the turbulent flow of liquid metals in tubes, *Atomnaya Energiya* 8 (1), 1960, pp 54–56.
- [143] Ede A. J., 1961, The heat transfer coefficient for flow in a pipe, *J. Heat Transfer*, vol 4, pp 105-110.

- [144] Notter R. H. and Sleicher C. H., 1972; A Solution to the Turbulent Graetz-Problem III Fully Developed and Entrance Region Heat Transfer Rates, Chem. Eng. Sci., Vol. 27, pp 2073-2093.
- [145] Kirillov P. L., Ushakov P. A., 2001; Heat transfer to liquid metals: specific features, methods of investigation, and main relationships, Thermal Eng. Vol 48 (1), pp 50–59
- [146] Cheng X, Tak N., 2006, Investigation on turbulent heat transfer to lead–bismuth eutectic flows in circular tubes for nuclear applications, Nucl. Eng. Des., 236, 385–393.
- [147] IAEA-TECDOC 1520, “Theoretical and Experimental Studies of Heavy Liquid Metal Thermal Hydraulics”, IAEA, 2006.
- [148] Chandra L., Roelofs F., Houkema M., Jonker B., 2009; A stepwise development and validation of a RANS based CFD modelling approach for the hydraulic and thermal-hydraulic analyses of liquid metal flow in a fuel assembly, Nuclear Engineering and Design, 239, 2009, pp 1988–2003.
- [149] Reynolds A. J., 1975; The prediction of turbulent Prandtl and Schmidt numbers.” Int. J. Heat Mass Transfer, vol 18, pp 1055–1069.
- [150] Gori F., El Hadidy M. A., Spalding D. B., 1979; Numerical prediction of heat transfer to low-Prandtl number fluids, Numer. Heat Transfer 2, pp 441–454.
- [151] Fuchs H., 1973; Wärmeübergang an strömendes Natrium, Eidg. Institut für Reaktorforschung, Würenlingen, Bericht Nr. 241, Schweiz.
- [152] Aoki S., 1963; A consideration on the heat transfer in liquid metal, Bull. Tokyo Inst. Tech. 54, pp 63–73.
- [153] Jischa M., Rieke H. B., 1979; About the Prediction of Turbulent Prandtl Numbers and Schmidt Numbers from Modelled Transport Equations, Int. J. Heat and Mass Transfer, Vol. 22, pp. 1547-1555.

- [154] Yakhot V. and Orszag S.A., 1986; Renormalization group analysis of turbulence”, J. Sci. Comput., Vol.1, 3-51.
- [155] Wolters J., Hansen G., Komen E. M. J., Roelofs F., “Validation of CFD Models with Respect to the Thermal-Hydraulic Design of the ESS Target”, IAEA-TECDOC 1520, IAEA, 2006.
- [156] PHOENICS ver3.6 user manual, CHAM, Feb 11, 2005.
- [157] Incropera, F.P. and Dewitt, D.P., 1996, Introduction to heat transfer, John Wiley and sons, New York.
- [158] Chen, C.J., J.S. Chiou (1981), “Laminar and Turbulent Heat Transfer in the Pipe Entrance Region for Liquid Metals”, International Journal of Heat and Mass Transfer, Vol. 24, pp. 1179-1189.
- [159] Shannon, R. L. and Depew, C. A., 1969, Forced laminar convection in a horizontal tube with variable viscosity and free convection effects, Trans. ASME 91C, 251.
- [160] Seban R. A., 1950; Heat Transfer Measurements on Lead Bismuth Eutectic in Turbulent Pipe Flow”, Inst. Eng. Res., Univ. Calif., (Contract N7-onr-29523, Phase(2), Proj. NR 035 324.
- [161] Johnson H. A., Harnett J. P. and Calbaugh W. J., 1954; Heat transfer to Lead-Bismuth and Mercury in Laminar and Transition Pipe Flow, Transactions of the ASME.
- [162] Lubarski B., 1951; Experimental Investigations of Forced Convection Heat Transfer Characteristics of Lead Bismuth Eutectic, NACA RM E51G02.
- [163] NEA Report, 2007; Best Practice Guidelines for the use of CFD in Nuclear Reactor Safety Applications, Report No: NEA/CSNI/R(2007)5.
- [164] Jaiswal, B.K., Vijayan, P.K., Maheshwari, N.K., Borgohain, A., 2008 Development of a computer code to study the steady state and the transient behaviour of liquid metal

- natural circulation loop, 19th National and 8th ISHMT-ASME heat and mass transfer conference, JNTU Hyderabad, India.
- [165] Idelchik I. E., Malyavskya G. R. , Martynenko O. G. and Fried E., 1988, Handbook of Hydraulic Resistance, 2nd edition, Hemisphere Publishing Corporation.
- [166] Distefano J. R. and Chitwood L. D., 2001, Oxidation and its effects on the mechanical properties of Nb-1Zr, J. Nuclear Materials 295, 42-48.
- [167] Petire J. C., Dickey B. R. and Legler B. M., 1967; Radiative and Convective heat transfer within vertical annular spaces open at the ends, TID 4500, U. S. Atomic Energy Commission Research and Development Report, Idaho Nuclear Corporation.
- [168] Wojcik C. C., 2001, "Thermomechanical Processing and Properties of Niobium Alloys" Proc. of International Symposium Niobium 2001, Orlando.
- [169] Kofstad P. and Espevik S., 1966, Low Pressure Oxidation of Niobium at 1200°–1700°C, J. Electrochem. Soc. 112, 155.
- [170] Delgrosso E. J., Krutenat R. C., Carlson C. E., and Carta J. S., 1963, "The Oxidation Characteristics of Niobium- 1 Zirconium Alloy, " J. Less-Common Metals 5, 57-77.
- [171] DiStefano J. R., Pint B. A. and DeVan J. H., 2000, Oxidation of refractory metals in air and low pressure oxygen gas, Int. J. Refractory Metals & Hard Materials 18, 237-243.
- [172] Jaques Al, 1988; Thermo physical Properties of Argon, Report No: TM-1517, Fermi National Accelerator Laboratory, February, 1988.